CRANFIELD UNIVERSITY

Sarah Thiollet

Development of a quantum dot-encoded microsphere suspension assay for the genotyping of single nucleotide polymorphisms

Cranfield Health

PhD THESIS

CRANFIELD UNIVERSITY

CRANFIELD HEALTH

Ph.D. THESIS

Academic Year 2009

Sarah Thiollet

Development of a quantum dot-encoded microsphere suspension assay for the genotyping of single nucleotide polymorphisms

Supervisors: Dr. Sarah L. Morgan
Dr. Nicola White

March 2009

This thesis is submitted in partial fulfilment for the Degree of
Doctor of Philosophy

To my parents, Catherine and Jacques Thiollet

.

ABSTRACT

This thesis describes the investigation of quantum dot-doped particle fluorescent technology commercially available for its application to analyte profiling in suspension.

The first part of the thesis described the characterisation of the quantum dot-encoded microspheres, QDEMs, developed by Crystalplex (PA, USA). The multiple fluorescence signatures of QDEMs were analysed using microscopy and flow cytometry technology which provided high-content measurements with a single excitation sources and multiple emission wavelength detectors. The sensitivity and stability of the materials was evaluated under typical biomedical conditions encounter in multiple analyte suspension assays. Novel analytical parameters were defined to study QDEM stability and confocal microscopy detection system was used to provide structural and fluorescent imagines of the fluorescent microspheres under various conditions. Composition of the aqueous environment, temperature and physical forces applied to QDEM induced changes in their fluorescent codes and structural properties. Optimal conditions were then defined for the application of the material to biomedical assays. In a second stage, a conjugation method was developed to produce optimised QDEM bioconjugates for the detection of single strand DNA in suspension. The impact of the conjugation buffer, the concentration and the structure of oligonucleotides was evaluated to optimise QDEM bioconjugates. Then, a novel approach was investigated to optimise the hybridisation of ssDNA to QDEM bioconjugates. Experimental design with response surface methodology determined optimum conditions for the hybridisation of oligonucleotides to QDEM surface in suspension array. Finally, the specific hybridisation of ssDNA to QDEM bioconjugates in a small liquid format adapted to single nucleotide polymorphism detection was demonstrated.

The work presented here shows the potential of QDEM bioconjugates for suspension array technology and DNA genotyping. Further, this report highlights the challenges that remain for QDEM fluorescent technology to be reliable for biomedical and suspension array applications.

ACKNOWLEDGEMENTS

I would like to express my gratitude to my supervisors Dr. Sarah L. Morgan and Dr. Nicola White for their guidance and support during my research.
I would like to thank Dr. Steve Dunn, Dr. Conrad Bessant, and Pr. Seamus Higson for their scientific advices and support in reviewing this manuscript.
I am thanking my former supervisors: Pr. Sally Saini, Dr. Steve Setford, who gave me the opportunity to undertake this research project, and Dr. Laurie Ritchie Dr. Jane Rixon, and Dr. Michael Malecha other former supervisors in this project.
My gratitude goes to the Head of Cranfield Health, Pr. Joe Lunec, for his commitment and his precious support in the final achievement of this project.
I do not forget all the researchers, engineers, academic staff, who have been of a great help all along this project, for practical work as for administrative tasks and daily problems to solve. For that I would like to sincerely thank them all.
I would like to particularly thank Dr. Catherine Boisson-Vidal, whose support was essential at the end of my research project, and Dr. Jerome Warrand for his scientific and sportive support along this PhD years.
I have a particular thought for my housemates, officemates and friends, who were my daily support and understood perfectly the difficulties I had to face in my work. I will not have made it without you. I also have a special thought for *Marc et Sophie*, who have been, and are of an undoubted support and friendship.
Special thanks to the farmers and the sheep who coped with my temper for free.

I dedicate this work to the only real doctor of the family, my beloved father, and to ‘my four generation of women’; you are the reasons why I keep running faster and longer.

TABLE OF CONTENTS

List of Figures

List of Tables

ABBREVIATIONS AND NOMENCLATURE

Abbreviations

%GC	Percentage of guanine and cytosine bases in a DNA sequence
2/3 D	2/3 dimensional
As	Arsenic
ASO	Allele Specific Oligonucleotide
a.u.	Arbitrary units
BSA	Bovine Serum Albumin
BP	Band Pass
bp	base pair
LP	Long Pass
C	Concentration
Cd	Cadmium
Ch	Channel
Cl	Chloral
Da	Dalton
ds	double strand
dNTPs	deoxyribonucleotides
D_o	Oligonucleotide density
DOE	Design of Experiment
FC	Flow Cytometry
cDNA	complementary DNA
Cy3	Cyanine-3-dUTP
Cy5	Cyanine-5-dUTP
ΔG	deltaG energy of initiation
DNA	Deoxyribonucleotide acid
dNTP	deoxyribonucleoside (5'-) triphosphate
FL1/2/3/4	Fluorescent channel

FSC	Forward Side Scatter
Gmean	Geometric mean fluorescent intensity
λe	emission wavelength
MFI	Median Fluorescence Intensity
MEF	Molecular Equivalent of soluble Fluorochromes
min	minutes
MRO	Multiple Response Optimisation
MW	Molecular Weight
Na	Sodium
NB	Number
Oligo	Oligonucleotides
Pb	Lead
PE	Phycoerythrin
PBS	Phospate-Buffered Saline
PCR	Polymerase Chain Reaction
QD	Quantum Dot
QDEM	quantum dot-encoded microsphere
RT	Room Temperature
RSM	Response Surface Methodology
S	Sulphide
Se	selenium
SNP	Single Nucleotide Polymorphism
ss	single strand
SSC	Side angle Scatter
SSC	Sodium Citrate buffer
STR	Short Tandem Repeat
TBS	Tris-HCl Bovine Serum
Te	Tellurium
Tm	melting Temperature
TMAC	Tetra Methyl Ammonium Chloride buffer

UV	Ultra Violet
USA	United States of America
UK	United Kingdom
Zn	Zinc

Nomenclature

- SI Prefixes for Units:

k	kilo- (10^{3})
m	milli- (10^{-3})
μ	micro- (10^{-6})
n	nano- (10^{-9})
p	pico- (10^{-12})
f	femto- (10^{-15})

- Units Notation:

°C	Degrees centigrade
g	gram
K	Kelvin
l or L	litre
m	metre
M	molar
v/v	volume per volume
w/v	weight per volume
S	surface
V	Volt

- Nucleic Acid Notation:

A	Adenine
C	Cytosine
G	Guanine
T	Thymine
U	Uracil

- Greek Alphabet Notation used:

β	beta
Δ	delta
λ	lambda
μ	mu

Chapter 1

Introduction and Literature review

1. INTRODUCTION AND LITERATURE REVIEW

The publication of the sequence of the human genome (Lander *et al.*, 2001) officially launched the 'omic' revolution in biology, transposing the traditional scale of research to a high throughput level. This genomic approach rapidly created a need for reliable, fast, cheap, and large scale biological experiments as well as efficient analytical processing of large amounts of data. Researchers point out the exigency of developing "human" size screening platform equipments in order to follow the growing scale of screening assay. In addition, a growing interest appears in the development of lab device miniaturisation for high throughput technology. In this respect, Nanobiotechnology described by Penn *et al.* (2003) as being "*the use of nanotechnology in biological systems*" offers promise to reach these objectives. Nanobiotechnology integrates the fields of chemistry, physics, material science, molecular and cell biology to fabricate nanostructures composed of organic and/or inorganic materials for bioanalytical applications. It also involves the design of instruments adapted to the synthesis and detection of the nanomaterials. Fluorescent and metallic nanoparticles have been used for optical and electrochemical detection (Authier *et al.*, 2001). Gold and silver nanoparticles coated with antibodies are used as substrates for multiplex bioassays. Jiang *et al.* (2008), recently showed that nanoparticles can not only be considered as carriers for biomedical applications but can also actively mediate functions in biological systems. Nanoparticles of various shapes, sizes and composition have the potential to fundamentally change the bioanalytical measurement landscape in biosciences by reducing the size of instrumentation while increasing the number of experiments and/or the number of analytes investigated (Penn *et al.*, 2003). An active area of research aim to use the unique properties of nanoparticles to improve molecular biological screening assays and to show their efficiency in terms of sensitivity, multiplexing, cost, ease of use and so forth, compared with existing bioanalytical technologies (Bailey *et al.*, 2004). Bioconjugated nanoparticles and quantum dots (QDs) are among the most promising nanomaterials for application to nanomedicine (Huo, 2007). Nanoparticles and QDs are conjugated with biospecific molecules, which act as recognition tags for biological applications. Antibodies, DNA, biotin, streptavidin, enzymes, or receptor ligands are

examples of biological tags attached to nanoparticles (Penn *et al.*, 2003; Grecco *et al.*, 2004; Lidke *et al.*, 2004; Medintz *et al.*, 2005). The binding of bioconjugates to their target is detected by the changes of single- or clustered-nanoparticles properties or by other response linked to the binding event of both target and probe bioconjugates. These applications are mainly based on the unique properties of the metallic or the semiconductor composition of the nanoparticles (Huo, 2007).

Semiconductor nanocrystal structures exhibit narrow, well-defined fluorescence emission spectra with a simple ultra-violet (UV) light excitation source, and are believed to significantly improve existing fluorescent labelling probes. Conventional dyes present emission spectra that largely overlap and prevent the fluorophores from being used in multiplex reactions. The unique photophysical properties of luminescent inorganic nanocrystal bioconjugates was demonstrated in multiplex bioimaging and sensing assays, and has the potential to enhance existing diagnostics assays. QD technology was also used to develop QD-doped particles. The fluorescent encoding properties of the QDs hold the potential to overcome many of the significant chemical and spectral limitations of conventional organic fluorophores bead-based technologies (Han *et al.*, 2001). Fluorescent semiconductor nanocrystals are encoded in microspheres which can subsequently be functionalised and used as bioconjugate fluorescent probes for multiplexed bioassays (Gao and Nie, 2004). Eastman *et al.* (2006) reported how QD-doped particles can be used for multiplex gene expression analysis. This technology has therefore the potential to improve current high throughput screening assay as genotyping platforms and therefore offer a promising contribution to the challenging field of "omic" analytical research.

The work presented in this thesis investigates the potential and pitfalls of QD-doped particle technology for DNA genotyping. Materials science and molecular biology were associated to address these issues. The following chapter presents an overview of both scientific fields involved in the research project. The review focuses on the QD technology and its applications, in order to highlight the potential of QDEM technology for the development of a genotyping assay.

1.1. Quantum dots technology (QDs)

1.1.1. Structural characteristics

Quantum dots (QDs) are nanometre (nm, 10^{-9} meter) sized particles, which are neither isolated small molecules nor bulk solids but are described as semiconductor nanocrystal materials (Bailey *et al.*, 2004). Modern QD technology originated from Brus and co-workers and the Ekimov and Efros group (early 1980s), which contributed to the understanding of the quantum confinement phenomenon that explains the colour-tunable properties of QD nanocrystals dependent on their sizes (Efros and Efros, 1982). Later Bawendi and Alivisatos discovered ways to make QDs water soluble and to conjugate them to biomolecules. They also improved QDs brightness by adding an inorganic shell around the nanocrystals (Alivisatos, 1996). Two types of QD structure can be distinguished by their properties of changing fluorescent emission wavelength depending on their size or on their material composition (Figure 1.1).

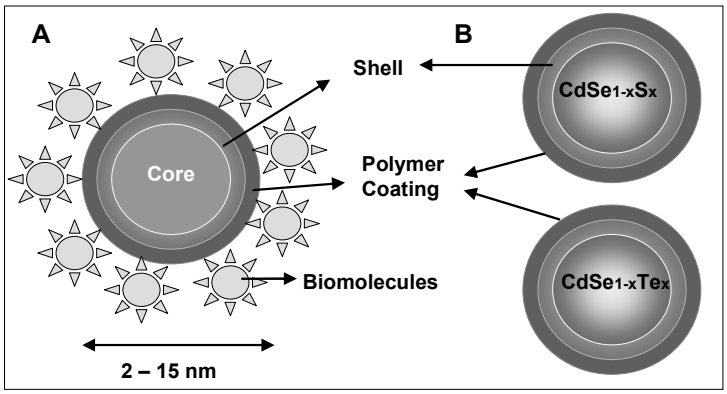

Figure 1.1 Schematic structure of conventional "size-tunable" QD conjugate (A) and example of "composition-tunable" alloyed QDs (B).

A: Size-tunable QDs with a core/shell structure, *e.g.*, CdTe/CdSe. **B**: Composition-tunable QDs, *e.g.*, $CdSe_{1-x}Te_x$, CdS_xSe_{1-x}/ZnS core/shell; Both QDs can be made water-soluble and biocompatible by surface-modification with a coating polymer to attach biomolecules (Bailey *et al.*, 2004; Maier *et al.*, 2007). Cd: cadmium, Te: telluride, Se: selenium, Zn : zinc, S: sulphide.

Conventional "size-tunable" QDs can be produced with different shapes such as rods, rice-shaped, and tetrapods (Peng, 2003). Spherical dots of 1-15 nm size range are the most commonly used for scientific applications. These QDs are composed of two major internal structures: the core and the shell (Figure 1.1A). The chemical composition of the core specifies the fluorescence properties of the QD. The core is confined and structurally related to the shell, an inorganic material purely protective and non-emissive, which confers robustness and tolerance to external conditions. The shell enhances the light emission and the specific optical properties of the QDs (Figure 1.1). The most common shell material is made of zinc sulphide (ZnS), a relatively inert material which insulates the core material (Dabbousi *et al.*, 1995).

Size-tunable QD are also called binary QD since the core of the nanocrystal is composed of two semiconductor materials of periodic groups II-VI, II-V, and IV-VI. II-VI semiconductors are synthesised using elements from the second and sixth group of the periodic table, *e.g.*, PbS, PbSe. IV-VI semiconductors are synthesised using elements from the fourth and sixth group of the periodic table, *e.g.*, InP, InSb; and III-V using third and fifth group elements, *e.g.,* CdSe, CdTe, CdHgTe, ZnS. The most common QDs used for life science applications are colloidal semiconductor nanocrystals made of CdS and CdSe core material overcoated with a layer of ZnS. The composition of their core material associated to the corresponding emission wavelength is presented in Table 1-1.

Table 1-1 Example of QDs core composition with corresponding emission wavelength *

Name	Structure	Corresponding periodic table group	Emission wavelength (λ_e) Range (in nm)
CdS	Cadmium Sulphide	II-VI	UV - blue (350- 500)
CdSe	Cadmium Selenide	II-VI	Visible (400 - 700)
CdTe	Cadmium Telluride	II-VI	Far infrared (600 - 1000)

* UV: ultra violet, nm: nanometre

Colloidal semiconductor nanocrystals are synthesised from precursor compounds dissolved in solutions, much like traditional chemical processes (Alivisatos *et al.*, 2005). QDs composed with other core materials have been prepared but issues of synthesis reproducibility and inorganic passivity remains (Medintz *et al.*, 2005).

Semiconductor materials can also be used to form alloyed nanocrystals (Bailey and Nie, 2003). An alloy is defined as a partial or complete solid solution of one or more elements in a metallic matrix. Complete solid solution alloys give single solid phase microstructure, while partial solutions give two or more phases that may be homogeneous in distribution depending on thermal (heat treatment). As an example, steel is a metal alloy whose major component is iron, with carbon content. Bailey *et al.* (2003) prepared alloyed nanocrystals, defined as ternary QDs (*i.e.,* three different semiconductor materials), composed of $CdSe_{1-x}Te_x$, with uniform size particles, and adjustable optical characteristics (Figure 1.1B). Zhong *et al.* (2003) described the synthesis of $Zn_xCd_{1-x}Se$ and $Zn_xCd_{1-x}S$ with comparable photoluminescence properties to the best of those reported for CdSe-based QDs. The emission wavelengths or colours of this new class of "composition-tunable" alloyed nanocrystals are determined by the relative concentration of the elements making up the core of the QDs (Maier *et al.*, 2007).

Core-shell materials are further insulted with a coating layer. An internal coating layer of inorganic ligands is covalently attached to the surface of the shell to further passivate the core-shell structure and acts as a glue to the outer layer of the coating. The outer coating layer determines the solubility and the reactivity of the QD material and is usually a mixed of hydro-phobic and -phillic polymers with carboxylic acid functionalisation. The hydrophobic part interacts with the internal inorganic coating and the hydrophilic part interacts with the environment to provide QD solubility in solvents. The example of coating with carboxylate groups on the external surface permits biological or non biological moieties to be attached on the QD, which therefore provides special properties to the material such as biomolecule binding capacities (Hezinger *et al.*, 2008). QDs stability toward external environment conditions depends on the thickness of the shells.

The modification of QD size and chemical composition tuned the fluorescent emission of the nanocrystals from the near ultraviolet (400 nm) to the near-infrared spectrum (2000 nm) (Figure 1.2) (Table 1-1).

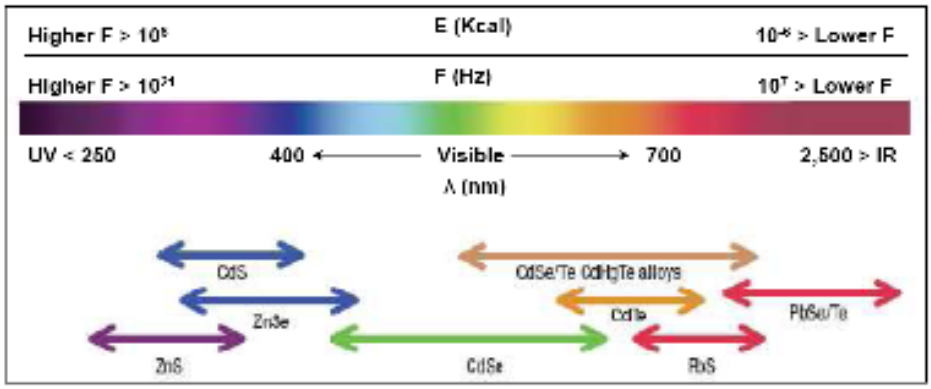

Figure 1.2 Representation of QD core materials as a function of their emission wavelength over the electromagnetic spectrum (adapted from Medintz *et al.*, 2005).

UV: ultra-violet, IR: infrared; Scales of the electromagnetic spectrum are represented with different units, E: energy in Kcal, F: frequency in Hz, and λ: wavelength in nm.

1.1.2. Optical properties

- **Photophysical properties: the quantum confinement**

A semiconductor under stimulation will absorb light and react like many atomic structures under excitation: electrons from inner shells within the structure are promoted from the valence band to the conduction band, leaving a positively charged hole due to the absence of the negatively charged electron. The particularity of the QD structure confines the electron's movement such that it cannot move freely and therefore exhibits atom-like quantised energy levels. Electron energy levels must be treated as discrete; there is a small and finite separation between energy levels which is called quantum confinement.

Under these conditions, the semiconductor material stops acting like a solid-state system and acts instead as a 'quantum dot'. The so-called electron 'confinement' process creates the particular electronic and optical properties of quantum dots (Brus, 1984; Chestnoy *et al.*, 1986). A large energy input is required to bring the QD into an excited state. For a given input energy, a QD only emits a narrowly defined emission spectrum. Fluorescence is generated when the electron and positive hole recombine. When electrons and holes (exciton pairs) generated by the incident photons are confined within a space or quantum box, smaller than the Bohr exciton radius (*i.e.,* the preferred electron-to-hole distance of an exciton pair of normal bulk material), the semiconductor's band gap widens and its fluorescence shifts towards the blue. The smaller the box, the shorter (bluer) the fluorescence wavelength. On the contrary, the larger the quantum box, the longer (redder) the fluorescence wavelength (Figure 1.2) (Dabbousi *et al.*, 1997). As the particle reduces further in size, the energy required to excite the structure increases and the absorption and emission wavelength correspondingly reduce (Electromagnetic spectrum Figure 1.2). The quantum theory predicts that the energy of emitted light will increase proportionally with the decreasing of quantum dot diameters.

The structure and nanosize of the QDs confers to the material unique optical properties of light absorption and emission. Figure 1.3 shows the absorption and emission spectra of equal concentrations of conventional dyes and six different size-tunable QD populations.

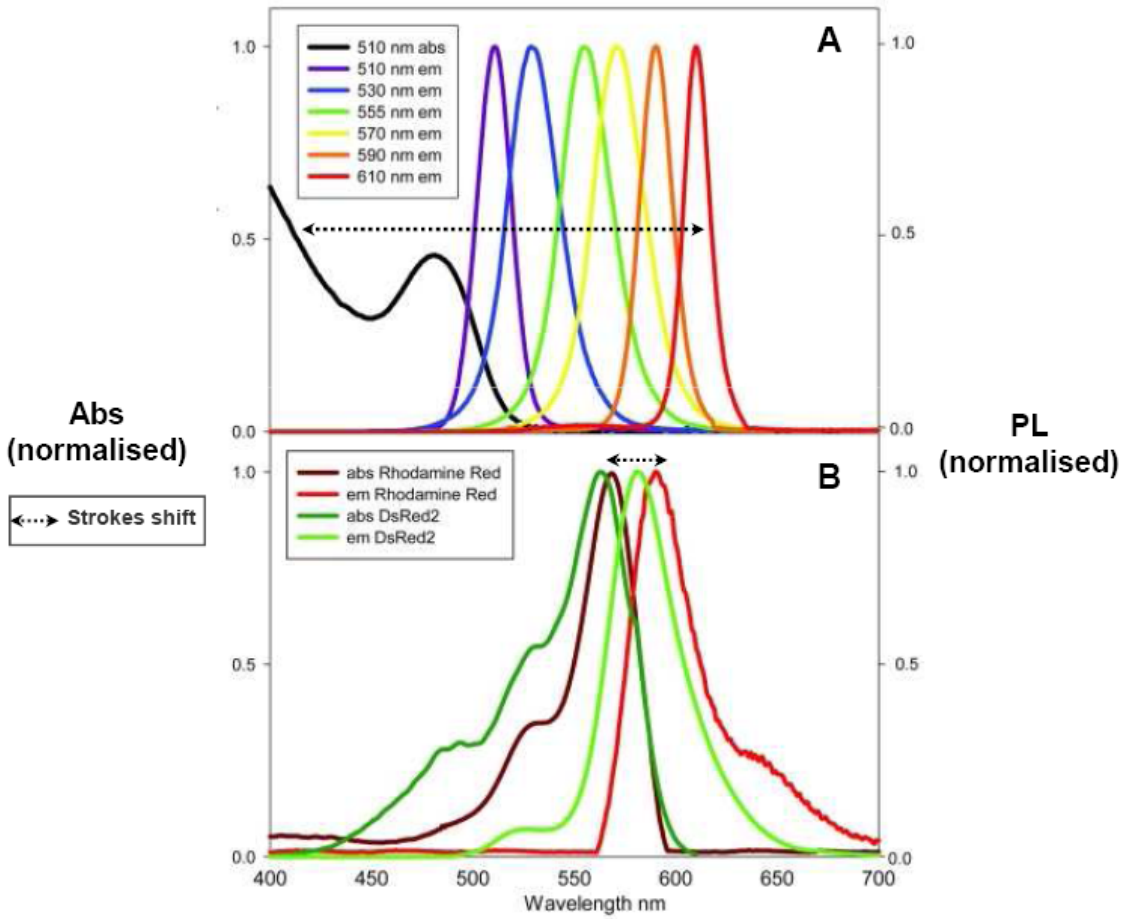

Figure 1.3 Comparison of QDs (CdSe/ZnS core/shell) spectral properties (A) to those of conventional organic dye (Rhodamine red/DsRed2) (B) (adapted from Medintz *et al.*, 2008).

Abs: Normalised absorbance is represented on the left y-axis; abs: absorption spectra. PL: Normalised photoluminescence is represented on the right y-axis; em: emission spectra. **A**: absorption and emission of six different QD populations. The black line shows the absorption at 510 nm of emitting QDs. **B**: absorption and emission of rhodamine red, a common organic dye, and of DsRed2 a fluorescent protein (Baird *et al.*, 2000). All samples were excited at 365 nm with a UV lamp. For the 610 nm emitting QDs, the pointed arrows illustrate the stokes shift of 610QD (~250 nm), and of rhodamine (~50 nm).

- **Absorption and excitation characteristics**

When UV light is absorbed, electrons are transferred from valence bands of the material (or orbital) to the conduction band. The energy of absorbed light must correspond very closely to the difference in energies between the energy levels involved in the absorbance event. As QDs are composed of a large number of nearly identical atoms it mimics a combination of large electronic possibilities in the valence band and conduction band, which allows a large number of combinations between orbital energy levels and the excited electron. QDs therefore absorb broad wavelength light. The higher the energies (Figure 1.2), the greater the number of potential combinations and the more QDs potentially absorb light. As a consequence, the enhanced absorbance of QDs converges directly into more intense signals and potentially higher fluorescent label sensitivity. An inexpensive UV lamp simultaneously excites multiple coloured QDs which is advantageous for multiplexed detection experiment (Figure 1.3A) (Medintz *et al.*, 2008). The excitation of QDs is flexible, easy and cost-efficient.

- **Tuneable emission pattern**

The emission pattern is an important factor in multiplex fluorescence assays to facilitate the specificity of detection and to achieve acceptable sensitivity. The unique internal atomic structure of nanocrystal semiconductors ensures QDs' extremely symmetrical narrow emission spectra compared with conventional fluorescent dyes (Figure 1.3A, B). Less overlap among QDs' spectra significantly reduces channel-to-channel detection crosstalk. Conventional dyes exhibit less intense and broader emission profiles (Figure 1.3B). The simultaneous detection of organic dyes is therefore highly limited by the difference in brightness and the overlap of their emission spectra (Medintz *et al.*, 2008).

The enhanced absorbance of QDs is directly translated into more intense signals and thus, potentially higher assays sensitivity. First, QDs' narrow wavelength distribution makes them compatible with narrow detection filters, which reduces background noise and auto-fluorescent contamination. The narrow emission spectrum also decreases the need for laborious and inaccurate compensation strategies for fluorescent detection, which produce enhance quantitative QD assays (Bruchez Jr *et al.*, 1998). Nevertheless, QDs present one form of emission broadening known as "inhomogeneous broadening", which is due to size distribution of the QD population. The narrower the size distribution, the smaller the spectral broadening. Ideally, a particular population contains "identical" QDs, but in reality different size diameters are obtained due to current uncertainty of the chemical synthesis process. Alloyed nanocrystals or composition-tunable QDs promise to resolve this limitation of the QD technology with a uniform particle size and adjustable optical characteristics (Maier *et al.*, 2007).

The Stroke shift of a fluorophore is the difference between the absorbance peak and the emission peak for a fluorophore. A shift between excitation light and emission light occurs because the excited fluorophore looses energy before re-emitting light due to vibrionic vibration. As a consequence, a fluorophore should always emit less energy than it has been receiving, which means that its emission wavelength should always be higher than its excitation wavelength. The stroke shift of QDs and fluorescent dyes are represented by the pointed arrow in Figure 1.3. Since QDs are more efficiently excited at wavelengths further displaced from the emission peak, their stroke shift appears greater than for the equivalent organic dyes (Figure 1.3A, B). The large strokes shift observed with QDs allows the use of broad excitation and emission filters that do not overlap, increasing brightness and sensitivity. The small distance between the peaks with Rhodamine requires filters with similar band gaps, thus reducing efficiency and brightness.

Conventional dyes are more sensitive to surface interactions, extreme pH changes and light. Even the act of measuring the fluorescent signal decreases their emission intensity. These external events denature the fluorophore structure, causing photobleaching: the fluorophore

will stop absorbing and as a consequence stop emitting light. QDs are more stable regarding time, intensity, wavelength, and do not bleach as organic dyes do (although QDs can be slowly degraded under intense UV conditions). The chemistry of their shell and the polymeric coatings are important structural characteristics that improve their robustness and stability (Chan and Nie, 1998).

- **QD tuneable properties**

The colours of both QDs absorption and emission can be tuned to any chosen wavelength by changing the size or composition of the dots due to their specific photophysical properties as explained previously. Most common dots are composed of CdSe and are available in the emission range from 510 nm to 665 nm (Figure 1.4) (Bailey *et al.*, 2004). QDs of the same chemical composition exhibit the same quantum yield (ratio between emitted and absorbed light: if r=1 all light absorbed is re-emitted), the same surface chemistry and the same environmental properties. As a consequence, QD CdSe of different sizes should have theoretically the same response to light whatever the colour they emit (Figure 1.4A). CdSe QD's emission wavelength range limitations are overcome by changing the composition of the core with new semiconductor materials. CdS material allows a wider range of emissions in the blue part of the spectrum and CdTe increases the colour possibilities in the red part (Figure 1.4-B) (Dabbousi *et al.*, 1995).

Alloyed nanocrystals show similar resolved electronic transitions and clear band-gap fluorescence emission to those reported for conventional QDs (binary QDs), but they also present a nonlinear relationship between the composition and the excitonic absorption and band-gap emission. Alloy nanocrystals have a thus a longer emission wavelength than conventional QDs due to this nonlinear relationship between the band-gap energy and the core composition (Figure 1.4B) (Bailey *et al.*, 2004). For alloyed nanocrystals, Bailey *et al.* (2003) have demonstrated that the quantum confinement effect could be controlled with three variable factors: particle size, composition and internal structure.

The composition-tunable emission of $Zn_xCd_{1-x}Se$ alloy nanocrystals have wavelengths ranging from 460 to 630 nm across the visible spectrum with a blue-shifts which gradually increase with the Zn content: the higher the concentration of Zn, the lower the emission wavelength (Zhong *et al.*, 2003).

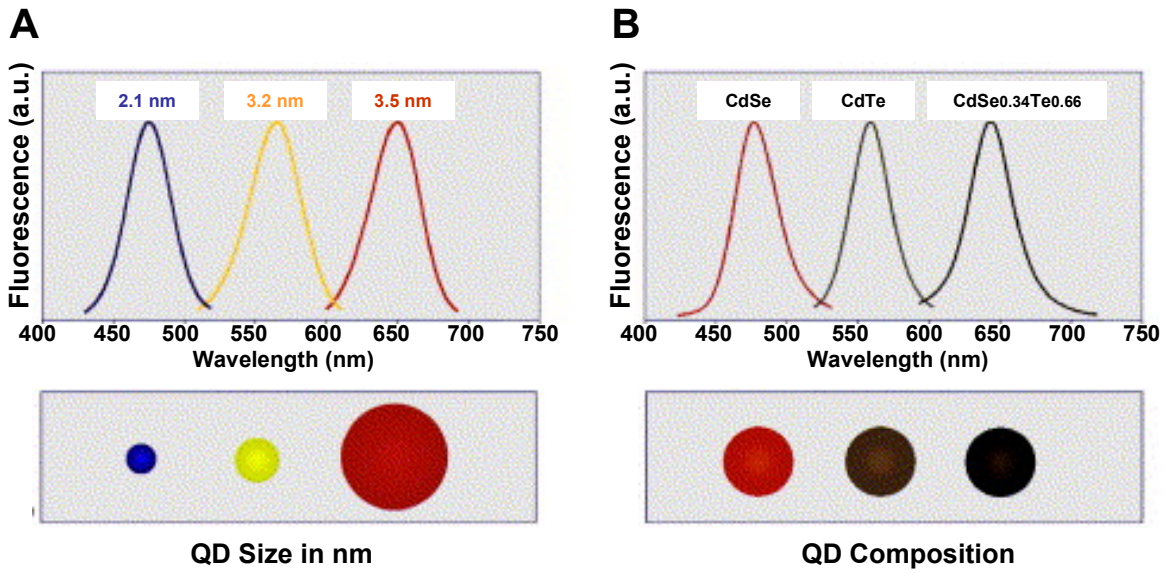

Figure 1.4 Tunable emission pattern of the QD emission wavelength by changing the nanoparticle size (A) or composition (B) (adapted from Bailey *et al.*, 2004).

A: The emission of a CdSe QD varies within the visible spectrum (450–650 nm) depending on the core diameter (2 to 7.5 nm). A schematic representation of the "size-tunable" CdSe particles is shown below the fluorescence (FL) spectrum. **B**: The emission maximum can be tuned to any wavelength between 610 and 800 nm by modifying the composition of the ternary alloy nanocrystals. Illustration of "composition-tunable" $CdSe_xTe_{1-x}$ nanoparticle of constant size (5 nm diameter) is represented below the FL spectrum.

1.1.3. Chemical synthesis and bioconjugation methodologies

A number of different approaches have been described for the synthesis of conventional binary QDs with high crystallinity quality and size distribution monodispersity. High yields of monodisperse and stable particles are obtained with an organometallic approach by undertaking chemical synthesis in organic solvents at high temperatures in the presence of organometallic surfactants (Figure 1.5). Under continuous stirring at high temperature (~320 C), selenium (Se) precursor dissolved in tri-n-octylphospine (TOP) is injected. Fast nucleation of CdSe nanocrystals is initiated and rapidly stopped, partially due to the prompt decrease in temperature (to ~290°C) caused by the injection of the room temperature (RT) solution. Then, the particle growth starts and when the desired size is obtained, the solution is cooled (~220°C) to stop the reaction. A protective shell of zinc sulphide can be grown by injection of Zn/S precursors dissolved in TOP. Core-shell CdSe/ZnS QDs are isolated via precipitation at RT (Figure 1.5).

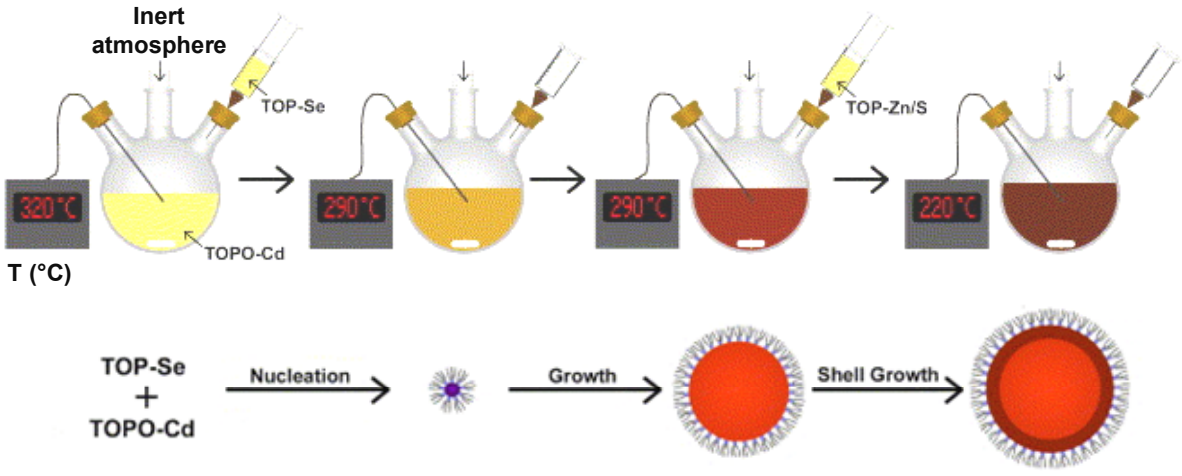

Figure 1.5 Schematic representation of high-temperature synthesis of size-tunable colloidal CdSe QD (adapted from Bailey *et al.*, 2004).

Cadmium precursor (Cd) is dissolved in trioctyl phosphine oxide (TOPO) in an inert atmosphere (argon or nitrogen flow). T: temperature in °C. Se: selenide, Zn/S: zinc sulphide.

Murray *et al.* (1993) described the synthesis of high quality colloidal QDs with high-temperature growth solvents/ligands (mixture of trioctyl phosphine/trioctyl phosphine oxide, TOP/TOPO), associated to the pyrolysis of organometallic precursors. The CdSe QDs produced presented high crystalline cores and size distribution. A wider band-gap semiconductor material (ZnS or/and CdS) was later added to the same reaction with appropriate precursors to coat the CdSe core and create the protective shell. This synthetic approach using high-temperature steps produces hydrophobic surfactant-coated nanoparticles which are well-dispersed in inorganic solvent (toluene, chloroform) but are not soluble in aqueous solutions. Cores are synthesised and their growth is monitored by absorption spectroscopy, based on the known size-dependent behaviour of conventional QDs (Figure 1.5). The growth is stopped by quenching the reaction when the desired core size is reached (Dabbousi *et al.*, 1997; Peng and Peng, 2001).

Aqueous synthesis methods have been described, where sodium hydrogen telluride (NaHTe) is produced in an aqueous solution and mixed with nitrogen-saturated cadmium chloride ($CdCl_2$) using mercaptoacetic acid to stabilise the solution. The mixture is heated to control the growth of the resulting CdTe nanocrystals. The reflux technique involving the condensation of vapours and the return of this condensate to the system from which it originated is then used (~100°C) to control the growth of the nanocrystals. The QDs synthesised are water-soluble, stable, biocompatible, less expensive and less pollutant than organometallic procedures (Zhang *et al.*, 2003). However, this approach cannot reach the QDs degree of crystallinity and of narrow size distribution obtained with organometallic methods which is only achievable with effective separation of the nucleation and growth steps with high temperature annealing (Gaponik *et al.*, 2002).

Preparation of alloyed nanocrystals is based on the high temperature organometallic approach described previously but all reagents are added in a single mix with precise control of the core elements molar ratios. Bailey *et al.* (2003) reported a procedure to produce alloyed QDs where the amount of injected cadmium (Cd) was either in large excess or in short supply relative to the total molar ratios of Selenium:Tellurium (Se:Te).

The QD composition is determined by the relative formation of both CdSe and CdTe and not by the total amount of Cd. Alloyed nanocrystals can be prepared in a wide range of composition dependent on the core elements molar ratio (Se:Te in this case). Thus, these types of composition-tunable QDs were described by the formula $CdSe_{1-x}Te_x$ (Bailey and Nie, 2003).

Recently, Liu (2008) described the preparation of $Zn_xCd_{1-x}Se$ QDs at low temperatures by a reaction mixing Cd, Zn, and Se elements and using a cysteine for surface stabilisation. As described before, QD spectral emission can be tuned depending on the Zn/Cd molar ratio and intrinsic Zn/Cd relativities towards the third element (Se), and range from 430 to 505 nm. Cysteine, an aminothiols which has been used previously for direct capping of Cd-based QD particles, is compatible with biomaterials (cell compatibility and conjugation to serum bovine albumin) (Liu *et al.*, 2008).

Traditional QDs can be made water-soluble by replacing the surfactant layer or by encapsulating the original nanocrystals in an additional layer of hydrophilic polymers. Most QD solubilisation strategies rely on the substitution of the original hydrophobic TOP/TOPO ligands with ligands, which carry on one side, functional groups reacting with the inorganic QD surface (*e.g.*, thiol (–SH) group), and on the opposite side, hydrophilic groups (*e.g.*, hydroxyl (-OH), carboxyl (-COOH)), which ensure water affinity (Chan and Nie, 1998). The growth of a silica shell functionalised with hydrophilic groups is an alternative strategy to insulate the hydrophobic nanocrystals (Bruchez Jr *et al.*, 1998; Gerion *et al.*, 2001).

Finally, a third method was recently developed to coat hydrophobic nanocrystals with amphiphilic polymers (polar and apolar molecules) that arrange themselves into bilayers, by positioning their polar groups towards the surrounding aqueous medium and their lipophilic chains towards the inside of the bilayer, defining a non-polar region where the nanocrystals is between two polar ones. The polymer shell is thus stabilised by cross linking the polymer chains (Pellegrino *et al.*, 2004).

Hydrosoluble QDs can be associated with biological molecules as protein, anti-body, oligonucleotide, or other small biological molecule, which give the nanocrystals binding properties or other biological functionalities. The biological molecules can be absorbed to the QD or bound to the hydrophilic shell (Figure 1.6).

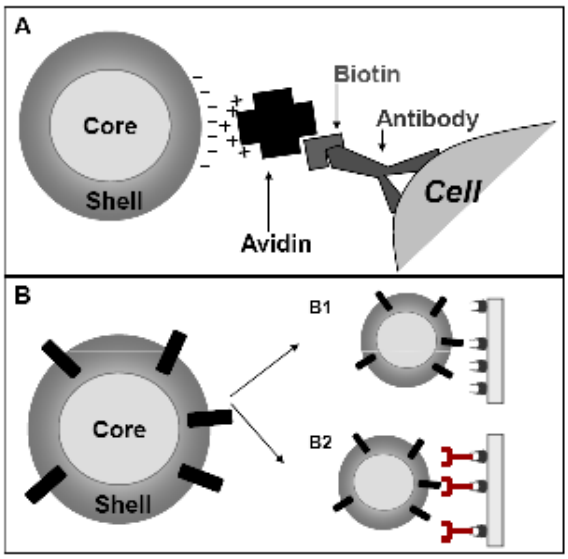

Figure 1.6 Schematic representation of QD bioconjugates.

A: Example of QD-avidin bioconjugate by electrostatic interaction, interacting with biotinylated antibodies; **B**: Example of absorbed QD bioconjugates that mediate direct or indirect binding functions.

QD biofunctionalisation is achieved by the interaction of the hydrophilic QD surface with the reactive chemical groups of biomolecules. An example is shown in Figure 1.6A with the electrostatically bioconjugation of a charged molecule (such as biotin) to the QD surface. Bioconjugation with covalent cross-linking typically uses carbodiimide coupling between carboxylated activated surfaces with amino modified molecules or maleinimide-catalised coupling between amine and sulfhydryl groups. Polyhistidine tags also provide the binding of biomolecules through mercapto (-SH) bond to the QD surface.

To resume, QD bioconjugates can perform direct identification of a specific target (Figure 1.6B1). The bioconjugation steps can also be repeated to add or change the functionalities of the QD. An example is the avidin or streptavidin QD bioconjugates which can be used in association with biotinylated proteins or antibodies as shown in Figure 1.6A. To generalise, a three-layer or "sandwich" approach using firstly an antibodies against a specific target, secondly a biotinylated secondary antibody against the first and a finally a streptavidin-coated QD offers also the possibility to label almost all types of biological targets (Figure 1.6B2).

QD bioconjugates are quickly replacing analogous conventional dye conjugates because of their superior optical performance: higher chemical- and photo-stability, lower limits of detection, which confer them higher levels of multiplex ability, and more quantitative results. Further, the optimisation of a given QD core structure bioconjugate population should be easily extrapolated to other types of populations. The development of multiplex assays is thus simplified and accelerated. A standard fluorescence microscope is an excellent and inexpensive tool for QD bioconjugate detection (Chan *et al.*, 2004). Examples of commercialised QD bioconjugates include QDs linked to biological species via streptavidin, protein A, and the biotin family (Figure 1.6A), which exhibit strong molecular interactions with their respective ligands.

1.1.4. Applications of QD technologies to life sciences

The broad excitation spectra of QDs allows the excitation of mixed QD populations with a single source of light (or single wavelength) far from their respective emission spectra with high efficiency, This optical characteristics and the QDs' tunable fluorescent emission properties are the two main advantages of QDs over traditional organic dye which have been exploited in analytical science and more specifically in life science (Jaiswal *et al.*, 2004). QDs have been commercialised even if current issues, potentially limiting their applications, have not yet been fully understood and thus need to be addressed further (Resch-Genger *et al.*, 2008). These limitations include photophysical properties (optical blinking, photostability), cytotoxicity, reproducibility and monodispersity of synthesis procedures, bioconjugation impact (biomolecule orientations, non specific attachment, sterical limitation due to increased size), and solubilisation (aggregation). The advantages and limits of the technology for biomedical applications are discussed in the final discussion of the thesis.

- **Commercialised QD materials**

Three companies were identified to provide commercialised size-tunable QD technologies: Invitrogen (Catlsbad, CA, USA), Evident Technologies (New-York, NY, USA), and NANOCO Technologies (Manchester, UK) through Sigma-Aldrich material science (Lumidots™, St Louis, MO, USA). Most of them offer an equivalent range of 7 different QD populations emitting from 380 to 700 nm with similar surface chemistries and bioconjugates tools.

Invitrogen (CA, USA) commercialise advanced antibody conjugation kits, western blotting kits and cell labelling kits which provide adapted protocols for the use of QD bioconjugates. Invitrogen promise real-time imaging, cell and tissues labelling, ligand-receptors tracking, and protein arrays with the panel of Qdot® commercialised products (Ballou *et al.*, 2004; Lagerholm *et al.*, 2004; Giepmans *et al.*, 2005; Lidke *et al.*, 2005).

In addition to the traditional range of CdSe QDs, Evident Technologies (New-York, NY, USA) provide lead sulphide (PbS) based QDs. Evidot® offers test kits with small quantities of a selection of nanocrystal wavelengths adapted to research teaching purposes, characterisation work or product development. The other originality of the company is the development of QD technology for use in other fields as light emitting diodes. Evident Technologies presents also other areas of research for the application of QD technology such as photonics and telecommunications, electroluminescence, security inks and solar cells. The photophysical properties of the QDs confer to them increased nonlinear absorption and refractive index which makes them attractive for optical switches, modulators and other devices that rely on nonlinear optics. Ink and paint formulation combining multiple QDs and other pigments can be created to provide unique fluorescent spectral barcodes for the identification of any object or document upon illumination (Chang *et al.*, 2004). QD-based ink can be applied to screen, gravure and ink jet printing processes, while paints are designed to be sprayed.

The third company, recently internationalised and originally from the UK, NANOCO Technology (Manchester, UK), provides CdSe (emitting from 480 to 640 nm), CdS (emitting from 380 to 480 nm), and cadmium free (CFQD™) NanoDots™ commercially distributed by Sigma-Aldrich material science. Their commercial activities are focus on electroluminescent displays, solid-state lighting, solar cells and life science applications, which are under development.

Only a single company, to our knowledge, was found to commercialise composition-tunable nanocrystals (TriLite™ nanocrystals), as well as quantum dots encoded into microspheres (PlxBead™). Crystalplex Corporation (Pittsburgh, PA, USA) develops and commercialises semiconductor nanocrystals for life science, optoelectronic (electroluminescent display, lighting), and security applications such as cryptography. Zhou *et al.* (2004) have demonstrated the utility of QD to create practically indecipherable cryptograms. The concept is to use a set of multiple single colour QD for creating highly secret codes based on their absorption/emission properties. The unique optical properties of QD make them a promising

tool in the area of security and encoded documents (Zhou *et al.*, 2004). For these applications, QDs with heavier atoms such as CdTe or HgSe or hybrids composed of PbSe have been studied due to their extended optical properties in the near-infrared region. Further details on the range of products available and their applications are detailed later in the thesis (Chapter 2, section 2.1)

- **Applications to life science**

Liposomes and polymer based micro and nanoparticles have been used and studied for a wide range of applications including pharmaceutics and physiology. A new generation of biosensors which employ colloidal gold and fluorescent nanocrystals have emerged and have been utilised in diagnosis, active agent detection and imaging (Medintz *et al.*, 2005). QDs are a promising tool for *in vivo* biomedical applications because of their inorganic nature which involves less interaction than organic dyes with their immediate *in vivo* environment. Pre-clinical drug screening and delivery are also other promising biomedical applications of QD technology.

Vu *et al.* (2005) developed QD conjugated to small hormone peptides to investigate ligand-receptor interactions, to activate cell surface receptor channels and to modulate downstream neurite sprouting. This work demonstrates the potential of QDs as drug carriers to specifically regulate cell functions. The functional groups covering the entire surface of the QDs imply multiple attachments of drug molecules to a single QD which might complicate and reduce the cell absorption. More molecules are needed to cover the reactive groups on the surface, which also potentially affects experimental costs. Synthesis control methods have been reported to reduce the number of surface groups surrounding a single QD (Qi and Gao, 2008). However, each of these methods adds to the final QD size, which is problematic especially for kinetic studies and the transport of drug molecules. Biotoxicity, size variation, bead aggregation, blinking and cell absorption are the principal issues to be addressed to in the development QD technology for drug discovery.

QDs are disguised as proteins for cell entry. Insights into receptor/ligand interactions and signal transduction have been studied with QD. Akerman *et al.* (2002) developed QD-peptide conjugates which bind directly and specifically to mice lung and tumour vasculatures. QD constant emission properties permit continuous imaging to follow the dynamics of biological interaction processes in real time (Grecco *et al.*, 2004). Direct interactions with native receptors were also characterised by Rosenthal *et al.* (2002) using serotonin conjugates. No increase in sensitivity over organic dyes is observed with QD-labelled antibodies, but the multiplex capabilities of QDs excited with a single source of light provide significant benefits for the detection of fluorophore labelled antibodies over conventional fluorophores.

The potential value of QD in bioimaging is due to (i) their photostability, which facilitates the long-term tracking of QD-labelled cells and molecules; (ii) their colour diversity, which enables the simultaneous tagging of several different population of cells and molecules; (iii) their broad excitation and narrow emission spectra, which facilitates the simultaneous detection of different QD-tagged cells; and (iv) the availability of common approaches to produce bioconjugates without compromising the molecular function, which allows *in vivo* and *in vitro* labelling of biomolecules (Figure 1.7)(Medintz *et al.*, 2005).

Observation of *Xenopus* embryos partitioning during development over days has been achieved by microinjecting QD bioconjugates into various cells (Dubertret *et al.*, 2002). This work demonstrated the high photostability and extended life time emission of QDs offering the possibility of long-term tracking of biological processes. QDs have also been conjugated with Streptavidin and IgG to label cell surface markers and nuclear antigens, and to stain microtubules and actin (Wu *et al.*, 2003). QDs have shown superior optical properties for high-resolution cellular imaging and the long-term observation of individual molecules and their movement within the cells.

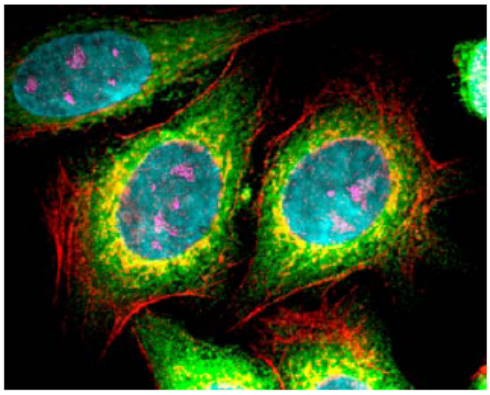

Figure 1.7 Illustration of cellular multicolour imaging with quantum dots (QDs) (adapted from Medintz *et al.*, 2005).

Pseudo-colour imagine of fixed human epithelial cells stained with five QDs: 655 nm QDs were used for the targeting of the nucleus in Cyan, 605QDs for proteins in magenta, 525QDs for mitochondria in orange, 565QDs for microtubules in green, and 705QDs for actin filaments in red.

The application of QDs to nanomolecular diagnosis has been described for the imaging of living tissues, and for cancer diagnosis tools. Researchers have injected live mice with QDs chemically-linked to monoclonal antibodies to detect the prostate-specific antigen on the cell surface of tumours. QDs simultaneous imaging of multiple molecular markers inside or on the surface of live cells could allow the early detection and identification of malignant tumours (Wu *et al.*, 2003). QD optical features make them ideal donors in fluorescent resonance energy transfer (FRET) mechanism, a physical phenomenon happening when fluorescent group of dyes are in close proximity to one another and when the emission spectrum of a fluorophore, the donor or quencher, overlaps with the excitation spectrum of another one, the acceptor or reporter. QDs have been recently reported as efficient FRET donors when coupled with a variety of acceptors such as organic fluorophores, as well as with other QDs or metallic nanoparticles. QD FRET potential has been tested *in vitro* and is likely to find widespread *in vivo* applications (Jaiswal *et al.*, 2004). Lim *et al.* (2008) demonstrated the efficiency of a QD-organic dye FRET system that provided mechanistic insight into the process of non-viral vector based gene delivery by tracking the intracellular modifications of the DNA.

An interesting application of FRET using a QD-based sensor has been demonstrated where the spatial reorganisation of the donor–acceptor pair in order to initiate the switching is not required. Sensing applications use QD properties to create an ‘‘on/off’’ switching capability via FRET mechanism. Instead, a photoactivated/deactivated acceptor is utilised. Advances in the design of these types of integrated devices, which incorporate an emission unit with a quenching unit that can be modulated by a biological stimulus, could lead to the creation of powerful and compact sensors (Mattoussi *et al.*, 2004). QDs are also particularly attractive for biosensor applications due to their long-term photostability allowing real-time and continuous monitoring. Goldman *et al.* (2002) demonstrated a working prototype of QD-based sensor, with the QD acting as the energy donor and functioning in sugar detection (Figure 1.8).

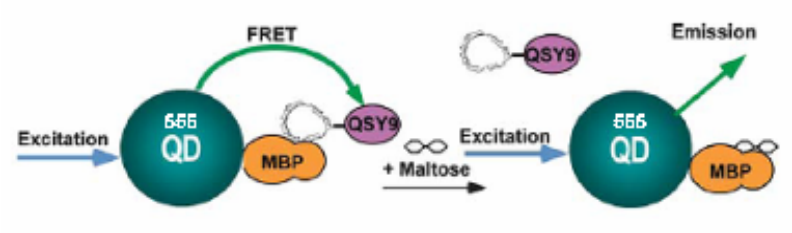

Figure 1.8 Prototype of QD-sensor (adapted from Mattoussi *et al.*, 2004).

555 nm quantum dots (QD) surrounded by 15-20 maltose-binding molecules (MBP). QD-MBP; β – cyclodextrin (CD)-QSY9: absorption max. ~565 nm; the QD-MBP / QSY9-β-CD complex quenches the emission of 555QD; Displacement of β -CD-QSY9 with maltose increase QD emission.

A 555 nm QD donor is conjugated to maltose-binding protein (MBP) that interact with β-cyclodextrin (β-CD), which has been labelled with a QSY-9 quencher. QSY9-labelled β -CD is captured within the centrally located sugar binding pocket of these MBP moieties. The favourable FRET distance between QD centre and QSY9-β–CD is able to induce a maltose concentration dependent quenching of the QD emission in solution format (Figure

1.8). Goldman *et al.* (2002) demonstrated that QDs can be employed as FRET donors for sensitive and specific biosensing.

Several papers published in the past few years suggested that the cytotoxicity of QDs, mediated by UV irradiation might be turned into a technique for killing cancer cells (Bakalova *et al.*, 2004). Tsay *et al.* (2007) presented their initial work on QDs as a novel photosensitiser or at least as a cofactor or components of conventional photosensitising agents used in photodynamic therapy. The group synthesised a peptide coated QD conjugated to a water-soluble photosensitiser, with intact photophysical properties and capable of generating singlet oxygen through oxidation or FRET mechanism. However, the application of QD-photosensitiser for *in vivo* imaging, targeting, and photodynamic needs to be demonstrated.

QDs have many advantages upon conventional dye for biological applications, and especially for *in vitro* bioimaging. Nevertheless, before QDs can find wider uses, several improvements are needed, such as the development of methods for delivery and efficient targeting in cells without altering the QD properties. There is still much left to understand for QDs to become a standard tool in biological applications.

1.2. Quantum dot-encoded microsphere (QDEMs)

Particle-based assays using flow cytometry detection have been used in the 1970s as solid support in suspension assay for the capture of antibodies in immunoassays (Horan and Wheeless Jr, 1977). Since that time, size- and colour-coded microparticles have become an essential analytical tool in biology for biological assays such as DNA identification, protein quantification, immunoassays, cell sorting and so forth. As described in the introductory part of this chapter, the need for highly parallel molecular analysis that has arisen with the development of genomics and proteomics has enhanced the research in fluorescent encoding technology to enable high throughput multiplex assays (Nolan and Mandy, 2006). Hence, microspheres of different sizes and encoded with various organic fluorophores have

been developed. Commercialised bead sets have been applied to high throughput suspension and array platform for clinical and research studies.

A new promising multiplex bead-based technology arises with the possibility to encode QDs into spherical polymeric beads with a diameter ranging from 20 nm to 150 microns, depending on the application (Figure 1.10). Different QDs emitting at different wavelengths are pulled together into a bead and illuminated at the same time with a single light source taking advantage of QDs narrow emission bandwidth.

The resulting emission spectrum is a unique spectral 'bar-code' encoded by:

- The QD composition: the nature of and/or the size determine the QD wavelength emission or colour;
- The QD intensity: the intensity is determined by the quantity of each QD's colour.

This combination promises to create hundreds of different spectral codes (Han *et al.*, 2001).

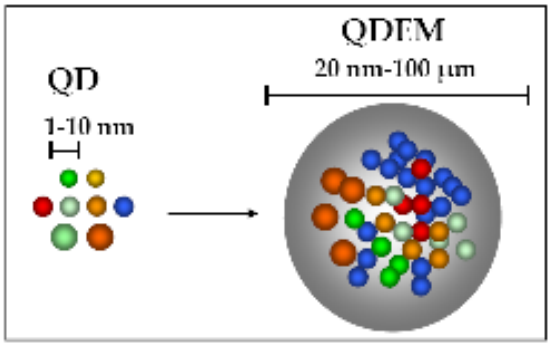

Figure 1.9 Schematic view of QD-encoded microspheres (QDEMs).

QD: quantum dots, QDEM: quantum dot-encoded microspheres. Each colour represents a specific nanocrystal population, size- or composition-tunable with distinct emission wavelengths. The number of identical colour nanocrystals illustrates the ratio of each population present in the microsphere: the intensity of each QD's colour is translated in a signal ratio.

1.2.1. Optical and structural specificities

Figure 1.10 presents the principle of encoded beads with multicolour QDs at predetermined intensity ratios. The colours of the sphere represent the different QD populations emitting at distinct wavelengths. The numbers of coloured spheres (orange, red, green, and blue) illustrate the levels of fluorescence intensity. Theoretically, the use of ten intensity levels (0, 1, 2, 3…) of a single QD emitting at one specific wavelength gives nine unique fluorescent codes since the "0" corresponds to the absence of the QDs. The combination of QDs increases then exponentially with the number of potential fluorescent code: n intensity levels with m QD wavelengths or colours generate (n^m -1) unique codes, where the "-1" correspond to the 0 intensity beads or non-encoded beads (or blank beads). The fluorescence intensity and specificity can be measured with multiple detector channel instruments (such as a flow cytometer, or a confocal microscopy). Figure 1.10 shows QD-doped particles with two and three colours with different codes: (3:3) (3:2), and (3:2:1) which are distinguished by both absolute intensities and relative intensity ratios at different wavelengths.

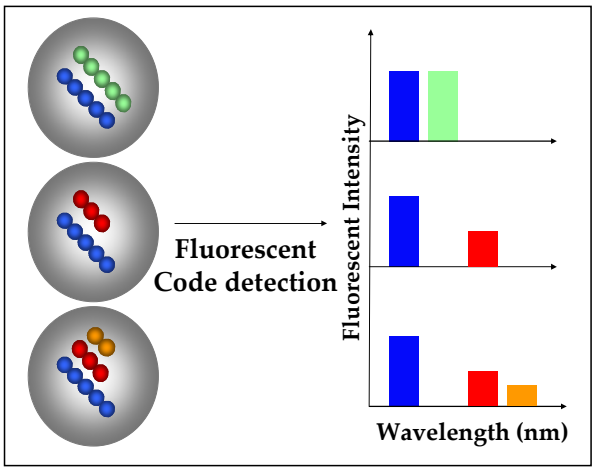

Figure 1.10 Illustration of QDEM encoding optical properties.

The nanocrystal composition (schematic nanospheres) in the microsphere is translated into a fluorescent code encoded in terms of fluorescent wavelength and intensity.

Han *et al.* (2001) described the first synthesis of multicolour optical encoded microspheres with different-sized QDs (core/shell CdSe/ZnS nanocrystals) (Figure 1.11). The preliminary work of Han *et al.* (2001) suggested that the number of fluorescent codes should first be increased by using more colours (Figure 1.11), since coding capabilities can still be limited by: (i) spectral overlap, (ii) fluorescence intensity variations difficult to control, (iii) QDEMs signal-to-noise that are highly dependent on the amount of QDs in the bead, on the optical properties of the different QDs and on the response of the measurement instrument to the emission wavelengths (Han *et al.*, 2001).

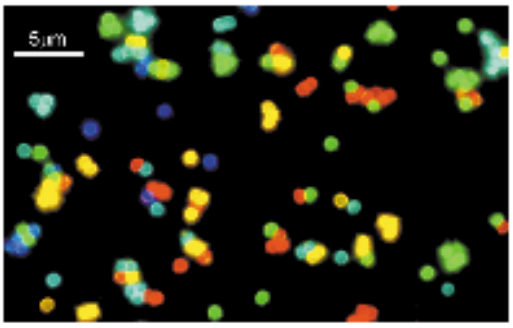

Figure 1.11 True-colour fluorescent micrograph of single colour CdSe/ZnS QDEMs (adapted from Han *et al.*, 2001).

Mixture composed of 484, 508, 547, 575, and 611 nm QDEMs. Observations on a glass surface, obtained with true-colour digital camera and a single light source (Han *et al.*, 2001).

1.2.2. Current synthesis strategies

Different groups have recently published various methods for QD-doped particles synthesis. Six methods have been reported thus far. The first method (1) consists of the diffusion of QDs into polystyrene microspheres by solvent swelling of the microbeads (Han *et al.*, 2001; Gao and Nie, 2004); (2) the second uses a layer-by-layer (LBL) strategy to deposit layers of charged QDs on the oppositely charged coating of the microsphere (Wang

and Tan, 2006); (3) the third one implies the growing of a silica protective shell incorporating QDs around preformed core silica microsphere (Chan *et al.*, 2004); (4) the fourth method synthesises QD-encoded polystyrene microbeads by a modified suspension polymerisation method (Li *et al.*, 2005); (5) the fifth approach is described as being an *in situ* encapsulation of QDs into polystyrene microspheres by using chemical bound of functionalised oligomeric phosphine ligands (Sheng *et al.*, 2006); (6) the last original method depicts a spray-dryness and thermal denaturation strategy to synthesise bovine serum albumin (BSA)-encoded microspheres (Chu *et al.*, 2006).

The first two methods have been shown to have biological applications for DNA genotyping by coupling the QD-doped particles to specific oligonucleotides. QD-doped microspheres from the third method have been applied to *in vivo* imaging. Crucial data are still needed for a relevant characterisation of QD-encoded bead obtained with suspension polymerisation (fourth method). Therefore no conclusion could be drawn on their utility for biological application. The BSA-QD microspheres synthesised with the sixth method also require better characterisation. In addition, without thermal denaturation following spray-dryness step, microspheres dissolve in solution: the microspheres are broken and QD leach out (method 6).

Sheng *et al.* (2006), initiators of the fifth method , affirm, without showing any data, that their beads are stable after high-frequency sonication, solvent exchange and long term storage. In addition this group mentioned that QD-doped particles synthesised with the first and second may not be stable when the chemical environment is changed and that QD may leach out of the microsphere under certain conditions (Sheng *et al.*, 2006). Chan (2004) mentioned the same phenomenon (method 3), which suggested that sonication and washes in polar or non-polar solvents could result in a loss of QDs (Chan *et al.*, 2004). The observed phenomena were not presented in the literature (method 1, 2, and 3).

Encoding procedures are still under optimisation and no unanimous methodology has yet emerged. Nevertheless, as previously described, QDEMs can be functionalised and molecular probes can be attached to the bead surface for biological binding and recognition functionalities as DNA–DNA hybridisation, antibody–antigen/ligand–receptor interactions, and/or streptavidin-biotin interactions (Gao and Nie, 2004; Riegler *et al.*, 2006; Wang *et al.*, 2007). Proof-of-principle work has been reported to demonstrate the interests of QDEMs for life science applications.

1.2.3. Applications and potentials of QDEMs technology

A wide range of microsphere surface coating permits the conjugation of the beads to various classes of biomolecules or ligands for bioassays. As a consequence, the entire assay is concentrated on the surface of the micro-sized spheres, which eases the detection of the signal and has been shown to enhance the sensitivity of detections. The detection signal is also exponentially amplified thanks to the increased binding surface area of the sphere compare with the QD bioconjugate surface (Salas *et al.*, 2008).

Another advantage of QDEMs technology is the flexibility and potential cost-effectiveness of the experimental design. First, a smaller amount of beads should be required per assay due to QDEMs brightness and enhanced emission signal intensity. Secondly, QDEM bioconjugation versatility could expand the range of applications of a unique set of QDEMs. The new technology of QDEMs promise novel properties for applied research that has been demonstrated in various assays as immunodetection, *in vivo* imaging, electro- and optical- sensing, and DNA hybridisation assays (Ma *et al.*, 2007; Suppl *et al.*, 2008).

QDEM bioconjugated to mouse antibodies were used for immunofluorescent detection of p-glycoprotein and showed higher detection limit in fluorescent microscopy with the detection of a single antigen molecule. The work reported by Stsiapura *et al.* (2004) allowed the reconstruction of the 3-dimensional distribution of the antigen in the cells using confocal microscopy. Ma *et al.* (2007) used four different QDEMs (designed with 2

colours, 3 intensity levels) to detect antigens in fluoro-immunoassays with a novel microfluidic on-chip detection device. Multicolour *in vivo* imaging was demonstrated with the illumination of 3 colour QDEMs (0.5 μm) in the same mouse (Gao and Nie, 2004). These results suggested new developments in cancer diagnosis with the simultaneous imaging of multiple biomarkers.

Wilson *et al.* (2007) demonstrated the advantage of QDEMs in multiplexed immunoassays with the detection of individual and mixtures of explosives. Three different types of explosives were specifically detected in suspension in the same sample, with three sets of QDEMs encoded with different spectral codes (Wilson *et al.*, 2007).

Silica microbeads embedded with QDs and iron oxide nanocrystals with magnetic separation properties promise novel platforms for biosensing and analytical detections (Sathe *et al.*, 2006). Guo *et al.* (2006) incubated animal cells with multifunctional luminescent/magnetic QDEMs and obtained micro-loaded cells via an undamaged endocytosis process. This work illustrates the potential of multifunctional QDEMs for fluorescent tracing and cytosolic delivery in targeted cells (Guo *et al.*, 2006).

Further, QDEMs present optical coding properties for electrical identification. Specific electrochemical signatures can be produced by encapsulating ZnS, PbS, CdS, InAs and GaAs QDs in polystyrene microspheres (Wang *et al.*, 2003). QDEMs electrochemical authenticity provides a useful tool for easy-to-use stripping analysers. The electrochemical test to identify a commercial product schematised in Figure 1.12 consists of: (A) casting QD-encoded particles identification layer on the packaging of a commercial product, (B) its rapid dissolution, (C) quantification of metal constituents with voltammetric stripping, (D) obtaining stripping peaks of metal related to the encoded QDs.

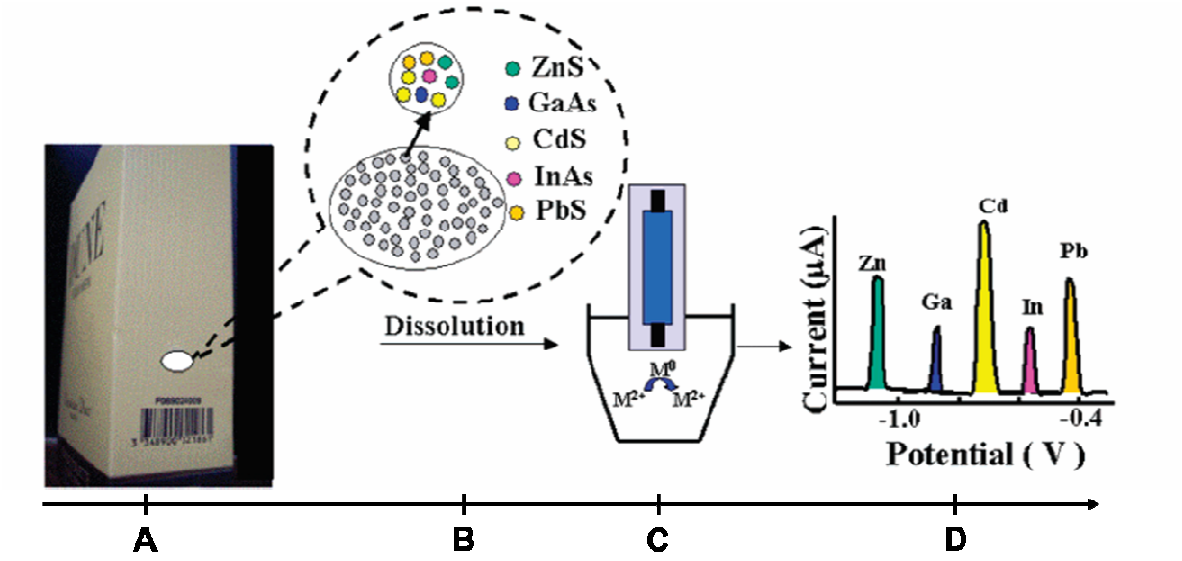

Figure 1.12 Schematic representation of the electrochemical application of the bar-coding system based on QDEM (adapted from Wang *et al.*, 2003).

The application of QDEMs to optical ion sensing was reported by Xu *et al.* (2007). QDEMs used in ion sensing were prepared by simultaneous doping of sodium ionophore X, chromoionophore II, a lipophilic tetraphenylborate cation exchanger, and TOPO capped core/shell 610 nm CdSe/CdS QDs and 700 nm CdTe/CdS QDs as fluorescent label. The ion exchangers measured the apparent charge of the QDs in the encoded microspheres for sodium ion-sensing. The sodium response of the QDEMs was recorded in a solution of magnesium acetate buffers and the full protonation and deprotonation of the QDEMs was observed. The modified QDEMs-sodium sensing showed satisfactory sodium response with satisfying selectivity (Xu and Bakker, 2007). This work illustrates the potential of QDEM for multiplexed sensing analysis systems using the QDEMs bar-code technology (Ma *et al.*, 2007).

Han *et al.* (2001) first reported the application of QDEMs in DNA assays. Later, Xu *et al.* (2003) presented a single nucleotide polymorphism (SNP) genotyping method using QD-encoded mesoporous microspheres (Qbead™ system). The quality of QDEM fluorescent code was individually tested to assure appropriate activity on a per-code basis, as opposed

to on a per-chip or per-slide basis. An allele-specific oligonucleotide assay was developed to genotype five SNPs at a time. An inorganic reporter dye (Streptavidin–phycoerythrin (PE)–Cy5 conjugate) was used to detect the complex formed by the hybridisation of the targeted DNA and the specific QDEM fluorescent probes. Flow cytometry instrumentation was used for fluorescent code detection. The Qbead™ genotyping platform is believed to have promising high throughput applications (Xu *et al.*, 2003; Gao and Nie, 2004).

Eastman *et al.* (2006) presented a nanobarcode gene expression monitoring system for multiplexed gene expression analysis, adaptable to potential miniaturised space applications. A combination of four different sizes of QDs (or different colour) in combination with 12 intensity levels for each of the QD gives a possibility of 20,736 nanobarcoded magnetic beads. Approximately 200 beads were selected and manufactured for the analysis of approximately 100 gene expressions. QDs were encoded in paramagnetic microspheres and each had a specific ratio of four colours providing a unique spectral code. The transcript-specific oligonucleotide probes were conjugated to the beads. Each barcode which detected a specific transcript was then hybridised with the biotinylated cRNA of the sample analysed. The complex was identified with 665 nm streptavidin QDs fluorescent reporters which allowed the quantification of the hybridised transcript. The magnetic bead were then captured at the bottom of the well and scanned for gene expression variation analysis by quantification of 665 nm fluorescent levels This bead system requires specific detection instruments and software to identify the bead codes corresponding to each gene targeted and to quantify the amount of target hybridised to each bead (the Mosaic Q1000 Scanner, Quantum Dot Corp, CA, USA). Authors claim the superiority of the system above classic microarray platforms (Eastman *et al.*, 2006; Ruan *et al.*, 2007).

The identification of close homologues in gene profiling experiments could be improved with QDs technology. Homologous targets could be accurately and confidently distinguished by adding several different probes for the same target with the optimal cost-time-accuracy ratios on a case-by-case basis. As a conclusion, QDs and QDEMs offer the potential to improve and facilitate multiplexed genotyping assays.

1.3. Genotyping platform technology

All human cells, other than mature red blood cells, possess a nucleus which contains the genetic material or DNA molecule. DNA molecules are enclosed within chromosome structures. The DNA molecule encoding the human genetic information is formed by two strands of nucleotides (Watson and Crick, 1953). The DNA sequence is composed of four units, the four bases adenine (A), thymine (T), cytosine (C), and guanine (G). The strands are linked upon specific hydrogen bonding between bases as base pairs (bp): guanine to cytosine, and adenine to thymine. Each individual possesses its own genetic complement, coming from its ancestry.

There are twenty-four different human chromosomes: 22 autosomal chromosomes (identified by a specific number) and 2 sex chromosomes, the X and the Y. Humans are diploid and possess 46 chromosomes per genome, grouped into 23 pairs. A diploid organism therefore carries two copies or alleles of their genetic material. An individual who has two identical copies or alleles of a gene is called homozygous, whereas an individual with two different versions or alleles is called heterozygous for this specific gene. The Y chromosome determines the sex of the individual. The female diploid karyotype found in a healthy cell equals 44 chromosomes (two sets of the 22 chromosomes) and XX. The male equivalent is 44 chromosomes and XY (Schröck *et al.*, 1996).

Ninety percent of the human genome is composed of non-coding DNA regions, which are generally not subject to the pressure of selection. Genetic variations or polymorphisms in these regions are thus mainly transmitted to offspring, increasing the genetic variability in the genome from generation to generation. These regions are useful for inter-individual genetic discrimination (Hurley *et al.*, 2004). A polymorphism is a genetic locus with two or more variants that occur with a frequency (> 1%) in a given population (Lander *et al.*, 2001).

Historically, the restriction fragment length polymorphisms (RFLPs), introduced in the 70's, were the first generation of DNA markers used for genetic mapping. The discrimination between RFLP markers were based on enzymatic digestion. Digested DNA fragments were separated by size and analysed by hybridisation with labelled probes. In the following decade, a new type of DNA variations, the minisatellites or variable number tandem repeats (VNTRs), were mainly used for DNA genotyping. VNTRs presented many alleles and higher heterozygosity than the RFLPs. The heterozygotie is a measure of the genetic variation obtained by the calculation of the frequency of heterozygotes in a population at one locus. Minisatellites were, therefore, more informative for genetic mapping. VNTRs consist of a short sequence of DNA (20-50 nucleotides) which is repeated a variable number of times. They are not uniformly distributed over the genome and are preferentially found at telomeres and in the hypervariable regions of the chromosome. The first "DNA fingerprint" was established based on VNTR analysis by Alec Jeffreys (1985) and was considered as the first forensic tool for DNA genotyping identification.

However, the techniques used for the genotyping of DNA variations were time-consuming, costly and required a large amount of DNA material (Botstein *et al.*, 1980). With the introduction of the polymerase chain reaction in 1986 (Mullis *et al.*, 1986), a new type of genotyping techniques were available for high throughput analysis. The latest generation of genetic markers, short tandem repeats (STRs) and single nucleotide polymorphisms (SNPs), replaced the other type of markers for biological genotyping applications. The development of massive parallel genotyping technologies started with the SNPs and genome mapping. The following review focuses on SNP, the genetic markers mostly used in genomics and other high throughput biological applications.

1.3.1. Single nucleotide polymorphisms: genetic markers for high throughput genotyping

As suggested by the acronym, a SNP marker is a single base change in the DNA sequence with usually two possible alternative nucleotides being substituted at a given position (Figure 1.13A). SNPs are therefore bi-allelic markers. Typically, any two sections of the human genome differ from one another by approximately 0.1% of nucleotide sites which correspond to one variant per 1,000 bases, on average, along the DNA sequence (Brookes, 1999). SNPs are therefore the simplest and the most abundant form of genetic polymorphism in the human genome, accounting for 90% of all human DNA polymorphisms. Around 4 million SNPs have been validated as polymorphic in at least one of the major population groups (InternationalHapMapConsortium, 2003).

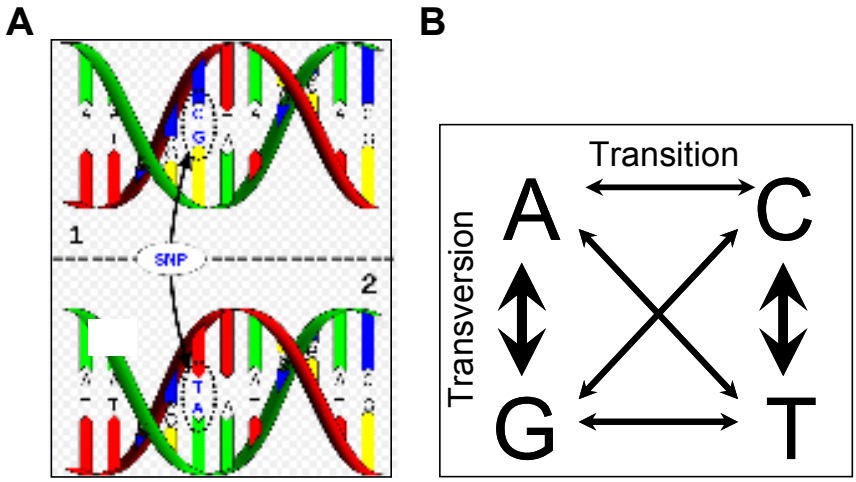

Figure 1.13 Schematic representation of a C/T SNP variation on a DNA molecule (A), and SNP nucleotide base substitution possible mechanisms (B) (adapted from D. Hall, 2007).

A: SNP: single nucleotide polymorphism; dsDNA: double-strand DNA. DNA molecule 1 differs from DNA molecule 2 at a single base-pair location, showing a C/T SNP. A: adenine, C: cytosine, T: thymine, G: guanine, bases of the DNA. **B**: Large arrows indicate transversion processes, whereas slim arrows indicate transition processes.

Two types of nucleotide base substitutions result in a SNP: (1) a transition substitution occurs between the purine bases (A and G) or between pyrimidine bases (C and T). This category represents around two-thirds of all SNPs, and (2) a transversion substitution occurs between a purine and a pyrimidine base (Figure 1.13B). Base pair 'indel' (insertion/ deletion) occurs by a different mechanism that the base substitution of SNPs. They are nevertheless commonly considered as a single mutation source of polymorphism in the human genome and they can be closely physically associated to SNP mutation (Longman-Jacobsen *et al.*, 2003).

SNPs are not uniformly distributed over the human genome; they are three times more frequent in non-coding regions than in coding regions. The sequence variations are, for instance, much lower for the sex chromosome. They are also not uniformly distributed over a chromosome. As an example, the sequence that encodes proteins, which present antigens to the immune system in the chromosome 6, displays a very high number of SNPs compared with other chromosomal regions (Horton *et al.*, 1998).

In coding regions, SNPs are of particular interest as they can induce two different effects on the expressed protein. Synonymous mutation occurs when the substitution of one base causes no amino acid change in the protein. This mechanism is also called a silent mutation where the phenotype stays unchanged. Non-synonymous mutation appears when the substitution results in the alteration of an encoded amino acid. A mis-sense mutation changes the protein by causing a change in a codon sequence. As an example, a non-sense mutation can result in a misplaced termination codon, stopping or preventing the protein synthesis. In one half of all coding sequences, SNPs conduct to non-synonymous codon changes. SNPs can also occur in genetic regulatory regions, and can thus change the amount or timing of a protein's production. Such SNPs are much more difficult to identify and to study (Brookes, 1999).

SNPs are validated as informative if they are genetically conserved, phenotypically not expressed, and represented at high frequencies in populations. The mapping of the human genome saw the development of a haplotype map (InternationalHapMapConsortium, 2005). By definition, haplotypes are sets of closely linked polymorphic genetic markers present on

the same DNA molecule. The 'HapMap' project lead by the HapMap Consortium, an association of international scientists and sequencing centres, is expected to provide useful information on human SNP variability and to be an essential resource to researchers for the discovery of genes and genetic variations that affect health, disease and responses to drugs and environmental factors. The identification of a minimal number of SNPs of interest could be related to a particular important gene in the metabolism for example. Another application of this project is to define relevant SNPs in the different regions of the human genome that will be sufficiently informative to predict insight about the common SNPs remaining in that particular region, using the property of SNPs to be strongly associated between each other (*i.e.,* genetic linkage disequilibrium). Consequently, the number of SNPs required to define haplotypes in a particular region could be restrained to a few numbers of this informative 'Tag' SNPs (InternationalHapMapConsortium, 2003).

In the medical field, because of their abundance, SNPs are the markers of choice for candidate gene association studies to identify genes involve in complex disorders. Asthma is a complex disease which involves genetic and environmental factors. A linkage refinement analysis using SNP genotyping on predicted loci linked with asthma-related phenotype concluded to a strong association between high-risk of asthma susceptibility and a 12.2 megabase (Mb) region of chromosome 2 (Pillai *et al.*, 2006). SNPs can also be used as pharmacogenomic markers for the analysis of individual variable response to drugs. It is now possible to interrogate more than 20,000 SNPs over the entire genome for association studies. Using this approach, a recent study demonstrated a strong statistical association between the major histocompatibility complex allele and clinically diagnosed hypersensitivity to abacavir, an anti-HIV agent, which varied between racial populations. The feasibility of screening population to identify patients who are predisposed to developing hypersensitivity reaction to abacavir, has been demonstrated (Mosteller *et al.*, 2006; Hughes *et al.*, 2008). SNPs have also important specialised applications in forensic sciences: first, as binary markers with a low mutation rates ($2 .10^{-8}$ per base per generation) they can be regarded as a unique events (mutations) in human evolution. Secondly, SNPs permit the reduction of PCR fragment sizes in genotyping assays which has shown its utility for the identification of body parts of

victims from mass disasters, *i.e.*, World Trade Centre (Hand, 2002), but is also crucial for the analysis of degraded samples from sexual assaults or soiled samples (Alonso *et al.*, 2005). Finally, SNPs also help for the definition of haplotypes (or haplogroups) to study male lineage (Jobling and Tyler-Smith, 1995; Brion *et al.*, 2005a).

1.3.2. The principles of current SNP genotyping technologies

Human DNA can be extracted and purified from a number of biological materials such as blood, urine, semen or saliva. Most current methodologies for marker identification begin with a PCR reaction of multiple DNA markers in a single-tube reaction. After this first step, techniques differ by the level of automation and multiplexing (number of markers and/or samples to be analysed simultaneously), the method of detection, and by their sensitivity.

The PCR amplifies or copies targeted DNA sequences, and creates typically >1x 10^6 copies of the template. The method exploits the natural function of the DNA polymerase enzyme which requires a DNA template molecule and two primers (short oligonucleotide sequences of 20-30 bp) which complement and define the target sequence to be copied (Figure 1.14). The targeted double-stranded DNA (dsDNA) is denatured by heating to obtain two single-strands of DNA (ssDNA). Then, the primers are hybridised or annealed to their complementary bases on the ssDNA. During the elongation step the polymerase synthesises a complementary DNA strand (with the four nucleotides available in the reaction mix), and the primers are used to initiate the replication reaction. The result is a new double-strand of DNA composed of one of the original strands assembled with a newly synthesised complementary strand (Figure 1.14). The synthetic cycle is repeated, usually thirty to thirty-five times, resulting in an exponential amplification of the DNA target (Mullis *et al.*, 1986). Multiplex PCR, *i.e.*, where multiple loci are simultaneously amplified in a single reaction, has greatly enhanced DNA genotyping by increasing the information obtained per unit of time, by enhancing the power of discrimination, by also diminishing the effort required to obtain results from multiple loci, and finally by reducing the amount of template consumed per profile (Henegariu *et al.*, 1997). The recent progress made in the area of SNPs multiplex PCR

amplification with a 35-plex on the Y chromosome and a 52-plex autosomal SNP assay (Sanchez *et al.*, 2003; Sanchez *et al.*, 2006) have considerably accelerated SNP genotyping processes.

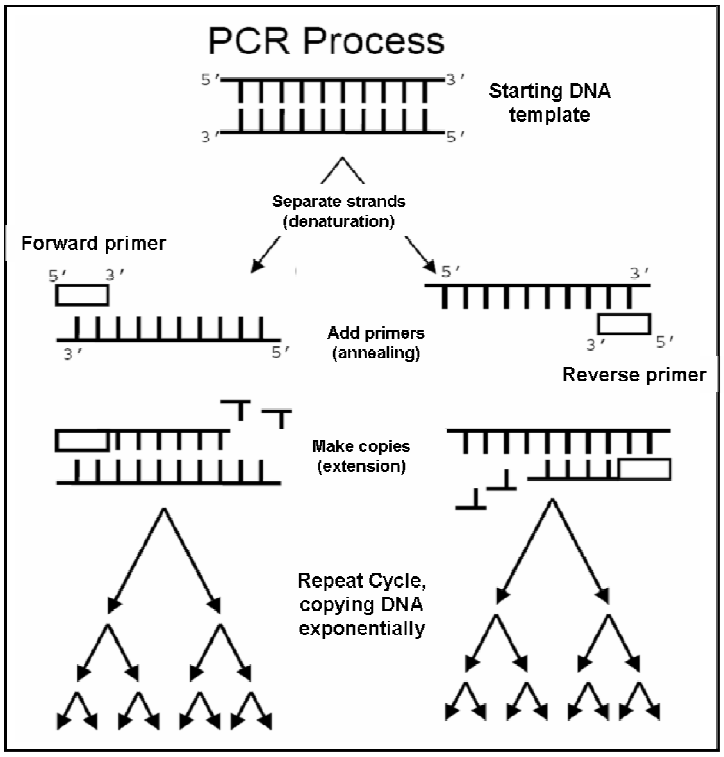

Figure 1.14 The polymerase chain reaction (PCR) (adapted from Butler, 2004).

The genotyping of SNPs relies mainly on the identification of base changes, which offers simpler techniques with higher throughput analysis compared with the methods for multiple-base variation genetic markers. SNP genotyping technologies can be distinguished by the method of allelic discrimination, the assay format, and the methods of detection. The following review presents examples of current SNP genotyping strategies employed mainly in the identification of known SNPs. Genotyping methods are introduced by their allele discrimination strategies. Genotyping assay format, suspension or solid, and the method of allele detections available are detailed in the following chapter section.

The molecular mechanisms for SNP allele discrimination include: allele specific hybridisation (ASO), primer extension (PE), oligonucleotide ligation (OLA), and invasive cleavage (Kim and Misra, 2007).

- **Hybridisation assay**

ASO methods rely on the intrinsic properties of the DNA to form duplex molecules by associating bases to bases in two complementary strands of DNA (Figure 1.15). ASO uses the thermodynamic differences between complete and single mismatch hybridisation. Two allele-specific probes are designed with a sequence complementary to the two SNP alleles. The polymorphic base of the SNP marker is usually positioned in the centre of the probe sequence. DNA hybridisation is performed in the optimal conditions for the probes to anneal only to their corresponding allele

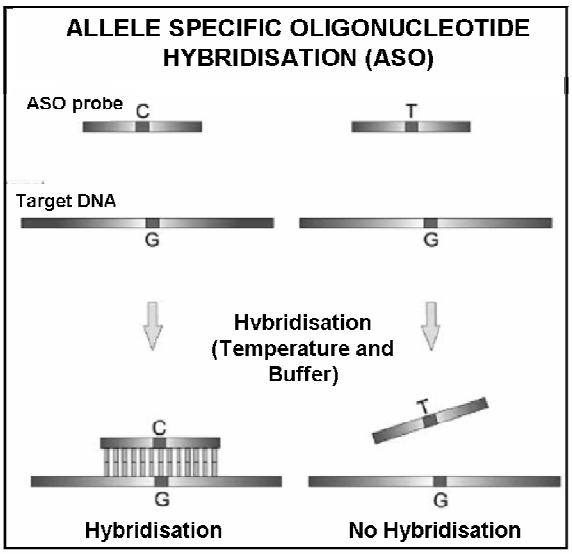

Figure 1.15 Schematic representation of the allelic specific oligonucleotide (ASO) assay (adapted from Sobrino *et al.*, 2005).

- **Primer extension**

PE depends on the DNA polymerase ability to incorporate specific deoxyribonucleotides or bases complementary to the sequence of a template DNA. Figure 1.16 presents the two forms of primer extension methods available: single base extension and allele-specific primer extension.

Single base extension (SBE) is a popular SNP genotyping method since it is adaptable to various detection platforms. The SBE extends a DNA strand or a primer by one base (Figure 1.16A). In the extension step, DNA polymerase extends the primer by the incorporation of a biotin-labelled dideoxynucleotides (ddNTPs). Extension only occurs if the 3' end of the allele specific primer is bound to the homologous allelic sequence. DdNTPs or terminators are used for the reaction because their specific structure prevents the polymerase from incorporating other bases after them, which stops the extension process. Products of SBE reaction generally need to be purified to remove non specific hybridisation and free terminators (Sokolov, 1990). This washing step increases experimental time, but improves the specificity and the success of the experiment. The multiplexing capacity of this approach depends on the technology used for allele detection. Genotypes can be identified using: fluorescent detection platform or molecular weight detection system depending on the experimental design.

Allele specific extension (ASPE) uses the property of the DNA polymerase to extend allele-specific primers only when the 3'end is perfectly complementary to the DNA template (Figure 1.16B). Two primers, one for each SNP allele, are required. The genotype of a sample is determined by the detection of the primers that has formed the extended product. A common reverse primer can also be added to the reaction and allows the amplification of the specific allele in a sample with the matching primers. This variant of ASPE is called allele-specific PCR. Tag-primers can be used to determine each PCR product. The genotype of a sample is thus determined with the detection of fluorescent primer that has formed the product on a microarray or on fluorescent labelled microbeads

which bind tagged primers. A variant of this reaction is using a common reverse primer in association with an allele specific forward primer. The matching specific primer allows the amplification of a specific allele in a sample, and in that case, the reaction is called allele-specific PCR (Newton *et al.*, 1989; Scott Higgins *et al.*, 1997).

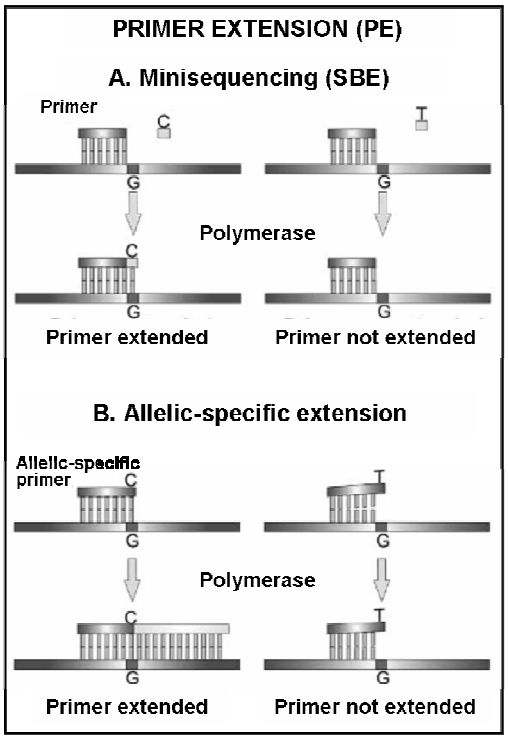

Figure 1.16 Schematic representation primer extension (PE) genotyping reactions (adapted from Sobrino *et al.*, 2005).

A: Minisequencing reaction or single base extension (SBE); **B**: Allele-specific extension.

- **Ligation assay**

The oligo ligation method (OLA) relies on DNA ligase capacity to join the end of oligo sequences annealed next to each other on a template (Figure 1.17A). Ligation products are synthesised only if the oligo sequences are perfectly identical to their templates at the ligation site. SNP can be genotyped by the detection of the ligation products formation for

the targeted SNP. Most experiments design allele-specific probes on the 3' and one common probe on the 5' end because DNA ligase discriminates mismatches on the 3' end with higher sensitivity. Thermostable DNA ligases are preferentially used as repeated thermal cycles produce linear increases of the ligation products. OLA methods were developed for SNP genotyping on genomic DNA (gDNA) and PCR products (Chen *et al.*, 2000). The differences between the methods depend on: the type of primers or probes, and the type of support used.

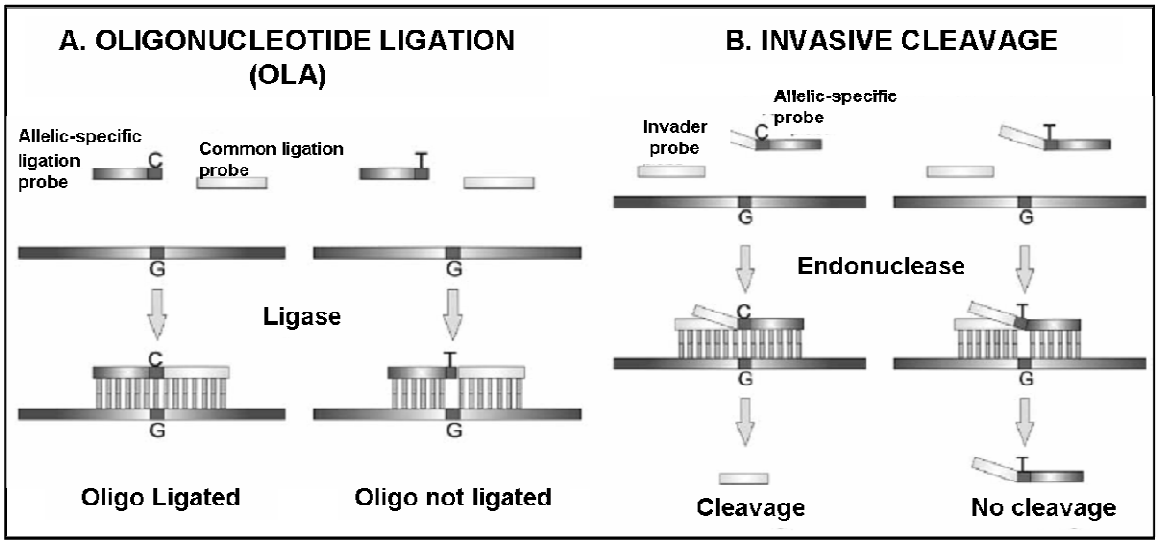

Figure 1.17 General diagram of oligonucleotide ligation assay (A) and invasive cleavage reaction (B) (adapted from Sobrino *et al.*, 2005).

The invasive cleavage assay relies on the Flap endonuclease's (FENs) property to remove the redundant portions (flap) from the 5' end of a downstream DNA fragment overlapping an upstream (invader) DNA fragment (Figure 1.17B). An invader oligonucleotide is therefore designed with a 3' end before the polymorphic site of the targeted SNP. Two allele-specific SNP signal probes are designed which overlap the polymorphic SNP site. After the slight change of location of the signal probes by the invader probe, the FEN cleaves only the perfectly matched allele specific signal probes (Lyamichev *et al.*, 1999).

1.3.3. Methods of detection and commercialised applications

The genotyping methods can be classified following two categories of assay format: the suspension format for reactions occurring in solution, and the solid format for reactions happening on a solid support (glass, slide, chip, and bead-chip). Detection technologies and instrumentations are adapted to the detection approach and the assay format. The products of the reactions that discriminate the SNP alleles are analysed for allele differentiation through three main detection methods: fluorescence technology, chemiluminescence reactions and molecular mass-based method.

- **Fluorescence-based detection method**

Fluorescent signal-based detection method has been the method of choice of the initial studies on SNPs and the high throughput sequence identifications (Lander *et al.*, 2001) because its execution is simple and fast with high sensitivity (Kim and Misra, 2007). A ladder of fluorescent extended-products is obtained with ddNTPs labelled with different fluorescent dyes and a Sanger sequencing reaction (Sanger *et al.*, 1977).

Fluorescent resonance energy transfer (FRET) is the fluorescent detection method mostly used with wide application in genotyping assays. FRET is a physical phenomenon happening when fluorescent group of dyes are in close proximity to one another and when the emission spectrum of a fluorophore, the donor or quencher, overlaps with the excitation spectrum of another one, the acceptor or reporter. In close proximity the fluorophore donor quenches the reporter dye and both fluorophores are "switch-off". As soon as the donor and acceptor are separated they can emit light when excited with the appropriate wavelength (Clegg, 1992). In most applications, the donor and acceptor dyes are different, in which case FRET is detected by the appearance of the acceptor fluorescence or by the quenching of the donor fluorescence. Oligo probe can be synthesised with a reporter dye and a quencher.

Commercialised FRET probes include the Taqman® probe assay (Applied Biosystem, CA, USA) and the molecular beacon probes which hold a hairpin-loop conformation (Figure 1.18). FRET is a popular mechanism for homogeneous genotyping assay (*i.e.,* one uniform format, generally liquid in tube, from the start to the end of the experiment) (Tyagi *et al.*, 1998; Myakishev *et al.*, 2001). For both FRET probes the hybridisation to a specific target will determine the switch "on/off" event of the probe.

The TaqMan® probe (Applied Biosystem) hybridises during the polymerisation step of the PCR reaction. During the elongation step, the 5'nuclease activity of the DNA polymerase cuts off the 5'end of the probe, which releases the reporter dye from the quencher. The reporter therefore, emits fluorescence directly proportional to the number of PCR product produced (Grove, 1999).

The molecular beacon probes hold a hairpin-loop conformation when it is not hybridised, and in this conformation the fluorescence of the reporter organic dyes is turned off by the adjacent quencher. When the beacon hybridises to a perfectly complementary target, the fluorophore is freed from the quencher and able to emit fluorescence (Figure 1.18) (Pierce *et al.*, 2000).

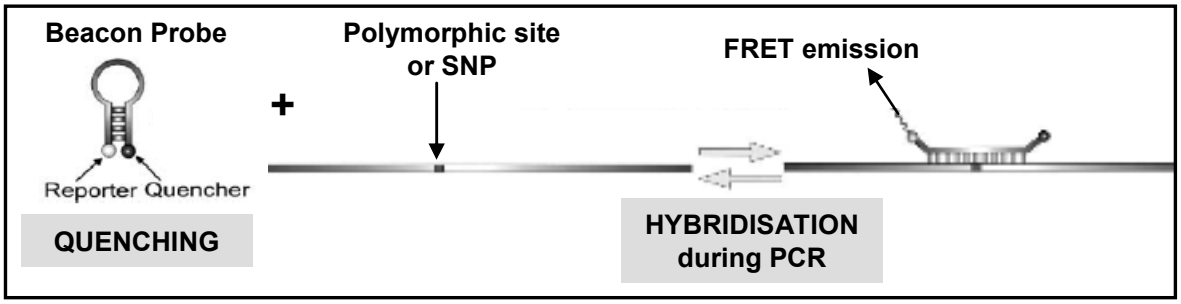

Figure 1.18 FRET and molecular beacons mechanism overview (adapted from Sobrino *et al.*, 2005).

Fluorescent technology can been applied to both solid and liquid format support and combined with different allele-specific methods. FRET probes are usually applied to ASO assays, allele specific PE, and invasive cleavage reactions (Invader® assay, Third Wave Technologies Inc., Madison, WI, USA). The fluorescence released by FRET probes can be measured with real-time PCR instruments, which allows the quantification of the DNA template amplified. However, real-time PCR reactions are limited by the number of fluorophores which can be used in a single experiment and efficiently detected (Brion *et al.*, 2005b).

- **Chemiluminescence-based detection method**

Chemiluminescence-based detection has been applied for SNP genotyping using a cascade of enzymatic reactions known as Pyrosequencing™ (Biotage, Sweden) with primer extension reaction. When the DNA polymerase incorporates a dNTP onto the SNP primer it produces a by-product, a pyrophosphate. This pyrophosphate is used in Pyrosequencing™ to trigger an enzymatic cascade (ATP sulfurylase, luciferase), which will produce a detectable luminescent signal. The four dNTP are added one by one in a specific order. When the appropriate dNTP is incorporated, the enzymatic reaction proceeds and generates light. If the added nucleotide is not incorporated, no light is produced. Pyrosequencing™ is a real-time luminescence detection method that can sequence a 20-30 bp DNA target in about 20 min (Alderborn *et al.*, 2000). Chemiluminescence provides high signal-to-noise, rapid detection, and automation, but this approach is limited in terms of multiplexing capacity, since real-time PCR limits the number of simultaneous colour detections.

- **Mass-based detection method**

Mass-detection method uses matrix assisted laser desorption/ionisation time-of-flight (MALDI-TOF) or mass spectrometry (MS) platforms for the mass analysis of biomolecules such as oligonucleotides (Karas *et al.*, 1990; Schram, 1990; Little *et al.*, 1994). It is the most direct method compared with the other fluorescence detection methods as it measures

the molecular weight (M.W. in Dalton Da) of the products of the allele-specific detection method. Several commercialised products have been developed in association with different allele-specific method. The PROBE assay (MWG Biotech, Ebersberg, Germany) combines the use of ddNTP and dNTP in a SBE reaction, whereas The MassEXTEND™ (Sequenom, San Diego, CA, USA) approach uses SBE or ASPE for SNP genotyping. The high resolution of MS enables to distinguish which ddNTP has been incorporated in the primer sequence extension.

MS detection can be quantitative and appears to be one of the best technologies for allele frequencies estimation. However, despite its high resolution it is still difficult to distinguish between A/T A/A T/T. The modified PinPoint assay (Applied Biosystem, CA, USA) uses mass-tagged ddNTP with primer extension to overcome this limitation by increasing the mass difference between extension products of SNP alleles. Another potential limitation of MS detection is the necessity of purification steps, as the MALDI-TOF assay is very sensitive to sample impurities. If the products have non-overlapping mass, the assay can be multiplexed. High throughput genotyping assay can also be achieved by adding a non-human "tail" sequence at the 5' end of the primer, as for the SNaPshot reaction. A twelve-plex has been described by Ross *et al.* (1998). Further, rapid detection by MALDI-TOF MS combined with reaction miniaturisation in a chip-based PE was reported to enhance the throughput of mass detection genotyping method while decreasing the cost (Tang *et al.*, 1999).

- **Assay format and high throughput genotyping platforms**

The most popular commercialised assays employ mainly flow cytometer and imaging systems (*i.e.*, fluorescent plate reader, microarray scanner) and capillary electrophoresis instruments as detection platforms, which implies that the genotyping methods can be performed in two types of formats (*i.e.,* in suspension or on solid surface). A selection of the most employed commercialised platforms is presented in detail.

Flow cytometry (FC) instrumentation used for bead-based suspension platforms, measures and analyses the physical characteristics of single particles as they flow in a fluid stream excited by a laser or any other excitation light source. The physical properties measured include the relative particles size, the granularity (internal complexity), and the relative fluorescence intensity. When a particle associated with fluorochromes is excited, it releases light which presents specific spectral properties. Scattered and emitted light from particles is converted to electrical pulses by optical detectors to produce digital signals. Common systems can have more than one source of excitation light and a range of three to eight detection channels (Simmer, 2008). Microspheres generally composed of polystyrene and silica materials have been used for biodiagnostic assays. Microsphere surface coating permits the conjugation of the beads to various classes of biomolecules and in particular to DNA molecules. Bead-based assays have been developed for SNP genotyping in suspension and in solid format (Kellar and Iannone, 2002; Oliphant *et al.*, 2002). ASO bead-based assays were the first bead-based SNP genotyping assays to be developed (Figure 1.19) (Authier *et al.*, 2001). Typically, a SNP allelic probe is attached on a bead surface, and a DNA heteroduplex is formed when the probe hybridises to its specific target. A reporter dye binds the PCR product or fluorescent PCR products are produced. The heteroduplex will therefore exhibit a unique spectral print composed of the microsphere fluorescent code and the PCR product fluorescent signal. SNP genotyping bead-based assay in suspension and solid format requires respectively flow cytometry and plate reader or scanner instrumentation, with one or multiple laser excitation and with multicolour emission detector channels.

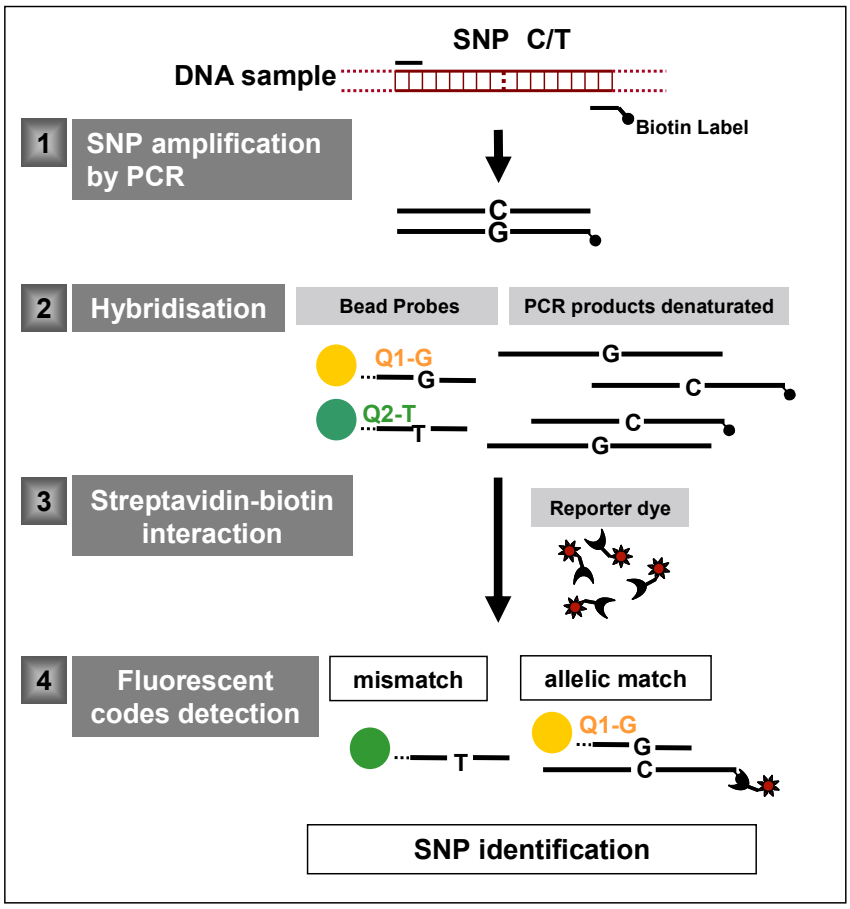

Figure 1.19 Schematic of the general principle of ASO bead-based assay.

Four main steps are involved in the bead-based assay **1**: selection of SNP markers and amplification of the DNA target with biotinylated primers; **2**: design of the fluorescent probe, heat-denaturation of the PCR products and hybridisation of the probes to the denaturated biotinylated PCR products; **3**: addition of the fluorescent reporter dye linked to a streptavidin and interaction with the complex [biotinylated target fluorescent probe]; **4**: detection of the fluorescent signals in the suspension. Each probe has a unique fluorescent tag. The detection of the reporter dye and the fluorescent probe simultaneously identify which allele has been hybridised.

ASO bead-based assay using inorganic fluorescent microspheres is still under development, whereas a multiplex microsphere-based platform encoded with conventional dye has been developed by Luminex Corp. (TX, USA). The Luminex®xMAP™ system offers the most advanced commercialised microsphere-based suspension array technology applied to SNP genotyping (Wetton *et al.*, 2005). A duo of organic dyes is used to encode a 100 bead library which theoretically permits the rapid identification of 50 SNPs in a single reaction vessel. An organic fluorophore (*R*-phycoerythrin, alexa 532, or cyanine 3) is used as a reporter dye to detect the hybridised product bound to the microspheres. The Luminex®xMAP™ assay requires a specific detection instrument, the Luminex 100 analyser, which functions on the same principles of a flow cytometer instrument (Fulton *et al.*, 1997; Dunbar, 2006).

The SNP stream system (Beckman-Coulter, CA, USA) is a SBE on a solid surface-based method of detection (Figure 1.20A) (Ye *et al.*, 2001). First, it involves the amplification of the targeted SNP. Then, cleaned PCR products are used as a matrix for the SBE reaction with tagged primers specific for each SNP. The SBE product is therefore associated to a specific SNP tag that finally binds to a specific spot or SNP address on a solid support (well, microplate, microbeads, microchips or bead-chips). The instrumentation that detects the fluorescent signals depends on the surface used: fluorescent plate readers are employed for microplates, flow cytometry for microbeads, scanner or other imaging systems for microarrays.

The SNPlex™ assay (Applied Biosystem, CA, USA) combines allele discrimination method with initially the traditional genotyping detection method of capillary electrophoresis (CE) (Figure 1.20B). Traditional gel electrophoresis is adapted to a capillar using polymers in solution to create a molecular strainer also known as replaceable physical gel. CE allows analytes which have similar charge-to-mass ratios to be resolved by size. This technique is commonly employed in the molecular weight analysis of proteins and the sizing of DNA molecules for sequencing and genotyping applications (Karger, 1996; Larsen *et al.*, 2000).

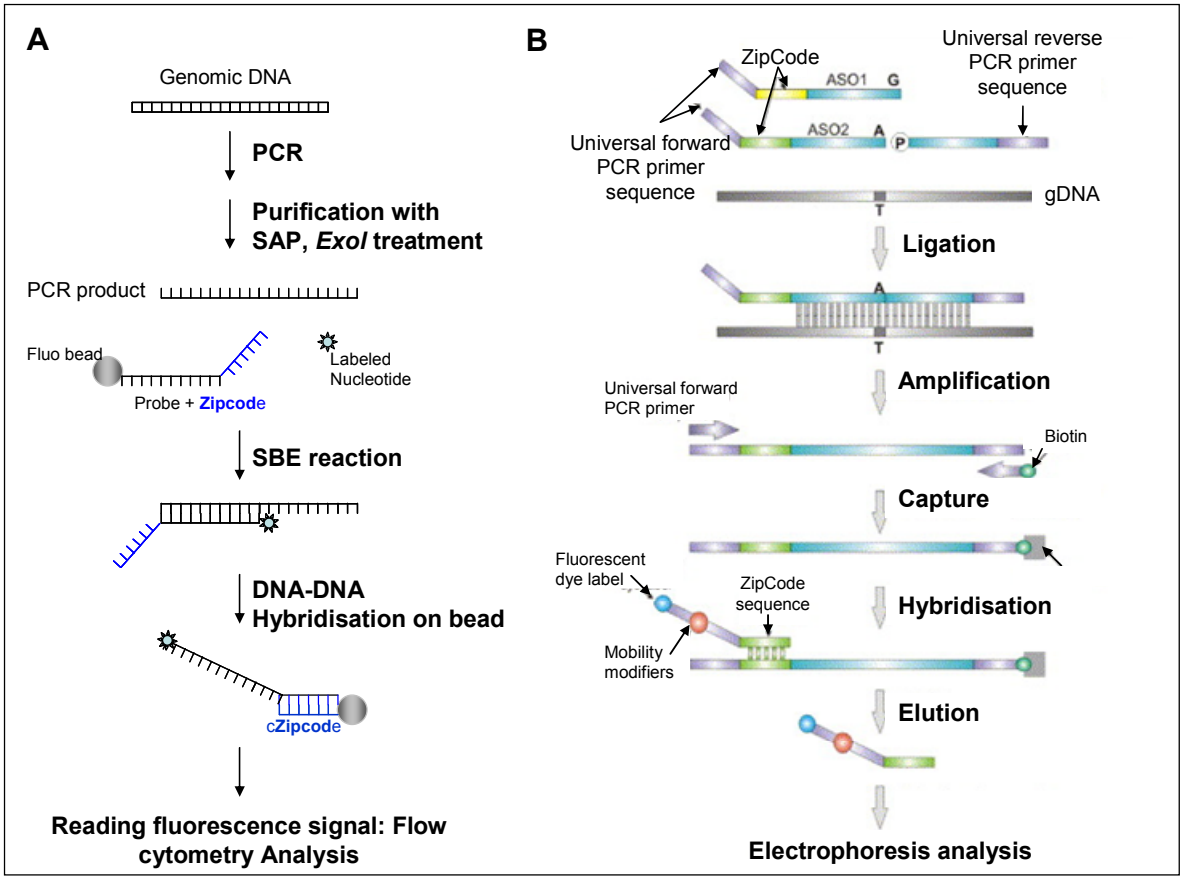

Figure 1.20 Schematic representation of bead-based SBE assay (A) (adapted from Hsu *et al.*, 2001) and the SNPlex™ genotyping system workflow using OLA (B) (adapted from Ballester *et al.*, 2007).

A: DNA sequence (called ZipCode) at the 5'end of the oligonucleotide probe allows the resulting SBE product to hybridise with its complementary sequence (cZipCode) which has been coupled to a specific fluorescent microsphere. The amplified products are treated with shrimp alkaline phosphatase (SAP) and exonuclease I (EXO I) to avoid the participation of the remaining PCR mix products in the subsequent extension reaction. **B**: gDNA: genomic DNA; uni: universal; 3730 DNA analyser (Applied Biosystem, CA, USA) is the method of detection.

The assay has also been adapted to bead-based and FC detection. In both case, the assay requires a common probe (the ligation probe LSO) composed of the specific targeted sequence and a universal PCR primer sequence, and two allelic probes composed of the SNP allelic sequence followed by a ZipCode and universal PCR primer sequence. When an allelic probe is perfectly matching the gDNA of the sample, the ligation product is formed and then amplified thanks to biotinylated universal primers. Biotinylated denaturised PCR products (ssDNA) are bound to a streptavidin-coated plate. A fourth fluorescent probe (ZipChute) identifies universal ZipCode amplified on the allelic probes immobilised on the plate. These ZipChute probes have a unique sequence complementary to a specific portion of the OLA PCR products, and they contain mobility modifiers. After elution, ZipChute probes can be separated by capillary electrophoresis under denaturing conditions with fluorescence detection or identify by FC if attached to fluorescent beads (Kuhn *et al.*, 2004; Tobler *et al.*, 2005). The Goldengate assay from Illumina Inc. (USA) differs from the SNPlex™ by an additional allelic-specific extension step to the ligation reaction.

BeadArray™ (Illumina, CA, USA) is a high throughput SNP genotyping method similar to the SNplex™ that uses ASO and OLA to generate allele specific PCR products. The Illumina BeadArray technology uses either fibre optic bundles or silicon slides as a substrate to embed silica beads covered with DNA probes for allele-product identification (Figure 1.21A). From 384 to 250,000 bead types are pooled and self-assembled in each particular well onto the BeadChip. Microarrays can be assembled on silicon slides that have been processed by micro-electromechanical systems (MEMS) technology to have nanowells which support self assembly of beads. Microbeads chip from Illumina needs a specialised reader instrument which costs more than half a million pounds (Shen *et al.*, 2005). The limitation of this approach arises when a large number of samples are tested as it is difficult to accommodate multiple sample analysis on a single array: it could lead to the misinterpretation of genetic profiles. The generation of large SNP multiplex PCR before hybridisation is another practical limitation of this technology format.

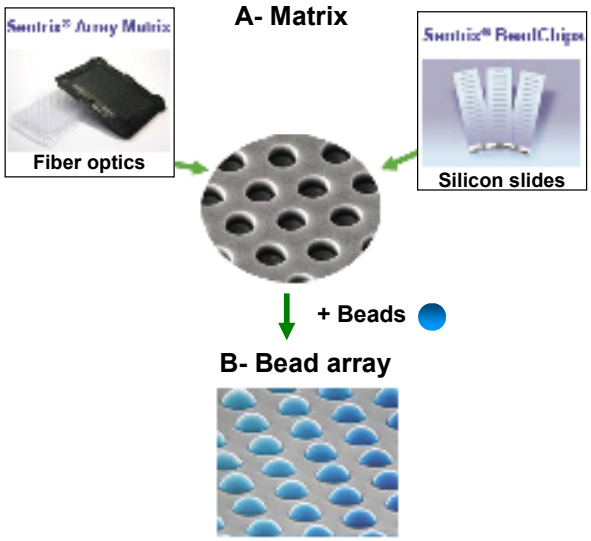

Figure 1.21 The BeadArray™ (adapted from Fan *et al.*, 2005).

The surface of the array is the matrix (A) made of fibre optics or silicon, where beads are embedded at a specific position with a specific code (B) to identify analytes that will specifically bind to each bead fluorescent signature in a multiplex format.

The classic microarray solid support approach utilises a relative small number of samples and large number of SNPs. ASO and SBE assays on solid arrays are achieved with fluorescent PCR products labelled during SNP amplification. On a small area of a solid support (1-1.5 cm^2), hundreds of short specific DNA sequences can be chemically attached as specific spots to create a microarray. On the other side, DNA genotyping on solid arrays with fluorescent detection requires expensive plate reader instrumentation. The GeneChip® system has overcome the difficulty to optimise the simultaneous analysis of thousand of SNPs (Affymetrix, Corp.CA, USA). This system uses tens of ASO probes for each SNP. The arrayed probes contain the two different sequences at the polymorphic site as well as some nucleotides of SNP flanking regions. Light-directed chemistry synthesises specific oligo probes covalently bound at defined locations on the chip (Pease *et al.*, 1994). Unlike flow cytometer, plate reader analyses the fluorescence well by well. A high-intensity lamp passes light to the microtiter well. The light emitted by the reaction happening in the well is then quantified by a detector.

- **Efficiency and limitations of current genotyping assays**

Common technical requirements for SNP genotyping technology involve high level of sensitivity, reliability, reproducibility, capacity of multiplexing, rapidity of analysis and cost per genotype efficiency. On the practical side, requirements can vary from one application to another depending on: (i) the type of DNA samples (low or high content of DNA, cellular or biological origin, degraded or ancient, or purity of the sample) (ii) the SNP markers to be genotyped (autosomal, mitochondrial, or on sexual chromosome) and (iii) the overall goals of the analysis (SNP detection, SNP identification, or Allele frequency investigation) (Kim and Misra, 2007). The overall accuracy and efficiency of SNP genotyping technologies depend on the pre-amplification strategy of the DNA template, the allele discrimination method and the detection format.

Method such as ligation assay can be performed with genomic DNA, which avoids the amplification step. A number of genotyping techniques, however, rely on PCR for target amplification. PCR efficiency and cost is a critical issue for multiplex amplification experiments and large scale sample analysis (Chen and Sullivan, 2003). Further, primer extension methods, unlike hybridisation or ligation assays, require a washing step after the PCR, which adds to the final time and cost of the assay.

Allele discrimination methods that do not interfere with target amplification are an advantage and authorise both experimental step to be performed in a single stage and closed-tube experiment (*e.g.,* ASO, OLA, FRET assays). However, allele discrimination efficiency is variable and depends on the enzyme-like activity specificity and the DNA properties. DNA ligase and endonuclease (OLA, invader assay) have the highest specificity. DNA polymerase synthesis activity can be very specific (SBE) or marginal (ASPE) if long DNA strands have to be synthesised. The hybridisation allele discrimination power is relatively low comparatively to other assays such as ligation (Sobrino *et al.*, 2005).

Most genotyping methods on solid support (*e.g.*, MS, ZipCode assay, Illumina beads arrays, microarray, and electrophoresis) necessitate a clean-up step before allelic products detection to prevent false positive detection and genotyping scoring error. The purification and the separation of allele-specific products from the experimental mix increase time experiment but provide superior detection sensitivity and multiplex capabilities. In contrast, homogeneous detection assays are more amenable to automation but have limited multiplex capacities (*i.e.,* no purification step). The absence of purification of the allele-specific products also increases the potential for false-negative detection. Therefore, these methods require higher optimisation and detection sensitivity to avoid interference with the non specific products of the reaction. (Chen and Sullivan, 2003). The efficiency of SNP genotyping technologies also relies on the speed of the detection method. Electrophoresis experiments can last hours whereas fluorescence intensity (FC instrumentation), absorbance, electric charge or MS method of detections can take less than a second. Automation of sample preparation, and algorithms for automated genotyping scoring can be applied to most of the platforms, but only a limited number of assay can provide quantitative information with allele detection, with limited multiplexing capacities (*e.g.,* MS, pyrosequencing). The level of throughput is limited for allele detection methods using organic dye (*e.g.,* FRET, dyed bead-based assay, pyrosequencing™) (section 1.1.4).

SNP genotyping technologies have rapidly evolved in the last decade, however technologies have not yet proven to fit all the requirements adapted to all biomolecular applications. Technical and practical considerations have to be studied when choosing a technology for a specific application. The development of new genotyping systems is still needed to enhance high throughput with quantitative and rapid information acquisition, and to answer the specific need of SNP genotyping applications (Kim and Misra, 2007).

1.4. Aims and objectives

The development of optimised screening assays continues to be an active area of research in the field of molecular diagnostics. New methodologies and technologies still need to be investigated to take up the challenges of optimising genotyping platforms that comprehensively satisfy the complex criteria involved in DNA marker identification for biomedical applications (Kim *et al.*, 2007). Subsequently, the review of the quantum dots technology presented before (Section 1.1) illustrates the multi-disciplinary potential applications of this innovative fluorescence technology.

The research project presented in this thesis aimed to design a new suspension genotyping platform based on quantum dot-encoded microsphere (QDEM) fluorescence technology and flow cytometry instrumentation. This project was adapted from previous work on bead-based assay and quantum dot-doped particle studies in the biomedical field (Lander *et al.*, 2001; Xu *et al.*, 2003; Dunbar, 2006). The novelty of the project lies in the development of a suspension array technology (SAT) using exclusively inorganic dyes, and in the bioanalytical evaluation of commercialised QD technology.

The aims of the research project were: to characterise and to investigate the properties of the first QDEM commercially available as fluorescent markers for suspension assay technology applications (SAT); to develop a QDEM bioconjugate adapted to high throughput genotyping suspension assays; to explore and develop a novel way to facilitate the optimisation of ASO suspension assay adapted to QDEM technology; and to evaluate the potential of QDEM bioconjugate for single nucleotide polymorphism (SNP) genotyping.

To fulfil these aims, several objectives were defined:

1. To characterise and identify experimental conditions adapted to TriLite™ QDEMs by: the investigation of the reactivity and the sensitivity of the QDEM technology to biomedical experimental conditions, and by the selection of optimal experimental conditions adapted to the QDEM technology.

2. To develop a fast and efficient conjugation method adapted to SAT by: the adaptation of the optimal conditions obtained from the previous investigation on the QDEM material, the study of the different factors influencing the conjugation efficiency, and the selection of optimal conditions for the development of an efficient bioconjugation method.

3. To demonstrate the accuracy, and the sensitivity of the assay using QDEM as fluorescent marker by: the optimisation of QDEM-probe hybridisation to DNA target to improve hybridisation suspension assay sensitivity, the characterisation of QDEM-probe hybridisation reaction with the titration of the SNP PCR products, and the demonstration of the probe specificity with competitive hybridisation experiments using specific and unspecific target.

4. To demonstrate the potential of QDEM-probe's specificity and sensitivity for SNP identification in single and multiplex format by the identification of SNPs using more than two different QDEMs in a single experiment.

Chapter 2

Characterisation of TriLite™ Quantum Dot-Encoded Microspheres

2. CHARACTERISATION OF TriLite™ QUANTUM DOT-ENCODED MICROSPHERES

2.1. Introduction

The use of inorganic fluorophores in bioscience has been described as a technological advance that has had a major impact in the field (Resch-Genger *et al.*, 2008). The initial work of Chan *et al.* (1998) highlighted semiconductor nanocrystal materials or quantum dots (QDs) as new optimum fluorescent dyes due to their unique size-dependent optical and electronic properties. Size-tunable QDs have been successfully applied in biomedicine for *in vivo* and *in vitro* assays, *e.g.*, bioimaging, immunoassays, molecular diagnostics, labelling, and sensing (Dabbousi *et al.*, 1995; Norris *et al.*, 1996; Chan and Nie, 1998; Bailey *et al.*, 2004; Medintz *et al.*, 2005; Derfus *et al.*, 2007). The use of size-tunable QDs was, however, found to be limited. Specific applications, such as *in vivo* imaging, required very small nanocrystals; yet multiplex bioimaging assays need a range of QD sizes to achieve multicolour detection. Size can also be a limitation when incorporating QDs in larger superstructure such as mesoporous microspheres. The multiple requirements, *i.e.*, size and multicolour, for a single assay were addressed with the development of alloy nanocrystals (Chapter 1, section 1.1.1), whose optical properties vary with composition (Swafford *et al.*, 2006). The colour of alloy QDs are tuned while maintaining a small size of particles. The multiplex capabilities of QDs are therefore enhanced by tuning simultaneously the nanocrystals size and composition. Alloy nanocrystals were described with a homogeneous composition or a gradient structure, *i.e.*, different composition of the alloy in different parts of the nanocrystal, depending on their synthesis procedure. Both present significantly different optical properties (Bailey and Nie, 2003). In Chapter 1, QD technologies were reviewed in detail in Chapter 1. The present work focuses on the QD technologies used in this research project and developed by Crystalplex Corporation (Pittsburgh, PA, USA).

Crystalplex (PA, USA) is the only company that was found to develop and commercialise CdS_xSe_{1-x}/ZnS core/shell alloy nanocrystals (TriLite™ crystals) (Figure 2.1). The emission wavelengths of TriLite^{TM} nanocrystals are determined by the relative concentrations of the mixture of the three elements (Cadmium, Cd, sulphur, S, and selenium, Se) of the nanocrystal core illustrated in Figure 2.1. Composition-tunable TriLite™ QDs are synthesised according to Murray's *et al.* (1995) method to obtain gradient alloy nanocrystal. Briefly, CdS_xSe_{1-x} are prepared under cadmium–rich (Cd) condition, a premixed solution of selenium (Se) and sulphur (S) are injected into a solution containing approximately height times more cadmium precursor at high temperature (~300°C) (Bailey and Nie, 2003).

Single CdS_xSe_{1-x}/ZnS core/shell nanocrystals are coated with conventional trioctylphosphine oxide (TOPO) ligand on the surface. TriLite™ alloy nanocrystals are manufactured in a uniform size, ranging from 4 to 5 nm, and with a gradient composition of CdS_xSe_{1-x} determining the wavelength emission. QDs can be produced with emission from 420 nm (stable blue and blue-green colours, wavelength < 525 nm), to 685nm (the far red region of the spectrum, wavelength > 660 nm) with little loss in stability (Figure 1.2). TriLite™ QDs are stable, and have quantum efficiencies of ~45%, with very narrow bandwidths (between 30 – 40 nm across the wavelength range) while keeping very broad excitation bands. All colours can be excited by single light source in the 250 – 480 nm excitation range (Maier *et al.*, 2007). QDs can be functionalised with carboxyl, amine, hydroxyl groups and avidin/streptavidin molecules.

Crystalplex currently provide 10 standard colours of nanocrystals that can be incorporated into acrylic beads (PLxBeads™ and MultiPLxBeads™) leading to customised QD-encoded microspheres (or QDEMs) with one or more colours. QDEMs can be functionalised with carboxyl groups and avidin/streptavidin surface chemistry for coupling to biomolecules. Microsphere sizes range from 1 to 20 μm (Maier *et al.*, 2007).

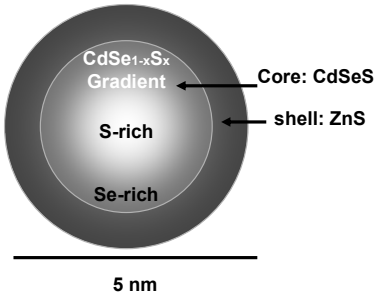

Figure 2.1 Schematic representation of TriLite™ nanocrystals composition.
Cd: cadmium, Se: selenium, S: sulphur, Zn: zinc. S/ Se gradient composition.

QDs are encoded with the method of Han *et al.* (2001). Purchased polystyrene/methacrylate beads, traditionally synthesised by polymerisation of styrene (98% vol/vol), divinylbenzene) (1% vol/vol), and acrylic acid (1% vol/vol). Polymerisation of methacrylate on the polystyrene beads (Tanaka *et al.*, 2000; Han *et al.*, 2001), was used for the incorporation of QDs by swelling the beads in a solvent mixture and by adding a controlled amount of QDs to the mixture (Chapter 1, section 1.2.2.). Further, a zinc-sulphate protective shell is added to the microspheres in order to seal in the QDs. The sealant layer is also added to the blank beads (non encoded beads) to enable relevant comparative studies with encoded beads. Multicolour QDEMs use an adjusted amount of QDs to experimentally compensate for the different optical properties of different coloured dots. The embedding process can be completed within ~30 min at room temperature. Encoded beads are protected with 3-mercaptopropyl trimetroxysilane, which polymerised inside the pores upon addition of a trace amount of water (Han *et al.*, 2001).

The optical specificities of the QDEMs were described as followed: diameter (in μm) ***λe*** gave the emission wavelength (in nm) of the QDs trapped in the microsphere; when the beads were encoded with 2 or 3 different QDs, the emission wavelength of the QDs was indicated in brackets; the intensity ***I*** described the relative intensity of each QD present in the bead compared with the others. The position of the intensity number in the brackets applied to the corresponding emission wavelength at the same position in the brackets. As

an example, a two-colour QDEM (525;575) (2:1) was composed of QDs emitting at 525 nm at the intensity level 2, and of QDs emitting at 575 nm at intensity level 1. Single-colour beads could have also variable relative intensity.

The precise amount of coloured QDs encoded in the microsphere defined the level of intensity. As an example, the 575QDEM of 20 μm diameters were encoded with four different levels of 575QDs intensity. Figure 2.2 illustrates how Crystalplex use nanocrystals to create MultiPLxBeads™ with specific photonic barcodes. Each QDEM is encoded with specific and varying concentrations of different composition-tunable nanocrystals. Large concentrations of a specific colour of nanocrystal create high intensity light. This technique, adapted from Han (Han *et al.*), treats each colour as a placeholder for a digit associated with the intensity of the colour.

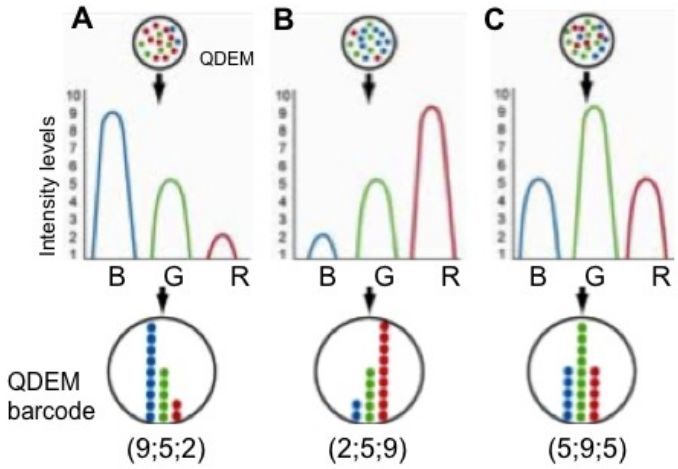

Figure 2.2 Schematic representation of multicolour QDEMs encoded with composition-tunable nanocrystals (adapted from Maier *et al.*, 2007).

A, **B**, **C:** different QDEM barcodes composed of B: blue, G: green, and R: red, coloured QDs.

Standard detection instrumentation with quantitative accuracy and multi-spectral resolution (flow cytometry, or imaging systems with multi detector channels) are required to identify and produce a unique optical signature for each QDEM, which illustrates the precise concentration of each colour within the microspheres. Figure 2.2A shows QDEMs embedded with nanocrystals with a blue intensity level of nine, a green intensity level of five, and a red intensity level of two, producing the code (9:5:2). The number of possible codes can be calculated by the number of available intensity levels (***I***) raised to the power of available colours (**c**), expressed as $\boldsymbol{I}^{\mathbf{C}}$. In the example of Figure 2.2, ten concentrations of three colours enable 10^3 different codes, or 1,000 unique fluorescent labels. As previously described, non encoded beads can also be used as a label described with intensity 0. The QDEMs available for the present study are presented in Table 1 of the Appendix A in the form of a 'bead library' listing 37 different types of QDEM populations.

The use of QD-doped microspheres represents an advance in fluorescent technology offering promise for high throughput screening assays. QD-encoded microspheres (QDEMs) have the potential to produce an unprecedented number of unique fluorescent codes, with higher chemical- and photo- stability, lower limits of detection, and higher level of multiplex abilities (Han *et al.*, 2001; Gao and Nie, 2004). The work presented in this chapter describes the characterisation of TriLite™ alloyed nanocrystal-encoded microspheres (QDEMs) provided by Crystalplex (PA, USA). Comparable mass and brightness is predicted for QDEMs of the same size, across the emission range they are synthesised, because of their composition-tunable properties. Therefore, the reactivity and sensitivity of a QDEM population can be extrapolated to the other coloured beads of the same composition-type. The general characteristics of QDEM encoded with 525 nm QDs were evaluated, and the impacts of the experimental conditions of bead-based assay on QDEM physical and optical properties were investigated. A specific study was undertaken to describe QDEM behaviour under experimental conditions such as buffers, temperature and time of incubation, and manipulation applied in suspension array assay.

2.2. Materials and methods

2.2.1. Materials

Tris-ethylenediamine tetra acetic acid (TE, pH 8.0), 1 M tris-HCl, 3 M sodium chloride (TBS, pH 7.5), phosphate buffer (TBS, pH 7.4), ethylenediamine tetra acid (EDTA, PH 8.0), 2[N-Morpholino] ethanesulfonic acid (MES), 1 M Tris-HCl, Tween-20, imidazole, azide, sodium dodecyl sulfate (SDS), and nuclease free water (nfH_2O, BRK200) were purchased from Fisher Scientific Ltd (Loughborough, Leicestershire, UK). Bovine serum albumin (7.5% BSA), 5 M Tetra methyl ammonium chloride solution (pH 8.0), sodium chloride, sodium citrate buffer (20X SSC, pH 7.0), and 20 M sodium saline phosphate EDTA (pH 4.0), were purchased from Sigma Chemical Co. (Poole, Dorset, UK). Centrifugation was performed in a mini-centrifuge (Microcentaur, MSE, Henderson Biomedical Ltd, London, UK). The effect of the temperature on QDEM was tested in water bath (Grant SUB6, Shepreth Cambridge Ltd, Cambridgeshire, UK). A sonicator instrument (Sonicator instrument Corp, Copiague, NY, USA), MS1 shaker (IKA®Works Inc, Wilmington, WC, USA), and rotamixer vortexer-mixer (Hook and Tucker Zenyx, Launch Diagnostics Ltd, Kent, UK) were used to resuspend QDEM solutions.

The carboxylated functionalised porous polystyrene microspheres encoded with quantum dots (QDEMs) used in the conjugation assay were 5 µm diameters non encoded (0QDEM), 525 (525QDEM), and 575 (575QDEM) beads; and 20 µm diameters non encoded and 575 beads (Appendix A). The beads were purchased from Crystalplex (Pittsburgh, PA, USA) and received in two different scales depending on the beads quantity needed, *i.e.,* 0.5 mg of encoded beads and 1 mg of blank beads (or non encoded) in 1 mL of deionised water (DI), with 1% BSA and 0.01% azide. The quantity of blank bead purchased was higher since it was used as a control for a majority of the experimental tests undertaken. The coefficient of variation (CV) of beads intensity from bead to bead was ± 10% (Appendix B).

2.2.2. QDEMs storage, handling, and quantification procedures

QDEM solutions were received in 1 mL tinted glass containers at room temperature (RT) in TBS pH 7.5, 1% BSA, and 0.01% azide storage buffer (Crystalplex, PA, USA). The first step consisted of the dispersion of bead aggregates by 10 s vortexing and sonication for a minimum of 20 s (50/60 Hz operating frequency). Beads were then washed in DI water containing 1% BSA and centrifuged at 8000 rpm for 1 min, resuspended in storage buffer with a minimum concentration of 1 mg/mL and transferred to a 1.5 mL eppendorf tube adapted to bench centrifuge instrument. The concentration of the transferred QDEMs or stock solutions was systematically evaluated. Diluted samples in TE (pH 8.0) buffer (typically 1 in 100) of QDEM stock solutions were deposited on the grid of a Neubauer haemocytometer (Reichert, Bright-line® NY, USA), and beads were observed and counted under a Axioskop2 plus fluorescent microscope (Zeiss, Germany). For detailed methodology see Appendix C. the coefficient of variation (CV) for duplicate measurements varied from 4 to 17%. Before using any QDEM solution, the samples were vortexed for 10 s followed by sonication for 20 s to 30 s, repeated three times. QDEM solutions were stored at 4°C in storage buffer.

2.2.3. Acid / base titration of carboxylated microspheres

The carboxylated groups (COOH) on the outer layer of the polystyrene microsphere determined QDEM's reaction to buffers. The estimation of the accessible (COOH) groups on the 5 μm diameter QDEM surface was determined by acid / base titration with NaOH (0.8 mM) and HCl (1 mM). A volume of 6 μL of blank QDEM stock solution (with 1.46 x 10^7 bead/mg) was mixed at room temperature (RT) with 5 mL of 0.8 mM NaOH, and titrated with 1 mM of HCl (Fisher). The resulting solution was back titrated with the base (NaOH, 0.8 mM). Acid-base equivalent points were determined potentiometrically. The titration curves were drawn with Excel (Windows software 2000, Microsoft Corp, USA), the volume of equivalence was determined, and the microequivalents of carboxyl groups per gram of particles were then calculated. (Appendix D).

2.2.4. Testing microspheres for suspension array conditions

- **QDEMs**

Two different populations of QDEM were tested: 525QDEMs and 575QDEMs. Three different manufactured lots of 5 μm diameter carboxylated QDEM (PA, USA) were tested: Lot 1 and Lot 2 encoded with 525 nm QDs (green bead) and Lot 3 encoded with 575 nm QDs. Within a lot, two different QDEM batches were tested. Non encoded beads (or Blank bead) were used as a control in comparison with colour beads (Appendix A).

- **Chemicals and conditions tested**

The structural and fluorescent stability of QDEMs was studied with traditional buffers employed with polystyrene microspheres and with chemicals implicated in particle-based assay in liquid format. Buffers for the specific application to nucleic acid detection in suspension array were also tested.

Storage buffers

The buffers usually recommended for the storage of polystyrene microsphere were phosphate buffer (PBS) at 0.01 M and pH 7.4, or TE buffer at 0.1 M and pH 8.0. Crystalplex (PA, USA) suggested to use 1 M tris-HCl, 3 M sodium chloride at pH 7.5 (TBS), with 0.01% azide and 1% BSA.

Coupling reactions and washing steps

Two recurrent methods have arisen from the literature when looking at the carbodiimide conjugation of carboxylated polystyrene microsphere to amino active oligonucleotide probes (oligo): MES buffer or imidazole buffer were used in association with 1-ethyl-3-(3-dimethylaminopropyl)-carbodiimide (EDC), and sulfo-*N*-hydroxysuccinimide (sulfo-NHS) for the coupling reaction (Spiro *et al.*, 2000; Xu *et al.*, 2003; Wittebolle *et al.*, 2006). EDC is a water-soluble derivative of carbodiimide that catalyses the formation of amide bonds

between carboxylic acids and amines by activating carboxyl groups. When carbodiimides react with carboxyls an intermediate is formed which can stabilise the reaction with amines through a peptidic bond without spacer length (Appendix E). Table 2-1 presents an overview of the experimental steps involved in the methods which were selected for the coupling of 10^4 QDEMs (Spiro *et al.*, 2000; Xu *et al.*, 2003; Wittebolle *et al.*, 2006).

Chemicals previously described in the literature for amino-carboxy coupling of oligonucleotide to microsphere and used in the first set of experimental tests were listed: MES (pH 4.5), BSA, SDS (pH 4.0), imidazole (pH 7.0), TBS (pH 7.4), TE (pH 8.0), Tween-20 (pH 4.0) (Fisher, UK); (Fulton *et al.*, 1997; Spiro *et al.*, 2000; Xu *et al.*, 2003).

Table 2-1 Experimental steps for the carbodiimide coupling of 10^4 QDEMs to oligos*

Steps	***Method 1***	***Method 2***
	10^4 QDEM in	10^4 QDEM in
Reaction Mix V= 25 µl	MES (0.1 M, pH 4.5) 1-2 µl EDC (10 mg/ml) 1-2 µl oligo (pmol)	IMIDAZOLE (0.1 M, pH 7.0) 1-2 µl EDC (10 mg/ml) 1-2 µl oligo (pmol)
Incubation under agitation (400-600 rpm)	RT 30 min-1 h	RT 2-4 h
Washing steps	in V=500 µl , 10 s vortex	
wash 1	0.02% Tween-20	H_2O
wash 2	0.5% SDS	
wash 3	0.1% SDS	
FC Buffer analysis	TE (0.1 M, p H8.0)	TE (0.1 M, pH 8.0)
Storage buffer	TBS (pH 7.5) 0.1% azide, 1% BSA	TBS (pH 7.5) 0.1% azide, 1% BSA

* V: volume of experiment; RT: room temperature; BSA bovine serum albumin; H_2O: nuclease free water

Hybridisation reactions and washing steps

Experimental conditions traditionally used for DNA-DNA hybridisation in particle based-assay were also selected from the literature (Table 2-2), (Xu *et al.*, 2003; Berkhout *et al.*, 2006; Cao *et al.*, 2006a; Dunbar, 2006; Eastman *et al.*, 2006).

QDEMs were then tested for the hybridisation buffers and washing solutions mainly used in DNA-DNA hybridisation suspension arrays, *i.e.,* 1.5X and 2X TMAC hybridisation buffers, (1 M and 2 M TMAC, 75 mM Tris-HCl, 7.5 mM EDTA, pH 8.0 (Sigma, UK)), SSC (3X and 6X from 20X SSC: 0.015% sodium citrate, 0.15 M sodium chloride, PH 7.0 (Sigma, UK)) 1.2X SSPE washing solution (20 M SSPE, 0.5% SDS, pH 7.0 (Fisher, UK)).

Table 2-2 Experimental steps for hybridisation of conjugated polystyrene microspheres to ssDNA in liquid format *

Steps	***Method 1***	***Method 2***	***Method 3***	***Method 4***
Reaction Mix V = 25 µl	10^4 bio-conjugate QDEMs in 2X TMAC + oligo (ssDNA)	10^4 bio-conjugate QDEMs in 1.5X TMAC + oligo (ssDNA)	10^4 bio-conjugate QDEMs in 3X SSC, 0.05% SDS + oligo (ssDNA)	10^4 bio-conjugate QDEMs in 6X SSC, 0.05% SDS + oligo (ssDNA)
Incubation (water bath)	55 °C 30 min	46 °C 1 h	45 °C 1 h	45 °C 1 h 55 °C 30min
Washing steps	in V=500 µl, 10 s vortex or 400-600 rpm shaking			
wash 1	RT 1.2XSSPE, 55 C°, 7 min	1X TMAC	1X SSC, 0.03% SDS	1X SSC, 0.03% SDS
wash 2	0.05% SDS	1X TMAC	0.2X SSC	0.2X SSC
wash 3			0.05X SSC	0.05X SSC
wash 4			DI water, 30 C°	DI water, 30 C°
FC Buffer analysis	TE (0.1M, pH8.0)	TE (0.1M, pH8.0)	TE (0.1M, pH8.0)	TE (0.1M, pH8.0)
Storage buffer	TBS (pH7.5)0.1% azide, 1% BSA	TBS (pH7.5)0.1% azide, 1% BSA	TBS (pH7.5)0.1% azide, 1% BSA	TBS (pH7.5)0.1% azide, 1% BSA

* DI water: deionised water

- **Methodology**

A volume equivalent to 10,000 QDEMs from the calculated concentration of the stock solution was used in all the experimental tests (Appendix C). Storage and analysis buffers were evaluated. The microspheres were incubated in 400 µl of TE buffer and storage buffer, vortexed for 10 s and incubated respectively at RT for 0 to 2 h. The experimental conditions of coupling were first tested with 525QDEMs in 25 µl of MES (pH 4.5) and imidazole (pH 7.0) buffers, and incubated at RT for 0 to 2 h, while shaking at 400 to 600 rpm. The impact of the coupling washing solutions (Tween-20, SDS) was tested at RT in 400 µl; the solutions were vortexed for 10 s, and incubated for 0 to 1 h, shaking at 400 rpm.

Secondly, 525QDEM structural stability for hybridisation conditions was tested with TMAC and SSC hybridisation buffer. 525QDEMs were incubated with 1.5X and 2X TMAC buffer for 0 to 2 h at 55°C, and with 3X and 6X SSC buffers both at 45°C and 55°C for 30 min and 90 min. 525QDEMs were diluted in 400 µl of 1.2X SSPE, 0.05% SDS hybridisation washing solution vortexed for 10s and incubated at RT and 55°C for 0 to 1 h, shaking at 400 rpm.

To be able to distinguish between the effect of the temperature and the reagents, the same quantity of microspheres was incubated in TE buffer at RT (24°C), 55°C and 72°C for incubation times ranging from 0 to 2 h.

Finally, the same experimental tests were applied to Lot 1 and 2 of 525QDEM and to 575QDEM stock solutions to investigate the role in the bead stability of the two parameters which defines the encoding of the QDEM: intensity, *i.e.,* nanocrystals concentration, and emission wavelength, *i.e.,* the QD emission wavelength dependent on the nanocrystals size and composition, as described in section 1.1.1.

After all incubations and tests in the different buffers, QDEMs were centrifuged (1 min at 8000 rpm), resuspended, and analysed on the flow cytometer.

2.2.5. Microscopy techniques

- **Scanning electron microscopy (SEM)**

The particle size, morphology and composition were examined with scanning electron microscope (SEM). The Environmental SEM Philips XL-30 ESEM, and a Phillips XL30 SFEG (Field emission Gun) microscope equipped with Energy Dispersive Spectrometry (EDS) to perform chemical composition analysis (Royal Philips Electronics, Netherlands) were used. Preliminary QDEM observations were undertaken with the ESEM. The samples were washed in a 50% methanol solution, resuspended in methanol, and then deposited on an aluminium plate. The plate was left to dry over night before analysis. 525QDEMs and a 50/50 mixture of (1:0:0:0) (0:1:0:0) QDEMs were observed under the ESEM. To obtain detailed structural observations, 0QDEMs and 575QDEMs of 5 µm and 20 µm diameters were prepared for XL30SEFG analysis by drying a dispersed solution on a aluminium tab and sputtering a thin film of carbon to avoid charging (CC7650 Carbon coater, Emitech, UK).

- **Fluorescence microscopy and confocal microscopy**

As previously described (section 2.2.2) fluorescence microscopy (Axioskop2 plus, Zeiss, Germany) was used to enumerate diluted QDEM stock solutions, and experimental samples with a haemocytometer (Reichert, Bright-line® NY, USA) (Appendix C).

Images and fluorescent spectra of QDEMs were recorded with a Axioskop2plus LSM 510 confocal microscope (Zeiss, Germany). Channel 1 (Ch1, green spectra) detected 525QDEMs with a 505-530 nm band pass filter (BP). Channel 2 (Ch2, yellow spectra) detected 575QDEMs with BP filter of 530-600 nm (Table 2-3). Both channels were excited at 488 nm (Argon laser, 2% power intensity). The same settings were applied for positive and negative controls. Blank QDEMs were used to normalise the fluorescence background. Three-dimensional (3-D) images of QDEMs were obtained by the optical sectioning of the

specimen. The scanner recorded numbers of single plane sections (or slices) while the specimen was being moved along the optical axis (z) with controlled increments. Images were treated through the LSM 5 Image Browser software (Zeiss, Germany).

Ten µL of diluted QDEM solutions from the stock solution containing a minimum of 1000 beads were prepared. A maximum of ten beads was observed on superfrost colour slides 76 x 26 mm, with coverglass 22 x 50 mm (Menzel-glaser, Germany). QDEM solutions were systematically resuspended to obtain homogeneous bead solutions concentration before placing a droplet of the suspension between the glass slides.

2.2.6. Flow cytometry

- **Sample preparation and analysis**

The materials related to flow cytometry (FC) were purchased from Beckman-Coulter Inc. (High Wycombe, Buckinghamshire, UK). QDEMs were analysed in 400 µL of filtered buffer. Depending on the colours of the QDEMs and the organic fluorophores used in the experiments, the samples were characterised using the adequate optical parameters of the flow cytometer: side angle scatter (SSC), forward angle scatter (FSC), 4 channels of detection (FL1, FL2, FL3, FL4) (Table 2-3).

Table 2-3 Detection system and fluorescent dyes characteristics *

Detection channel Microscope / FC	**Band pass filter (in nm)**	**Visible colour**	**Emission λ (in nm)** QD / Fluorochrome
Ch1 / FL1	505-545	Green	525
Ch2 / FL2	560-590	Yellow-Orange	575 / PE, Cy3
FL3	605-635	Red	630
FL4	660-700	Deep Red	665 / Cy5

* Ch: channel; FL: fluorescence λ: wavelength; FITC: fluorescein isothiocyanate; PE: phycoerythrin; Cy: cyanine dye

Data were acquired in a four-decade logarithmic scale, using the System II Data Acquisition & display software, version 2.0 (Beckman-Coulter, FL, USA). Samples were vortexed before the run through a Coulter Epics XL-MCL flow cytometer equipped with an air-cooled 488 nm argon-ion laser (Beckman- Coulter Inc, purchase through LabX, Ontario, Canada). The Flow-check beads were used for daily optical alignment of the flow cytometer instrument.

- **Data acquisition and analysis**

FC data (fcs data files) were acquired in each detector channel. FC data files were analysed with WinMDI 2.8 (Joseph Trotter, The Scripps Research Institute, La Jolla, CA, USA), and FloJo 7.2.2 (Tree Star Inc, Ashland, OR, USA) software.

The median fluorescent intensity (MFI), the coefficient of variation, and the percentage (%) of events were calculated on gated population using WinMDI2.8 software (CA, USA). The QDEM stock solution was used as a control to define a region for the QDEM population of interest and to calculate the MFI base-line. Three to six replicates were run per experiment. The average coefficient of variation was calculated between all the positive samples for the conjugation and the hybridisation experiments.

- **Statistical calculation and representation**

The following nomenclature was used for the statistical analysis: ***s*** for samples, ***n*** for negative control experiment or background measurement, ***c*** for control population. The numerical results are presented as the mean of replicates ± the standard error (SEM). Curves and statistical tests were calculated with GraphPad Prism5.01 (GraphPad Software, San Diego, CA, USA) and Excel (Microsoft Corp, USA).

- Corrected MFI (RMFI) was calculated by subtracting negative control values (n) to values obtained with the positive samples (s) of the same batch experiment (in arbitrary units, a.u.);

- The relative variation of QDEM fluorescent code was evaluated by estimating by the comparison with the initial fluorescence of the QDEM control population as (in a.u.):

$$\% \text{ FL} = 100 \times \text{MFI}^{\text{FL}}(s) / \text{MFI}^{\text{FL}}(c)$$

- To evaluate the number of QDEMs in the experimental tube, the percentage of events was recorded during sample analysis and a relative percentage of events compared with the control population was calculated:

$$\% \text{ Events} = 100 \times \% \text{ Events}(s) / \% \text{ Events}(c)$$

Principal component analysis (PCA) and mesh plot representation were generated with MATLAB software applications (Forsythe *et al.*, 1977) using MFI (± SEM) values calculated with the WinMDI software (La Jolla, USA).

2.3. Results

2.3.1. Concentration, size, composition, morphology, and surface properties

- **Concentration**

Carboxylated functionalised QDEMs (Crystalplex Corp, PA, USA) were described as 5 µm diameter porous polystyrene microspheres, with a protective shell placed on the surface of the beads after encoding with QDs. The QDEM solutions were evaluated by the manufacturer at ~1.46 x 10^7 beads/mg, and therefore by extrapolation at 7.3 x 10^6 beads / 0.5 mg. The concentration of 0.5 to 1 mg of QDEM suspensions (in TBS, 1% BSA, 0.01% azide) was systematically re-evaluated after the transfer to 1.5 mL eppendorf tube in order to accurately employ the expected number of microspheres in the experimental tests (Section 2.2.2). The calculated concentrations were typically between 1.1 x 10^6 to 6 x 10^6 beads / 0.5 mg, and 9 x 10^6 to 1.1 x 10^7 beads per mL. This step was essential to be able to work quantitatively (with known quantities of materials) in the characterisation experiments and in the optimisation assays.

- **Size and morphology**

A XL30 SFEG scanning electron microscope (Philips, Nertherlands) was used to characterise the surface and the morphology of the carboxylated porous polystyrene microspheres. Typical examples of the SFEG images recorded with 0 and 575QDEMs of 5 µm and 20 µm diameters are presented (Figure 2.3, Figure 2.4, Figure 2.5, and Figure 2.6.

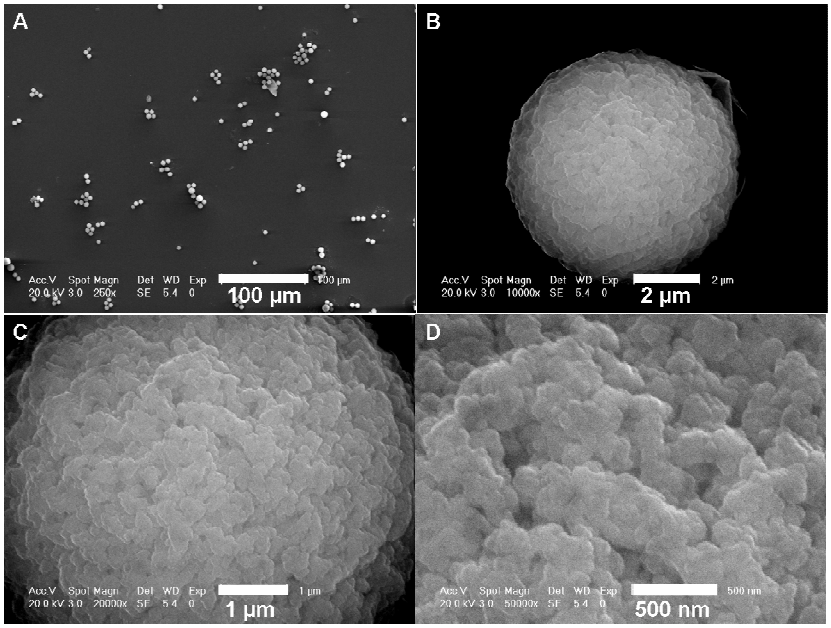

Figure 2.3 Typical SFEG images of 5 µm diameter non encoded QDEM.

Micrographs taken with 20.0 kV; the scale bars were redrawn for clear observation.

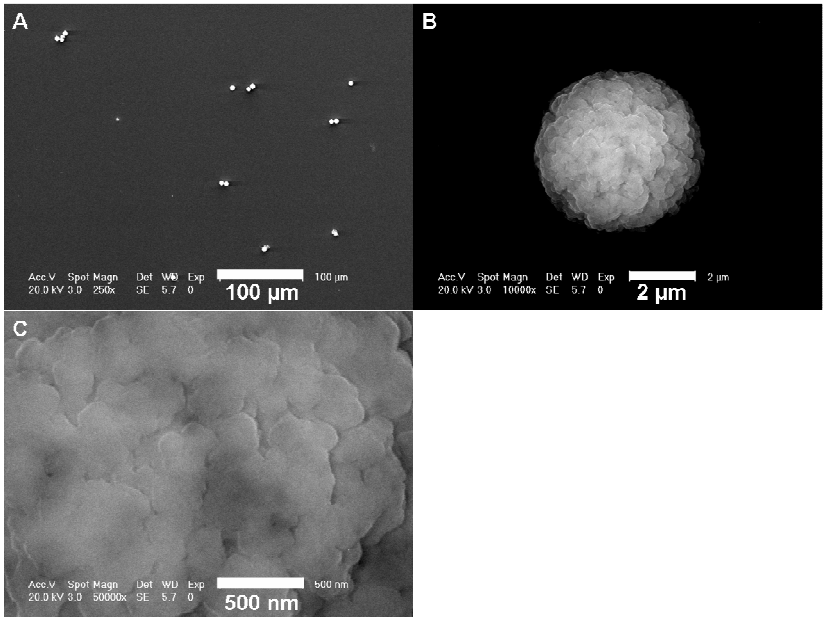

Figure 2.4 Typical SFEG images of 5 µm diameter 575 encoded QDEM.

Micrographs taken with 20.0 kV; the scale bars were redrawn for clear observation.

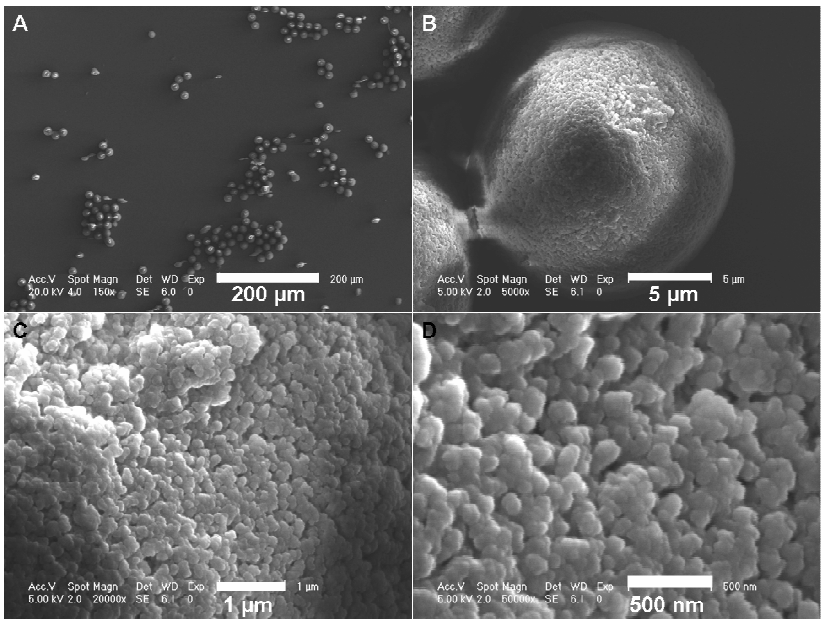

Figure 2.5 Typical SFEG images of 20 µm diameter non encoded QDEM.

Micrographs taken with 10.0 kV (A, D) and 5 kV (B, C); the scale bars were redrawn for clear observation.

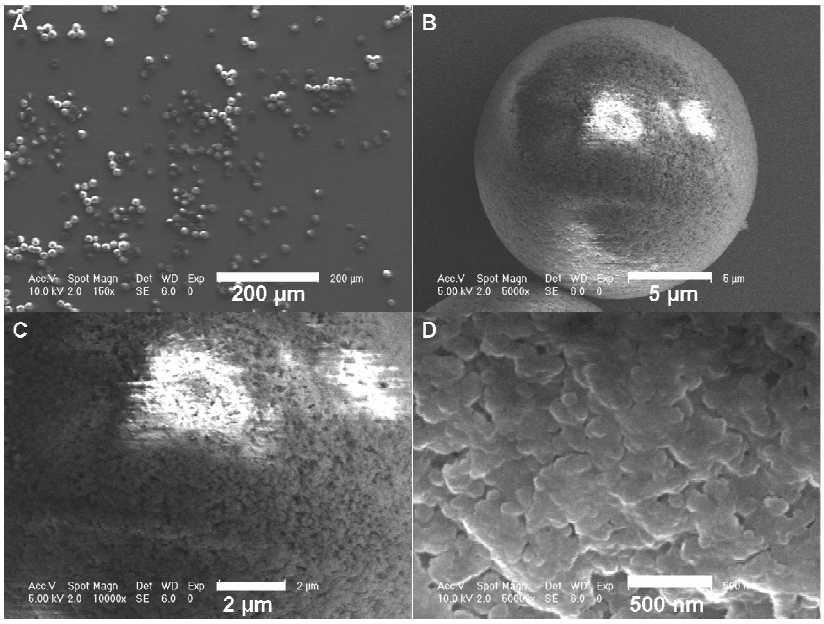

Figure 2.6 Typical SFEG images of 20 µm diameter 575 encoded QDEM.

Micrographs taken with 20.0 kV (A), and 5.0 kV (B, C, and D); the scale bars were redrawn for clear observation.

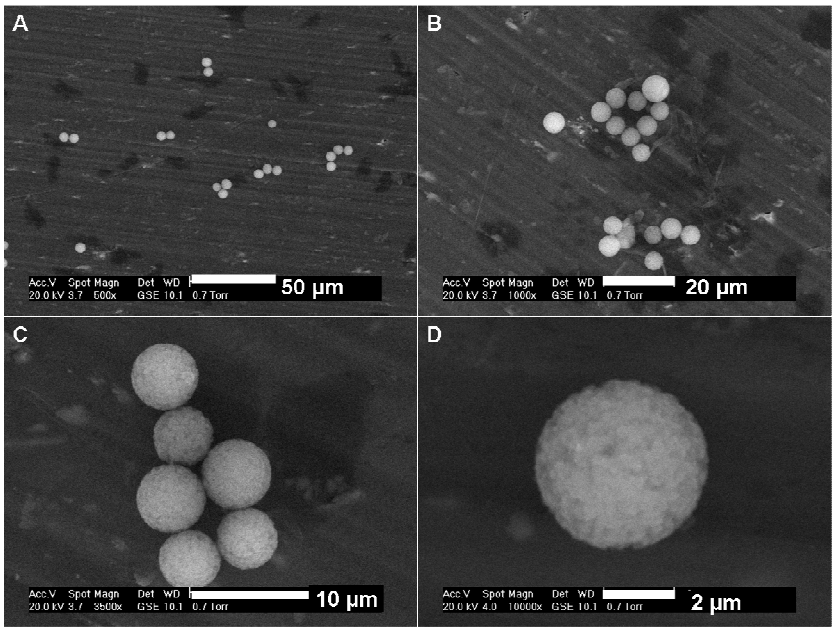

Figure 2.7 Typical SEM images of 5 µm diameter 525 encoded QDEM.

Micrographs taken with 20.0 kV, the scale bars were redrawn for clear observation.

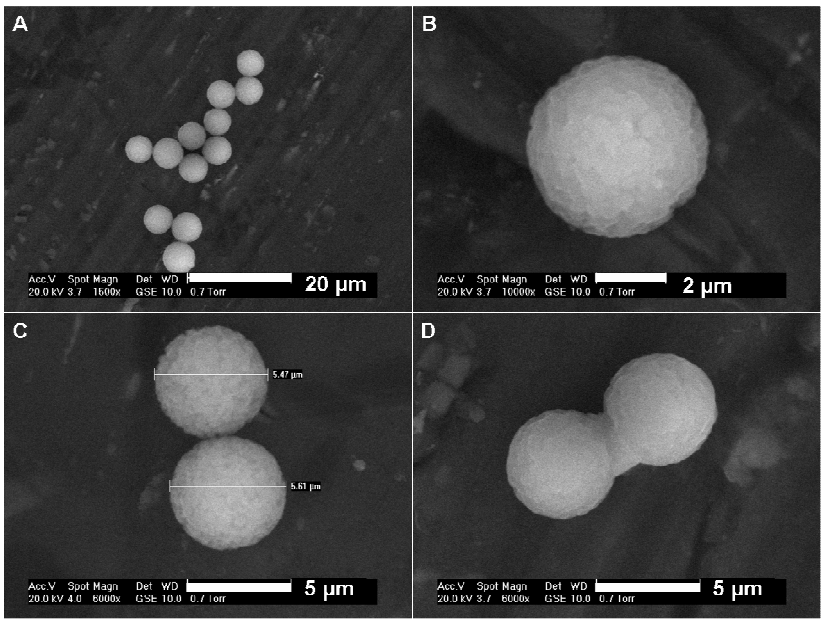

Figure 2.8 Typical SEM images of a 50/50 ratio mixture of (1:0:0:0) and (0:1:0:0) intensities of (525;575;630;665) QDEMs.

Micrographs taken with 20.0 kV; the scale bars were redrawn for clear observation.

In the SFEG images, QDEMs had a spherical regular shape. The surface of QDEMs appeared rough and presented a pleated aspect. The pores appeared to cover the bead surface, which indicated an increased surface area and pore volume. The observations of multiple 0QDEM (non encoded) events were similar in morphology and topography to encoded microspheres (Figure 2.3D, Figure 2.5D, Figure 2.6D, and Figure 2.4C).

Figure 2.7 and Figure 2.8 present the typical images observed under SEM with respectively (525) and (525;575;630;665) QD-doped microspheres of 5 µm diameter. Images with different magnification are displayed. The (525) and (525;575;630;665) QDEM populations presented a uniform spherical shape and size distribution. QDEMs encoded with one type of nanocrystals or four different types of nanocrystals presented the same morphology with SEM analysis (Figure 2.7 and Figure 2.8). The comparison between Figure 2.8C and D showed a particular formation in (D) which was not present in (C). The density and colour of the bridge observed between the two QDEMs in Figure 2.8D was similar to the microsphere surface.

- **Composition**

The qualitative analysis of 525QDEM of 5 µm diameters was undertaken on an aluminium surface with the A XL30 SFEG scanning electron microscope (Philips, Netherlands), with different acceleration voltage to compare the composition of superficial layers and deeper layers of the microsphere. Blank and 525 encoded QDEMs of 20 µm diameter were quantitatively analysed in the same conditions, on a small silicon surface to be able to compare the composition of encoded and non encoded microspheres. The analysis of the superficial layer of the 5 µm 525QDEM structure presented a higher content of carbon, oxygen, zinc and sulphur composite than the analysis of the deeper internal structure of the bead (Figure 2.9A). The amount of aluminium detected was approximately twenty times superior with deep analysis. Copper and calcium were also detected whereas these elements were absent from the superficial analysis. The same ratio of chlorine was detected in both analyses. The elements composing the core of QDs were not detectable with 5 µm beads.

Zinc and sulphide elements were detected in high quantity in 20 µm 0QDEM (respectively ~2.0% and 1.0%) in comparison with 525QDEMs (respectively four times less, and two times less). A high concentration of carbon and oxygen were detected with 20 µm 525QDEMs.

Traces of cadmium and selenium (traces <0.5%) were detected with the quantitative analysis in 20 µm diameters 525QDEMs (Figure 2.9B) but not in 0QDEMs. The high proportion of silicon corresponded to the silicon surface on which the samples were deposit for the analysis.

The proportion of zinc/sulphur in the different population of QDEMs showed a similar distribution, ~70/30 between all the samples except for the 525QDEMs of 20 µm diameter which presented a ~50/50 ratios (Table 2-4).

Table 2-4 Proportion of zinc and sulphide in the different QDEMs analysed *

Samples	Diameter (µm)	Ratio in % Zn:S
Superficial	5	70 - 30
Deep		68 - 32
0QDEM	20	65 - 35
525QDEM		54 - 46

* %: percentage

- **Surface properties**

The loading capacity of the accessible carboxyl group on the polymer microspheres was determined by acid/base titration. The volume of equivalence was determined with the titration curve (Appendix D). The result indicated a (COOH) coverage of ~26.3 µeq/g.

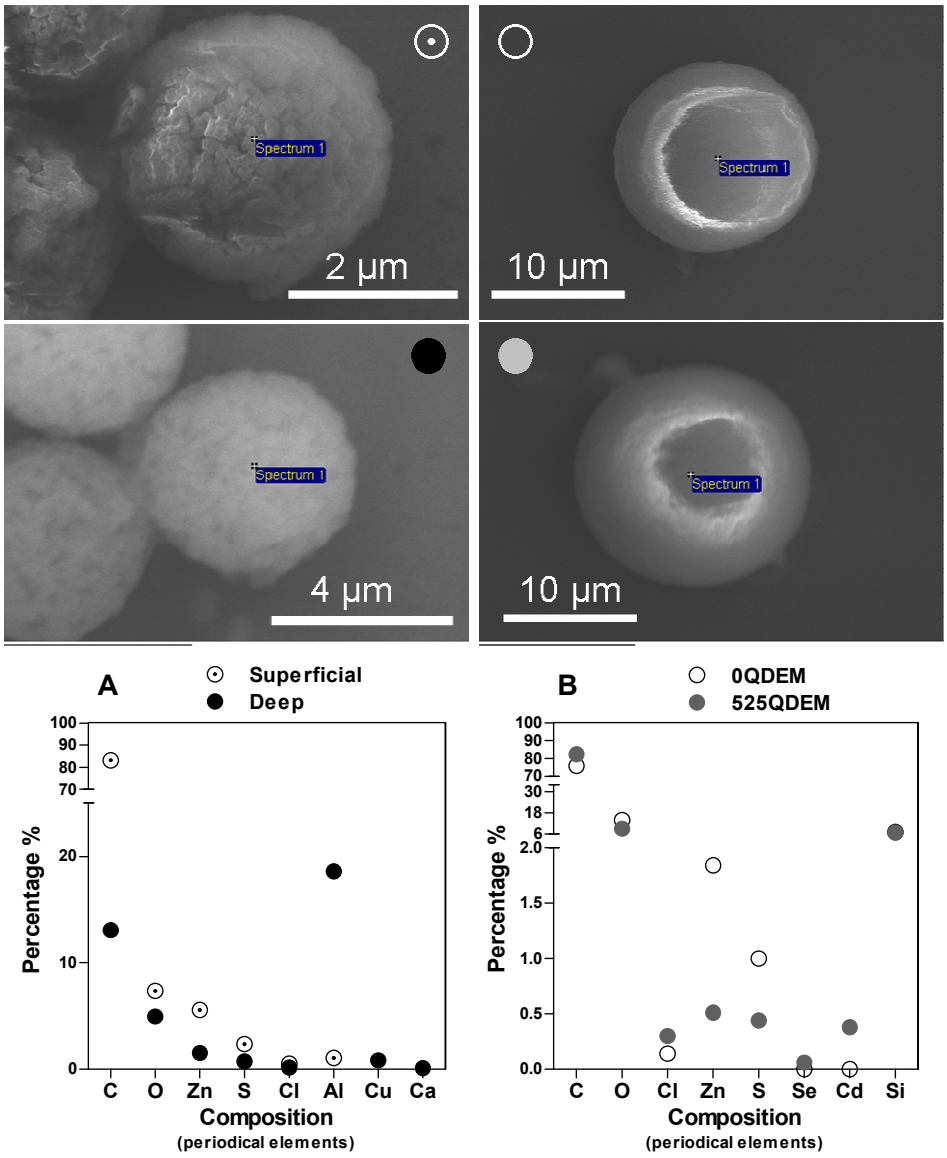

Figure 2.9 Representation of the SFEG composition analysis.

A: (⊙) superficial (10 kV) and (●) deep (20 kV) qualitative analysis of the composition of 5 µm 525QDEMs; the percentage of each elements is represented with GraphPad Prism5.01 (CA, USA); C: carbon, O: oxygen, Cl: chlorine, Zn: zinc, S: sulphur, Se: selenide, Cd: cadmium, Si: silicon, Al: aluminium, Cu: copper, Ca: calcium; **B**: Quantitative composition analysis of (○) 20 µm non encoded QDEM, and (●) 20 µm encoded 525QDEM, with 20kV accelerated voltage; The SEFG micrographs showed the position of the spectrum for each analysis on each QDEM. SEFG images and compositions analysis were chosen since they were typical of the QDEM populations analysed (with an average variations of the values < 5% from the means). The scale bars were redrawn for clear observations.

2.3.2. Fluorescent characterisation of single QDEM

QDEM fluorescence and structural properties were examined under fluorescence microscopy with an Axioskop2plus LSM 510 confocal scanning fluorescence microscope (Zeiss, Germany). The beads showed a strong green photoluminescence (PL) under argon laser excitation (488 nm) (Figure 2.10 and Figure 2.11).

- **3-Dimensional view (3-D)**

The first observations were made on QDEMs encoded with 525 nm QDs after medium speed vortexing with the rotamixer (Zenyx, Kent, UK). Figure 2.10 presents typical 3-D frozen images of 10 µm 525QDEMs. The optical sectioning of the scanner recorded 70 single plane sections (or slices), with the specimen being moved along the optical axis (z) by controlled increments of 0.20 µm. The scanning of the specimens provided a collection of Z-stacks (*i.e.,* collection of emission wavelengths in the spatial z axis) which allowed the reconstruction of a 3-D view of the microsphere. The 3-D data set provided information about the spatial structure of the object scanned.

The microsphere showed a regular fluorescent spherical profile (Figure 2.10 A,B). The confocal optical slices suggested that the microsphere was hollowed. The cross section analysis used to produce the 3-D images revealed a specific distribution of the QDs fluorescence within the sphere: the maximum intensity was found toward the surface of the sphere; a lower fluorescent signal was observed towards the centre of the sphere (Figure 2.10A).

The images of the sectioning corresponding to approximately the radius of the sphere were presented in the fourth line of the gallery A of Figure 2.10, in the inset 7 to 7.2 µm. These images illustrated the specific localisation of the fluorescence on the external surface of the microsphere.

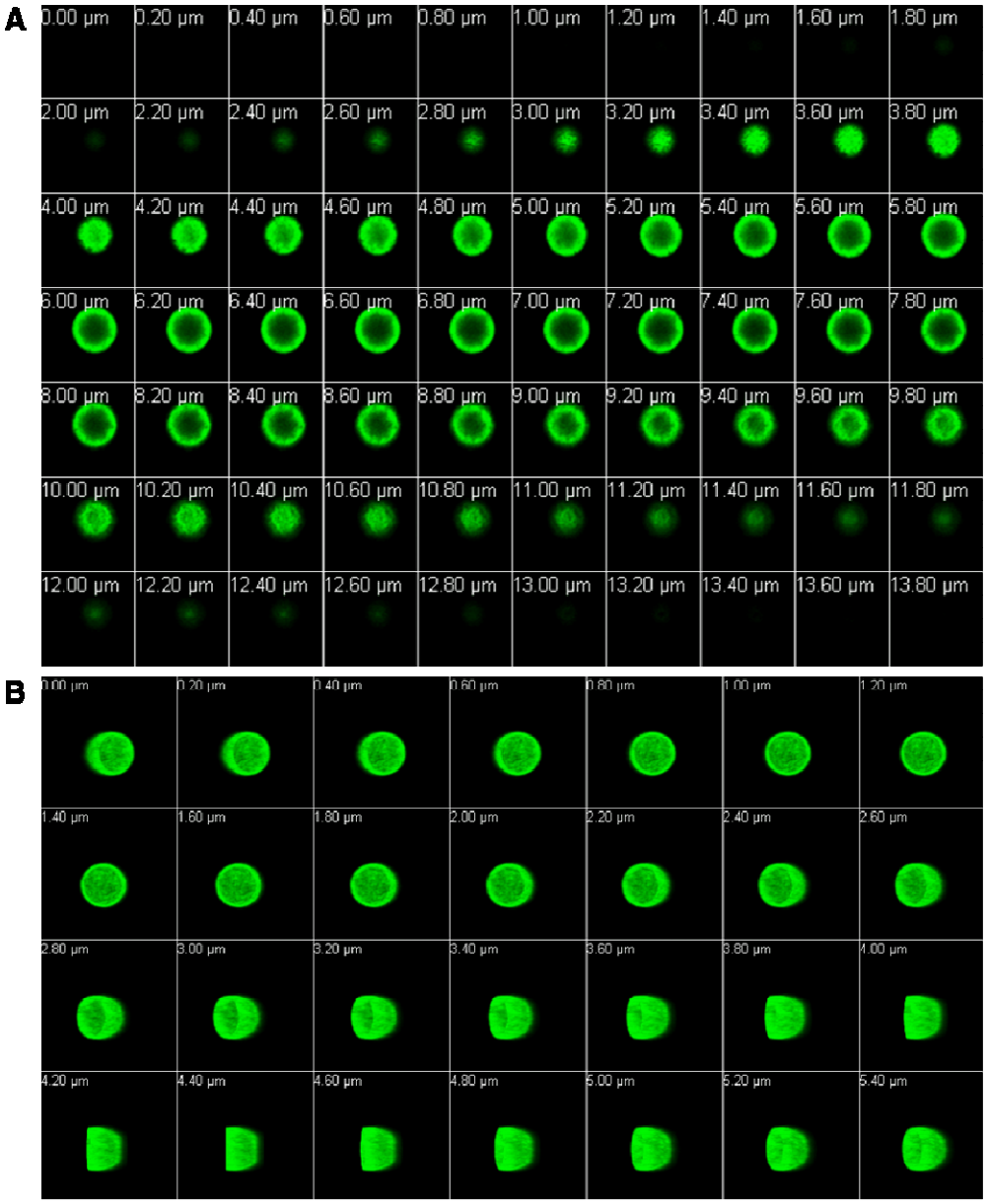

Figure 2.10 Laser cross sectional confocal imagines and 3-D images of a 525QDEM.

Gallery (**A**): z- stacks gallery; sections of the 3-D data set of the 525QDEM; data comprised 70 images; the distance from one scan slice to the following one is indicated in the up left corner (in µm); slices are 200 nm apart. Gallery (**B**): selective scans of the 3-D images; rotation increment (200 nm steps) are indicated in the up left corner of each imagine of the gallery. Typical images of 525QDEMs from stock solutions after medium vortexing..

- **Fluorescent profile before and after homogenisation**

The PL profiles of the 525QDEMs observed in 3-D were analysed after vortexing the samples at medium speed (Figure 2.11). Previous observations on the 3-D images were confirmed by the fluorescent spectra of the same 525QDEM population. A difference of ~88.4% of PL intensity was calculated between the extremity and the centre of the sphere, within a distance corresponding to the radius of the sphere. No fluorescence was detected in channel 2. The majority of the QDEMs observed on the slide presented the same characteristics as in Figure 2.11A. The second set of observations was made on sonicated and vortexed QDEM solutions. A change in the PL profile was observed, and the QDs' fluorescence within the sphere appeared more uniformly distributed than before sonication. A low background fluorescence, ~5 a.u., was detected in channel 2. These observations were made on different cross sections of the QDEMs. The dispersion of the fluorescence was observed on the different scans performed. After only 20 s of sonication at 50/60 Hz operating frequency (the average frequency used for microspheres separation in solution) the difference in PL intensity from the centre to the surface of the sphere decreased from ~88.4% to 61%. Longer time exposure to sonication reduced it approximately to zero (Appendix F). An estimation of the fluorescence distribution was calculated in using the distance (in μm) covered by the PL pick relatively to the radius of the beads. The PL profile showed that the fluorescence was located on average in the outer 33% of the QDEM radius for Figure 2.11A, and in the outer 53% for Figure 2.11B

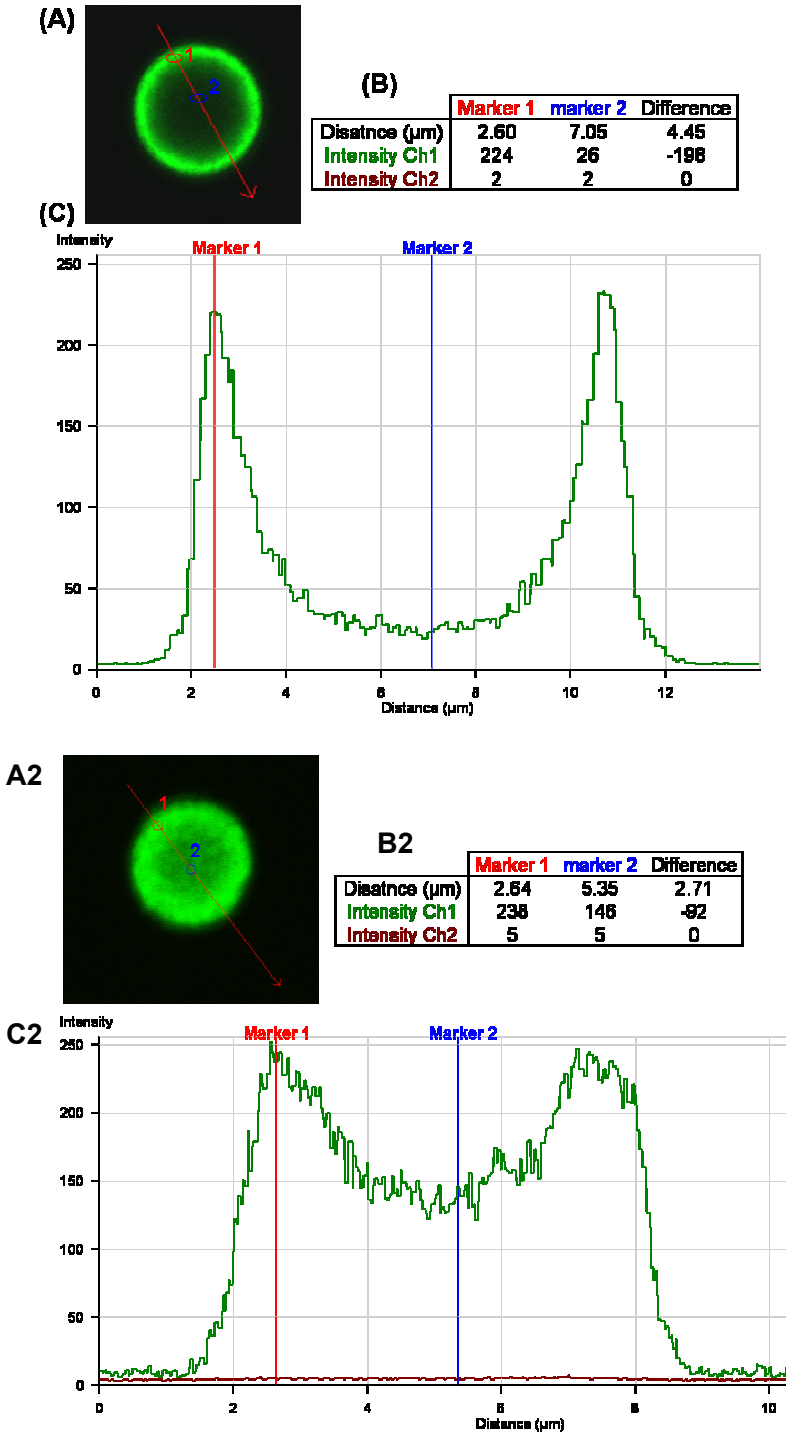

Figure 2.11 Fluorescent profile of 525QDEM obtained with confocal microscopy.

Typical images of 525QDEM before (**1**) and after sonication (**2**); **A**: 525QDEM imagines with marker 1 (red) and 2 (blue) positions; **B**: Fluorescent intensity values (in a.u.) detected in Ch1 and Ch2 (Table 2-3); (C) PL spectra of 525QDEM.

2.3.3. Read-out and protocol conceptualisation for multiplex QDEM fluorescent code analysis

- **Observation of 5 levels of intensity of a QDEMs population**

A mixture composed of equivalent quantities of 20 µm QDEMs non encoded and encoded with 1, 2, 3 and 4 increasing level of 575 QDs were analysed under confocal microscopy (Figure 2.12). The different QDEM populations mixed in the samples were distinctively identified. The red arrows point out QDEMs identified with different PL intensity on the imagines. The contrast was increased in the same magnitude for both imagines in order to be able to visualise the spherical print of the blank beads.

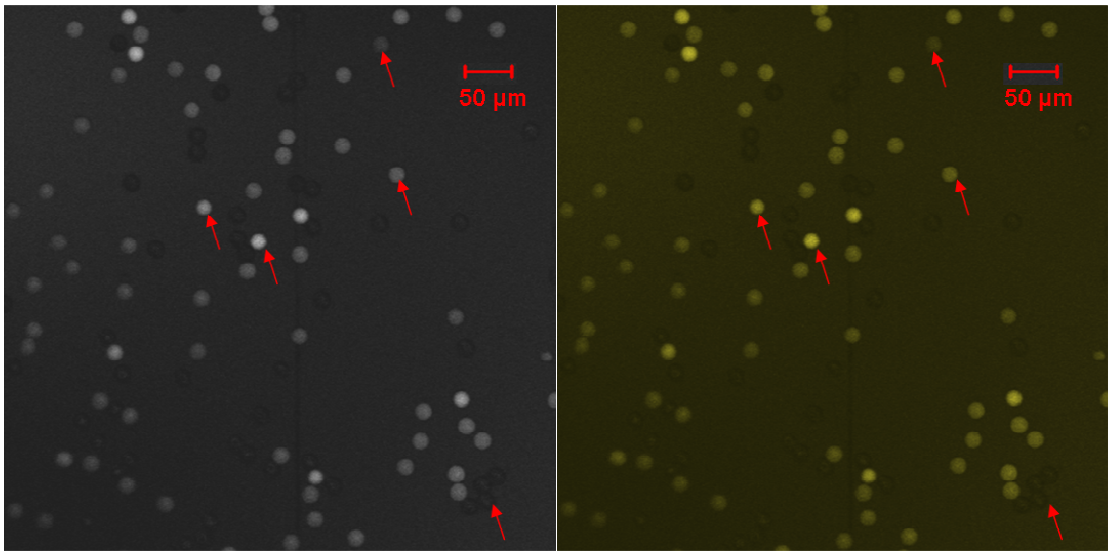

Figure 2.12 Confocal images of a mixture of 575QDEMs.

True-colour and range indicator images of a mixture of 575QDEM; the red arrows on the pictures point out the different 575QDEM encoded with 0, 1, 2, 3, or 4 level of intensity; the scale bar was retyped in the right corner of each image for clear observations.

- **Analysis of 15-plex QDEM fluorescent codes**

QDEMs encoded with two QD colours (525;575), and with four levels of intensity (0, 1, 2, and 3) generated [4^2 – 1]: 15 unique fluorescent codes (see introduction). The mesh plot presented in Figure 2.13 was obtained with the collaboration of Crystalplex using the median fluorescent intensity data (MFI) and the percentage of events of the 15 two-colour QDEM populations run through an Epics Coulter (Beckman-Coulter, USA) (personal communication with Jenny Crawford, PA, USA). The height of the picks corresponds to the density each QDEM population represented in the mixture analysed. The alignment of the QDEMs on the x coordinates is proportional to the intensity of the 525QDs encoding. In the same extent, the different QDEMs were aligned on y-axis coordinate proportionally to the intensity of the 575QDs encoding. This result illustrates the process of modifying the molar concentration of 525 and 575QDs to obtained 15 unique codes with variable ratio of each of the QDs. Figure 2.14 demonstrates a highly specific identification of 15 different QDEMs encoded with two different colours with flow cytometry instrumentation.

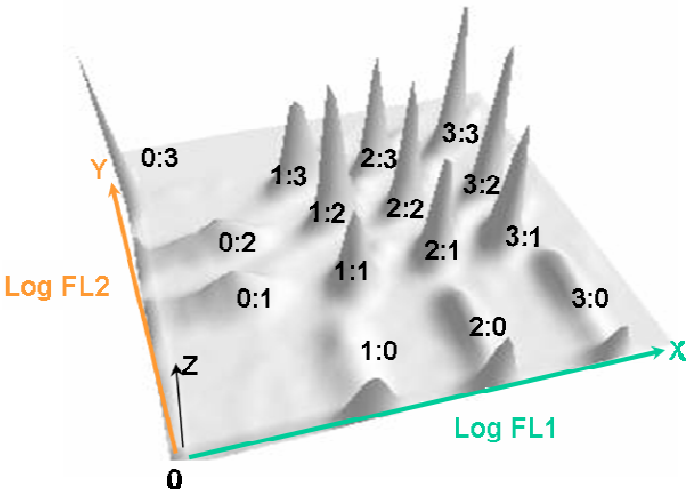

Figure 2.13 3-D plot of 15 individual QDEM codes.

(x, y) axis are in logarithmic scale; (z) axis represents the count of events in numerical values; single QDEM at 525 nm (green) and 575 nm (yellow) and two-colour beads (525;575) at different intensities are represented. Codes are indicated for each emission pick.

- **Analysis of a 20-plex QDEM library**

The same quantity of twenty different QDEM populations was pulled together in a single tube experiment to evaluate the specificity of the QDEM fluorescent codes and to develop multi-fluorescence analysis protocols for FC. Very simple analytical tools were used to distinguish between the different QDEM populations. The QDEM library (Appendix A) was run through the flow cytometer with nor compensation nor gating, to check the fluorescent codes of QDEM populations. The average MFIs of 20 different QDEMs were plotted with the FloJo software (Tree Star Inc, USA). The settings of the 20-plex protocol were established using the single QDEM as calibration tool. A simple dot plot successfully identified 20 distinct QDEM codes (Figure 2.14).

A poor resolution of the codes (0:1:1:1) and (1:1:0:0) were noticed. Only two populations, the Blank (0), and (525;575)(1:2) had a majority of the events out off scale, meaning that the average MFI was not reliable and therefore the fluorescent code non-informative. Fluorescent overspill in FL2 were observed for 525 and 575 QDEMs. The main observation revealed the impact of the difference in fluorescence intensities between high intensity single-colour beads and multi-colour beads. Figure 2.14 shows the detection of 525 and 575 single-colour beads in the last log scale of the dot plot, with an emission intensity approximately two log scale higher than the multi-colour beads in the same detector channel (for the same QDs).

The average MFI of the twenty QDEM samples were recorded in each detectors channel. A PCA was performed using the six flow cytometer parameters to calculate the coordinate of each QDEM population (Table 2-3). This experiment illustrates an initial test to use an analytical method in order to identify the fluorescent signal of the QDEMs taking into account all the data provided by the FC instruments.

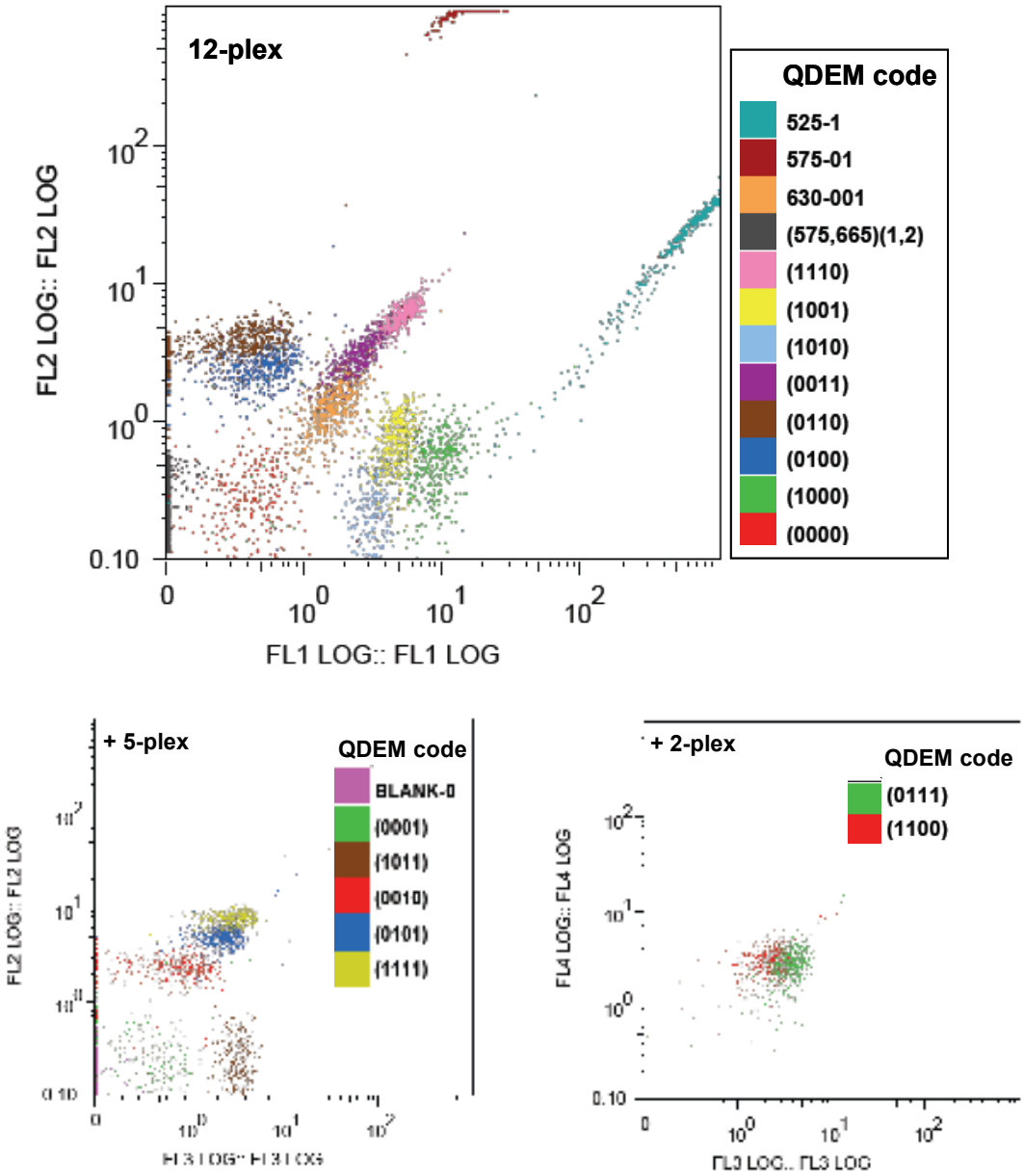

Figure 2.14 Dot plots of twenty different QDEM population.

QDEM populations were visualised by using different channel detector to plot the data. Runs with single QDEM were undertaken to design the settings of the FC protocol, and to tag each population with a colour code.

The PCA was used to establish a profile of the QDEMs using the six flow cytometer parameters characterising the microspheres. The PCA was also performed to potentially identify patterns in the fluorescent codes of QDEM and highlight their similarities and differences. Each QDEM of the twenty codes were specifically represented on the plot. The PCA analysis confirmed the observations made in Figure 2.14: the single-colour beads (525), (575) and blank beads (0) fluorescent parameters strongly diverged from the rest of the QDEM populations. Single-colour beads defined the two components PC1 and PC2 (lines indicated in Figure 2.15). The circle in Figure 2.15 was grouping four-colour beads and the 630 and 665 single-colour beads, which illustrated the similarities between the characteristics of these microspheres, and especially between 665QDEM and 0011QDEM, presenting very similar coordinates.

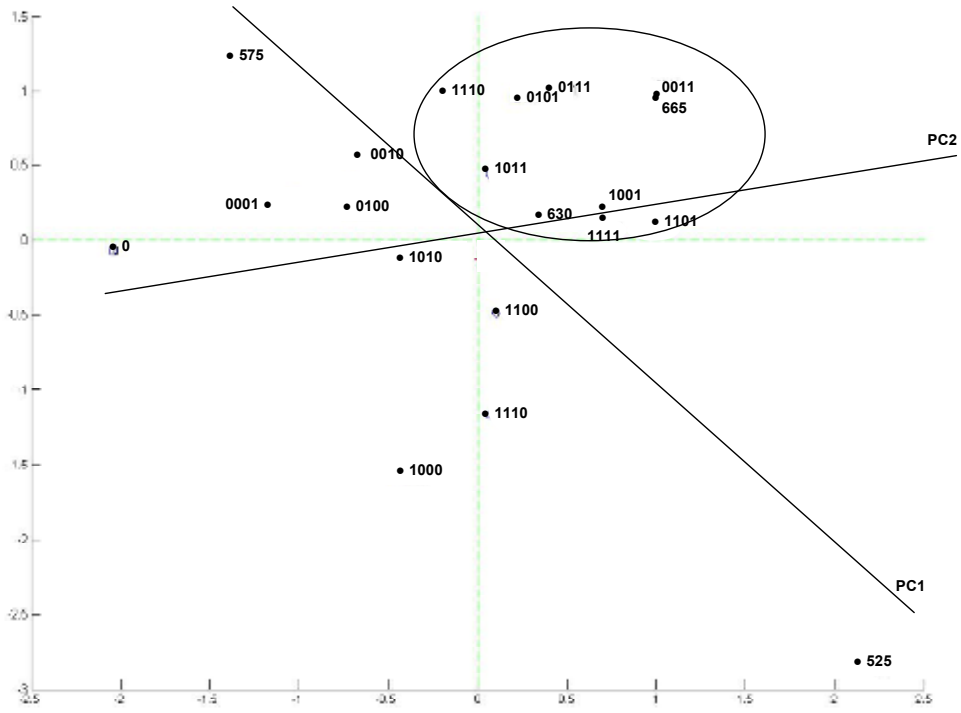

Figure 2.15 PCA bi-plot of twenty QDEM codes.

(●) the position of each QDEM are indicated with the corresponding fluorescent codes: the twenty QDEM are composed of single-colour and four-colour beads (Appendix A).

2.3.4. QDEM response to suspension array experimental conditions

- **QDEM stability and storage buffers**

Figure 2.16 presents the variation of the percentage of events and of the fluorescent code of 525QDEM stock solution incubated at RT over time in TE (pH 8.0) and TBS (pH 7.4) storage buffer. After 2 h incubation at RT, no significant variation of the MFI and the percentage of events were noticed in TBS storage buffer. A decrease of 10% (± 4) of the percentage of events was observed after 5 min incubation and a decrease of 20% (± 10) of the percentage of events was noticed after 1 h incubation in TE buffer. The fluorescence intensity was stable over time for both in TE and TBS storage buffer.

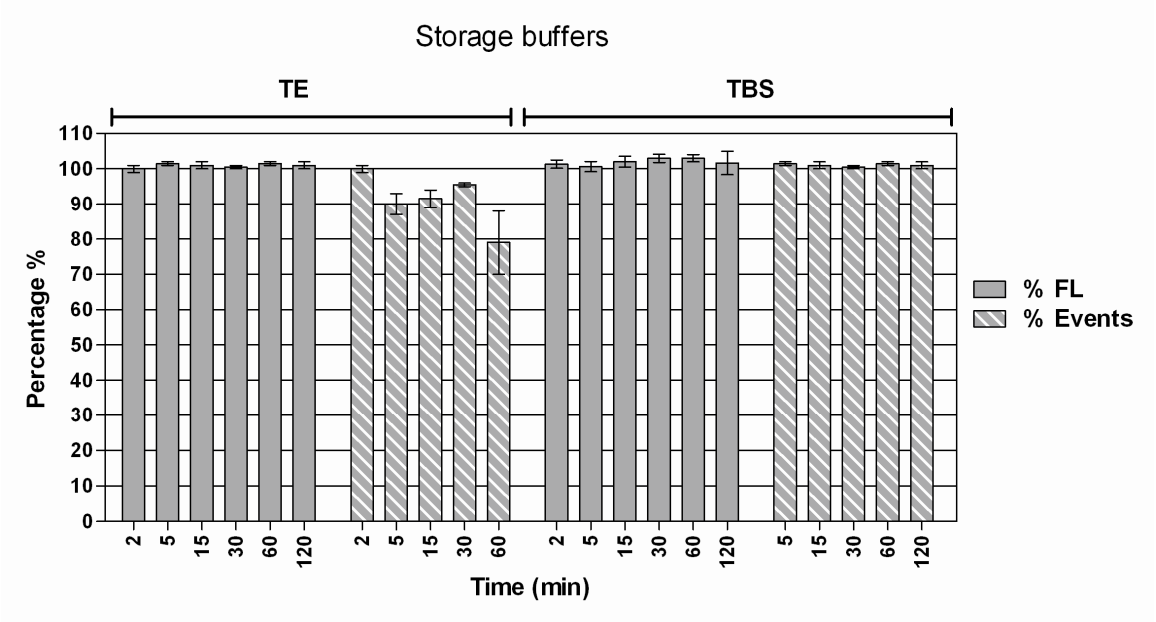

Figure 2.16 Chart representing the relative number of events and the relative MFI (in % ± standard error of the mean, SEM) versus time (in min), detected on 525QDEM population incubated in TE and TBS at RT over a time range of 2 min to 120 min.

% FL: percentage of fluorescence; % Events: relative percentage of events (refer to section 2.2.6).

Long-term storage was also investigated. The fluorescent code and intensity as well as the microsphere concentration were stable in TBS storage buffer after months, whereas in TE buffer a significant decrease of the fluorescent code and of the number of QDEMs appeared after 24 h (Appendix G). The fluorescence and the number of events of the QDEM population was stable (~100% of control population) in TE buffer in the range of time used for flow cytometry analysis whereas after 1 min, half of the QDEM fluorescence was detected under flow cytometry in PBS buffer (Figure 2.16) (Appendix G).

QDEMs were found less stable in PBS buffer than in TE buffer over the same range of incubation time (Appendix G). As a first finding, the QDEM were highly sensitive to stringent salt solutions. The comparison between different storage and running buffers resulted in the choice of TBS (1X TBS 1% BSA, and 0.01% azide, pH 7.5) for long-term storage, and TE (0.1M, pH 8.0) was chosen as a running buffer in the rest of the study. QDEMs were recommended to be stored with a minimum of 1% proteins (Crystalplex). The BSA in the storage buffer composition helped to stabilize the QDEM for long-term storage.

- **Effects of the coupling and hybridisation conditions on QDEM properties**

Coupling conditions

Figure 2.17 represents the variation of the percentage of events and of the fluorescent code of 525QDEM population incubated over time with MES and imidazole coupling buffers. The time range was chosen to illustrate the average incubation conditions used in the literature for high throughput carbodiimide coupling: conjugation experiment required typically a minimum of 30 min to a maximum of 2 h incubation time (Table 2-1). After 2 min of incubation in MES buffer, the relative percentage of events of the QDEM population started to diminish, reaching a minimum of 77% (± 10) events after 5 min. Similarly the relative MFI decreased after 2 min and stayed low with longer incubation times. The diminution of the QDEM fluorescence ranged from 40% (± 16) to 28% (± 10).

Incubation in imidazole demonstrated a low significant decrease of fluorescence after 2 h of incubation (~5% ± 2). The relative percentage of events decreased of ~10-15% (±10-21) at 15 min and continued to fall until 2 h (left side of the Figure 2.17). The fluorescent intensity of the bead was significantly lowered (23% (± 10)) when incubated with MES buffer whereas imidazole buffer showed a smaller impact on QDEM fluorescent code stability (5% ± 2). The dispersion of the error bar of the relative percentage of events for the time range of 15 to 120 min in imidazole indicated that the decrement of population was not significant in comparison with the control population (time 0). The comparison with the relative percentage of events recovered after incubation indicated a ~20% difference between MES and imidazole. QDEMs presented higher instability in MES buffer than in the imidazole buffer. These results also showed a reduction of the QDEM fluorescent intensity in parallel of the reduction of the number of the microsphere recovered after incubation with MES.

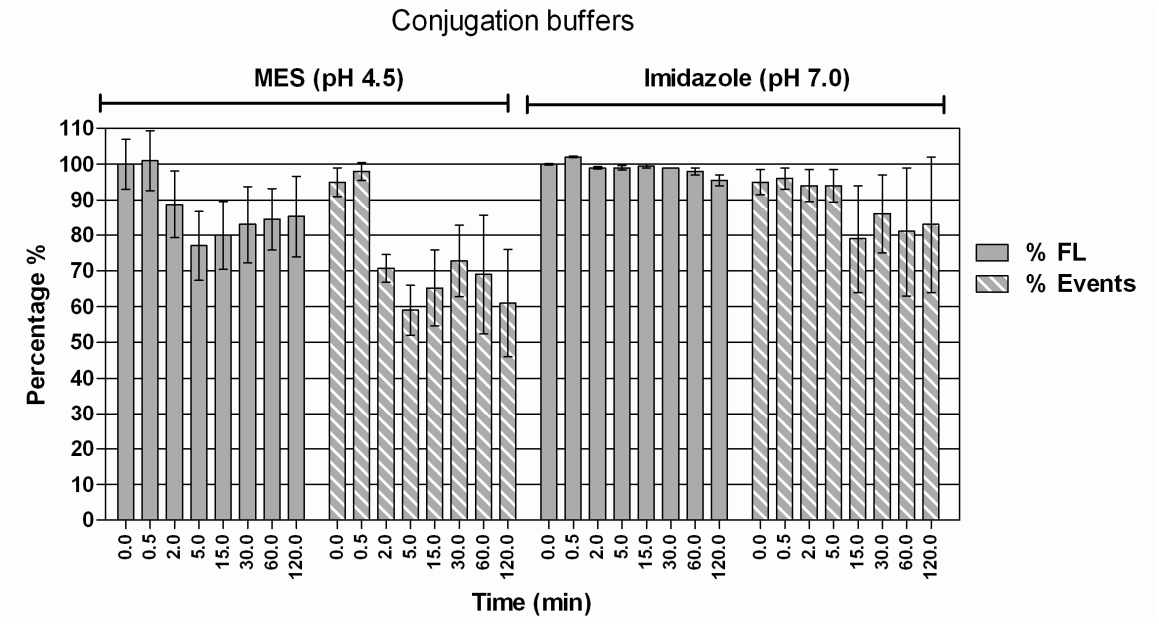

Figure 2.17 Chart representing the relative number of events and the relative MFI (in % ± SEM) versus time (in min), detected on 525QDEM population incubated in MES and imidazole.

Data are presented as the mean ± SEM; % FL: percentage of fluorescence; % Events: relative percentage of events.

Hybridisation conditions

Figure 2.18 reports the variation of the percentage of events and of the fluorescent code of 525QDEM incubated over time with TMAC (Figure 2.18A) and SSC (Figure 2.18B) hybridisation buffers. The temperature and the range of time were representative of the conditions used in bead-based assays for oligo detection (Table 2-2). A global decrease of the percentage of fluorescence and events is observed in Figure 2.18A, for both 1.5X and 2.X TMAC tested buffers. First, an immediate drop of the percentage of events is observed after 2 min reaching respectively 78 and 72% (±8-10). A decrease of ~13% of fluorescence is observed after 5 min incubation with 1.5X TMAC. After 2 h only 66% (± 20) of the initial 525 nm emission is detected in half of the initial population. The negative impact of 2X TMAC buffer on QDEM fluorescence is detected after 15 min with a diminution of 1-2%. After 2 h only 48% of the initial 525 emission is detected in less than half of the initial bead population. In Figure 2.18B, the percentage of fluorescent globally decreased from 30 min to 90 min for both 3X and 6X SSC buffers. The tendency of the percentage of events is less obvious. The variations of percentage of events follow the variations of the percentage of fluorescence with 3X SSC buffer, but not with 6X SSC. The recovery of the bead was higher with the less stringent buffer at 45°C, whereas no significant difference of percentage of events was observed between the two buffers at 55°C. Likewise, the decrease of the percentage of MFI was higher and faster at 45°C with 3X SSC, whereas the decline of the fluorescent was comparable between 3X and 6X SSC buffer at 55°C for both incubation time.

The first global comparison of the graph A and B in Figure 2.18 revealed a higher negative impact of TMAC buffer on both the percentage of fluorescence and the percentage of events in comparison with SSC hybridisation buffer.

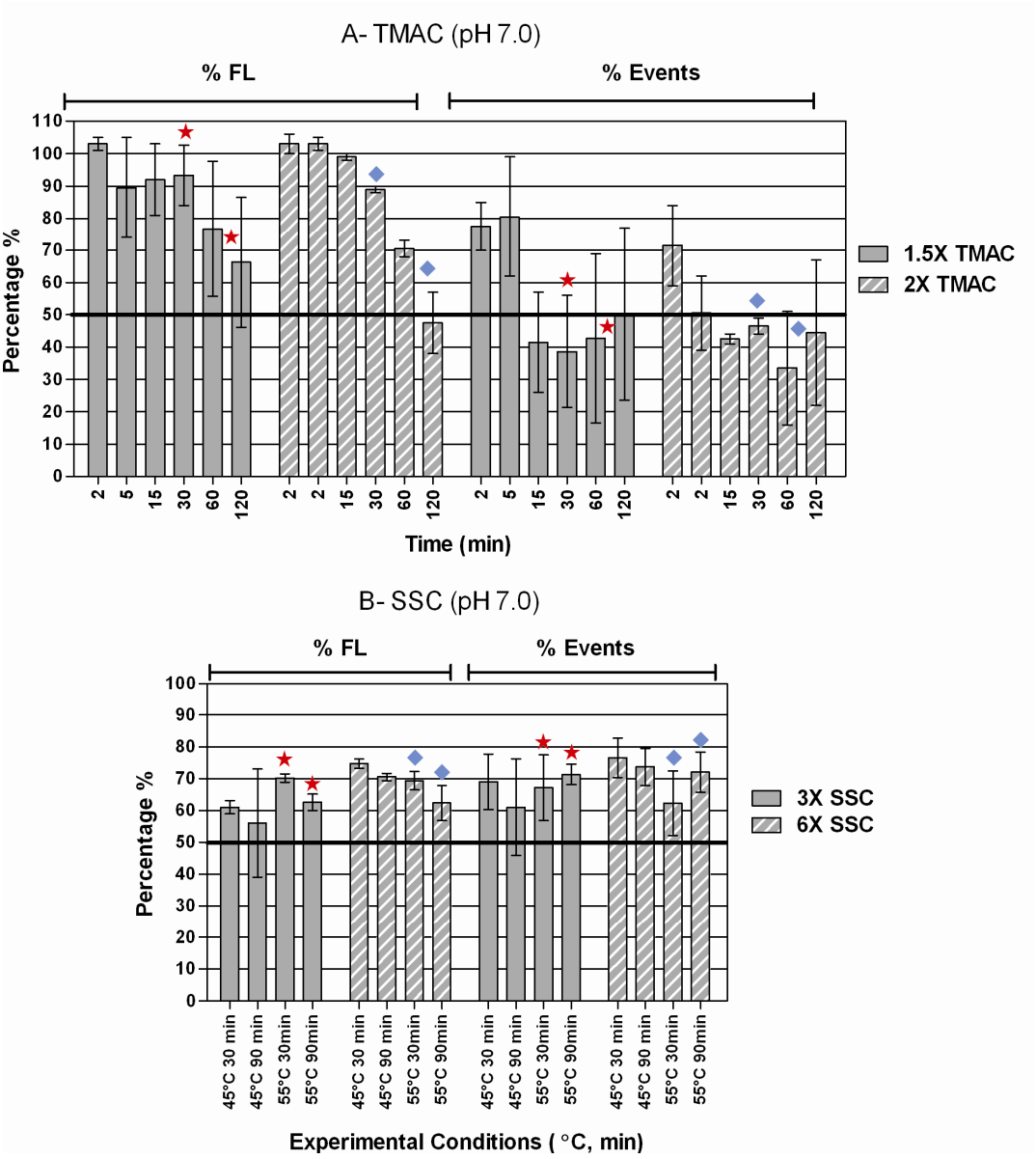

Figure 2.18 Chart representing the relative number of events and the relative MFI (in % ± SEM) versus time (in min), detected on 525QDEM population incubated in hybridisation buffer over a time range of 0 to 120 min.

A: Incubation with 1.5X and 2X TMAC buffer (0 to 120 min at 55°C); **B**: Incubation with 3X and 6X SSC buffer (30 and 90 min at 45°C and 55°C); % FL: percentage of fluorescence; % Events: relative percentage of events; Comparison points at 55°C between (★) high stringent hybridisation buffer (1.5X TMAC and 3X SSC) and low stringent hybridisation buffer (◆) (2X TMAC and 6X SSC) in the same range of incubation time (30 min, and between 60 to 120 min); the horizontal bar corresponded to the 50% limit on the y-axis graph of the percentage of events.

The mean of the percentage of events at 55°C was calculated between 1.5X and 2X TMAC buffer at 30 min and 90 min. The same calculation was performed for the percentage of fluorescence. The means was also calculated for the data obtained with 3X and 6X SSC buffer (Table 2-5).

Table 2-5 Mean of the percentage of fluorescence and events detected with TMAC and SSC buffers at 30 and 90 min *

	% FL		% Events	
	★	◆	★	◆
MEAN (~) ± SD	30 min	90 min	30 min	90 min
SSC	70 ± 2	62 ± 3	65 ± 7	72 ± 4
TMAC	92 ± 5	48 ± 1	66 ± 8	39 ± 8

* Comparison points at 55°C between high (★) and low (◆) stringent hybridisation buffer

Although the mean of percentage of fluorescent is 18% higher, the mean of the percentage of events is similar for TMAC and SSC hybridisation buffers after 30 min of incubation at 55°C. After 90 min, SSC buffers presented a mean percentage of fluorescent superior by 14%, and a mean percentage of events superior by 33% to the mean values obtain with TMAC. The significant effect of the hybridisation conditions on the QDEM stability in the time scale usually expected for bead-based ssDNA detection assays was demonstrated in Figure 2.18.

The results presented Figure 2.18 and in Figure 2.19 showed a significant effect of the hybridisation conditions on the QDEM stability in the time scale usually expected for bead-based ssDNA detection assays. These results showed that the more stringent the buffer, the stronger was the negative effect on the microspheres. The SSC buffer presented the higher rate of bead recovery with the highest fluorescence emission over time compared with the TMAC buffer. SSC buffer were therefore considered as the most suitable buffer to develop a QDEM hybridisation assay. The temperature also played an important role on the QDEM stability, dependent on the time of incubation.

Washing conditions

Figure 2.19 illustrates the variation of the percentage of events and of the fluorescent code of a 525QDEM population incubated at RT, over time in SDS and Tween-20 coupling washing solution, and in SSPE hybridisation washing solution (Table 2-2). A continuous loss of fluorescence was observed over time (0.5 to 120 min) in the different washing solutions. The percentage of events decreased simultaneously. The decline of the relative percentage of fluorescence was greater and faster with the Tween-20 solution than with the other washing solutions: after 5 min incubation with Tween-20 only 74% (± 10) of fluorescence was detected whereas 95% (± 2) and 99% (± 1) was detected with SDS and SSPE solutions. The strongest effect on QDEM is observed after 2 h incubation in SSPE buffer: 26% (± 10) of the fluorescence is detected in 54% (± 10) of the bead population. The effect of SSPE washing solution was also tested at 55ºC (Table 2-1). The increase of the temperature during the incubation conducted to a higher and faster diminution of the QDEM fluorescence and the percentage of events (Appendix G). The results of the experiments presented in Figure 2.19 were taken as a model to define the general behaviour of the QDEM towards detergent solutions.

- **Impact of the temperature**

Figure 2.19 reported the variation of the percentage of events and of the fluorescent code of a 525QDEM population incubated in TE buffer at different temperatures (20-25°C, 55°C, and 72°C). After 2 h incubation no significant variations of MFI were noticed at 20-25°C and 55°C, while a significant decline of the bead population was observed (dropping of ~20% (± 9-11)). The most dramatic effect was reported at 72°C, with the decrease of ~80% (± 3) of the MFI after 2 h and ~50% (± 26) of relative percentage of events recovery.

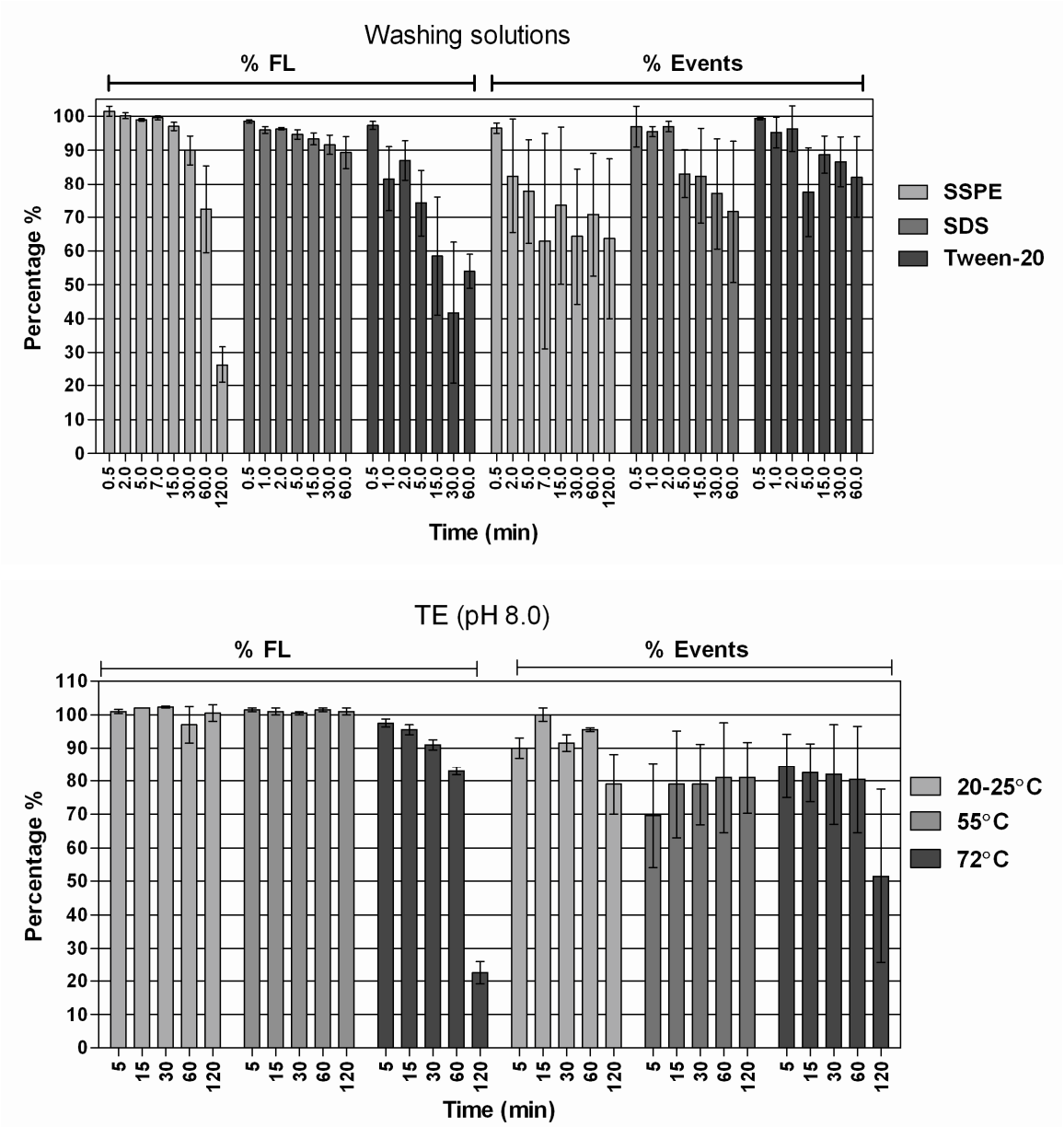

Figure 2.19 Chart representing the relative number of events and the relative MFI (in % ± SEM) versus time (in min), detected on 525QDEM population incubated in SSPE, SDS and Tween-20 washing solution over a time range of 30 s to 60 or 120 min (A) and in TE at RT, 55°C, and 72°C over a time range of 5 min to 120 min (B). % FL: percentage of fluorescence; % Events: relative percentage of events.

- **Batch-to-batch variations study**

The variations between manufactured batches of QDEMs were investigated. The first results obtain on QDEM stability in conjugation buffer in Figure 2.17 were obtained with the first batch of QDEMs, *i.e.*, Lot 1, purchased from the supplier (Crystalplex, USA). This population was encoded with high intensity of 525QDs and was used to perform the majority of the test-experiments presented in this study. The data obtained with Lot 1 (Figure 2.17) were compared with the results reported in Figure 2.20A, obtained with Lot 2: a new batch of 525QDEM (green spectra) purchased 1 year and a half after Lot 1, encoded with a lower concentration of 525 nanocrystals but that had higher quantum efficiency (personal communication with J. Crawford, Crystalplex, USA). The MFI detected (time 0) with the initial 525QDEM population of Lot 1 was approximately 15% superior to the MFI of Lot 2. Lot 3 represented a batch purchased at the same period of time that Lot 2, encoded with high intensity of 575 nm nanocrystals (yellow spectra). This Lot was used to validate the observations made on 525QDEM with another type of encoded colour bead.

Lot 2 showed a diminution of the percentage of fluorescence and the percentage of events that did not exceed 11% from 7 min to 120 min in MES. The percentage of fluorescence was stable in imidazole, whereas the percentage of events showed a diminution < 10% along the time scale. The percentage of fluorescence and of events was stable over time in MES for the 575QDEM in Figure 2.20. A low continuous decrease of the 575QDEM percentage of fluorescence was observed in imidazole. After 2 h the initial fluorescence declined of 6.5% (± 0.5). The percentage of events of the 575QDEM population stayed above 90% over time both in MES and imidazole.

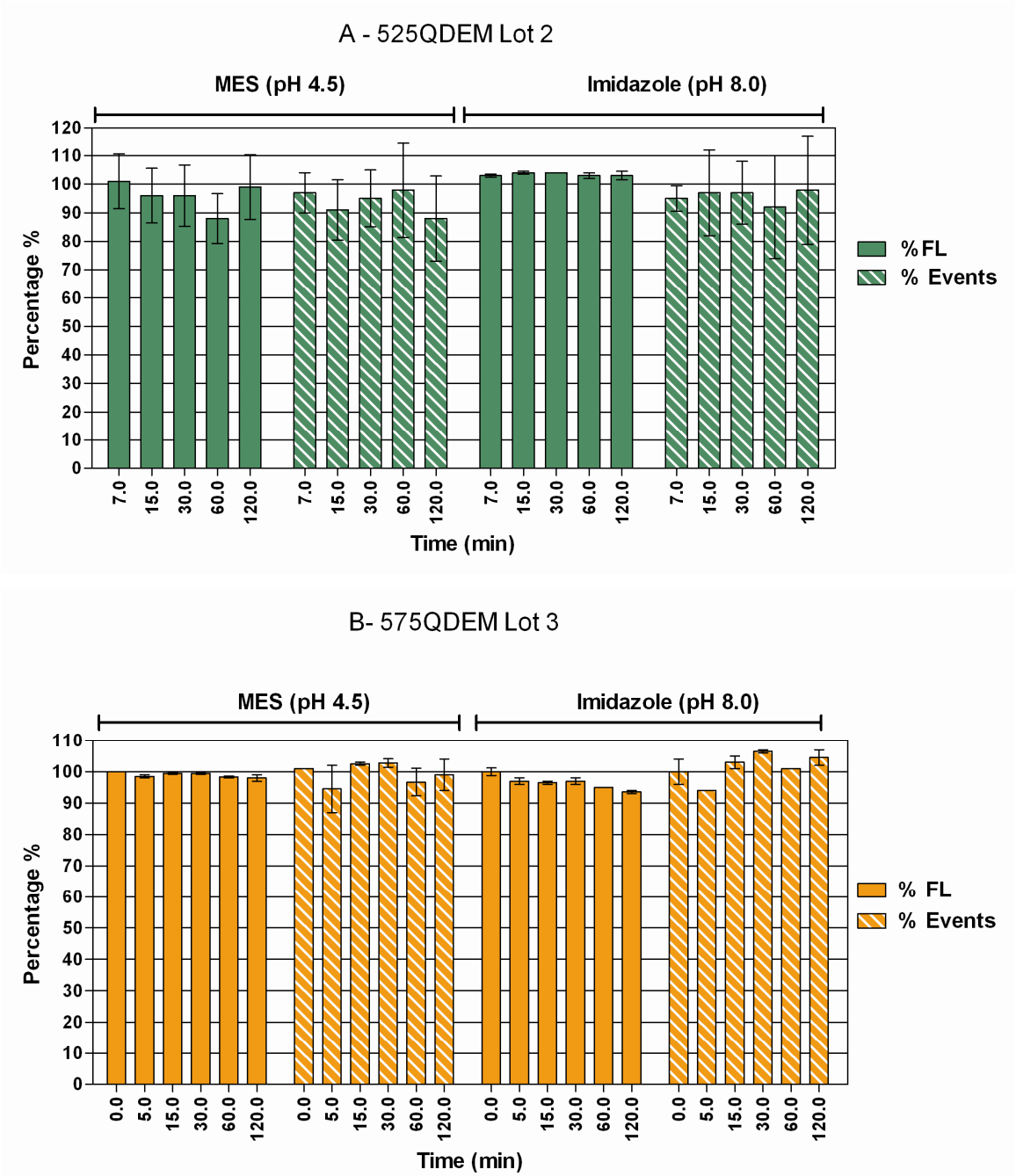

Figure 2.20 Chart representing the relative number of events and the relative MFI (in % ± SEM) versus time (in min), detected on (A) 525QDEM Lot 2 and (B) 575QDEM Lot 3, incubated in imidazole and MES at RT over a time range of 0 to 120 min.

% FL: percentage of fluorescence; % Events: relative percentage of events. To facilitate the interpretation, and illustrate the different population code, graphs are coloured in green (525 nm QD emission wavelength) and in yellow (575 nm).

The mean of the percentage of fluorescence and events was calculated over time for MES and imidazole experiments for the three QDEM populations tested. The results were presented as the mean of all the time point ± SD (Table 2-6). Table 2-6 resumed the average impact of the buffers over time on the different lot of QDEM tested. The fluorescence and percentage of events of 525QDEM Lot 1 were, on average, lowered in MES, (respectively by ~18% and 38%) compared with Lot 2 (~4 and 6%) and Lot 3 (~1 and 2%). In imidazole, Lot 1, 2, and 3 presented a similar fluorescence mean average over time. However, the percentage of events declined over time (decline of ~16%) in Lot 1, compare with the other Lot that were stable.

Table 2-6 Mean of the percentage of fluorescence and events detected in MES and imidazole over time (0 to 120 min), for 525 (Lot 1 and 2) and 575 QDEMs (Lot 3).

	MES		Imidazole	
MEAN (~) ± SD	***% FL***	***% Events***	***% FL***	***% Events***
525 Lot 1	82 ± 3	62 ± 3	98 ± 2	84 ± 6
525 Lot 2	96 ± 2	94 ± 2	103 ± 0.3	96 ± 1
575 Lot 3	99 ± 1	99 ± 1	97 ± 1	102 ± 2

These results first confirmed the higher sensitivity of QDEMs to MES compared with imidazole observed in previous results (Figure 2.17). Lot 2 and 3 presented on average a higher percentage of fluorescence and of events over time in conjugation buffer. No differences were observed between the different colour QDEM populations recently manufactured. A period of time estimated of 10 months separated the first experiment performed with the 525QDEM Lot 1 stock solution and aliquots and the other QDEM Lot.

- **Confocal imagines of treated and untreated QDEMs**

Figure 2.21 presents the effect of 575QDEM incubation in imidazole and MES over time. The fluorescent profiles of four treated beads (Figure 2.21B, C) were compared with the untreated bead (Figure 2.21A). The fluorescence was regularly distributed and localised toward the external surface of the microsphere (Figure 2.21A). The four treated bead exhibited distinctive fluorescent profiles from the control. Two microsphere with a low fluorescent hallow were detected in proximity to a 575QDEM emitting a brighter spectra (Figure 2.21A). Two disruptions points in the fluorescence profile, localised in the external surface of the bright 575QDEM are pointed out by the red arrows on the picture. The 575QDEM in Figure 2.21C also shows a point of disruption in the microsphere structure. The shape of the microsphere was no longer spherical and the intensity of the distribution of the fluorescence in the structure is more diffuse in comparison with the control.

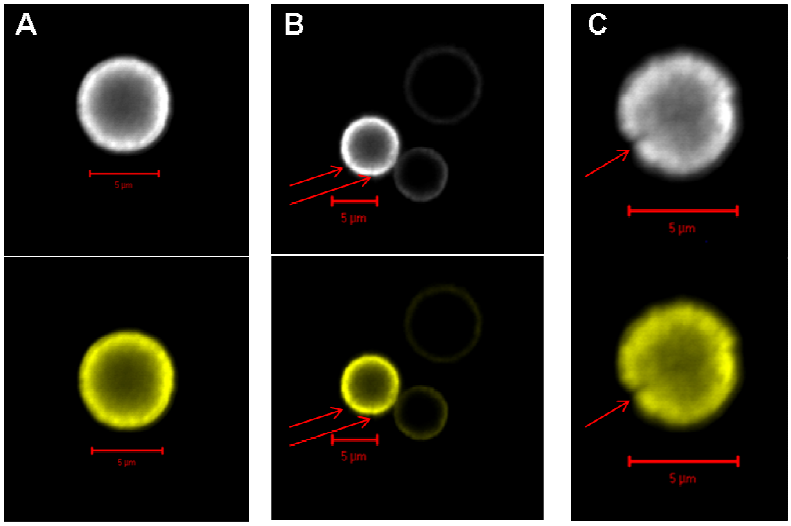

Figure 2.21 Confocal images of 575QDEMs.

A: 575QDEM control population (t = 0 min); **B**: Typical images of 575QDEM after 24 h incubation in imidazole; **C**: Typical images of 575QDEM after 24 h incubation in MES; 5 µm scale bar indicated in red; top imagines: range indicator; bottom imagines: colour detected in channel 2; imagines were taken under the same gain and voltage with a 530-600 nm BP filter; The red arrows indicated abnormalities of the fluorescent profiles compared with the control.

The Figure 2.22 presented confocal imagines of 525QDEM before (A) and after (B) treatment with conjugation experimental conditions. The control (Figure 2.22A) presented a similar profile as the control observed in Figure 2.21A. A difference of intensity was observed between the 525QDEM after 15 min incubation in MES and the control population (Figure 2.22C). After 30 min incubation in imidazole, the polystyrene structure of the microsphere appeared broken and cracks were visible under confocal microscopy (Figure 2.22C). The 525QDEM still emitted fluorescence but with a lower intensity than the control.

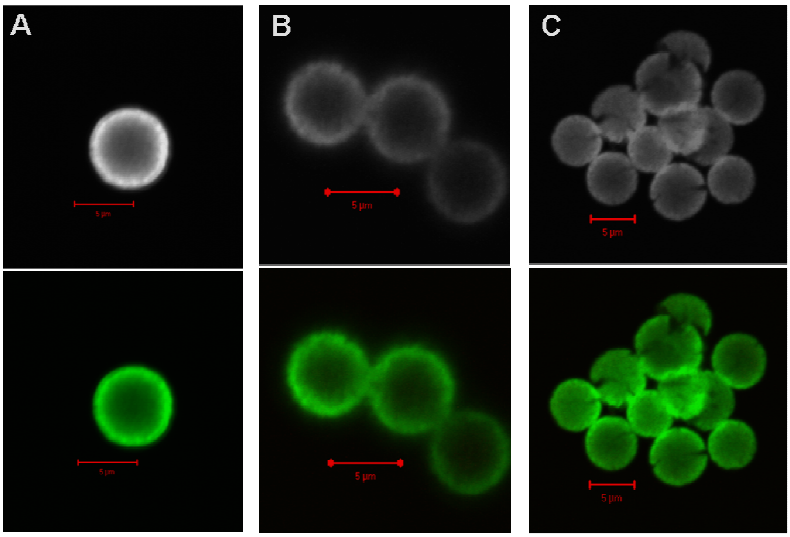

Figure 2.22 Confocal images of 525QDEM

A: 525QDEM control population (t = 0 min); **B**: Typical images of 525QDEM after 15 min incubation in MES; **C**: Typical images of 525QDEM after 30 min incubation in imidazole; 5 µm scale bar indicated in red; top imagines: range indicator; bottom imagines: colour detected in channel 1; imagines were taken under the same gain and voltage with a 505-530 nm BP filter.

2.4. Discussion

2.4.1. Structural characteristics of TriLite™ QDEM commercialised solutions

The characterisation of the CdS_xSe_{1-x}/ZnS core/shell nanocrystal-encoded porous polystyrene/methacrylate carboxylated microspheres, or QDEMs (Crystalplex, PA, USA) was undertaken to evaluate the chemical and fluorescent properties of the material (Figure 2.1). The understanding of the reactivity and the sensitivity of this new technology was essential for the development and the optimisation of a suspension array assay. QDEMs were obtained from the first and unique suppliers (Crystalplex, PA, USA) found to provide a large panel of fluorescent code microspheres that have a size adapted for analytical bioassays (5 µm diameters bead). The quantification of the QDEM solution indicated that the handling from 1 mL glass vial to 1 mL plastic tubes could generate 15% up to 60% of QDEM loss (Section 2.3.1). QDEM solutions shipped in containers ready to be used in routine bench-work laboratory would avoid this drawback.

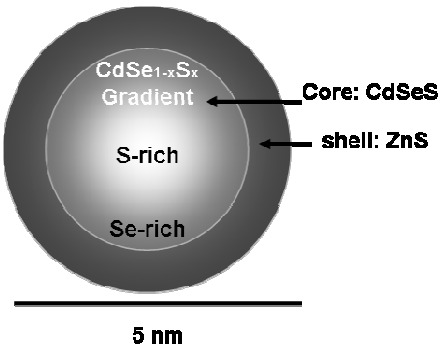

Figure 2-1 Schematic representation of TriLite™ nanocrystals composition (reprinted).

The first observation on QDEM control populations under scanning electron microscopy (SEM) revealed no differences between non encoded and encoded microspheres. The surface morphology and topography show the asperity of the bead surface, which indicated the porous nature of the beads (Figure 2.3 to Figure 2.6). The main components detected with the chemical analysis of QDEMs were carbon and oxygen elements, which corresponded to the main elements that compose the chemical formula of carboxylated polystyrene/methacrylate structures. The solid surface where the sample were analysed, *i.e.*, aluminium and silicon, were also detected with a high level. A higher content of aluminium was detected with deep spectral analysis than with superficial analysis, which confirmed the good penetration of the electron beam (Figure 2.9A).

The presence of cadmium and selenide (Cd, Se) in the proportion of respectively 0.44% and 0.06% illustrated the detection of the main elements composing the core of the TriLite™ nanocrystals in the 20 µm diameter QDEM encoded with 525QDs (Figure 2.9B). The alloy nanocrystals were synthesised in cadmium rich conditions with gradient of CdS_xSe_{1-x}, which explain the high proportion of Cd and S, and the detection of traces of Se (Dabbousi *et al.*, 1997; Maier *et al.*, 2007). The absence of the main elements of the core materials (Cd and Se) in 5 µm diameter 525QDEMs indicated that QDs were preferentially detected when the diameter of the QDEM was 20 µm diameters. The higher concentration of QDs in microspheres with larger sizes facilitates the detections of QDs elements with the SFEG instrument. Zinc and sulphur (Zn, S) elements were detected in all the samples analysed. The qualitative analysis showed that these elements participated to the composition of the microsphere matrix with a Zn/S ratio of 70/30 (Table 2-4). The composition of the blank QDEM presented on average a similar level of zinc and sulphur composites than the encoded microspheres. These elements composed the protective and sealant coating applied to the microspheres after encoding but also applied to non encoded beads. The 50/50 ratios found with 20 µm diameter 525QDEM corresponded to the enrichment in S due to the presence of CdS_xSe_{1-x} nanocrystals detected with SEFG in the larger beads.

The detection of chloride, copper or calcium (Cl, Cu, Ca) was interpreted as the presence of residual contaminants left during the synthesis of the polymers composing the microspheres. Polymerisation of methacrylate on polystyrene bead surface is enhanced by the addition of metallic catalysts to obtain size and weight distribution uniformity. Contaminants coming from these catalysts can be trapped in the pore of the microspheres during synthesis and depending on the level of purification of the polymers, traces can be found when using accurate method of detection as the SFEG instruments. The presence of these elements was considered to have no significant effect on the beads reactivity.

The same chemical process of protective coating was applied to the microsphere surface of all the different QDEM populations so they would be no differences between encoded beads and beads lacking of nanocrystals (personal communication with J. Crawford, Crystalplex, USA). Blank beads are preferably used for the optimisation process of chemical reactions, *i.e.*, bioconjugation, since they are the less expensive materials to work with. The observations of similar structural aspects and chemical composition between non encoded and encoded beads are an essential result to enable the comparability of empirical tests run with blank beads and encoded beads. These results also support that the observations made on one population could be extrapolated to other QDEM populations.

The carboxylation coverage of microsphere was therefore calculated with blank beads. The thermo-sensitivity of carboxylated microspheres is dependent on the ionization (COOH/COO-) of the carboxylic groups. QDEM with low exchange capacity (low carboxylic group coverage, *i.e.,* <0.5 meq/g are thermo-sensitive both in the protonated and deprotonated form of (COOH) group. At higher exchange capacity, *i.e.,* >2 meq/g, the microspheres are mostly not able to swell in the protonated form and swell extensively in the ionized form (up to twenty-eight times), losing therefore their thermo-sensitivity properties (Fundueanu *et al.*, 2008). QDEM of 5 µm diameter presented a (COOH) coverage of ~26.3 µeq/g, which indicated thermo-sensitive properties and that the modification of their surface ionisation should not have a major impact on their structural behaviour in solution.

Preliminary results of beads composition and structural aspects identified the main differences between population as the level of encoding which was thus detected and analysed through photoluminescence characterisation.

2.4.2. Optical characterisation of TriLite™ QDEM solutions

Fluorescent profiles sectioning of a green photoluminescence (PL) 525QDEM population after long term storage and middle speed vortexing for resuspension showed that QDs preferentially localised close to the surface of the polystyrene microsphere (Figure 2.10A). These first set of observations of the QDEMs PL fluorescence matched the observations reported in the literature that after encoding using the swelling method, QDs mainly localised toward the exterior of the microsphere. Gao *et al.* (2001) reported that under confocal microscopy QDs were preferentially located in the outer 25% of the polystyrene microspheres' radius, a similar spatial distribution to organic dyes in polystyrene beads. Approximation of the PL distribution show similar results (33%) (Figure 2.10). Sectioning and 3-dimensional images confirmed that the differences observed in the fluorescence distribution in the microsphere structure were specific and not an artefact due to differences in the position of the optics in the z-axis or due to differences in the sectioning. (Figure 2.10 and Figure 2.11).

Hydrophobic QDs (coated with TOPO ligands, section 1.1.3) are trapped into the pores of the polystyrene microsphere by hydrophobic interactions. The penetration depth of the QDs in the porous microsphere is dependent on the level of porosity of the bead matrix. Gao *et al.* (2004) reported that QDs penetration was limited to 10-20 nm below the surface, in microspheres that have low porosity and are sealed by a dense layer (~300 nm) on the surface. On the other side, QD-doped polystyrene microsphere with mesoscale 2-50 nm pores sizes (mesoporous beads) showed uniform fluorescent signals across the internal areas of the beads illustrating the uniform penetration of QDs in the bead's interior. However, it is possible to achieve the same distribution by changing the extent of the microspheres swelling in solvent mixtures (Bradley *et al.*, 2005). The presence of a

methacrylate layer increasing the density of the polystyrene bead's surface is in accordance with the 3-D sectioning and PL profiles observed in Figure 2.11A. The QD localisation is also therefore typical of limited penetration of QDs in a microsphere with a low level of porosity. These results show that nanoparticle penetration could be used to explore the internal porosity structure of microspheres with confocal microscopy (Bradley *et al.*, 2005). A second set of observations with 525QDEM population after repeated vortexing and sonication showed a modified PL profile, with a diffuse distribution within the sphere (localisation in the outer 53% of the beads radius). The observations reported in this study suggested that sonication could increase the swelling of the 525QDEM and therefore increase the uniform disposition of the QDs within the polystyrene sphere. The formation, growth, and implosive collapse of the bubbles produced by ultrasonic irradiation (sonication) can generate intense shock waves that travel through the liquid solution at the speed of sound (Suslick, 1995). The "bubbles" and shock waves could modify the hydrophobic interactions between QDs and the polystyrene matrix, leading to an alteration of the QDs distribution within the sphere by "pushing around" the QDs in the pores of the polystyrene network. The energy provided by the sonication could also increase the diffusion of the QDs due to the expansion and the contraction of the lattice of the beads. The sonication effect would therefore modify and displace the QDs distribution in the matrix that initially trapped the QDs inside the microsphere after diffusion in the sphere's pores. This model explaining the differences observed is reinforced by the assumption that hydrophobic interactions are easily susceptible to break under mechanical effects (Gao and Nie, 2004). The effects of ultrasound sonication are further discussed later in the text.

The analysis of a selection of multicolour QDEMs from the QDEM library available (Appendix A) illustrated the potential and limitations of the TriLite™ QDEM barcode technology (see introduction). The quantitative doping of the polystyrene microsphere with QDs is achieved by controlling the amount of molar concentration of the different QD's colours in the doping solution. Fluorescence intensity ratios are obtained by modifying the QDs concentration of the different QD's colours.

The results of the multiplex fluorescent code analysis demonstrated that multiple intensity single-colour beads and multicolour beads could be identified under confocal microscopy and flow cytometry analysis with high specificity (Figure 2.13 and Figure 2.14). Higher level of multiplexing where analysed to further test the high throughput potential of QDEMs technology with flow cytometry detection mixing single-colour beads and multicolour beads. The expected 20 fluorescent profiles of a mixture of single-colour beads and multiple-colour beads on the same dot plot illustrate the difference of intensities or ratio of the QDs encoding single- and multiple-colour beads (Figure 2.15).

The association of one-colour bead with four-colour beads was successfully plotted using FC analysis but the resolution of the QDEM fluorescent barcode identification was higher using a computational tool such as PCA (Figure 2.16). Both Dot-plot analyses and PCA representation of the average MFI of the QDEM samples showed that high intensity single-colour QDEMs had a specific fluorescent signature, isolated from the rest of the QDEMs tested. Other low intensity single-colour QDEMs (630QDEMs and 665QDEMs) were grouped with the four-colour beads and spectral overlaps of fluorescent profiles were observed (665QDEM and 0011QDEM). QDEM technology does not exclude the potential overlap of QDEM fluorescent code in multiplex assays with FC analysis. Therefore, the specific identification of four-colour QDEMs simultaneously with one- and two- colour beads showed the relative specificity of QDEM codes identity for suspension array technology (SAT) (Figure 2.14 and Figure 2.15). A limitative step in the development of SAT is the development of FC protocol that allows the discrimination of multiple QDEM fluorescent codes. The results presented in this study illustrate that automated identification of fluorescent code is required to facilitate and accelerate the QDEM multiplex SAT analysis. Wu *et al.* (2002) reported the development of a prototype instrument for decoding paramagnetic QD-doped beads directly in the wells of high-density microplates with the adaptation of a commercial instrument to read and decode 24 spectral barcodes (three-colour beads with different intensities). However, this prototype is limited to plate reader format. FC offers the advantage of single particle signature analysis with higher quantitative and multiplex capabilities than plate reader.

Current QD technology research needs to focus on the development of analytical tools adapted to the specific identification of multiple QDEMs fluorescent signatures. A research project that offer promises for the development of analytical software adapted to QDEM multiplex experiment was undertaken in relation with the research presented in this thesis using Crystalplex QDEMs (Clarke *et al.*, 2005). This work aimed to evaluate conventional statistical methods as a support for the detection of 16 unique QDEMs using the same standard flow cytometer (Coulter Epics XL-MCL, Beckman, USA) (Clarke *et al.* under revision). The report presented a promising support vector machine learning approach for the identification of QDEMs from FC data. The model developed by Clarke *et al.* (under revision) showed the accurate recognition of QDEM fluorescent signature classification and sensitivity. Further work is still needed to develop and prove the validity of the model at a higher throughput level.

These results highlighted the challenges and limitations of the application of the QDEM barcode technology to high throughput assays, which leads to several conclusions. First, the detection of multicolour encoding of polystyrene microsphere with QDs needs to improved further. While waiting for these technological improvements, QDEMs encoded in the same range of intensities should be used in multiplex experiment to avoid QDEM signal overlap, and to obtain a high resolution analysis of the fluorescent spectra of the probes as shown in Figure 2.13.

2.4.3. Study of TriLite™ QDEMs in particle-based bioassay conditions

The analysis of QDEM populations under the experimental conditions mostly used for bead-based bioassay was evaluated by the variations of the percentage of events detected and by the changes in the fluorescent intensity signal of the samples compared with the initial population. These series of experiment represented an important first step in the development and optimisation of a QDEMs suspension assay for the detection of ssDNA. The buffers and conditions had to be selected from the various experimental conditions available in the literature on particle-based bioassay.

Two distinguishable phenomena were identified when manipulating the Crystalplex TriLite™ QDEM: (1) a significant decrease of the number of QDEMs detected with the flow cytometer, and (2) a significant decrease of the fluorescence intensity of the QDEM population under study. Resuspension treatments (sonication frequency, vortex intensity), time exposure and the nature of solvents used for microsphere suspension showed to have a significant impact on QDEM stability in solution.

First the images showing the disruption of the microsphere and the visualisation under FC of a significant amount of debris confirmed the degradation of the QDEMs under a majority of the treatments applied (Figure 2.21C Figure 2.22C). Molecular bonds can be disrupted due to ultrasound sonication with sufficient intensity passing through them (Vijayalakshmi and Madras, 2004). The main effects produced by ultrasound sonication are: heat, cavitation, agitation, acoustic streaming, interface instabilities and friction, diffusion and mechanical rupture. All these effects impact on the polystyrene/methacrylate microsphere stability. The impacts of ultrasound sonication are named sonochemical effects. Due to its powerful mechanical and chemical effects, ultrasound sonication has been used in diverse areas including polymerisation, sonochemically-assisted modification of polymer surfaces modification of polyethylene surfaces, cleavage of polymer chains in solution, dispersion of fillers and other components in polymers matrix and finally the encapsulation of inorganic particles with polymers (Shim *et al.*, 2002).

Polymer degradation in solution was reported under cavitation, *i.e.*, the production of microbubbles formed by acoustic pressures (Price and Smith, 1991). Suslick *et al.* (1986) described that each cavitation bubble acts as a localised microreactor which, in aqueous systems, generates instantaneous temperatures of ~5000°C, pressure in excess of about 1000 atmospheres, and heating and cooling rates above 10^{10}K/s (Kelvin/second). This theory named as the 'hot spot' approach explains the energy release involved with cavitation that can cause chemical bond rupture (Suslick *et al.*, 1986). Repeated sonication treatment was therefore considered as the major factor facilitating the degradation of polystyrene microspheres in buffers.

Two main sonochemical effects were found to participate to the disappearance of QDEMs from the initial gate defined with the control QDEM population. Multiple observations under SEM and confocal microscopy confirmed the potential formation of a "neck" between two microspheres of 5 to 20 µm diameters spatially close after resuspension Figure 2.8D, Figure 2.5B, Figure 2.22B). These structures were observed both in the control and in treated samples after vortexing and sonication. These results strongly suggested that this "neck" was composed of polystyrene. The formation of a "neck" has been described before and is more frequent when polystyrene microspheres are in methanol suspension. The formation of these structures could be associated to the agglomeration of particles observed under ultrasonic irradiation. Prozorov *et al.* (2004) described the agglomeration of particles under sonication, highly dependent on particle size. Particles smaller than micrometers and bigger than tens of micrometers were not found to agglomerate because of the insufficient inter-particle collisions. Large particles, corresponding to the 20 µm in our study, were described to weld by collision with smaller particles. These observations were also supported with the property of polystyrene to polymerise under ultrasound effect, which could create polystyrene bridge between two microspheres. These observations could explain mechanically the formation of the neck structures observed in Figure 2.5 and Figure 2.8. The creation of these QDEM "secondary structures" strongly suggested a negative impact on the QDEM detection. The modification of the external morphology and structure lead to the simultaneous detection of the QDEMs in the flow stream of the flow cytometer. As a result, it incurs diminution of the percentage of events and a potential lost of information by losing events, and losing fluorescent reporters. As a conclusion, this phenomenon was described as an observable effect explaining the decrease of the percentage of events of treated samples.

Ultrasound sonication was not only capable of disrupting chemical bonds of the microsphere but was also though to induce re-modelling of the polymer lattices. Sonochemical effects could induce phenomena of extension (swelling) and contraction, disruption of the Zn/S protective shell, and remodelling of microsphere methacryltate coating. These changes could explain as well the decrease of fluorescent intensity observed

during the treatments. The initial sonication and vortexing of the particle to resuspend them, associated to the dilution of QDEMs in a large volume of reagents could wash out the protective layer sealing the microsphere pores to trap the QDs inside the beads of the microsphere and therefore facilitate the leaking of the QDs out of the microsphere lattice. This phenomenon was illustrated by the "ghost" bead observed under confocal microscopy in Figure 2.21B.

Sonochemical changes in the polystyrene matrix associated to sonomechanical forces can induce changes in the distribution of the fluorescence in the microsphere, and induce the redistribution of QDs in the lattice of the polystyrene beads. Sonication effects could provoke higher probability of the QDs to move towards each other and to couple with each other in the beads. QDs aggregation could cause problems such as spectral broadening, self-quenching, and wavelength shifting (Gao and Nie, 2003) leading to a decrease of the global fluorescent intensity of the beads. Fluorescence energy transfer (FRET) could also be produced with QDs spatially close to each other, which would impact on the fluorescence intensity or induce a spectral shift (Gao and Nie, 2004). Further, in the same extent the formation of beads duplets not only change the forward scatter detection of the QDEMs by FC but it can also lead to FRET and quenching of the bead fluorescence close to each other, leading to the decrease of fluorescence intensity codes observed under FC and confocal microscopy. These results provided important information for QDEM application to biological assays. The localisation of the QDs within the particle influence the characteristics of the bead population detected under flow cytometry, and depending on the QDs distribution the emission signal of fluorescent molecules attached to the surface of the microsphere could also be affected (by FRET, quenching, emission or absorption spectra overlap).

No significant variations in fluorescence and QDEMs structural stability were observed between different Lot of manufactured QDEMs. The lower stability of QDEM Lot 1 compared with other Lots was explained by the repeated sonication and vortexing applied to the stock solution to re-suspend the bead. These treatments were necessary to obtain an

homogeneous concentration of QDEMs in the solution and to be able to performed quantitative experiment. The manipulation of Lot 1 QDEM stock solution to prepare aliquots and the repeated use of aliquots showed to have an impact on the overall stability of the beads on the long term.

Gao *et al.* (2003) observed leaching of QDs in chloroform or other non polar solvents, whereas QDs where stable overnight in water or polar organic solvents (*e.g.,* ethanol, acetone). The stability of TriLite ™ QDEMs was tested in polar organic solvents and water (*e.g.,* TE buffers, PBS, Imidazole, MES, and Tween-20). The first step when testing the QDEMs solution was to resuspend the samples by sonication/vortexing repeated treatments (respectively 20 s, 10 s, three times). This step was essential to be able to disperse the beads in solution and to obtain homogeneous concentrations that allow the analysis of the same quantity of beads for each experiment. This treatment was believed to initially weaken the structure of the polystyrene microspheres which would later lead to higher degradation of the structure in the different buffer. QDEMs could therefore be more sensitive to swelling with the diffusion of water molecules and chemical component in the weaken structure leading to a burst of the structure. This theory would explain for example the high degradation of QDEMs in high saline solution as PBS.

The combined effects of the different treatments (sonication, vortexing), time exposure, temperature and the nature of the solvents used for microsphere suspension was believed to have a direct impact on the number of QDEMs recovered with a conserved fluorescent code at the end of the bioconjugation procedure. The long term effects of the manipulation of the QDEMs also have to be considered for the planning of the experiments. The main objective of the empirical tests undertaken in this study was achieved by modelling the behaviour of QDEMs to predict the most suitable solutions and treatments for QDEM SAT bioassays. First, QDEM solutions should be stored in TBS with 1% BSA to maximise the QDEM stability. QDEM stock solutions should be aliquoted once. The stability of aliquots should be checked after repeated exposure to sonication and vortexing for re-suspension. QDEM aliquot solutions should not be used if a decrease of the intensity or a significant number of

debris is observed under FC. TE buffer should be used as running buffer for FC analysis. The pH of storage and reactive buffers should be kept as neutral as possible (~pH 8.0). Imidazole and SSC buffers should be used respectively for conjugation and hybridisation experiments. The hybridisation temperature for bead-based DNA detection assays should be kept as low as possible. Washing solutions and more generally washing steps should be empirically adapted to limit the use of detergent solutions while proving an efficient elimination of non specific binding. An increased number of washing steps performed with low stringent solutions, such as TBS storage buffer and TE solution could be an alternative for efficient washing while limiting QDEM instability.

These empirical data on the bioconjugation treatments and procedures were crucial to optimise the recovery of conserved QDEMs and to progress to the optimisation of oligo probe attachment to the QDEM surface. Important observations on the QDEM structure and reactivity were described which represented a significant contribution to the understanding and the evaluation of the potential use of QDEMs for suspension array platforms applied to biological applications.

Chapter 3

TriLite™ Quantum Dot-Encoded Microsphere Bioconjugates

3. TriLite™ QUANTUM DOT-ENCODED MICROSPHERE BIOCONJUGATES

3.1. Introduction

Flow cytometry (FC) technology is based on the general approach of performing sensitive multiparameter optical measurements in a flowing stream. The development of a new set of fluorescent-encoded microspheres has been a key factor in the wide application of FC technology for molecular analysis and measurements using microparticles as a solid support. As mentioned previously, fluorescent bead technology (Luminex Inc., USA, Chapter 1) now allows the discrimination of 100 different microspheres, similar in function to planar microarray, but in the latter case a single microsphere is used as a single element or "spot" of the array in a two dimensional space. Traditional planar DNA microarrays (or DNA chips) are highly efficient methods to analyse in parallel a high number of molecular targets from a single sample, but are not adapted to large scale samples analysis. Each array has the capacity to screen hundreds to thousands of markers for one sample at a time. The preparation and the measurement analysis of one array measurement is highly time consuming, therefore the analysis of series of samples is not time efficient. In contrast, suspension array assays offer higher level of serial analysis, with high speed fluidic detection (Nolan and Sklar, 2002). A need for multifunctional polymer particles with tailored surface properties has therefore been growing in the pharmaceutical industry, in medical diagnostics, and in biotechnology, molecular biology, or analytical sciences. As a result, microparticles of functionalised polystyrene-, PMMA-, silica-, and melamine resin particles have been developed and commercialised for these applications. The research field of nucleic acid sequence detection and sequence analysis is one of the scientific field that has particularly benefit from the development of suspension array technology, with optically encoded microspheres associated to FC detection (Salas *et al.*, 2008).

DNA sequence analysis mainly involves the study of variations in the nucleic acid sequence, and especially single nucleotide polymorphisms (SNPs) detection. The combination of the high level of multiplexing of optical encoded microspheres associated with the high level of serial analysis of FC instruments makes suspension array technology a more suitable format than flat microarray for applications such as disease diagnostics, drug discovery, bacterial identification and forensic analysis. The first step in the development of a microsphere array for nucleic acid analysis is the functionalisation of the microsphere surface with nucleic acids or oligonucleotides (oligos) to obtain fluorescent probes. The nucleic acids are mostly synthetic oligos. Acid nucleic sequences do not naturally contain any reactive sites (*e.g.*, primary amines, sulfhydryls, carboxylates, or phenolates) and are not naturally reactive with the majority of the common bioconjugate reagents. As a consequence, oligos need to be modified for their conjugation to a fluorescent probe or microsphere. Chemical and enzymatic techniques can add a functional group or a label to an individual nucleotide, by derivatisation through discrete sites on the bases, sugars, or phosphates groups that comprise the nucleic acid. Modifications are usually placed on the 5'-end of the oligonucleotide sequence since it is easier to incorporate the modification in the last step of the automated process of oligo synthesis (synthesis from 3' end to 5' end). Factors, such as steric inhibition, electrostatic repulsion, and binding kinetics influence the hybridisation efficiency. Highly active bioconjugates, therefore, generally require a longer distance between the oligo and the point of attachment on the solid surface to produce sensitive hybridisation assays that quantify and/or identify the binding of the oligo to its complementary single-strand DNA (ssDNA) in complex mixtures. The inclusion of multi-carbon linker or spacer was reported to improve hybridisation efficiency to solid surface, though the degree of improvement varies (Nolan and Mandy, 2006).

Oligos have been immobilised on various solid surfaces (*e.g.,* glass, ceramics, silicon, magnetic beads, nylon, polymers and membranes) through non covalent interaction such as physical adsorption or entrapment, affinity binding interactions, and covalent conjugation (chemical binding). Adsorption interactions are mostly adapted for attachment on glass

surfaces and present a relative lack of stability (Sklar *et al.*, 2007). Since current commercialised quantum dot-doped particles (QD-doped) are polymer-based beads, the adsorption method was not considered as suitable for the development of DNA-QDEM bioconjugates. Affinity tag interactions (*e.g.,* biotinylated oligos/streptavidin) are generally strong and specific, but not as stable as covalent binding. Furthermore, they usually incur more non specific binding on the targeted solid surface (Hermanson, 2008). The covalent DNA binding to solid surfaces has been demonstrated to be superior to other methods in terms of stability, specificity, reproducibility and repeatability of the bioconjugation and to improve the hybridisation efficiency signals obtained with DNA bioconjugates (Douglas and Monteith, 1994; Dugas *et al.*, 2004). Covalent attachment was described as the best strategy to attach DNA to any type of microsphere using a single point of attachment, preferably at the 5' end or 3' end of the oligo sequence. A variety of functionalities (Figure 3.1) can be used to covalently couple biomolecules to microsphere through the appropriate chemical reactions corresponding to the chemical nature of the group (carboxyl coupling, amino coupling, maleimide coupling, and so forth) (Wong, 1991; Hermanson *et al.*, 1992).

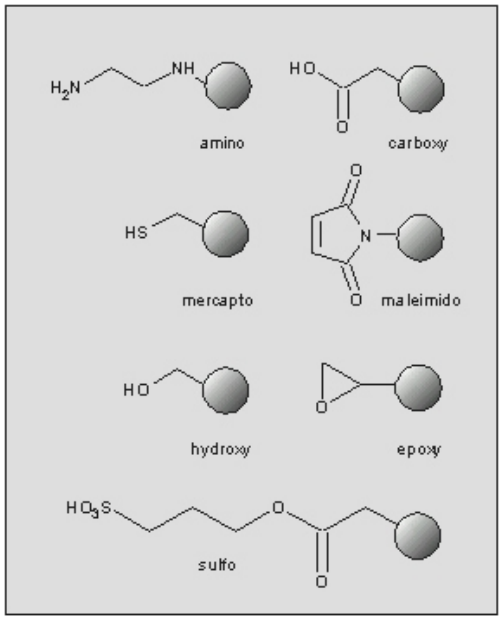

Figure 3.1 Typical polystyrene microspheres surface functionalities (MicroParticleGmBh, March 2008).

The carboxylation provides covalent attachment through a functional group added during the last step of oligo synthesis (on the 5' end) to maximise bioconjugation stability and efficiency. It also insures that only full-length oligos are attached to the polystyrene QDEMs. Carboxylated particles can then be conjugated to amine-labelled oligos. The most frequent reaction strategy in suspension (aqueous) format involves a two-step coupling process using 1-ethyl-3-(3-dimethylaminopropyl)-carbodiimide (EDC) and *N*-hydroxy-succinimide NHS or sulfo-NHS to form an amide bond. Sulfo-NHS facilitates the reaction through a sulfo-NHS ester intermediate, which has a higher reactivity for the amine coupling than the initial EDC-reactive ester (Appendix I). The two-step reaction enhances coupling and provides an improved control of each step in the process. This is advantageous as it avoids the formation of microsphere clusters and the cross linking of the ligands itself. This reaction is called carbodiimide coupling, which occurs between carboxylated microspheres and amino-modified oligos (Nakajima and Ikada, 1995).

Microspheres, in the size range of three to fifteen microns, coated with carboxyl groups have previously been used in suspension array platforms for immunoassays and genetic analysis (Salas *et al.*, 2008). Suspension array technology (SAT) has been applied to identify and quantify ssDNA by carbodiimide coupling of carboxylated microspheres to specific oligos (Lowe *et al.*, 2004; Hanley *et al.*, 2007). This method was especially adapted to allele-specific oligonucleotide (ASO) hybridisation assay for single nucleotide polymorphism (SNP) genotyping (Fulton *et al.*, 1997). To date, the Luminex platform™ (Austin, TX, USA) represents the most advanced commercial SAT on the market and uses a duo of organic dyes to encode a 100 bead library composed of 5.6 micron-sized polystyrene microspheres. However, this method is limited since it depends on multiple excitation spectra and is restricted by the overlapping emission spectra of organic fluorophores. The detection method is restrained to the Luminex 100™ analyser, a simplified version of a flow cytometer instrument, which requires the use of two lasers: one to excite the beads and one to excite the reporter dye attached to the bead (Dunbar, 2006). The Luminex platform™ incurs high costs and reduces the flexibility of the bead-based assay since it prohibits the enlargement of the number of fluorescent codes. The other ASO

methods available employ organic dyes, and are highly time consuming, costly and/or not adapted to multiplex analysis (Kim and Misra, 2007). The unique optical properties of QD-doped particles previously described (section 1.1.2) represent an advance in fluorescent bead technology that offers promise for the improvement of high throughput SAT.

Functionalised QD-doped particles have higher chemical- and photo- stability and lower limits of detection associated to high binding capacities and surface groups' availability (Han *et al.*, 2001). As a result, the most significant advance of the QD-doped particles is their multiplexed coding capabilities (Chapter 1). Studies that reported the use of QD-doped particles in suspension for immuno- and DNA-detection assays are limited and mainly designed to establish the proof-of-principles. ASO assays based on QD-doped particles and FC or fibre optic spectrophotometry detection methods have been described for the genotyping of single nucleotide polymorphisms (SNPs) (Cao *et al.*, 2006b; Wang *et al.*, 2007). These methods were not efficient since they were developed with large volumes of microspheres conjugated to one type of DNA probes (*i.e.,* 50 mg or 20–30 millions of particles) which then were encoded with QDs. The biochemistry equipments, reagents and processes required for the production of QD-doped particle DNA probes were not optimum for the initial development of a QD-doped particle suspension assays.

An initial study to overcome the current limitations of SAT and QD-doped particles assay was undertaken with this research project. A new carbodiimide bioconjugation methodology adapted to the TriLite™ alloyed nanocrystals carboxylated encoded microspheres (QDEM) of 5 micron-sized (± 10%) (Crystalplex, Pittsburgh, PA, USA), was developed for the detection of ssDNA with FC detection in a small suspension format. Flow cytometer instruments typically incur low running costs, are flexible, and adaptable to high throughput analysis, which offered many advantages over the Luminex instruments for the development of the assay (Chen and Sullivan, 2003; Sklar *et al.*, 2007). The impact of the conjugation procedure on the QDEM materials was also investigated.

The use of qualitative and quantitative methods to characterise and evaluate the microsphere bioconjugates is necessary for the optimisation of the conjugation procedure. The optimisation of the attachment of the oligo probes to the QDEMs surface is one of the factors that determine the later hybridisation efficiency and sensitivity of the bead-based allele-specific oligonucleotide hybridisation assay. Various techniques, including light scattering, spectroscopy, microscopy, and flow-adhesion assays have been developed to structurally characterise bead bioconjugates. The light scattering is an essential parameter that most flow cytometers can measure (Figure 3.2). Forward scattered light emission (FSC) and side scatter light emission (SSC) are commonly used to estimate the relative size and internal density of individual biological cells (Tycko *et al.*, 1985). SSC and FSC parameters can also characterise the differences between encoded microsphere populations. Several factors were identified as a potential source of the modification of the FSC and SSC directions between the different bead populations (Figure 3.2):

- The surface topography: degree of porosity, density of oligo or fluorophores attached on the bead surface, coating of the bead,
- The bead shape: size, spherical shape or the identification of broken particles,
- The internal composition of the bead: intensity or number of fluorophore trapped in the sphere, distribution of the dye within the sphere, microsphere chemical composition (bead matrix, internal coating), degree of porosity

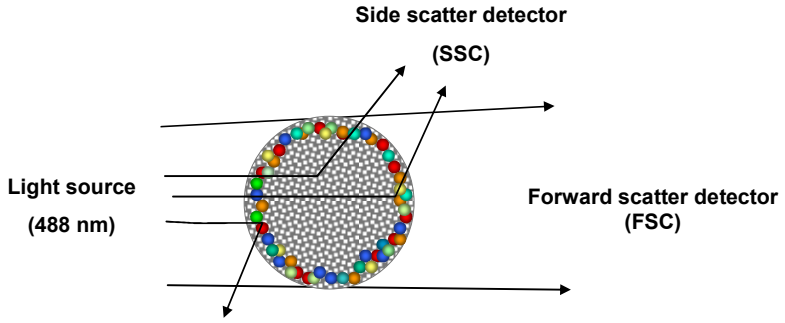

Figure 3.2 Light scattering detection properties of an encoded microsphere.
Arrows represent the elastic light scattering in the forward (FSC) and perpendicular directions (SSC).

Quantitative FC can be used to evaluate the bioconjugation efficiency. The number of oligos per bead can be estimated by commercially available fluorescent beads as follows. The amount of fluorescence relative to the peak obtained in a detector channel (peak channel) by FC can be quantified with a standard curve obtained with the commercial beads available. It is then possible to quantify the fluorescence intensity of an unknown sample, with the same instrument fluorescent settings used with the standard, by putting the peak value obtained in the standard curve. The number of fluorescent molecules per cell or per bead can therefore be estimated and expressed generally using two units: The ABC (antigen binding capacity) and the MEF (molecules of equivalent soluble-fluorochrome) (Morilla and Scolnik, 1998). In cell biology and bio-diagnostic research, the quantification of antigen (with ABC unit) on the cell surface has important applications such as looking at the differentiation of antigens during the activation of neutrophils in infectious events, or looking at the antigen expression regulation in immunophenotyping and pathological situation (parasitic or viral infection). Quantitative FC provides also useful parameters for clinical applications such as ascertaining malignancy by evaluation of cell-associated antigen density under- or over-expressed on malignant cells (Farahat *et al.*, 1995).

Spiro *et al.* (2000) was the first to use fluorescent calibration kits and fluorescent amino-modified oligos to quantify in MEF the conjugation and the hybridisation efficiency in a particle-based assay that detect specific DNA analytes in environmental samples. However, a limited number of studies were found to quantify of the number of fluorescent molecules attached to the beads in microsphere-based flow cytometric assays. A specific study of conjugation optimisation was reported by Wittebolle *et al.* (2006). The oligo density or number of soluble fluorochrome per μm^2 of bead surface was defined to evaluate the conjugation efficiency and coverage on the microsphere surface. The MEF values offer the advantage to quantitatively evaluate conjugation methods, and to determine optimal conditions and probe concentrations for the coupling to a specific type of microsphere.

The potential and efficiency of QD-doped particles for the detection of DNA in suspension arrays has not been quantitatively and specifically addressed. At the time of writing, only one type of QD-doped particles has been commercialised and available with different QDs fluorescent codes. No data on the reproducibility, batch-to-batch variation, stability and the quantitative evaluation of the QD-doped-particle bioconjugates were reported. The current development of a new suspension array method started with the optimisation of the attachment of the oligo probe to carboxylated QDEMs by carbodiimide coupling. Conjugation efficiency was functionally assessed and compared using direct coupling of amine active probes linked to cyanine organic fluorophores. The effects of the coupling buffers, and the concentration and the structure of the oligos were first studied to optimise the conjugation efficiency. The advantages and adaptability of QDEM bioconjugates for biomedical application are also discussed.

3.2. Materials and methods

3.2.1. Materials

- **Oligonucleotides and QDEMs technology**

Oligonucleotides (oligos) were obtained from Thermo Electron (Bremen, Germany). Specific fluorescent ssDNA probes were designed to study the chemical binding of oligos to the QDEM carboxylated surface. The *in silico* probe design was based on previous methodology (Xu *et al.*, 2003; Wittebolle *et al.*, 2006). **"**Direct" oligo probes for conjugation had an amino active group attached through a carbon spacer (6 or 18 carbon spacer) at the 5' extremity of a 18-mer poly-adenine (NH2-poly$(A)_{18}$) sequence, and with or without a cyanine fluorophore (Cy3 or Cy5) at the 3' extremity (Table 3-1).

Table 3-1 Oligos used for the optimisation of QDEM bioconjugates optimisation *

Name	Structure 5' → 3'	Specification
Direct Cy5 probe	NH2 – 6C – poly(A) – Cy5	20 (A) mer, Cy5 emitting at 670 nm
	NH2 – 18C – poly(A) – Cy5	20 (A) mer, Cy5
Direct Cy3 probe	NH2 – 6C – poly(A) – Cy3	18 (A) mer, Cy3 emitting at 565 nm
Direct NF probe	NH2 – 6C – seq – poly(A)	22 seq mer, 18 (A) mer

* NF: non fluorescent; NH2: amine active group; 6/18C: carbon spacer; (T)-mer: thymine polymer; (A)-mer: adenine polymer; seq: oligo sequence, GC content <50%; Cy3/5: cyanine fluorophores

Five types of 5 µm diameter carboxylated QDEMs were used in this study (Crystalplex, USA). Non-encoded beads (0QDEM), and 525 nm QDEM (525QDEM) were used for the bioconjugation study. Single colour beads, *i.e.,* 0-, 525-, and 575QDEM, and two-colour QDEM, *i.e.,* (525;575) with intensity codes of (1:1) and (2:1), were used to compare the fluorescent code of bioconjugates to non conjugated beads (Appendix A, Table 1). The 525 and 575 nm emission wavelengths of the QDEMs were respectively detected in the flow cytometer detectors FL1 and FL2. QDEMs of 5 µm diameter were chosen since their size was adapted to high throughput bead-based assay in suspension format (Iannone *et al.*, 2000).

- **General materials and chemicals**

Bovine serum albumin (BSA), 1-ethyl-3-(3-dimethylaminopropyl)-carbodiimide (EDC), sulfo-*N*-hydroxysuccinimide (sulfo-NHS), 2[N-Morpholino] ethanesulfonic acid (MES), sodium dodecyl sulfate (SDS) and organic solvent were purchased from Sigma Chemical (Poole, Dorset, UK). Imidazole, azide, 1 M Tris-HCl, 3 M Sodium chloride (TBS, pH 7.5), Tris-ethylenediamine tetra acetic acid (TE, pH 8.0), ethylenediamine tetra acid (EDTA, pH 8.0), Tween-20, sodium dodecyl sulfate (SDS), and nuclease free water (H_2O) were purchased from Fisher Scientific (Loughborough, Leicestershire, UK).

QDEMs bioconjugate solutions were quantified as previously described with a Neubauer haemocytometer (Reichert, Bright-line®, NY, USA) and the Axioskop2 plus fluorescent microscope (Zeiss, Berlin, Germany) (Appendix C). Scanning electron microscope (Philips XL-30 ESEM and a Phillips XL30SFEG microscope, Philips Electronics, Netherlands), and fluorescent microscope (Axioskop2plus LSM 510, Zeiss, Germany) were used as previously described to characterise QDEM bioconjugates (Section 2.2.5). All the materials related to FC was purchased from Beckman-Coulter (High Wycombe, Buckinghamshire, UK). All the centrifugations were performed in a mini-centrifuge (Microcentaur, MSE, Henderson Biomedical, London, UK). A sonicator instrument (Sonicator instrument, Copiague, NY, USA), a MS1 shaker (IKA®Works Inc, Wilmington, WC, USA), and a rotamixer vortexer-mixer (Hook and Tucker Zenyx, Surrey, Croydon, UK) were used to resuspend QDEM solutions.

- **Flow cytometry**

All the materials and methods related to the flow cytometer were as previously described in section 2.2. In addition, a specific protocol was designed using control QDEM population corresponding to the emission wavelength of the QDEMs and the organic fluorophores implicated in the bioconjugation experiment. The samples were characterised using the appropriate flow cytometer detector channels identifying the expected fluorescent codes highlighted in bold in Table 3-2.

Table 3-2 Fluorescent detection channel used in bioconjugation studies*

Detection channel Microscope / FC	**Band pass filter (in nm)**	**Visible colour**	**Emission λ (in nm)** QD / Fluorochrome
Ch1 / FL1	**505-545**	**Green**	**525**
Ch2 / FL2	**560-590**	**Yellow-Orange**	**575 / PE, Cy3**
FL3	605-635	Red	630
FL4	**660-700**	**Deep Red**	**665 / Cy5**

*Ch: channel; FL: fluorescence λ: wavelength; FITC: fluorescein isothiocyanate; PE: phyco-erythrin; Cy: cyanine dye

The Coulter Epics XL-MCL flow cytometer (Beckman-Coulter, UK) was use to measure light scattering simultaneously to fluorescent emissions intensity (BD Biosciences, 2000). The forward-scattered light (FSC) and the side-scattered light (SSC) detectors were used to record light deviation dependent on the physical characteristics of the particles (Section 2.1). FC data (fcs data files) were acquired in a four-decade logarithmic scale, using the System II Data Acquisition & display software, version 2.0 (Beckman-Coulter, FL, USA). A region was defined for the QDEMs population of interest. Three replicates were run per experiment.

3.2.2. Coupling of QDEMs to oligonucleotides

- **Experimental scheme**

The carbodiimide conjugation assay shown in the schematic of Figure 3.3 was adapted from Spiro *et al.* (2000).

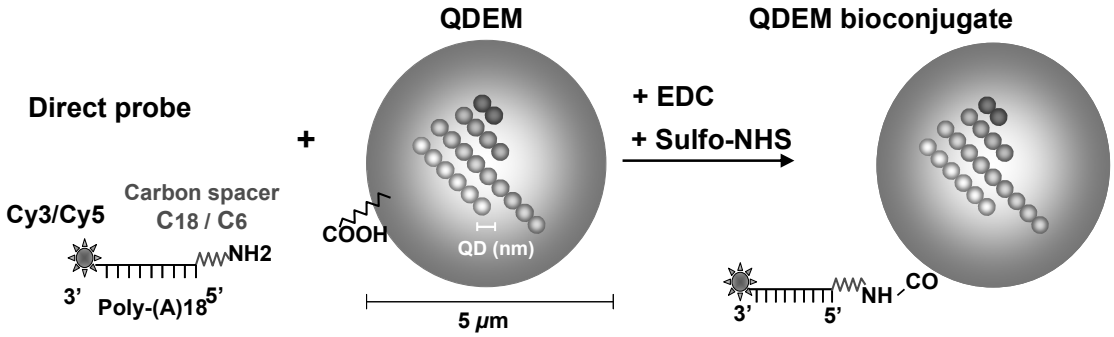

Figure 3.3 Direct conjugation experimental design.

The conjugation was achieved by a carbodiimide reaction: the oligo's amino group (NH2) reacted with the QDEM's carboxylated groups (COOH) mediated by active agents (EDC, Sulfo-NHS) (Appendix E). QDEM specific signal encoded in terms of colour and intensity for the discrimination between QDEM and the probe signal.

The amino-carboxyl coupling reaction was mediated by water-soluble carbodiimide active compounds: EDC, combined with sulfo-NHS, increases the coupling efficiency by creating a stable amine-reactive product (Appendix E). The conjugation efficiency was functionally assessed and compared using carbodiimide coupling with variable quantities (from 0 pmol to 400 pmol) of amine active probes directly linked to a cyanine organic fluorophore. The organic dyes Cy3 and Cy5, detected respectively in FL3 and FL4, were chosen in order to avoid emission overlap with the QDEM signals used in this study.

- **Conjugation protocol**

A volume equivalent to ~10,000 QDEMs (measured by haemocytometer, Appendix C) was conjugated by amino-carboxy coupling to a range of 1 to 400 pmol of direct fluorescent probes in 20 µL of MES (pH 4.5) buffer. Centrifugations were performed at 1133x g for 4 minutes (min). QDEM solutions were systematically homogenised by 15 second (s) of vortex and 20 s of sonication, repeated three times; 2 µL of fresh carbodiimide activators, *i.e.,* EDC (10 mg/ml in nf-H_2O) and sulfo-NHS (10 mg/ml in nf-H_2O), were added to the mix and incubated for 30 min at room temperature (RT) shaking at 500 rpm. The previous step was repeated and samples were then washed at RT (3 min, 400 rpm) successively in 400 µL of 0.02% Tween-20, 0.5% SDS, and 0.1 M of TE (pH 8.0).

The same protocol was repeated with imidazole (pH 7.0) coupling buffer until the washing steps. After incubation, samples were washed (RT, 4 min, 400 rpm) twice in imidazole (pH 7.0) and once in 0.1 M TE (pH 8.0). QDEMs were resuspended in 400 µL of 0.1 M TE for FC analysis or in 15 µL of storage buffer (1X TBS, 1% BSA, 0.01% azide) and kept at 4°C. Before storage, QDEM bioconjugates were enumerated by haemocytometer, and the concentrations of the QDEM bioconjugate in solutions were calculated (Appendix C).

Three types of negative controls were used: 1) QDEM stock solution, 2) QDEMs incubated with clean water, and 3) QDEMs incubated with fluorescent probe but without the initiators (EDC, Sulfo-NHS). Controls 1) and 2) were used to evaluate the fluorescent noise inherent to the flow cytometer and the effect of the procedure on the QDEM emission signal. Control 3) was used to quantify the fluorescent background due to non specific binding. Negative controls were performed for each batch experiment. Experiments that involved organic fluorophores were performed in the dark (experimental tubes covered with foil).

3.2.3. Data analysis

FC data were analysed with WinMDI 2.8 (The SRI, CA, USA). The median fluorescent intensity (MFI), the geometric mean (Gmean) and the percentage (%) of events were calculated on gated populations. The QDEM stock solution was used as a control to define the gate and its MFI was used to control QDEM specific fluorescent code (control 1), section 3.2.2). The background signal was determined for each batch conjugation experiment (control 1) and 2), section 3.2.2). The quality of probe attachment was evaluated by the amount of non specific binding (control 3), section 3.2.2).

- **Quantitative analysis**

Fluorescent probes, emitting at the same wavelength as phycoerythrin (PE) fluorophore were used to evaluate the number of direct probes attached to QDEMs encoded with 525 nm QDs (525QDEM). In this study, the QuantiBRITE PE bead calibration kit (Becton Dickinson, BD, biosciences, UK) was used to evaluate the conjugation efficiency since it was adapted to the flow cytometer Coulter Epics XL-MCL (Beckman Coulter) and presented the same detection properties as the Cy3 fluorophore (Table 3-2) (Schwartz *et al.*, 1998; Kulwinder *et al.*, 2001).

QuantiBRITE PE was used as previously described to calculate the molecules of equivalent soluble fluorochrome (MEF) values (Spiro *et al.*, 2000; Wittebolle *et al.*, 2006). Briefly, QuantiBRITE PE tubes that contained a mixture of four levels of phycoerythrin (PE emission peak at 572 nm) were reconstituted in 500 µL of TE (pH 8.0) buffer. The number of PE molecules per bead for each intensity level was specified in the manufacturer guidelines.

The mean fluorescence intensity (MFI) was acquired for each intensity peak (Figure 3.4A), and a calibration curve was calculated by correlating the MFI data of each population to the corresponding MEF values given in the kit (Figure 3.4B) (Kulwinder *et al.*, 2001). The fluorescence intensity detected in FL2 channel was converted into the number of PE molecules per event (or microsphere). QuantiBRITE kit was run on the flow cytometer and a calibration curve was calculated for each replicate. Figure 3.4A represents the typical histogram analysis of a QuantiBRITE tube for a batch of experiment. The standard curve relating the fluorescence to PE molecules presented in Figure 3.4B is calculated with the equation (1):

$$y = mx + c \qquad (1)$$

where y is the Log_{10} of the fluorescence detected, and x is the Log_{10} of PE molecules per bead. The FL2 Log(Gmean) of the sample analysed is substituted in the equation which is then solved to obtain the Log MEF. The anti-log is finally calculated to get the MEF values. Samples have to be run with the same FC settings than the kit to be able to perform quantitative analysis.

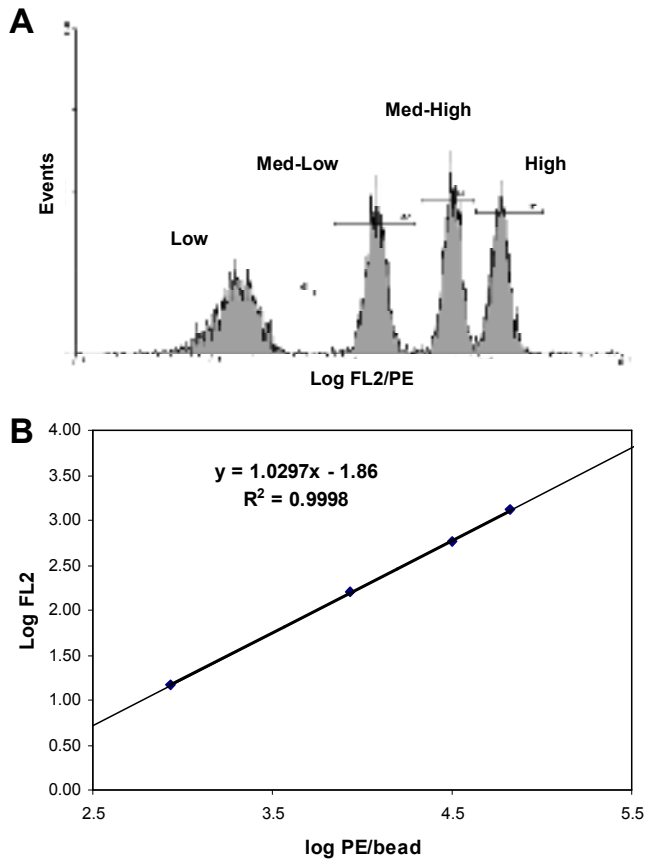

Figure 3.4 Typical calibration graph used for MEF calculations.

A: FL2 histogram of the four fluorescent intensity peaks (Low, Medium-Low, Medium-High, and High) detected with a tube of the QuantiBRITE-PE kit obtained with WinMDI v2.8 software (CA, USA); **B**: Linear regression plot of Log(Gmean) in FL2 versus Log(PE molecule/bead), calculated and represented in Excel (Windows 2000, Microsoft, USA)

- **Analysis of the MFI, the MEF and the percentage of events**

The following nomenclature was used for the statistical analysis: ***s*** for samples, ***n*** for negative control experiment or background measurement, ***c*** for control population, ***d*** for the diameter of the bead, ***S*** for the surface of the microsphere calculated with the formula *($S = \pi * d^2$)*. Data were presented as the mean of three to six replicates ± the standard error (SEM). Statistical analysis included the following calculations:

- Corrected MFI (RMFI) and corrected MEF (RMEF) were calculated by subtracting the negative control values (n) from the positive samples values (s) belonging to the same batch experiments (in arbitrary units, a.u.),

$$RMFI = MFI\ (s) - MFI\ (n)$$
$$RMEF = MEF\ (s) - MEF\ (n)$$

- Conjugation efficiency was described using the oligo density (D_o) corresponding to the number of fluorescent molecules covering the microsphere surface S (in oligo/μm^2) (Wittebolle *et al.*, 2006),

$$D_o = RMEF / S$$

- The fluorescent code consistency was evaluated by estimating the relative variation in the fluorescent code detected in the FL channel from the initial blank or 525QDEM control population (in a.u.),

$$\%\ FL = 100 \times MFI^{FL}(s) / MFI^{FL}(c)$$

- The variations in SSC and FSC detector channel of bioconjugates in comparison with a control population were calculated (in a.u.),

$$\%\ SSC\ (or\ FSC) = 100 \times MFI^{SSC}(s) / MFI^{SSC}(c)$$

- To evaluate the number of QDEMs in the experimental tube, the percentage of event was recorded during sample analysis and a relative percentage of events, compared with the control population, was calculated,

$$\%\ Events = 100 \times \%Events\ (s) / \%Events\ (c)$$

- **Statistical tests on MFI data**

A minimum of eleven replicates (samples) was required to test the normality distribution of the replicates and to undertake comparative tests on the different QDEM population data.

Replicates of the 0QDEM and 525QDEM bioconjugates were statistically analysed with GraphPad Prism5.01 (CA, USA). For each replicates a control sample was run simultaneously. The number of events and the MFI data of bioconjugates and controls were collected on populations gated with the region defined with the control population. A D'Agostino and Pearson normality test was run for each parameter of each population. Populations presenting a Gaussian distribution were analysed with one-way analysis of variance (ANOVA).

Populations before and after conjugation were compared for each flow cytometer parameter. Paired tests were chosen since the conjugation procedure was repeated more than ten times and for each replicate, control and treated bead were run in parallel. For each parameter and replicate, the data were corrected by subtracting the bioconjugate value to the control value. A D'Agostino and Pearson normality test was then run for each pair of corrected data (control minus bioconjugate) with each parameter analysed. Populations presenting a Gaussian distribution were analysed by a paired t test. If the data failed the normality test (p-value < 0.05), a Wilcoxon matched pairs non parametric t test was used instead of a paired t test

Light scattering (SSC and FSC) MFI data, and the percentage of events were compared between control and bioconjugate populations. The corrected paired data were used to compare 0QDEM to 525QDEM light scattering variations. These comparisons were not assimilated to a paired experiment, since the data were not collected from the same replicates and the bioconjugation were not undertaken at the same time. MFI data and percentage of events were analysed separately as they represented two different types of data (different units, and order of magnitudes)

If the paired data presented a Gaussian distribution (*i.e.,* data that passed the D'Agostino and Pearson normality test) a one-way analysis of variance (ANOVA) followed by Tukey-Kramer's multiple comparison test was performed to compare the data. ANOVA's post analysis evaluates statistical differences among the parameters (SSC, FSC) for 0QDEM and 525QDEM populations.

When only two groups were compared, the Tukey-Kramer's multiple comparison test was not adapted, and a unpaired t test was then performed.

The corrected percentage of events for 0 and 525QDEM population following a Gaussian distribution was analysed by an unpaired t test.

Data were presented as the mean of the replicates ± the standard deviation (SD). The full table of results are reported in Appendix I (Excel, Windows 2000, Microsoft, USA).

- **Graphical representations**

Graph (curves, scatter plots) and statistical tests were calculated with GraphPad Prism5.01 (GraphPad Software, CA, USA) and Excel 2000 (Microsoft, USA). A Mesh plot was generated with MATLAB software applications (Forsythe *et al.*, 1977) using MFI values calculated with the WinMDI software (CA, USA).

3.3. Results

3.3.1. Study of QDEM conjugation efficiency under different experimental conditions

- **Impact of buffers on the conjugation efficiency**

Two of the most common carbodiimide coupling buffers, MES and imidazole, were compared with evaluate the effect of modifying the coupling buffer on the conjugation efficiency. The oligo density (D_o in oligo/μm^{-2}) was calculated for direct Cy3 fluorescent probe (Cy3-oligo) quantities ranging from 0 to 400 pmol. Different levels of the direct fluorescent probe were used, depending on the precision needed to assess the general pattern of the graphs presented in Figure 3.5. The maximum saturation D_o for imidazole and MES was respectively approximately (~) 12,500 and 5000 oligo/μm^{-2} for 300 pmol of oligo (Figure 3.5). Therefore the D_o max of MES plot corresponded to ~40% of the D_o max imidazole plot. The titration curves of 525QDEM conjugated to Cy3 oligo with imidazole buffer presented a coupling saturation point at 200 pmol with a maximum D_o of ~12,588 oligo/μm^{-2} (± 2,477). To reach MES coupling saturation point, the same quantity of probes was needed, but in comparison, the maximum D_o (4796 (± 343) oligo/μm^2) was almost three times less (Figure 3.5). The study of the dependence between Cy3-oligo quantity and the D_o was undertaken (insets of Figure 3.5). A linear quantitative relationship was found with a coefficient of regression $r^2 = 0.941$ and a p-value < 0.0061 for imidazole in the dynamic range of the titration. MES linear regression was obtained with $r^2 = 0.969$, and a p-value< 0.0001.

From these results, the optimum probe quantity was defined. The oligo quantity equivalent to a third of the quantity at the D_o saturation value, *i.e.,* 60–70 pmol, was chosen to obtain an optimum probe coverage while avoiding fluorescent and steric inhibition due to probe saturation (Peterson *et al.*, 2001).

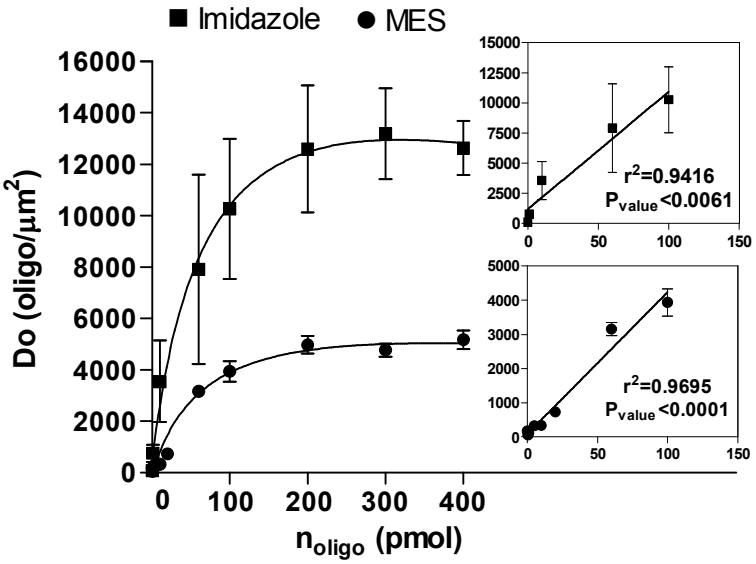

Figure 3.5 QDEM bioconjugation titration to Cy3-oligo in imidazole and MES buffer.
Titration curve: plot of Do (in oligo/µm^2) versus oligo quantity (n_{oligo} in pmol) independently obtained by a non linear fit model. Insets show the linear regression with the coefficient of regression (r^2) and the p-value (p) for probe quantity before saturation. Data presented as the Do ± standard error (SEM) of three replicates.

- **Impact of molecular 6-amino-caproic acid spacer arm**

The carbon spacer that separates the oligos from the microsphere was described as a flexible structure, resistant to bending or shortening, and was reported to minimise steric and electrostatic interferences between the two entities, which potentially favours conjugation reactions (Agrawal *et al.*, 2008). Previous work demonstrated that a six carbon spacer arm (6C) significantly enhanced the carbodiimide coupling reaction (Pack *et al.*, 2007). Cy5 probes with 6C and 18C spacer arm were conjugated in imidazole and MES buffer to 525QDEM in a range of 0 to 500 pmol to investigate the effect of carbon spacer on coupling (Figure 3.6). Preliminary coupling experiments with direct Cy5 probes were undertaken to create a FC protocol which detected a maximum of Cy5 signal in detector channel 4, while minimising the overspill in the other detector channels.

The qualitative analysis of the corrected median fluorescent intensity (RMFI) detected in FL4 showed no significant increase of the fluorescence with 18C Cy5 probe after 1 hour of incubation (Figure 3.6). The experiment also confirmed imidazole buffer as the most efficient buffer: the RMFI was ~500 a.u. with imidazole against ~200 a.u. with MES buffer for 100 pmol of Cy5 probe (Figure 3.6). Comparatively to Cy3 RMFI values (Figure 3.6), Cy5 values were approximately 200 a.u. lower. This difference was interpreted as overspill residues of the Cy5 emission fluorescence in close detector channels (FL2, FL3).

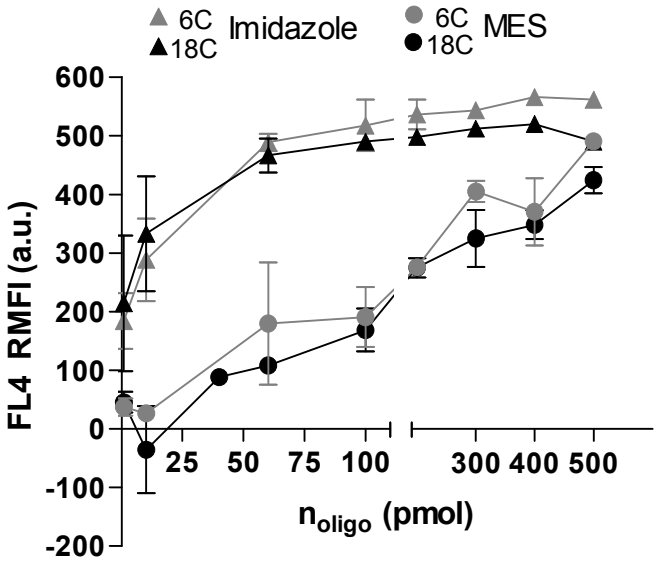

Figure 3.6 Impact of carbon spacer (6C/18C) on the bioconjugation in imidazole and MES buffer assays

Corrected median of fluorescence intensity (RMFI ± SEM of three replicates) in arbitrary units (a.u.) versus oligo quantity (pmol). Cy5 reporter dye detected in FL4. Overspills were noticed in other detector channels with high quantity of reporter dye. X-axis scale extended from 0 to 150 pmol to improve graphical representation.

- **Influence of time**

The benefit of increasing the incubation time from 1 h to 1h 30 was investigated. The direct conjugation procedure with Cy3 fluorescent probe was carried out with extended incubation times. The mean of RMFI (± SEM) was calculated for the emission spectra of 525QDEM detected in FL1 and Cy3 detected in FL2 (Figure 3.7).

Figure 3.7 shows a similar slope for both curves, with an increase of the RMFI for Cy3-oligo quantities ranging from 0 to 100 pmol. Both curves reached a saturation point of ~800 a.u. RMFI at 100 pmol of Cy3-oligo. From 100 pmol to 400 pmol of oligo, extending the time of conjugation from 1 h to 1h 30 min did not increase the probe fluorescent signal. Longer incubation times (>1h 30 min) were not investigated since the objective was to develop a rapid conjugation method for the production of multiple bioconjugates.

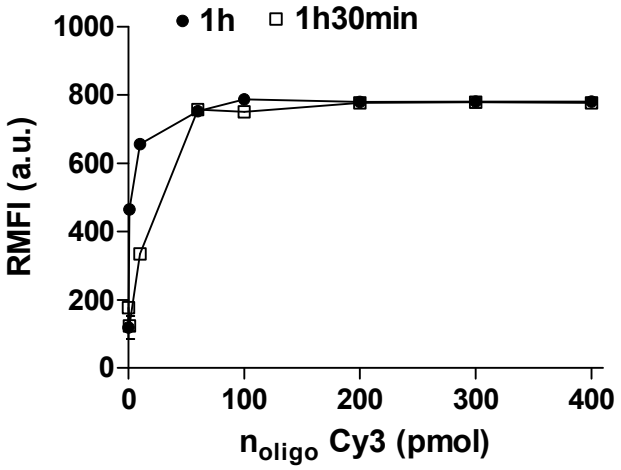

Figure 3.7 Impact of time on the coupling efficiency with imidazole buffer.
525QDEM were incubated for 1 h and 1h 30 min with 0 to 400 pmol Cy3 oligo probe, following the conjugation procedure. A negative control was performed for each replicate by coupling 525QDEM with DNase free water. Data were presented as the corrected MFI detected in FL2, RMFI (± SEM).

3.3.2. Sensitivity of carbodiimide coupling with imidazole buffer

A first set of optimum conditions for the QDEM carbodiimide coupling procedure was defined from the results obtained in Figure 3.5, Figure 3.6, and Figure 3.7: the imidazole buffer (0.1 M, pH 7.0) was used with C6 amino modified direct probe, in the optimum range of 60–70 pmol, with 1 h incubation. To evaluate the specificity of the covalent attachment to the QDEM surface, the activators of the carbodiimide reaction (EDC and sulfo-NHS) were replaced by H_2O. The samples were analysed under confocal microscopy and FC. Confocal microscopy was used to observe the coupling specificity with an optimum Cy3-oligo quantity (65 pmol), and to describe the impact of the procedure on QDEM's structure and fluorescent intensity (I) (Figure 3.8A, B, and C).

TriLite™ 525QDEM control population exhibited a very bright (I > 200 a.u.) and regular fluorescent profile (Figure 3.8A). The distribution of the fluorescence indicated a preferential localisation of QDs toward the exterior of the polystyrene microsphere. The high sensitivity of the confocal microscope detected a red background signal (I < 100 a.u.) with the negative control (Figure 3.8B). The Cy3 signals of the positive samples were detected with an I > 100 a.u. (Figure 3.8C). The detection of femtomole quantities of fluorescent oligos and the physical observation of QDEM bioconjugates were successfully achieved on confocal microscopy, which appeared as a valuable alternative analytical technique.

The FL2 background signal of the 525QDEM stock solution detected with FC was low (~6563 MEF (± 88)) and approximately equivalent to the fluorescence detected with 0 pmol of direct Cy3 probe (~6210 MEF (± 94)) (Figure 3.8D). A maximum of 11% non specific binding was detected at saturation, with 400 pmol of oligos. No significant background noise was detected in the optimum oligo range, *i.e.*, 60-70 pmol with confocal microscopy and FC analysis.

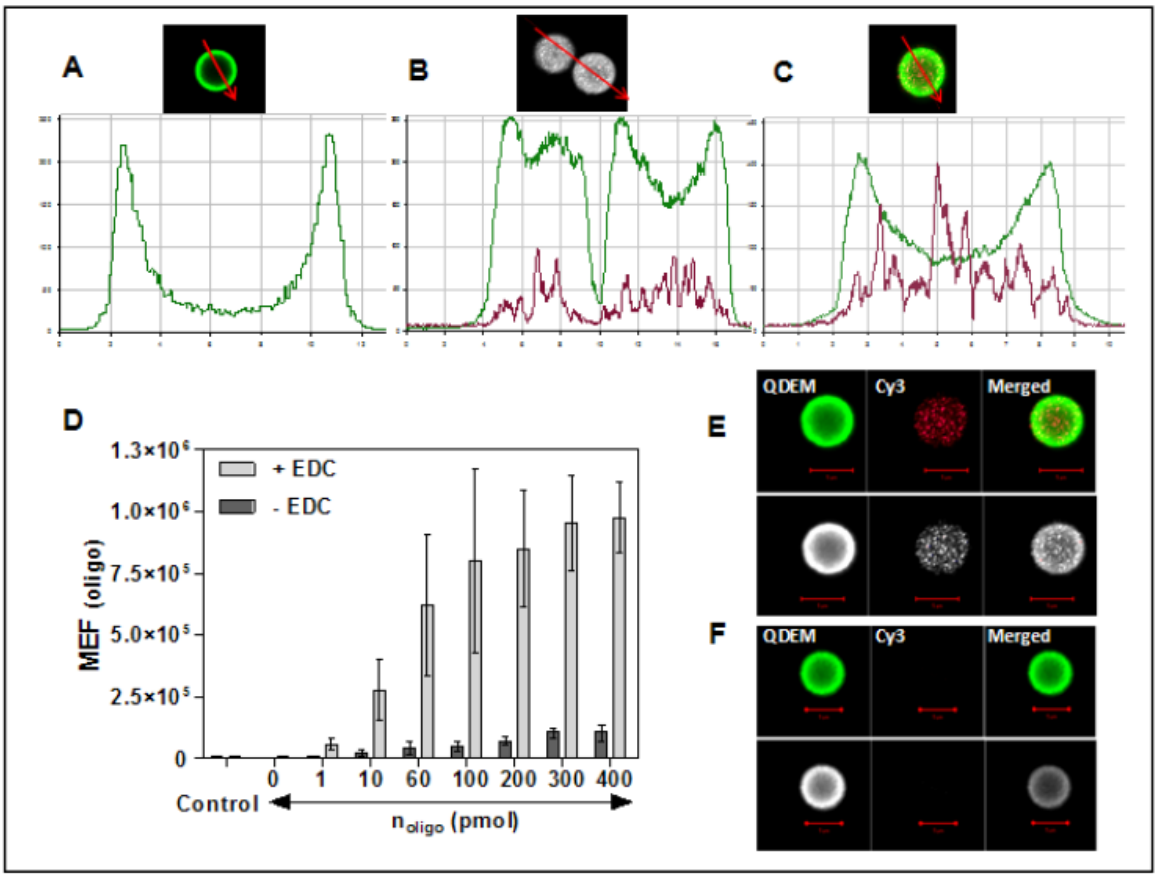

Figure 3.8 Study of the background noises of the carbodiimide coupling reaction in imidazole buffer.

A to C: Confocal images and spectra of 525QDEM conjugated with 0.1 pmol of Cy3 probe. **A**: Control population before treatment, **B**: Negative control (without activators), **C**: Positive control. The red arrows indicated the position of the fluorescent spectrum. Spectra represented the fluorescence intensity (A, B, C grid interval of 50 a.u.) versus the distance (grid interval of 2 µm for A and B, of 1 µm for C). The fluorescence detected for 525QDEM and Cy3 was represented respectively by a green and a red spectrum. **D**: Control: 525QDEM before treatment; 0: DNase-free water incubation, 0 to 400 pmol: incubation with direct Cy3 with or without the activators. MEF: molecules of fluorophore, data were presented as the mean (± SEM) of replicates. Confocal images (true colour and range indicator) of (**E**) positive control and (**F**) negative control of 525QDEM conjugated with 65 pmol of Cy3 probe (5 µm red scales bar).

3.3.3. Impact of the coupling procedure on QDEM structural and fluorescent characteristics

The QD-doped particles are a recent technology. Since the initial publication of Gao *et al.* in 2000, limited data has been published relating to the stability and efficiency of the fluorescent code of the beads in biomedical applications (Gao and Nie, 2004). The stability and the code consistency of the QDEMs were therefore investigated on the conjugation data obtained previously and with a new batch of experiments using blank beads (0QDEMs) conjugated non fluorescent probe (70 pmol of direct NF-oligo) in the optimised conditions defined previously (section 3.3.1).

- **Comparison between 0QDEM control population and 0QDEM bioconjugates**

Flow cytometry results

A marked shift of the fluorescence intensity in both FL1 and FL2 was observed after attaching direct NF probes to the blank QDEMs (0QDEM). The signal intensity of 0QDEM conjugated to NF-oligo increased from ~0 to ~log10 (in a.u.) in both channels. No changes in the fluorescence intensity were observed in the other detector channels (Figure 3.9 and Figure 3.10). The shift in the bioconjugate fluorescence signal, from ($I \leq \log10$) to ($I \geq \log10$), was specific to the intensities detected in FL1 and FL2 as shown in Figure 3.9.

QDEMs encoded with QDs detected in FL1 and FL2 were then chosen to investigate the impact of the fluorescent shift of 0QDEM bioconjugates on the multiplex abilities of the QDEM technology. QDEMs with barcodes susceptible to overlay the 0QDEM bioconjugates signal were thus plotted simultaneously on a mesh plot diagram. All the QDEM fluorescent codes were specifically identified and separated as shown in Figure 3.9. No overlay was observed between QDEM populations (0:1), (1:1), (2:1), (1:0) and the 0QDEMs bioconjugates (Appendix A).

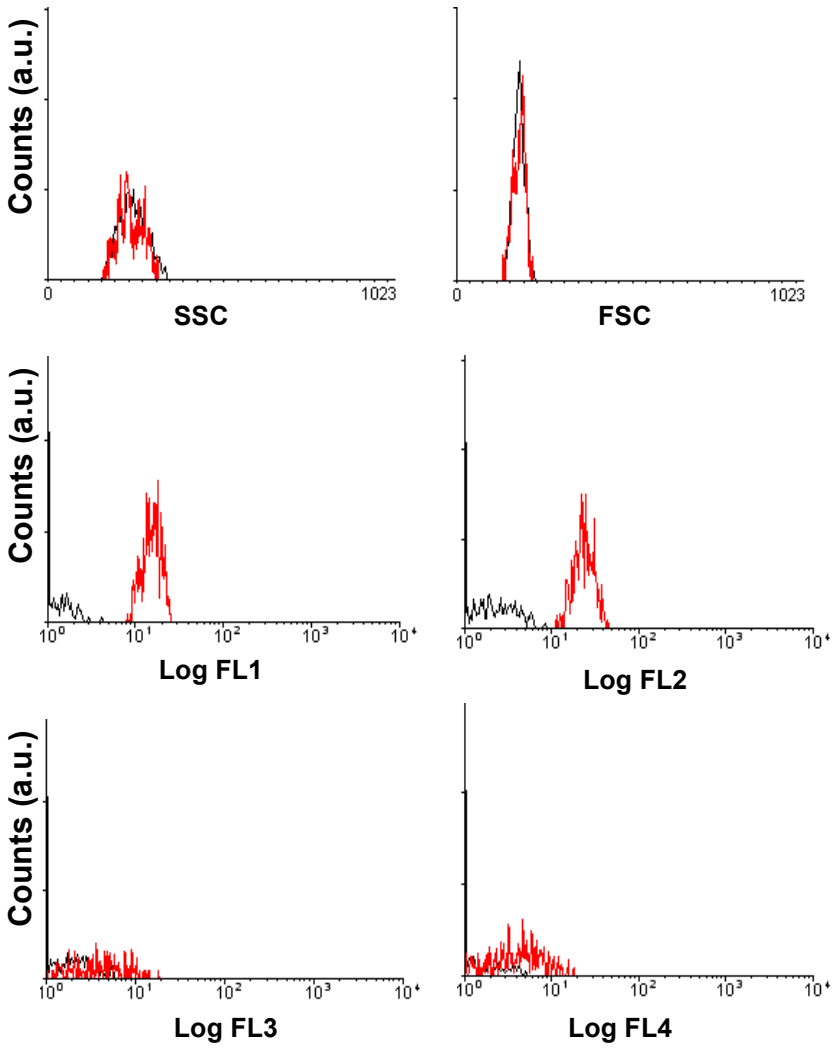

Figure 3.9 Flow cytometry histogram of 0QDEM control population (in black) and 0QDEM bioconjugated with direct NF probe (in red).

Events count (in a.u.) function of intensity detected in each detector channel (in a.u.); y-axis: linear representation; x-axis: (SSC, FSC) linear representation, (FL1,2,3,4,) logarithmic representation; histograms obtained with WinMDI 2.8 (CA, USA) from one replicate.

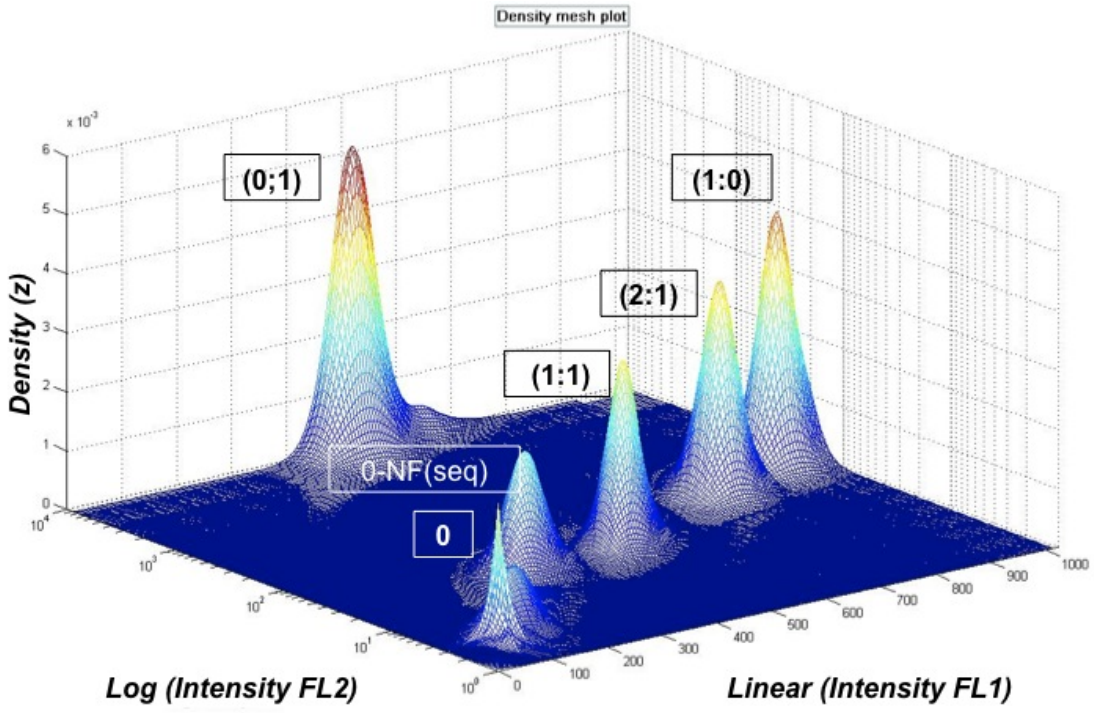

Figure 3.10 Density mesh plot of selective QDEM population and QDEM bioconjugates.
Each peak is associated to its QDEM fluorescent code (Appendix A, Table 1) indicated in the squared boxes; 0-NF(seq): non encoded microspheres conjugated to non fluorescent oligo. Data were presented as the mean of the MFI of three replicates for each peak; x-axis: linear MFI ^{FL1}, y-axis: log MFI ^{FL2}, y-axis: number of events detected in the gate.

Statistical analysis of the MFI data

Conjugation was performed with the optimum conditions defined previously with 0QDEM. Samples were run on the flow cytometer and a gate was defined with the 0QDEM control population. The number of events and the MFI data were collected on gated population for eleven of 0QDEM controls and 0QDEM bioconjugates. The computed data set is reported in Appendix I (Table 1a, b). The MFI data in FL3 and FL4 were excluded from the statistics analysis since MFI ~0 for both the control and the bioconjugates.

The D'Agostino and Pearson normality test indicated that MFI data had a Gaussian distribution for all the FC parameters (Appendix I, Table 2a, b). The statistical significance between the control and the bioconjugate populations was then investigated by one-way analysis of variance (ANOVA). The overall ANOVA test of the 0QDEM population had a very low *p*-value ($p<0.001$). The null hypothesis, which consider that all the data are sampled from groups having the same mean, was therefore rejected (Appendix I, Table 3).

After these first results, the data were compared as two paired groups. The D'Agostino and Pearson normality test indicated that the paired MFI data had a Gaussian distribution for all the parameters except FL1 (Appendix I, Table 4). The paired t test was then used to compare control and bioconjugate data, except for FL1 data. The paired t test measured the differences between each set of pairs for the FC parameters and analysed the list of differences based on the assumption that the differences in the entire population follow a Gaussian distribution (Appendix I, Table 5). The paired MFI collected in FL1 for the control and bioconjugate of each replicate were compared with a Wilcoxon matched pairs nonparametric test since for this parameter, the paired population failed D'Agostino & Pearson normality test (Appendix I, Table 6).

Figure 3.11A presents a scatter plot of the FC data with the results of the paired t-test. The asterisks represent the significance level related to the *p*-value. A *p*-value below 0.05 was considered significant. All the MFI row data are represented on a scatter plot as the mean (± SEM), and the results of the t test comparing each population for each parameter are indicated with their significance level. The MFI in FL1 and FL2 significantly increased after bioconjugation (Figure 3.11A), with a difference in the mean equal to an increase of respectively ~144 (± 30) and ~193 (± 11) a.u. The FL1 increase in fluorescence presented a low level of significance ($p = 0.0112$) compared with FL2 ($p<0.0001$). On the contrary, the MFI of FSC emission was significantly lower in the bioconjugates than in the 0QDEM control population, with a low significant level ($p = 0.0271$) and a difference in the mean equal to a diminution of ~- 71 (± 28) a.u. The number of 0QDEM also significantly decreased of ~29% (± 4) after treatment (Figure 3.12).

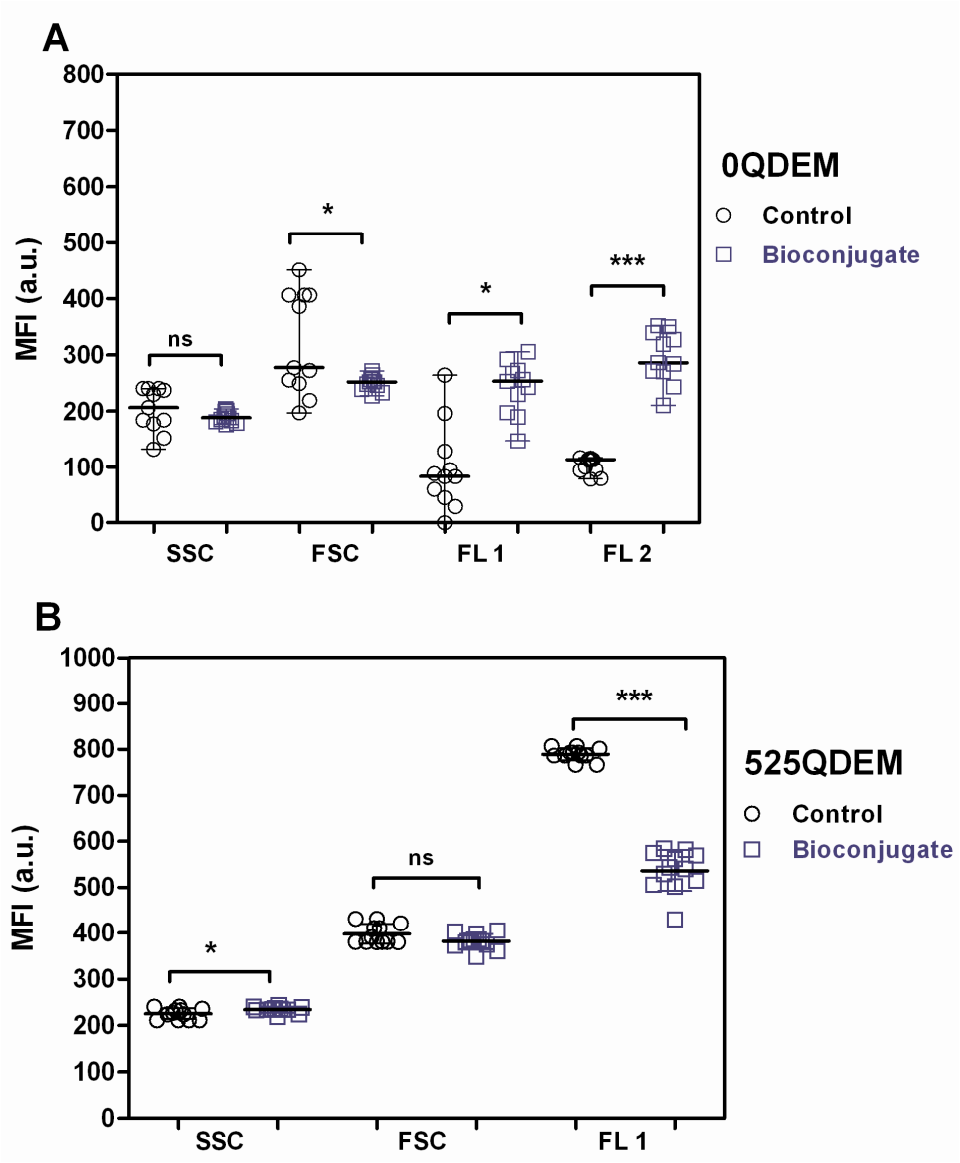

Figure 3.11 MFI data scatter plot and paired t-test results.

The scatter plot represents all MFI data for each parameter for the (**A**) 0QDEM and the (**B**) 525QDEM populations; data are presented as the mean (± SD); horizontal lines mark the median; post-analysis paired test was used to evaluate statistical differences among populations for SSC, FSC and FL2 parameter; Wilcoxon test was used to evaluate statistical differences between FL1 paired data; ns for not significant (p>0.05), * significant at p<0.05, and *** significant at p<0.001 (Appendix I, Table 4, Table 5, Table 6).

- **Comparing 525QDEM control population and 525QDEM bioconjugates**

The same experimental procedure and statistical analysis described with 0QDEM (section 3.3.3) was performed with twelve replicates to study the variation of the FC parameters and the percentage of events on the 525QDEMs (Figure 3.11B). MFI data collected in FL2, FL3, and FL4 were excluded from the analysis since MFI ~0 for both control and bioconjugate samples. The fluorescence detected in FL1 was significantly lower for the 525QDEM bioconjugates in comparison with the control (mean difference equal to a diminution of ~233 (± 14) a.u.). Figure 3.11 reveals a low significant increase of the SSC of the bioconjugates in comparison with the control, with a $p<0.05$ and a mean difference of ~9 (± 3) a.u. No significant difference was found between FSC data of the control and the bioconjugates. The percentage of events significantly decreased in the bioconjugates population in comparison with the control 525QDEMs (20% (± 4)) (Figure 3.12A). Finally, the effect of the procedure on 0QDEM and 525QDEM number of events was compared (Figure 3.12A). The Mann-Whitney tests demonstrated that there was no significant difference of percentage of events between the 0 and 525QDEM control, and between 0 and 525QDEM bioconjugates ($p>0.05$).

- **QDEMs analysis with SSC and FSC parameters**

The last statistical analysis was performed on the SSC and FSC data to compare the variation of light scattering between blank QDEMs (0QDEMs) and encoded QDEMs (525QDEMs) before and after the bioconjugation procedure (Figure 3.12B). No significant difference was observed for the SSC data between both the control and the bioconjugates, whereas a high significant variation of FSC emission was observed between both QDEM populations tested, with $p<0.001$. An increase in the FSC was observed for 525QDEM control and bioconjugate populations compared with the 0QDEM with a mean difference of respectively 77.8 and 132.6; the 95% confidence interval for the difference between the means extended respectively from 125-31 and 180-86 (in a.u.).

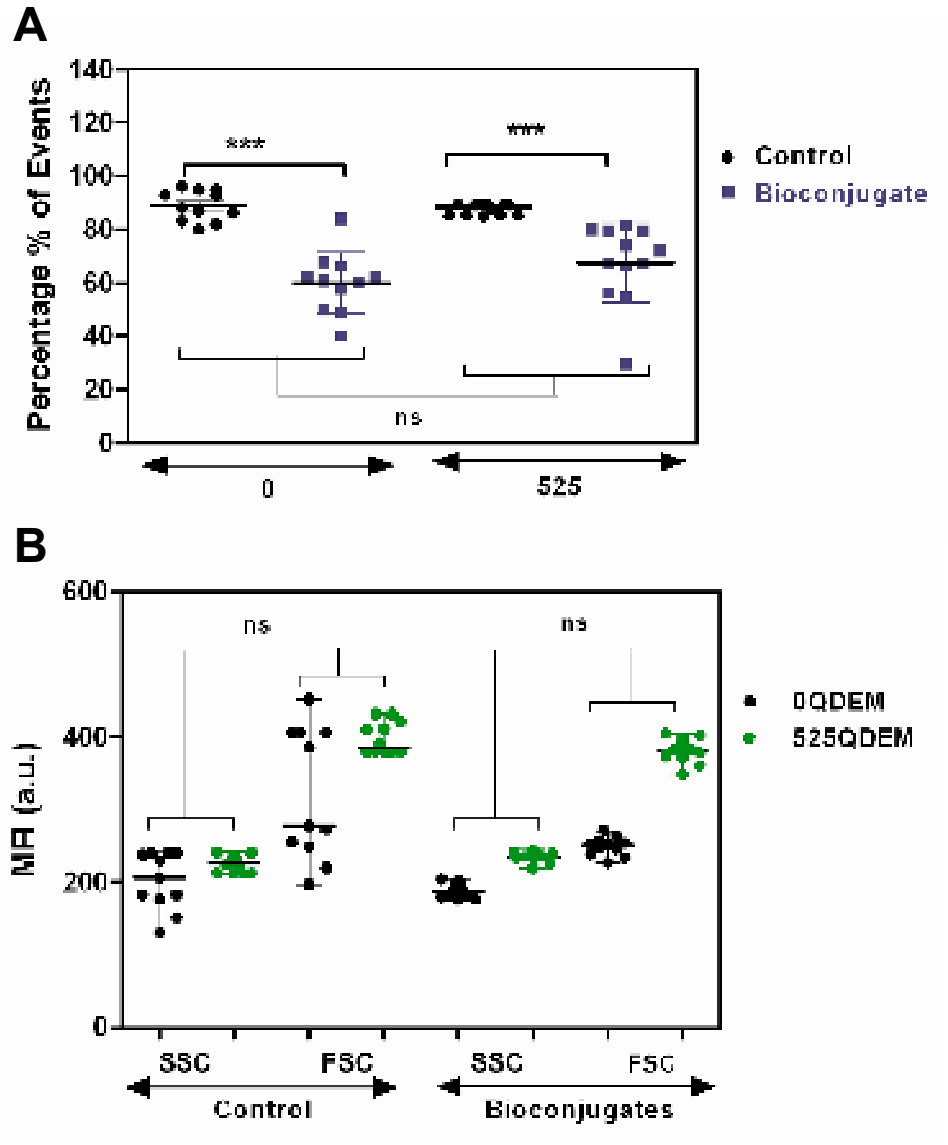

Figure 3.12 Scatter plot comparing 0QDEM and 525QDEM % Events data (A), and SSC/FSC intensity data (B).

A: a paired t-test evaluated the statistical differences between controls and bioconjugates of the same QDEM population; a Tukey-Kramer multiple comparison test was used on the row data to compare the percentage of events between 0 and 525QDEM samples that had the same treatment; **B**: A Tukey-Kramer multiple comparison test was used on the FSC and SSC corrected median fluorescent intensity (RMFI, in a.u.) data to evaluate statistical differences in the MFI among populations. The scatter plot represents all the data for each population of 0 and 525QDEM; data are presented as the median (± SD); horizontal lines mark the median; ns: not significant (p>0.05), *** significant at p<0.001 (Appendix I, Table 7, Table 8).

- **Structural and fluorescent characteristics of QDEM after bioconjugation**

The QDEM bioconjugates were observed under the high resolution SEM. The images in Figure 3.13 resulted from the observation of a minimum of 10 QDEMs in each sample. The QDEMs observed in Figure 3.13A, and B presents a rough surface and no differences were observed with the bioconjugate micrograph in Figure 3.13C. Figure 3.13D reveals a spherical and partially spherical microsphere observed in the bioconjugate samples. The comparison of the micrograph A and D demonstrated significant modifications of the microsphere shape, size and structural appearance.

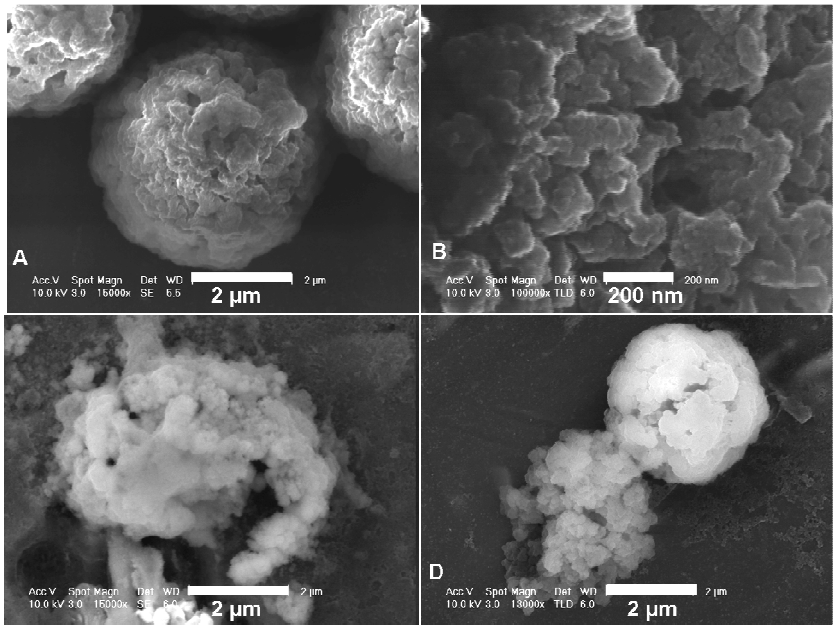

Figure 3.13 SFEG images of 5 µm diameter 525QDEM and 525QDEM bioconjugates.
Micrographs taken with 10.0kV. (**A,B**): 525QDEM before treatment; (**C,D**): 525QDEM bioconjugated to NF oligo. The scale bars were redrawn for clear observation.

Figure 3.14 shows confocal imagines of a batch of 525QDEMs bioconjugates with 70 pmol of Cy3-oligo. The white arrows on the pictures designate the typical imagines of bead structures observed after bioconjugation with Cy3-oligos. Bead number 1 illustrates the uniform distribution of the 525 emission, represented in green, inside the beads after treatments. The bead 2 shows a green fluorescence distributed in the outer skirt of the microsphere. Bead 3 shows approximately no green fluorescence but a high red signals. Bead 4 illustrates a QDEM with a broken shell structure, still emitting green and red fluorescence. Figure 3.14 also shows the disparity of Cy3 fluorescence among the different beads: QDEMs bioconjugates have different red fluorescence intensities.

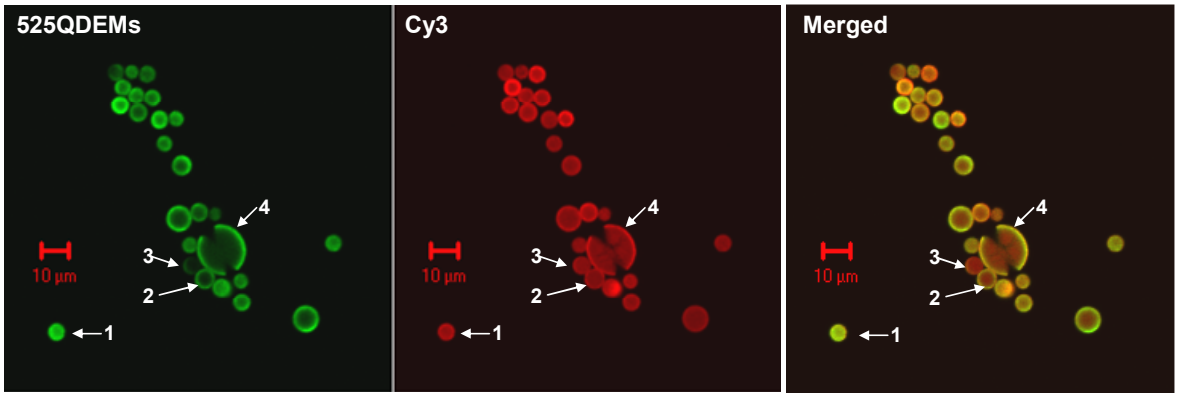

Figure 3.14 Images of 525QDEMs bioconjugates to Cy3-oligos.

True colour imagines obtained with confocal microscopy. QDEM Bioconjugates with 70 pmol of Cy3-oligos. Different QDEM bioconjugates profile indicated by the white arrows with **1**: uniform 525QD emission profile, **2**: localised 525QD fluorescent profile, **3**: with high Cy3 emission profile and quenching of 525QD emission, **4**: degraded structural properties. (10 µm red scales bar). Channel 1 (green spectra) detects 525QDEMs with a BP 505-530 nm, excited at 488 nm (Argon laser, 2% laser power intensity). Channel 2 (Red spectra) detects the Cy3 emission fluorescent with a 543 nm excitation wavelength (HeNe Laser, 60% intensity) and 560-615 nm BP filter. .

3.4. Discussion

A limited number of studies have reported on the application of QD-doped particles in bead-based genotyping assays. Most of the previous research work described different techniques for encoded QDs in microspheres (such as polystyrene, silica) or established the proof-of-principle of allele-specific oligonucleotide hybridisation (ASO) assay. The potential and the efficiency of QD-doped particles as bioconjugate probes for the detection of DNA in suspension arrays was not found to have been quantitatively and specifically addressed in the literature (Resch-Genger *et al.*, 2008).

An initial study was undertaken to evaluate the TriLite™ QDEM technology (Crystalplex, USA) for its sensitivity to biomedical experimental conditions. The results of this work presented in the precedent chapter (Chapter 2) first permitted the selection of buffers and treatments adapted to the development of QDEM-probes for genotyping assay. Secondly, it revealed that QDEM fluorescence code consistency and structural stability needed to be considered as major factors to take into account during this process since QDEM fluorescent and structural properties were sensitive to chemical and mechanical treatments. The second stage of the development of a suspension array using QD-doped particles consisted of the optimisation of short DNA probe attachment to TriLite™ QDEMs, with a quantitative study for its application to ASO genotyping.

The optimal amount of oligo probe to be conjugated to a microsphere depends on: (i) the length of the oligos (in bp), (ii) the nature of the modifications added to the probe (*e.g.,* fluorophore, amino groups, carbon spacer, or ligand), (iii) the size of the targeted DNA to hybridised with the probe, (iv) the size of the microsphere, and (v) the density coverage of the carboxyl (COOH) groups on the microsphere surface. Thus, to enable the development of a genotyping assay, the titration of the probe input to the particular carbodiimide coupling of QDEM was of a critical importance (Crystalplex, USA) (Lowe *et al.*, 2001; Kellar and Iannone, 2002).

A single strand fluorescent oligo directly binding the QDEM surface was used to qualitatively and quantitatively evaluate the fluorescence conjugated to the QDEMs (Figure 3.3). This optimisation strategy assessed the impact of the conjugation buffer, and the influence of the concentration and the structure of the oligos on the conjugation efficiency with 5 µm diameter QDEMs, an optimal bead size for high throughput bead-based assay (Iannone *et al.*, 2000).

Data reporting on the QD-doped particles coupling efficiency with MES or imidazole buffer were not found in the literature, whereas studies on the coupling of dyed beads were available. Spiro *et al.* (2000) obtained a mean signal of ~300,000 to 500,000 oligo/bead, with 5.5 – 5.6 µm diameter beads (Bangs Laboratories, Fisher, IN, USA) corresponding to a D_o of ~2865 to 4775 oligo/µm^2. A specific study in MES buffer was carried out by Wittebolle *et al.* (2006) using 100,000 polybeads of 3 µm diameter (Polysciences, Warrington, PA, USA) with a maximum D_o ~1345 (± 112) oligo/µm^2. In comparison, the maximum conjugation efficiency obtained in the TriLite™ QDEMs study was 2.6 to 4.4 times higher in imidazole buffer, and ten times superior with MES buffer. Heterogeneity in the carboxylation coverage of the different type of beads could explain partially these results, since the number of carboxyl groups on the bead surfaces determines the number of potential sites of attachment for the amino-modified oligos.

The results of the acid/base titration of TriLite™ QDEMs indicated a relative high (COOH) density of ~26.3 µeq/g compared with other carboxylated fluorescent microspheres used for conjugation experiment. As an example, Bangs' carboxylated fluorescent microspheres with a 5 µm (± 0.31) diameter (IN, USA) were described with a 2.0 µeq/g surface charge. Cyto-plex™ carboxylated microspheres of 5 µm (± < 2%) from Duke scientific (Palo Alto, CA, USA) were described to have a 35 µeq/g surface functionalities, but no reports were found on their binding efficiency. Further, the global higher mean of fluorescence observed with imidazole in the bioconjugation experiments performed with probes holding different carbon spacer length (Figure 3.6) confirmed the superiority of using imidazole buffer, and demonstrated the high efficiency of the QDEM conjugation method.

As stated earlier, different parameters known to facilitate the interaction between probes and ssDNA or to increase conjugation efficiency were tested in the QDEM bioconjugation experiment. The carbon spacer that separates the oligos from the microsphere is described as a flexible structure, resistant to bending or shortening, and is reported to minimise steric and electrostatic interferences between the two entities (Agrawal *et al.*, 2008). Previous work demonstrated that a six carbon spacer arm significantly enhanced the carbodiimide coupling reaction (Pack *et al.*, 2007). The elongation of the carbon spacer from six to eighteen carbons (6C, 18C) did not increase the conjugation efficiency in the work presented here (Figure 3.6 and Figure 3.7). The benefit of increasing the incubation time from 1 h to 1h30 was also investigated, showing no significant improvement in the conjugation efficiency. These experiments demonstrated that the conjugation procedure could be undertaken with high efficiency in a short time of incubation and with low cost modified oligos.

Moreover, to evaluate the specificity of the imidazole conjugation method, the activators of the bioconjugation procedure were replaced with H_2O. No significant background noise was detected with 0 to 400 pmol fluorescent probes. The non specific binding ($< 1.25 \times 10^5$ oligos) found with high concentration of fluorescent probe could illustrate the natural tendency of cyanine fluorophore to react with the polymer surface without active agents (Wittebolle *et al.*, 2006) (Figure 3.8D). Cyanine, globally positively-charged molecules, are sensitive to the polarity of their local environment, and could thus interact with the negative charged carboxyl groups attached to the microsphere surface (Ernst *et al.*, 1989). In addition, DNA carrying amine groups and thus potentially positively-charged in ionic buffers, could also interact with the carboxyl groups of the bead surface (Pack *et al.*, 2007). The limited non specific binding obtained with the QDEM method could be due to the accumulation of bovine serum albumin (BSA) protein on the bead surface because of the long term storage buffer used for QDEMs containing 1% of BSA. Native BSA is widely used in microsphere covalent binding assays as a blocking agent for the coverage of hydrophobic surfaces and its protection from non specific interactions (Men'shikova *et al.*, 2001). The buffer could therefore act as a blocking agent, which could explain the high

specificity of the bioconjugation method developed here. Blocking agents and efficient washing steps therefore assured a specific and efficient bioconjugation.

For ~n_{oligo} > 120 pmol the D_o values started to saturate, and after 400 pmol a decline of the conjugated fluorescence was observed in imidazole (Figure 3.5 and Figure 3.6). The carboxylated capacity of the microsphere and/or steric hindrance could explain physical saturation, leading to a restriction of the quantity of fluorescent probe potentially binding the bead surface, as described earlier. Fluorescence saturation could also occur when dye molecules absorb the light emission of other fluorophores that are physically close. First, the close proximity of Cy3 molecules on the QDEMs surface could lead to self-quenching between identical fluorophore species (Wang and Tan, 2006). Secondly, fluorescence resonance energy transfer (FRET), highly dependent on the distance separating the donor of energy to its acceptor, was discovered between 525 nm QDs and the Cy3 fluorophores covalently attached through a well-characterised construct (Clapp *et al.*, 2004). The most effective FRET interaction was found for distances separating both materials within a range of 5 to 10 nm. Although the spectral overlap between 525QDEM and Cy3-probes was probably ideal and the high level of functionalisation could potentially facilitate the interactions described in the work of Mattoussi *et al.* (2004), FRET was considered to have a minor role in fluorescence quenching, in this study, because of the distance separating QDs in the microsphere from the external Cy3 fluorophore.

The construct presented in this study separates the 525QDs, potential donor, from Cy3 molecules of fluorophore (acceptor) by a polystyrene matrix coated with a methacrylate layer and a (6C) carbon spacer attached to a 18-mer ssDNA. Although the 6C spacer arm could confer a relative flexibility of the oligo strand, the length of 6C and 18-mer oligo would nevertheless be in the range of ~7 nm, a theoretical distance calculated from the work of Agrawal *et al.* (2008). In the hypothesis that QDs can be localised close to the surface of the polystyrene microsphere, the Cy3 fluorophore would then be separated from the core of the QDs by the QD protective shell and coating, and the microsphere matrix adding to the minimum distance calculated of 7 nm. Therefore, FRET could occur during

conjugation but depending on the distribution of the QDs within the sphere, its impact on Cy3 fluorescent efficiency should be limited. The phenomena of FRET could explain why the variations between samples during imidazole conjugation seemed higher than the variations between samples observed with MES buffer. The wide error bars observed with imidazole could be linked to a higher variable inhibition process due to a global higher concentration of fluorescent probes on the QDEM surface, which could increase the potential of transitory quenching events. Finally, fluorescent measurements reaching the detection limit of the FC optical detectors could be the last factor participating to the fluorescence saturation (Enderlein, 2005).

Ideally, an optimum bioconjugate implies an optimum coverage of the bead surface with oligos, which avoids saturation or/and steric interaction. A high density of probes on the bead surface could result in steric hindrance, lower diffusion of ssDNA, and repulsion due to negative forces of molecule, all of which would inhibit the DNA interactions, and hence the hybridisation of ssDNA with the probes attached to the bead in the final ASO assay (Peterson *et al.*, 2001). Both fluorescence and steric saturation limits the hybridisation of the probe to its target and fluorescent detection during the hybridisation process. From these observations, the optimum probe quantity to conjugate to the QDEMs was chosen to be largely lower to the saturation point of conjugation, while still providing an optimum probe coverage. The value of the direct probe quantity was calculated from the imidazole and MES titration results and a linear relationship was found between the oligo quantity and the number of oligos attached on the bead surface (Figure 3.5). The optimum range of the direct probe was determined with the most efficient buffer as the equivalent to the quantity needed to reach approximately half of the first saturation point, *i.e.,* ~60 to 70 pmol. This value presented high conjugation efficiency (D_o ~7900 – 10,000 (± 3600 - 2700) oligo/μm^2) with high probability of avoiding the drawback of oligo saturation observed for high quantity of direct probe. The high specificity and sensitivity of the assay was demonstrated since no significant background noise was detected in the expected optimum oligo range (60 – 70 pmol) (Figure 3.8D). The specificity of QDEM bioconjugation with 65

pmol was confirmed with the absence of Cy3 signal on the confocal microscopy images of the QDEM bioconjugates (Figure 3.8E,F).

The observation of the different fluorescent sectioning profiles of initial untreated QDEMs and QDEM bioconjugates (Figure 3.8A,B,C, and Figure 3.14 arrow 1,2) confirmed the observations made previously in the characterisation of the material (Chapter 2): the resuspension treatments applied to the bead during the procedure, and especially repeated sonications/vortex processes, provoked a redistribution of the QDs inside the polystyrene lattice. Under ultrasound sonication the swelling of the polymer induce the QDs to "soak" in the matrix, and to penetrate the interior of the microsphere, creating the images of a uniform QDs distribution in the QDEMs (Figure 3.14).

The bioconjugation procedure exhibited two other distinguishable effects on the QDEM optical and structural properties that could be a limitation during the hybridisation process. The effect of the bioconjugation procedure on the QDEMs was systematically evaluated by comparing a control population against treated QDEMs. The specificity of the code identification and the sensitivity of the target detection in suspension assays are typically limited by the amount of background noise detected on the bead population at a specific wavelength. Fluorescent signal due to non specific binding on the microspheres was found to be blocked by the 1% BSA present in the QDEM storage buffer. The background signal detected in the QDEM assay was therefore mainly composed of autofluorescence: the fluorescence associated with the microsphere substrate and the attached probe or DNA target. First, an increase in the intensity of a 10-fold log scale was specifically detected in FL1 and FL2, for non encoded microsphere conjugated to 60 pmol of a 40 bp oligo mainly composed of purine bases (Figure 3.9 and Figure 3.10). The statistical results comparing 0QDEM bioconjugates to the control population confirmed that the increase in FL1 and FL2 in the bioconjugate population observed on the histograms and mesh plot graphical representations were statistically significant (Figure 3.11A). In contrast, the fluorescent code of the 525QDEM initial population, detected in FL1, decreased with a high level of significance in the bioconjugate population (Figure 3.11B). Confocal images of 525QDEM

bioconjugates illustrates both phenomena with the significant decrease or absence of 525 nm emission (Figure 3.14, bead 3) and the destruction of the spherical structure (Figure 3.14, bead 4). As detailed before, the conjugation buffer, and the different treatments (washing steps, vortex, sonication, agitation) applied to the QDEM solution during bioconjugation experiment had a significant negative impact on the QDEM fluorescence and structural stability. The decrease of QD fluorescence emission in the microsphere can be related to fluorescence quenching or washing out of the QDs out the beads due to the bioconjugation treatments (Section 2.4).

The effect of the overall bioconjugation process was evaluated to assess its consequences on the method's efficiency. The mean of the relative percentage of fluorescence and events was calculated with the QDEMs replicates before and after bioconjugation (Table 3-3).

Table 3-3 The statistical differences between 525QDEM controls and bioconjugates *

525QDEM	FL		% Events	
	Control	*Bioconjugate*	*Control*	*Bioconjugate*
Lower 95% CI of mean	780.7	508.1	86.1	57.9
Upper 95% CI of mean	797.6	564.2	88.75	76.8
Relative % CI of mean	~ 65 - 71		~ 67 - 87	

* CI: confidence interval; CI data taken from Appendix I, Table 2.b

The results demonstrated that the choice of buffer and handling has been optimised since it minimised the bead loss: ~67% of the initial QDEM population were recovered at the end of the procedure. The diminution of QDEM-probes during the conjugation experiment involves a loss of fluorescent probes which implies a loss of quantitative and qualitative information on the bioconjugation efficiency. It is also not cost efficient since it potentially incurs higher experimental cost due to the need of an initial higher number of QDEM materials to obtain the expected quantity of fluorescent probe for analyte detection.

The bioconjugation procedure had a major impact on the fluorescent code of the beads with the diminution of 30 to 35% of the fluorescence emission intensity of the QDEMs. The impact of autofluorescence on the 0QDEM fluorescent code and the modification of the 525QDEM fluorescence code due to washing-out of the QDs out of the microsphere or other structural modification could be a limitation to the high throughput of multiplexed QDEM assay (Section 2.4). Further, the changes in 0QDEM and 525QDEM signals present the potential of the encroachment of the fluorescent codes when the number of QDEM codes increases, but also when the complexity of the QDEM codes detection intensifies. The potential overlap of fluorescent profiles could reduce the number of QDEM fluorescent codes that could be used in a single experiment. The impact of encroachment upon bead signals for a subset of QDEM before and after bioconjugation would need to be modelled and empirically evaluated to optimised code detections adapted to QDEM bioconjugates. However, it has been shown that the encroachment on the analyte signal was not expected to be significant if effective gating and mean analyte signal algorithms were employed (Yang *et al.*, 2007). Consequently, it was necessary to use the bioconjugate population as the population of reference to identify and gate the QDEM populations on the flow cytometer. Specific FC protocols had to be adapted to the modified QDEM bioconjugate fluorescent code in order to successfully plot and collect the mean of intensity of multiplex QDEM-bioconjugate populations.

The second effect of bioconjugation on the bead stability appeared to be independent of the encoding of the QDEM. Broken microsphere structures were observed in the bioconjugate population and identified as damaged materials. The destruction of the bead chemical shell was then confirmed as one of the mechanisms potentially responsible for the diminution of the percentage of events after bioconjugation (Figure 3.13 and Figure 3.14 bead 4).

Elastic light scattering in the forward, (FSC) and perpendicular (SSC) direction were used to characterise the QDEM populations under study, *i.e.,* non encoded QDEM, 525QDEM, control and bioconjugate QDEM populations (Section 1.1). A significant increase in FSC was observed with 0QDEM bioconjugates but not with the 525QDEM bioconjugates

(Figure 3.11). The significance of the variation between the control and the 0QDEM bioconjugates was at a low level ($p = 0.0271$). FSC is mainly proportional to the size and shape of the particle detected: the larger the QDEMs the more light is scattered, hence the higher the MFI. The increase in FSC for 0QDEM bioconjugate population could be first explained by a general increase in the size and shape of the beads due to the conjugation of probes on its surface, and due to the swelling of the microsphere under sonication treatments. The hypothesis that the observed variations were linked to the QDEM size variation within the control population was excluded since the quantity of QDEMs analysed for each experiment represented less than 1% of the total QDEM initial concentration with a coefficient of size variation of 10%. The increased in FSC was then related to the changes in the surface topography of the microsphere after conjugation, due to the treatments and the attachment of oligo on its surface.

In contrast, a difference between 525QDEM control and bioconjugates was observed for the SSC with a low level of significance ($p < 0.0291$) (Figure 3.11) whereas no significant variation was calculated with 0QDEM bioconjugates ($p = 0.2549 >> 0.05$). The limited diminution in SSC was related to the leak of QDs during bioconjugation procedure and/or the redistribution of the QDs within the sphere. The loss of QDs could change the refractive index of the microsphere, and therefore modify the SSC MFI. These observations were confirmed by the absence of variation in SSC in the non encoded microsphere bioconjugates. A variation in FSC between 525QDEM control and bioconjugate was expected as the modification of the surface with oligonucleotides should have increased the FSC values as observed with the 0QDEM bioconjugate population. The detection of the SSC and FSC variations are dependent on the sensitivity of the optical detector of the FC instrument. FSC variations could be missed by the FC instrument if the variation of the light emitted was in a constrained range of values inferior to the standard limit of detection. These limitations could explain the result of the statistical analysis of the FSC comparison between 525QDEM control and bioconjugate, which gave a *p*-value with a very low level of non significance at $p = 0.069$, just above the 5% limit of significance (Appendix I, Table 5).

The initial differences of the 0QDEM and 525QDEM structure and composition due to the encoding procedure could also have had an impact on their response to light scattering, leading to a different pattern of the FSC and SSC variations upon treatments. The impact of the bioconjugation procedure was then compared directly between 0 and 525 QDEM populations. The variation in the scattering light emissions (SSC, FSC) and the percentage of events was investigated on the corrected paired data of both 0 and 525 QDEM populations. No significant differences were observed for all the parameters (Figure 3.12). The variation of the percentage of events between 0 and 525QDEM did not show any significant difference, whereas both types of QDEMs were affected by the treatment and the recovery of the QDEMs after the bioconjugation was significantly lowered by an average of 20% (Appendix I, Table 4, Table 9.). The same variations observed for both populations illustrated the reproducibility of the bioconjugation procedure for separated batch experiments. Secondly, the stability of the SSC and FSC signal, and the percentage of events were independent of the fluorescent code of the QDEM populations. These observations can also be explained by the identical post-encoding synthesis procedure applied to blank beads: the same protective layer is applied to both encoded and non encoded microspheres (Chapter 2).

QDEM technology is still under development and the optimisation of QDEM bioconjugates have to consider this constraint; however, it is important to develop a method for future efficient high throughput suspension assays. In summary, TriLite™ QDEMs could be conjugated to small quantities of short oligo probes within 1 hour, reaching higher conjugation efficiency than previous work, and using only a 6 carbon spacer. The assay utilised also minute quantities of QDEMs (~10,000), which is well adapted to future research in high throughput format. The impact of the treatments applied to the QDEM during bioconjugation was minimised through the selection of buffer and experimental conditions adapted to the bead structural and optical sensitivity. A good reproducibility of the bioconjugation procedure enabled, on average, the recovery of ~75% of initial QDEMs, with a relative code consistency of ~81%, taking 525QDEM as a encoded population model.

Chapter 4

Optimisation of QDEM-based DNA Hybridisation Assay using a 'Design of Experiments' Approach

4. OPTIMISATION OF QDEM-BASED DNA HYBRIDISATION ASSAY USING A 'DESIGN OF EXPERIMENTS' APPROACH

4.1. Introduction

An efficient method was developed in the previous chapter (Chapter 3) to synthesise QDEM probes specifically adapted to DNA identification in suspension format. The optimisation of the hybridisation of the QDEM bioconjugates to a DNA target in solution represented the second main experimental stage in the development of the QDEM allele specific oligonucleotide (ASO) genotyping assay (Figure 1.15). At this stage, the perspective of developing an assay for highly specific and sensitive recognition of DNA targets in complex mixtures with the QDEM-probes required a powerful optimisation strategy.

Specific protocols and empirical studies have been reported on hybridisation in solution with flow cytometry (FC) detection. Commercially available sets of dyed-microsphere have been optimised for high throughput multiplexed DNA detections for clinical and research applications (Spiro *et al.*, 2000; Hurley *et al.*, 2004; Dunbar, 2006). Technical reports that describe methodologies for bead-based assays adapted to QD-doped particle DNA probe are limited, and no commercial products could be found to help in the optimisation of the assay by standardised conditions. QD-doped particles were mostly used in previous studies as fluorescent probes to establish their potential in genotyping assays (Sukhanova and Nabiev, 2008). The literature illustrates thus the need to develop optimised hybridisation protocol in suspension specifically adapted to QD-doped particles (Resch-Genger *et al.*, 2008). The first set of QD-encoded polystyrene porous microspheres commercially available, the QDEMs, but also the most common type of QD-doped particles, were used in this research study to develop a specific hybridisation genotyping method adapted to FC detection.

The experimental factors that needed to be optimised in order to reach reproducible, efficient and sensitive hybridisation response were: the QDEM-probe quantities, the target quantities, the hybridisation buffers, and the hybridisation incubation conditions (temperature, and time). The results obtained from the study of the QDEM material and from the optimisation of the QDEM bioconjugates highlighted new parameters to be taken into consideration for the optimisation of the suspension hybridisation assay adapted to QDEMs. To summarise, the studies and results from chapter 2 and 3 showed that the effect of the experimental procedure on the fluorescent code and structural stability required to be investigated for the use of QDEMs in bioassays. The stability of the QDEM material was therefore added to the response factors to be optimised in the development of the allele-specific oligonucleotide (ASO) QDEM-based hybridisation assay. The response factors to be optimised were therefore: the QDEM stability and the hybridisation efficiency and sensitivity.

The optimisation of DNA hybridisation for genotyping assays is an overall complex experimental approach since it is dependent upon multiple initial parameters. The initial challenge when optimising a system which is dependent on a large number of parameters is to decide which factors are to be considered in the optimisation process. This selection is generally based on the literature rather than on empirical study, which is largely due to the still incomplete knowledge of the physical aspects of the assay. The selection of more than two or three factors to optimise, multiplies the number of experiments needed, especially if a sequential method is used. The sequential empirical work not only augments the number of experiments, but also completely ignores all interactions between the different factors. This method of optimisation can also be biased toward the first parameters to be optimised if the optimisation of the following parameters is performed based on the optimum conditions found for the first parameter optimised. Consequently, the basic approach of variation of the concentration of one factor while keeping the other factors fixed, appeared inefficient, biased, and poorly informative for the objective of the research, considering the numerous factors involved in the optimisation of the QDEM-based genotyping assay (Kim and Kalb, 1996; Wrobel *et al.*, 2003).

The necessity of the optimisation of the hybridisation step suggested the use of a more sophisticated approach than the sequential strategy. The design of experiments (DOE), described as a strategy to plan research, was first introduced in the early 1920s to enable the execution of valid experiments in the presence of many fluctuating conditions such as temperature, soil conditions and rainfall. Since then, the DOE has been applied to food industry, military applications, and health-care industry (Altekar *et al.*, 2007; Drago *et al.*, 2008). The DOE is an efficient and simple statistical approach suitable to select parameters of influence and optimise the hybridisation procedure (Montgomery, 1997). The main advantages of this approach for the optimisation of the assay were: to be unbiased towards any factors, to reduce the number of experiments needed to determine the optimum of each parameter, and to improve the statistical interpretation options. With the DOE, the number of experiments is directly linked to the amount of information gained from it. Overall it offers promise to reduce the analytical time while it increases the information gained and reducing consumables consumption.

A limited number of studies were found to report the recent use of DOE in molecular biology, even though it is a common approach to comparable issues in other scientific fields such as biosensors and analyte identification (Boleda *et al.*, 1996; Singh *et al.*, 2005; Ryan *et al.*, 2009). However, Boleda *et al.* (1996) described the use of experimental design techniques to improve the PCR optimisation (*i.e.,* easier, quicker and cheaper) of DNA from blood spots. The factors affecting the product yield (screening factors) were first determined, and the quantity of template DNA and the Mg^{2+} concentration needed for the PCR were then optimised (factors to optimise). Wrobel *et al.* (2003) demonstrated that the DOE significantly improved the optimisation of cDNA-microarray experimental protocols. Hence, response surface methodology (RSM), the statistical experiment designs mostly used in the DOE was chosen to accelerate and improve the optimisation of the hybridisation step in the QDEM suspension array (Haaland, 1989).

The nomenclature used in the DOE applied to the QDEM hybridisation assay includes (Lutz *et al.*, 1996):

- *Factors* are experimental (independent) variables that can be changed by the experimentator (in this case: temperature, time or hybridisation buffer);
- *Levels* represent the specific settings associated to each factor for a given experiment;
- *Interactions* illustrate the different combination of relationship between factors (*e.g.*, interactions between time and temperature);
- *Responses* are the variables (dependent) or the quantity that the experimentator aims to optimise (*e.g.*, hybridisation signal in median of fluorescent intensity, yield in a chemical reaction);
- *Effects* represent the magnitude of the changes in response as factors are varied;
- A *run* is a specific experiment performed for specific settings established for each factor implicated in the reaction;
- The *main effects* estimate the standard deviation or significance of the parameters associated with each factor in the statistical model.

Experimental design is based on the initial choice of factors and responses. Factors' selection depends on the investigator and corresponds to the parameters that are believed to have an effect on the responses under study. Different types of designs are available to sample the space defined by the factors. The choice of a design depends on the objectives of the experiment, and on the actual knowledge about the experiment environment, *i.e.,* on the number of factors and their possible ranges or levels. Popular designs include 'screening designs', and 'Response surface modelling' (RSM). Screening design investigates experimental strategies when little is known about the effects. Essential information on the effects can be obtained from this DOE but interactions cannot be interpreted. The screening experiment was not adapted to the optimisation process undertake in this study (Altekar *et al.*, 2007).

Response surface modelling (RSM) provides precise information about factors' effects including magnitude and direction. The number of factors is typically between two and six. RSM uses a regression equation to describe the relationship between factors and responses. This design intends to select the optimal settings of a set of experimental factors, which have to be quantitative (or numerical) factors. RSM provides the prediction of the responses under study within the experimental space of study and allows the identification of optimum experimental conditions to obtain optimum response values. RSM is based on factorial design and involves at least three levels of the experimental factors. Factorial design can be represented by geometric shapes: a square for 2-factor, 2-level design, and a cube for a three-factor, two-level design. Additional data are collected in RSM to improve the definition of the response: first a centre point is established at the centre of all of the design points and then "star points" are added to cover regions away from the design points (Figure 4.1). These designs are called central composite designs or CCD (Myers and Montgomery, 2002; Altekar *et al.*, 2007).

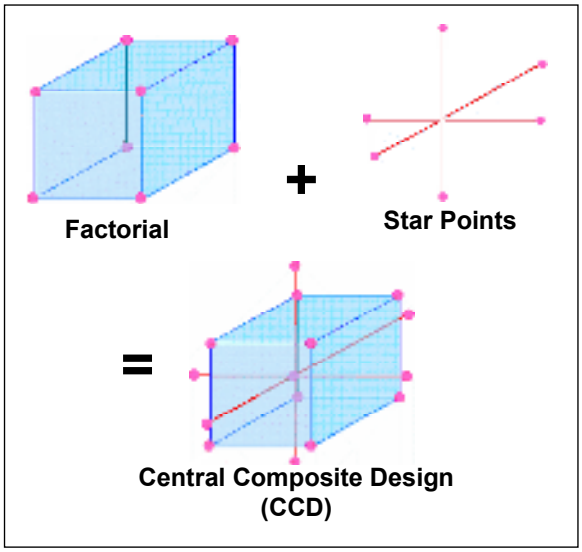

Figure 4.1 Graphic representation of central composite design (CCD) and star points (adapted from Altekar *et al.*, 2007).

Response surface methodology was used to study the relationship between the parameters influencing the hybridisation reaction (factor variables) and the different responses (response variables) of the hybridisation experimentation. The most frequent conditions used in multiplex ASO genotyping studies were defined in Chapter 2. Preliminary experiments were carried out to screen the appropriate parameters and to determine the experimental ranges of investigation (Chapter 2). Four primary experimental parameters had a major impact on the hybridisation procedure:

1. Hybridisation buffer
2. Single strand target oligo quantity
3. Time
4. Temperature

In order to be able to quantify the hybridisation efficiency, a specific experimental protocol was undertaken using a fluorescent oligo which hybridise the QDEM-probes. Therefore the four experimental factors listed before were expected to have a major effect on the two response variables analysed:

1. The hybridisation of a fluorescence oligo on the bead surface, measured in median of fluorescent intensity (MFI) (FC measurements)
2. The QDEM structural stability, measured as the percentage of events recovered at the end of the procedure (FC measurements)

Hybridisation buffer being a categorical factor (not quantitative), it could not be added as a factor in a RSM strategy. Hence, the impact of two buffers on the hybridisation responses was evaluated individually, with two RSM. These first experimental design approaches were also used to evaluate the level of the other quantitative factors and define optimum range values. A central composite design (CCD) with two-level factorial design, central points, and star points, [2^3 + star], was chosen to study the effects of three factors. The number 3 corresponded to the number of independent factors (X): temperature (degree Celsius, °C), time (minutes) and oligo quantity (molar).

The [2^3 + star] design is represented in Figure 4.1 and expressed in standard units where -1 and +1 represent respectively the low and high level of each factor. The additional star points are shown in the run 9 to 14. The star point's values were set equal to specific numbers to be able to produce desirable properties (see below). Table 4-1 represents the series of runs to be performed with different combinations of the three independent factors at different levels. For each experiment, three replicates were undertaken to estimate assay variability. The interpretation of the results and identification of significant differences between the factors tested in the assay is possible and depends on the estimation of the variability.

Table 4-1 Factor levels of the experimental design

	Factors (X)		
Run	Temp (°C)	Time (min)	Target (pmol)
1	-1.0	-1.0	-1.0
2	1.0	-1.0	-1.0
3	-1.0	1.0	-1.0
4	1.0	1.0	-1.0
5	-1.0	-1.0	1.0
6	1.0	-1.0	1.0
7	-1.0	1.0	1.0
8	1.0	1.0	1.0
9	-2.0	0.0	0.0
10	2.0	0.0	0.0
11	0.0	-2.0	0.0
12	0.0	2.0	0.0
13	0.0	0.0	-2.0
14	0.0	0.0	2.0

The RSM approach was also selected since it allowed the optimisation of the QDEM assay for multiples responses variables.

The multiple response optimisation (MRO) approach is used to determine which settings of the experimental factors achieve the desired characteristics for more than one response simultaneously. To use MRO, the RSM data are first analysed for each response variable to create a model for each separately. The desirability function (d(y)) is then constructed based on the values obtained for each optimised response. The desirability function of each response is combined in a later stage into a single function that can be maximised, minimised or set at a specific value (Myers and Montgomery, 1995). The data from each RSM analysis are collated to perform the joint optimisation of the two QDEM responses. Hence, MRO was used to optimise the two desirable responses of the hybridisation assay: the hybridisation signal and the QDEM recovery.

MRO approach assumes that the response values equal to (y) can be modelled through the desirability function d(y), where the desirability ranges from 0 to 1. The desirability function depends on the objectives of the response optimisation, which are defined by the MRO analysis options. The objective in this study was to maximise the fluorescent hybridisation signal and the QDEM recovery. The desirability function for the maximisation of the hybridisation responses was therefore defined by the following equation (StatPoint, VA, USA):

$$d = \begin{cases} 0 & \hat{y} < low \\ \left(\dfrac{\hat{y} - low}{high - low}\right)^{s} & low \le \hat{y} \le high \\ 1 & \hat{y} > high \end{cases} \qquad (1)$$

Where y is the predicted value of the response variable, *low* is a value below which the response was unacceptable, and *high* is a value above which the desirability was at its maximum. The low and high limits were defined as default values corresponding to the lowest and highest value obtained from the experimental data (Table 4-6). The function was represented as a plot in Figure 4.2.

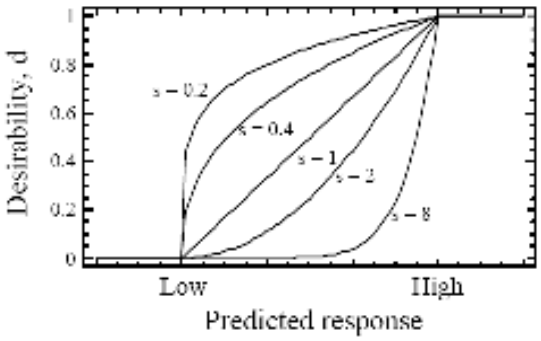

Figure 4.2 Desirability function for the maximisation of the response variables (StatPoint, VA, USA).

The parameter *s* defines the shape of the function. For $s = 1$, the desirability rose linearly from 0 at the *low* value to 1 at the *high* value. For $s < 1$, it increases quickly at first and then horizontalises. For $s > 1$, it increases slowly at first and then faster. The *s* parameter can be set large if it is very important to be close to the maximum level or small if anywhere over the specified response range is approximately equally desirable.

To combine the desirabilities of *m* responses, a single composite function *D* is created. For all the DOE, both response variables are considered to be equally important, and the composite function is the geometric mean of the separate desirabilities given by the following equation (Statgraphic, VA, USA):

$$D = \{ d_1 d_2 \ldots d_m \}^{1/m} \qquad (2)$$

The work presented in this chapter aimed to optimise the hybridisation of oligos to QDEM-probes. The two main objectives were to maximise the hybridisation signal detected through continuous FC by the attachment of fluorescent oligos to QDEM-probes, and to maximise the percentage of QDEMs recovered at the end of the assay. Hybridisation buffer, time, temperature and oligo target quantity were selected as the main parameters influencing the hybridisation reaction. RSM and MRO were used to predict optimum conditions, which were then empirically evaluated.

4.2. Materials and Methods

4.2.1. Materials

Materials, chemicals and instrumentation were as previously described (Section 3.2).

- **QDEMs and oligos**

The specificities of this study involved the use of two types of 5 µm carboxylated QDEM control populations (Appendix A): non encoded beads (0), and 525 nm QDEM (525)(1;0) (Crystalplex, USA). The direct non fluorescent conjugation oligos (NF-oligo) to be attached on the QDEM surface were designed as previously described (Section 3.2.2).

Specific fluorescent single strand DNA probes (ssDNA) were designed to study the kinetic and specificity of oligo hybridisation to the QDEM bioconjugates (Table 4-2). The *in silico* probe were designed according to previous methodology (Han *et al.*, 2001; Xu *et al.*, 2003). The "Indirect" probes consisted of a 18-mer poly-thymine ($poly(T)_{18}$) modified with a Cy3 at the 3' extremity, and complementary to the $poly(A)_{18}$ of the NF probe attached to the bead (Table 4-2). The organic fluorophore Cy3 was chosen in order to avoid emission overlap with the QDEM emission signal. Oligos were obtained from Thermo Electron (Bremen, Germany).

Table 4-2 Oligos used for the optimisation of the hybridisation experiment *

Name	Structure 5'→ 3'	Specification
Direct NF probe	NH2 – 6C – seq – poly(A)	22 seq mer, 18 (A) mer
Cy3 hybridisation probe	Poly(T) – Cy3	18 (T) mer, Cy3

* NF: non fluorescent; 6C: 6 carbon spacer; (T)-mer: thymine polymer; (A)-mer: adenine polymer; seq: oligo sequence with a GC content < 50%; Cy3: cyanine 3 fluorophore emitting at 575 nm

- **Flow cytometry**

All the materials and methods related to the flow cytometer (Coulter-Epics XL-MCL, Beckman-Coulter, USA) were as previously described in section 2.2.6. A new FC protocol was designed for the hybridisation optimisation procedure to specifically characterise the fluorescent signal of the control QDEM (0 or 525) and the hybridisation signal (Cy3). The QDEM control populations from the working solutions were used to define the region of the population under study. The mean fluorescence intensity (MFI) was then recorded on gated QDEM populations in the detector channels FL1 and FL 2 highlighted in bold in Table 4-3.

Table 4-3 Fluorescent detection parameters used in the hybridisation optimisation experiments

Detection channel Microscope / FC	Band pass filter (in nm)	Visible colour	Emission λ (in nm) QD / Fluorochrome
Ch1 / FL1	**505-545**	**Green**	**525**
Ch2 / FL2	**560-590**	**Yellow-Orange**	**575 / PE, Cy3**
FL3	605-635	Red	630
FL4	660-700	Deep Red	665 / Cy5

4.2.2. Conjugation protocol

The method for coupling NF-oligos to QDEMs was as previously described (Figure 3.1, section 3.2.1). The methodology was modified following the optimum conditions obtained from the results of previous experimentation obtained in Chapter 3). Briefly, a volume equivalent to 10,000 QDEMs (enumerated with a haemocytometer, Appendix C) was conjugated by amino-carboxy coupling to 60 pmol of NF-oligo in 20 µL of imidazole (pH 7.0) coupling buffer. Centrifugations were performed at 1133x g for 4 min. After incubation, samples were washed (RT, 4 min, 400 rpm) once in 300 µL of imidazole (pH 7.0), twice in the storage buffer (1X TBS, 1% BSA, 0.01% azide). QDEMs were resuspended in 15 µL of storage buffer (1X TBS, 1% BSA, 0.01% azide) and kept at 4°C.

Before storage, QDEM bioconjugate solutions were quantified (Appendix C). The quantification of bioconjugate samples with the haemocytometer method provided an average recovery of 8000 QDEMs (two measurements for each batch of bioconjugates). The stored beads were washed in 300 µL of hybridisation buffer (3X SSC or 6X SSC) for 20 s at RT, centrifuged and resuspended in the volume used for hybridisation experiment just before starting the hybridisation procedure. In most experiments, the freshly made bioconjugates were directly used for hybridisation. In the later case, the last wash was performed in the hybridisation buffer and QDEM bioconjugates were resuspended in the volume required for the hybridisation experiment.

Negative controls were used as previously described (Section 3.2.2): QDEM stock solutions and QDEMs incubated with clean water were used to evaluate the fluorescent noise inherent to the flow cytometer and the effect of the procedure on the QDEM emission signal. Negative controls were performed for each batch of bioconjugates prepared for the hybridisation study.

4.2.3. DNA hybridisation experiments

- **Experimental scheme**

An "indirect" fluorescent oligo (the target) was designed to specifically hybridise with the oligo sequence covering the surface of the QDEMs (the QDEM-probe). The hybridisation efficiency was evaluated through the fluorescent signal of a Cy3 organic dye attached at the 5' extremity of the indirect oligo (Figure 4.3). The poly(T) sequence hybridised with the poly(A) of the conjugation probe on the QDEM surface.

QDEMs incubated with NF-oligo but without the activators (EDC, Sulfo-NHS) were used as negative controls to quantify the non specific hybridisation. The fluorescence detected with untreated QDEMs and the initial QDEM working solutions were used as a baseline to correct the fluorescence detected in FL1 and FL2 for the different batch experiments.

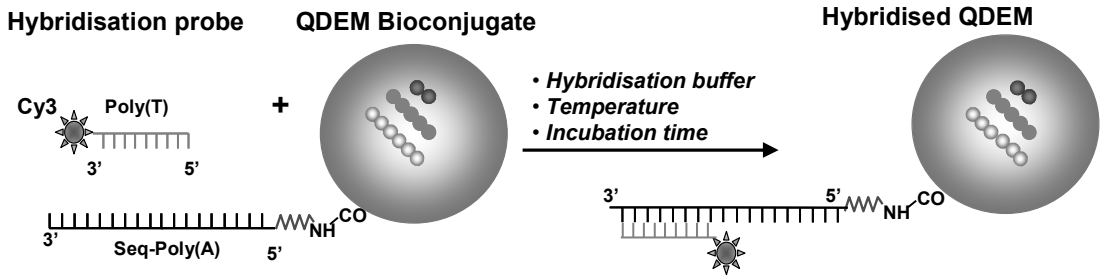

Figure 4.3 The experimental scheme of the hybridisation optimisation assay.
Hybridisation with fluorescent indirect probes; QDEMs are encoded with different ratios of QDs emitting at different wavelengths. QDEMs specific signal encoded in terms of colour and intensity, allowed the discrimination between QDEMs and the attached fluorescent probe**.** Oligo sequences poly(T) and poly(A) are complementary. Cy3: cyanine 3 organic fluorophore.

- **Experimental protocol**

Hybridisation experiments were performed in the dark (experiments covered with aluminium foil). Blank QDEM bioconjugate samples were incubated in 15 µL of prewarmed hybridisation buffer (3X SSC or 6X SSC from 0.015% sodium citrate, 0.15 M sodium chloride, pH 7.0) in the conditions defined by the design of experiments (DOE) approach (Section 4.2.4). All the hybridised samples were washed at room temperature (RT) under 400 rpm, in 400 µL of 0.5X SSC / 0.05% SDS for 4 min, then in 400 µL of storage buffer for 2 min, and another 1 min, and finally in TE (pH 8.0) for 1 min. Samples were analysed in 400 µL of TE (pH 8.0) on the flow cytometer.

4.2.4. Hybridisation optimisation with 'design of experiments'

The hybridisation conditions of the QDEM suspension assay were optimised through experimental design (DOE), with the response surface methodology, which is the statistical experiment design mostly used in DOE (Haaland, 1989). The central composite design (CCD) was employed in this regard (Montgomery, 1991). Experimental design and data analysis were calculated and represented graphically with StatGraphics Centurion XV trial version for Windows (StatPoint, Herndon, VA, USA).

Preliminary experiments were carried out to screen the experimental parameters in order to ease the selection of the experimental ranges of investigation. The study of the QDEM material in chapter 2 and 3 identified the sodium citrate buffer (SSC) as the most suitable buffer to develop a QDEM bead-based assay (Sections 2.3.4 and 3.3.3). As a result, two levels of categorical factors were chosen: a low and high stringent SSC buffer, respectively 3X and 6X SSC. Temperature and time conditions were also investigated. The selection of temperature ranges of 45 to 60 °C and incubation time range of 30 to 90 min were based on the literature and the results obtained in Chapter 2. The oligo quantity was determined from the literature and the quantity range corresponded to the expected quantity of a sensitive hybridisation assay (Spiro and Lowe, 2002; Lowe *et al.*, 2004; Horejsh *et al.*, 2005). All

factor ranges are summarised in Table 4-4. As an example, the experimental points undertaken for the DOE -1 with 3 X SSC buffer are presented in Table 4-5. The other tables can be found in Appendix I.

Table 4-4 Factor levels of the experimental design DOE-1 and DOE-2

DOE-1	*Level*	*Temperature (°C)*	*Time (min)*	*Oligo Quantity (pmol)*
3X SSC	– 1	45	30	0.05
	0	50	60	50.025
	+ 1	60	90	100
6X SSC	– 1	45	30	0
	0	53	60	50
	+ 1	55	90	1000
DOE-2	*Level*	*Temperature (°C)*	*Time (min)*	*Oligo Quantity (fmol)*
optimal SSC buffer	– 1	45	30	0.5
	0	50	60	50.25
	+ 1	55	90	1000

Table 4-5 Experimental runs to performed for DOE-1, 3 XSSC buffer

DOE-1 3 X SSC	Factors variables		
Number of Replicates	**Temp (ºC)**	**Time (min)**	**Conc (pmol)**
3	60	60	0.05
3	45	60	0.05
3	52.5	30	100
3	52.5	60	50.025
3	45	60	100
3	60	30	50.025
3	45	90	50.025
3	52.5	90	100
3	52.5	30	0.05
3	60	90	50.025
3	45	30	50.025
3	52.5	60	50.025
3	52.5	60	50.025
3	60	60	100
3	52.5	90	0.05

The multiple response optimisation (MRO) was used to optimise the two desirable responses analysed in the assay. The desirability functions ($d(y)$) for the maximisation of the hybridisation signal and the maximisation of the QDEM recovery were described by the following equations (StatPoint, VA, USA):

$$d_{\mathrm{RMFI}} = \begin{cases} 0 \\ \left(\dfrac{\mathrm{RMFI\ calc} - \mathrm{RMFI\ min\ obs}}{\mathrm{RMFI\ max\ obs} - \mathrm{RMFI\ min\ obs}} \right) \\ 1 \end{cases} \qquad (1)$$

$$d_{\%\mathrm{R}} = \begin{cases} 0 \\ \left(\dfrac{\%\mathrm{R\ calc} - \%\mathrm{R\ min\ obs}}{\%\mathrm{R\ max\ obs} - \%\mathrm{R\ min\ obs}} \right) \\ 1 \end{cases} \qquad (2)$$

Where RMFI and $\%R_{\mathrm{calc}}$ were the predicted values of the optimised hybridisation signal and the percentage of bead recovery; $[\mathrm{RMFI} / \%R]_{\mathrm{min\ obs}}$ were the minimum RMFI / %R values obtained from the experiments, below which, the response was unacceptable, and $[\mathrm{RMFI} / \%R]_{\mathrm{max\ obs}}$ were the maximum RMFI / %R values obtained from experimental data, above which, the desirability was at its maximum. Table 4-6 illustrates the analysis options defined for the MRO analysis of the different RSM.

Table 4-6 Responses variables and criteria of analysis for MRO*

Responses	*Data*	*Units*	*Low/High*	*Desirability*
QDEMs Recovery	Relative % Events	% (a.u.)	default	maximise
Hybridisation signal	RMFI of FL 1	% (a.u.)	default	maximise

* a.u.: arbitrary units; Default: values over which response variables were optimised separately

The desirabilities of the two responses were combined and a single composite function *D* was created by the software (Statgraphic, VA, USA). Both hybridisation signal (RMFI in arbitrary units) and QDEM stability (QDEM recovery in Relative % of events) were considered to be equally important in all the DOE; the weight of the responses for computational analysis was similar and an equivalent impact coefficient was given to the responses in DOE-1 and -2. By default, values of the impact coefficients were set to three (Statgraphic, VA, USA). The composite function was the geometric mean of the separate desirabilities given by the following equation (Statgraphic, VA, USA).

$$D = \{ d_{RMFI} \times d_{\%R} \}^{1/2} \quad (3)$$

4.2.5. Statistical analysis

- **MFI data and the percentage of events**

Three replicates were performed for each hybridisation experiment. For each batch experiment, a region was designed to target the untreated control population of the working solution. This region was then used to gate the samples run through the flow cytometer and to standardise the median fluorescent intensity (MFI). The MFI, the coefficient of variation for each parameter (CV), and the percentage of events (% Events) were calculated on gated population using WinMDI2.8 software (Joseph Trotter, SRI, La Jolla, CA, USA).

Corrected MFI (RMFI in arbitrary units, a.u.) was calculated for the DOE by subtracting the control population (c) values to the hybridised samples (s) values of the same batch experiment ($RMFI = MFI^{FL}(s) - MFI^{FL}(c)$) (Section 3.2.3).

The QDEM recovery was calculated as the percentage of events recovered in the gate at the end of the procedure compared with the percentage of QDEMs before treatment (% Recovery = 100 x% Events (s) /% Events (c)) (Section 3.2.3).

- **DOE step-by-step data analysis**

The data set obtained with the 0QDEM hybridised in the conditions defined by the DOE contained: (1) the relative percentage of events, and (2) the RMFI of the Cy3 hybridisation signal.

Data were first manually validated to ensure confidence in the agreement across replicates and the identification of outliers. Data were screened to verify that the expected range of values had been obtained, and the best results identified.

The data set was then imported in Statgraphic Centurion XV statistical package. The best model was constructed and identified with the results of the analysis of variance (ANOVA). The predicted values of the model were compared with the observed (or experimental) best values. Parameters influencing the reaction and the hybridisation responses were identified

The DOE data were first analysed separately to optimise the experimental parameters for each response. Details on the statistical analysis and results of the response optimisation of each DOE are presented as supplementary materials available in Appendix J and K.

- **Interpretation of RSM and MRO statistical results**

The analysis of variance (ANOVA table) of each response, *i.e.,* hybridisation signal and percentage of events, was performed to test the statistical significance of the effects and check the validity of the best model through different diagnostic tests. The ANOVA table partitioned the variability in Cy3 into separated pieces for each of the effects. It then tested the statistical significance of each effect by comparing the mean square against an estimate of the experimental error. ANOVA results determine which factors significantly affect the dependent variable of interest.

In the RSM experiments, ANOVA results determined which temperature, time and target concentration had a significant effect on the increase of the MFI of the hybridisation signal and on the percentage of events. The important results from the ANOVA table were the lack-of-fit and the R-Squared statistic, the equation that fitted the model, and the optimum response.

The lack-of-fit test is designed to determine whether the model created for a response is adequate to describe the observed data, or whether a more complicated model should be used. The test is performed by comparing the variability of the current model residuals to the variability between observed replicates for the same factors' settings. In this study, a lack-of-fit with a *p*-value ≥ 0.05 was considered not significant. As a consequence, the model was adequate to describe the observed data at 95.0% confidence level.

The R-squared statistics indicate, in percentage, how the model explains the variability of the response studied. In the R-squared statistics, the coefficient of determination (r^2) was used for the interpretation of the results. These statistic tests, additionally to the ANOVA tables were used to conclude if factors time, temperature, and target concentration significantly affected or not the resultant responses values in an additive manner; it meant that if no interactions was observed between the parameters then all the differences betweens the means could be sufficiently explained by the simple additive model for those three factors.

The DOE constructs a response surface equation fitting the data for each response. This equation or function is then evaluated and plotted. Hence, the model provides the optimum responses with the combination of the parameter levels which maximise the response studied over the range of values used to build the model. The model also predicts the responses for any conditions within the experimental space.

4.2.6. Graphical representation tools

The graphical tools available with the DOE statistical package were an essential part of the method to analyse and evaluate the experimental data against the model. The plots assisted in the identification of significant effects, the verification, and the interpretation of the model. The normal plot was used to distinguish between the positive and the negative effects. The investigation of the correlation between the model's predicted relative data and the observed data was used to validate the model. This type of plot was referred to as: actual versus predicted plot (Appendix).

Two dimension (2-D) contour plot and 3-D response plot showed the behaviour of the response studied as a function of two significant factors while the other significant factor was held constant (generally at its centre point value or at the optimum value). Coloured dots on the 3-D response plot indicates the actual experimental points (observed data) undertaken with the hybridisation protocol of the RSM. These graphical representations were chosen to interpret the results of the DOE.

4.2.7. Experimental validation: hybridisation titration

The experimental protocol described in section 4.2.3 was used to perform the hybridisation titration. The titration of the hybridisation signal was undertaken with increasing quantity of fluorescent indirect oligo ranging from 0.5 fmol to 1000 pmol in order to validate the optimum conditions obtained through the DOE analysis (Horejsh *et al.*, 2005). 525QDEMs from the untreated working solution were incubated directly with fluorescent probe as a negative control for each oligo quantities tested in the experiment of Cy3 oligo titration. Three replicates were run per oligo quantity tested. The geometric mean was calculated on gated population using WinMDI2.8 software (the SRI, USA) for each replicate.

The QuantiBRITE PE calibration kit was used as previously described to evaluate the molecules of equivalent soluble fluorochrome (MEF, in oligo) corresponding to the hybridisation signal detected in FL2 (Section 3.2.3.). Form this value, the corrected MEF (RMEF, in oligo) was calculated by subtracting negative control values (n) to positive samples values (s) of the same batch experiment (RMEF = MEF(s) – MEF(n)). The hybridisation signal (Cy3 RMEF in oligo) exclusively due to the oligos hybridised on the QDEM bioconjugates was plotted and a linear regression analysis was performed on the initial range values of the titration where the MEF values increased. The hybridisation detection limit was determined as a molar concentration, as follows: the lowest quantity of Cy3-oligo detected in the hybridisation assay was divided by the suspension volume of the hybridisation experiment (15 µL).

The code consistency of the hybridised samples was evaluated by estimating the relative variation in the fluorescent code detected in the FL detector channel from the initial blank or 525QDEM control population (% FL = 100 x MFI ^{FL}(s) / MFI ^{FL}(c), in a.u.).

The average coefficient of variation was calculated between all the positives samples of the hybridisation experiment for the QDEM fluorescent code and the Cy3 hybridisation signal. Data were presented as the mean of replicates ± standard error (SEM). Curves and statistics were calculated with GraphPad Prism5.01 (GraphPad Software, San Diego, CA, USA).

4.3. Results

4.3.1. DOE-1: Testing hybridisation buffers and factors' behaviour

The specific experimental protocol presented in Figure 4.3 with indirect fluorescent DNA target aimed to evaluate the validity of the DOE approach for the optimisation of the QDEM-based DNA hybridisation assay. The objective of the first batch of DOE was to assess the hybridisation buffers and to optimise the hybridisation conditions (or factors). A high and a low stringency SSC buffer were used with similar experimental factor ranges (Table 4-4) (Fuja *et al.*, 2004; Cao *et al.*, 2006a; Wang *et al.*, 2006).

- **DOE-1: single response analysis**

The ANOVA analysis of the overall data set of 3X SSC and 6X SSC DOE indicated that the target quantity had a significant effect on the responses studied (Appendix J and K). The lack-of-fit was not significant for the two responses investigated with the 3X SSC and 6X SSC hybridisation buffer. These results illustrated that the models constructed for each response were adequate to describe the observed data at the 95.0% confidence level (Table 4-7). The statistical analysis of the model also showed that the coefficients of determination, R-squared (r^2), were superior to 0.5 for 3X SSC. A high predictability of the model with no significant lack-of-fit therefore demonstrated that the model was adequate to describe the observed data. The coefficients of determination of the percentage of recovery and the hybridisation signal for 6X SSC were respectively 0.76 and 0.90. No significant lack-of-fit was found for the percentage of recovery data whereas a p-value<0.001 was found for the hybridisation signal. The model built for the percentage of recovery was therefore adequate to describe the observed data. The contradictory results were obtained with the hybridisation signal data.

Table 4-7 ANOVA lack-of-fit and coefficient of determination of the selected models

Buffer	*Target*	*Response*	*R-squared*	*Lack of fit*	
				p-value	*Conclusion*
3 X SSC	pmol	% Recovery	0.59	0.6643	Adequate
		Hybridisation signal	0.93	0.4155	Adequate
6 X SSC	pmol	% Recovery	0.72	0.37	Adequate
		Hybridisation ignal	0.89	0.0007	Inadequate

The two responses of 3 XSSC hybridisation experiments were analysed and after verifying the validity of the model (Section 4.2.4), the response surface plots were used to interpret the behaviour of the factors on the model. Figure 4.4 shows the response surface plots for the percentage of recovery and the hybridisation signal as a function of temperature and time, for 50.025 pmol of Cy3 targeted oligo.

Graphs in Figure 4.4 illustrate a tendency to find the optimum values in the middle range of temperature and time factors. The rising ridge response plot in Figure 4.4A shows that time had an optimum at ~60 min, and that increasing temperature was detrimental. Numerical prediction of optimum percentage of recovery was ~73% at 45ºC for 50 to 70 min incubation time (Figure 4.4A). The optimum hybridisation signal was found at ~305 a.u. for temperature ranging between ~49 and 53ºC and for incubation time ranging from 40 to 60 min (Figure 4.4B).

The response surface in Figure 4.4A also demonstrates that the lowest value of percentage of recovery (~64.5%) was obtained with the highest time and temperature values. The same tendency was observed for the minimum hybridisation signal responses at ~245 a.u. (Figure 4.4B). According to these results, high temperature and long time incubation in 3X SSC buffer were detrimental to QDEM stability, resuming in a global low efficiency of hybridisation.

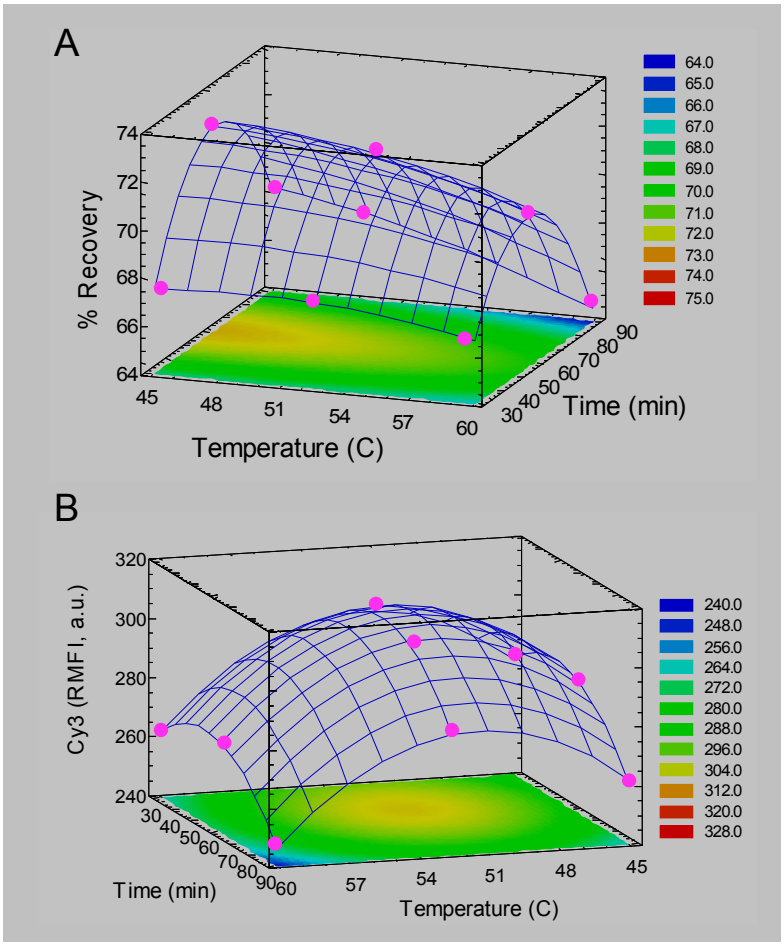

Figure 4.4 Response plots for the optimisation of the two responses with 3X SSC buffer as a function of time (min) and temperature (ºC).

Two- and three- dimensional contour plots show interaction between temperature and time for **A**: the QDEM recovery response, in percentage (%) of Events; and **B**: the Cy3 hybridisation signal response in RMFI (arbitrary units, a.u.); the quantity factor was held at its central point value, 50.025 pmol, for both graphs. The pink dots represent the actual experimental points or observed data, undertaken with the optimisation hybridisation protocol and needed for the RSM.

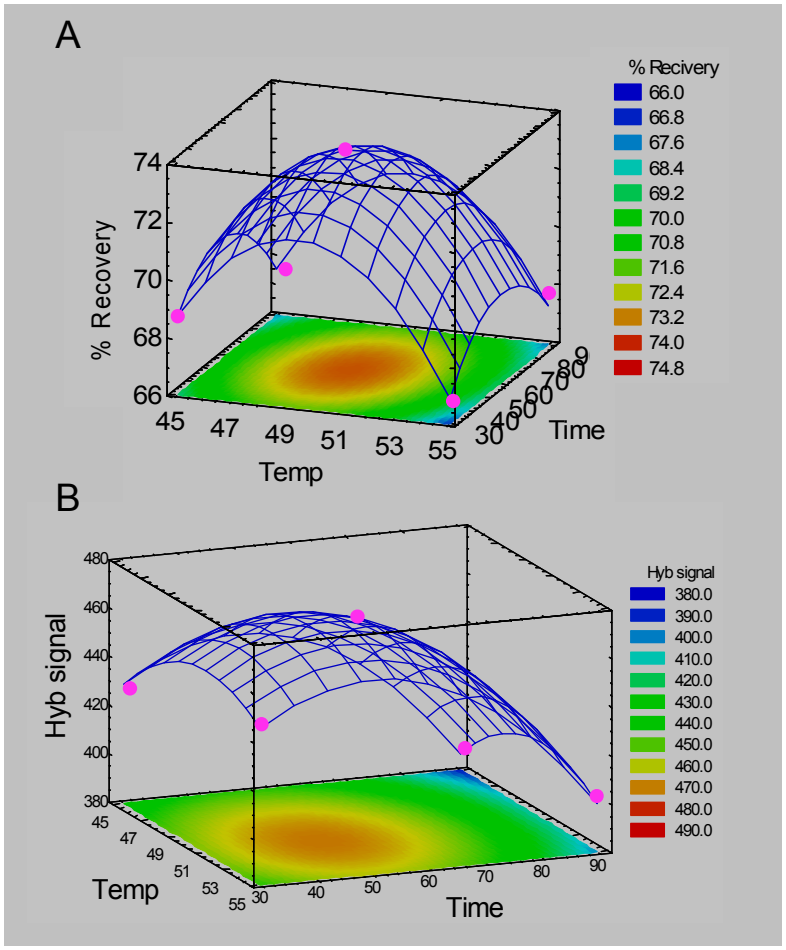

Figure 4.5 Response plots for the optimisation of the two responses with 6 X SSC buffer as a function of time (min) and temperature (ºC).

Two- and three- dimensional contour plots show interaction between temperature and time for **A**: the QDEM recovery response, in percentage (%) of Events; and **B**: the Cy3 hybridisation signal response in RMFI (arbitrary units, a.u.); the quantity factor was held at its central point value, 500 pmol, for all the graphs. Temp: temperature. The pink dots represent the actual experimental points or observed data.

The response plots obtained with 6X SSC present a tendency of low responses at high temperature (Figure 4.5). The minimum of recovery (~66.5%) and the lowest hybridisation signal (~400 a.u.) were found at 55ºC and 90 min (respectively Figure 4.5A and B). The optimum values corresponded to ~74% of recovery and ~470 a.u. hybridisation signal with approximately the same range of factors values as with the 3X SSC DOE: 48-52ºC for 45-55 min. The minimum of recovery with 6 X SSC was 2% higher than with 3 X SSC. The results obtained with 6X SSC were overall superior to the results obtained with 3X SSC buffer in terms of optimisation when comparing maximum and minimum values for both responses.

- **DOE-1: multiple response optimisation**

The statistical results of the first stage of the model analysis were used to develop the multiple response optimisation (MRO) as previously described (Section 4.2.4). The outputs of the MRO included: (1) the minimum and maximum values of the response variables over the experimental runs, (2) the parameters of the desirability function, (3) the observed values for each response, and the predicted and observed values of desirability (Appendix C). The predicted desirability was based on the values obtained with the model developed for each response optimisation, and the observed desirability values were based on the observed values obtained with the empirical experiments (supplementary materials in Appendix J, K).

The desirability function was plotted as a response surface plot which estimate the optimum point of the model constructed for the maximisation of the hybridisation signal and bead recovery in 3X and 6X SSC buffers (Figure 4.6).

The MRO with DOE-1 results calculated an optimum of 73% bead recovery, and 335 a.u. hybridisation signal for the incubation of ~8000 QDEMs with 100 pmol of Cy3 oligo at 57ºC for 90 min in 3X SSC hybridisation buffer. The MRO reached the middle range of the desirability function with a *d*-value of 0.55 (Figure 4.6A).

Numerical prediction of optimum responses and conditions with 6 X SSC hybridisation buffer presented a maximum of 74% bead recovery and 503 a.u. hybridisation signal for the hybridisation of ~8000 QDEMs with 642 pmol of oligo Cy3 at 47ºC for 38 min. The maximum of desirability was reached for these conditions with a *d*-value equal to 0.76 (Figure 4.6B)

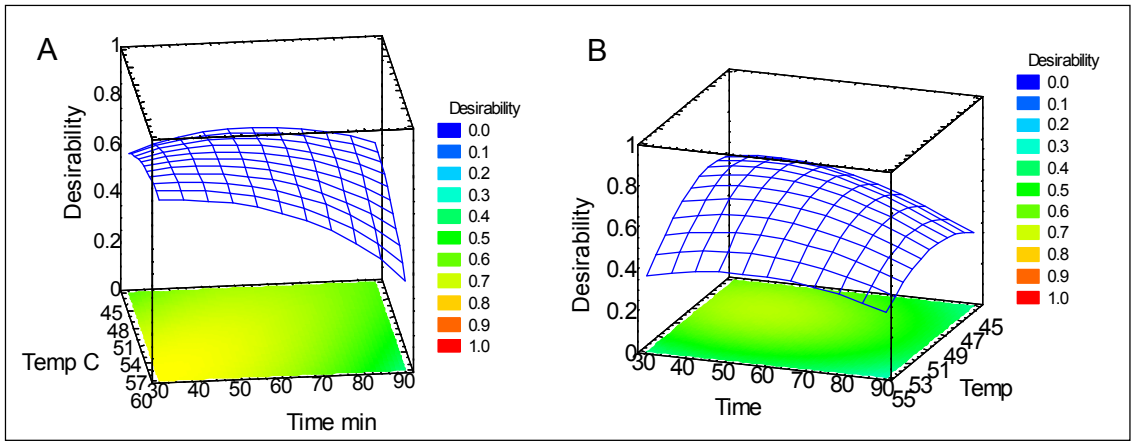

Figure 4.6 Response surface plot for the multiple response optimisation of the hybridisation signal with (A) 3X SSC and (B) 6X SSC buffer as a function of time (min), temperature (ºC) and desirability.

Two- and three- dimensional contour plots show the interaction between temperature (Temp) and time; target oligo quantity at (**A**) 50.025 pmol and (**B**) 500 pmol. The desirability function *d*(y) expressed the desirability of the response value equal to y on a scale of 0 to 1 indicated in the legend on the right side of the graph.

The modelling of the multiple response surface of 3X SSC showed that high temperature was more detrimental than long time of incubation in the hybridisation optimisation (Figure 4.6A). The lowest desirability was observed at 60ºC, with *d*-value ~0.2. The highest values of desirability (~0.55) represented by the hill of the 3-D graphs in Figure 4.6A were obtained for relative low temperature range (~48-51ºC) and for a wider range of incubation time (30-90 min).

The 3-D representations of the 6X SSC multiple responses illustrate that incubation times and temperature had approximately similar disadvantageous effects on bead recovery and hybridisation signal efficiency. Figure 4.6B shows a maximum of desirability at ~0.8, for low level of time and temperature factors. The minimum desirability at ~0.35 was observed for the highest values of temperature and time. The differences of 0.4 in desirability, between the maximum and minimum, indicate that in 6X SSC the level of temperature and time for the range of 0 to 1000 pmol of fluorescent target had a significant impact on the behaviour of the hybridisation responses (Figure 4.6B). The difference of ~0.3 desirability between maximum and minimum in 3X SSC shows that the factors and the hybridisation responses in the range observed were less correlated than with the 6X SSC buffer (Figure 4.6A).

The MRO of DOE-1 provided information on DNA hybridisation kinetics in solution. With low concentration of targeted DNA, longer time with higher temperature was required to optimise the hybridisation efficiency (3X SSC optimum conditions: 100 pmol of target, 57ºC, 90 min). The comparison between 3X SSC and 6X SSC multiple response optimisation showed that the optimum conditions defined by the MRO with 6X SSC were more efficient in terms of time than with 3X SSC. The disadvantage of 6X SSC in comparison with 3X SSC was the high quantity of oligo to be used for optimisation and the lack-of-fit of the hybridisation response. To resolve these issues a new DOE using the 6X SSC buffer was undertaken with lower concentration of fluorescent probe.

4.3.2. DOE-2: optimising hybridisation efficiency and sensitivity

Results of the DOE-1 and previous experiments evaluating hybridisation buffer impact on QDEM stability (Figure 2.18) showed that 6X SSC, the less stringent buffer, was more suitable to optimise the QDEM suspension assay. The results obtained with DOE-1 also determined which factor ranges best fitted the objective defined for the development of a QDEM suspension assay. The time and temperature levels were, on average, satisfactory and predicted adequate models. The results of 6 X SSC DOE-1 showed nevertheless a

significant lack-of-fit for the hybridisation signal: the levels and ranges of oligo quantity were respectively too high and too wide. The optimum oligo quantity defined by the MRO was also too high for the requirement of an efficient ASO assay. Oligo quantities in the femtomolar ranges were thus chosen in the final DOE in order to optimise the sensitivity of target detection. The DOE-2 aimed to improve the fitted model for the hybridisation response of the QDEMs. Table 4-8 presents the factors' levels used in the second DOE with 6X SSC buffer.

Table 4-8 Factor's levels of the experimental design DOE-2

DOE-2	*Level*	*Temperature (°C)*	*Time (min)*	*Oligo Quantity (fmol)*
optimal SSC buffer	– 1	45	30	0.5
	0	50	60	50.25
	+ 1	55	90	1000

- **DOE-2: single response analysis**

The analysis of the hybridisation signal responses revealed that the constructed model explained ~81% of the variability in the hybridisation signal data and ~72% of the stability data. The model designed was thus adequate to describe the percentage of recovery and observed hybridisation signal at the 95% confidence level since both responses *p*-value were ≥ 0.05 (Table 4-9).

Table 4-9 ANOVA lack-of-fit and coefficient of determination of the selected model

Buffer	*Target*	*Response*	*R-squared*	*Lack of fit*	
				p-value	*Conclusion*
6 X SSC	fmol	% Recovery	0.72	0.3726	Adequate
		Hybridisation signal	0.81	0.1282	Adequate

Figure 4.7 presents the 2-D contour plot, the 3-D response plot of hybridisation signal and QDEM stability in response to the oligo quantity, temperature and incubation time. The response surface design predicted the response curvature and resulted in a maximised hybridisation response at ~420 a.u. with 70 to 80 min incubation at 49-51ºC, and a maximised stability with ~73% of recovery for 50 to 60 min incubation at 49-51ºC.

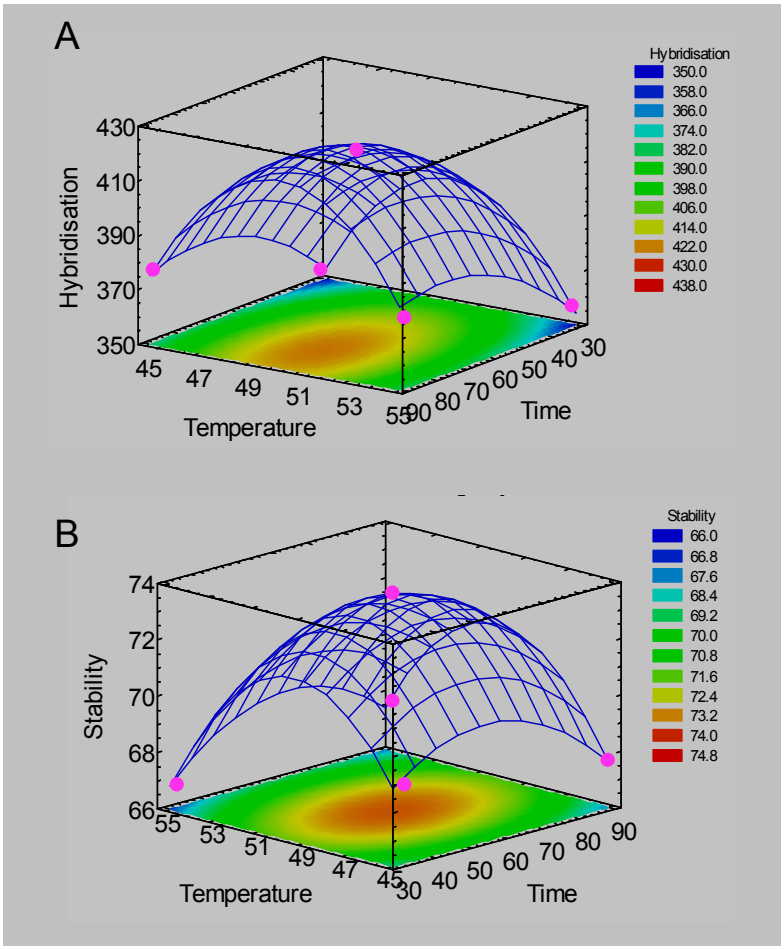

Figure 4.7 Response plots for the optimisation of the 2 responses with 6 X SSC buffer as a function of the time (min), the temperature (ºC).

Two- and three- dimensional contour plot showing interaction between temperature and time for **A**: Percentage (%) of recovery response; **B**: Cy3 hybridisation signal response in RMFI (a.u.); the quantity factor was held at its central point value, 500 fmol, for all the graphs. The pink dots represent the actual experimental points or observed data.

The response surfaces were the lowest at high temperature (55ºC) and short incubation times. Figure 4.7 shows that high temperature and short time of incubation were more detrimental for QDEM stability and hybridisation efficiency than low temperature and longer time of incubation. The variation between the lowest and highest predicted values of the hybridisation signal and the QDEM recovery was ≥ 10%. These differences were significant in the objective of optimising an experimental process. Therefore the DOE predicted values were found significantly relevant to optimise the experimental conditions (Table 4-10).

Table 4-10 Variations between low and high predicted values of the model *

Reponses	*Predicted values*		*Ratio (%) (1-L/H)*100*
	Highest	*Lowest*	
Hybridisation signal (RMFI, a.u.)	420	350	17%
% Recovery (%)	73.5	66.5	10%
Desirability	0.9	0.5	44%

* L: lowest, H: highest, a.u.: arbitrary units

- **DOE-2: multiple response optimisation**

The optimum conditions determined by the MRO maximised the percentage of recovery at ~76.5%, and the hybridisation signal at 450 a.u. with a *d*-value of ~0.9. To obtain these optimum values the hybridisation conditions needed the incubation of 1,341 pmol of the Cy3-oligo target for 58 min at 49ºC. The desirability function was plotted as a response surface plot, which illustrated the optimum point of the model (Figure 4.8).

The desirability function predicted conditions of hybridisation with the lowest desirability at 0.5 whereas the responses were maximised with a desirability of *d* ~0.9. The ratio calculated in Table 4-10 showed that the input of the MRO was significant to define optimum conditions since almost 50% differences were observed between the lowest and highest desirability values.

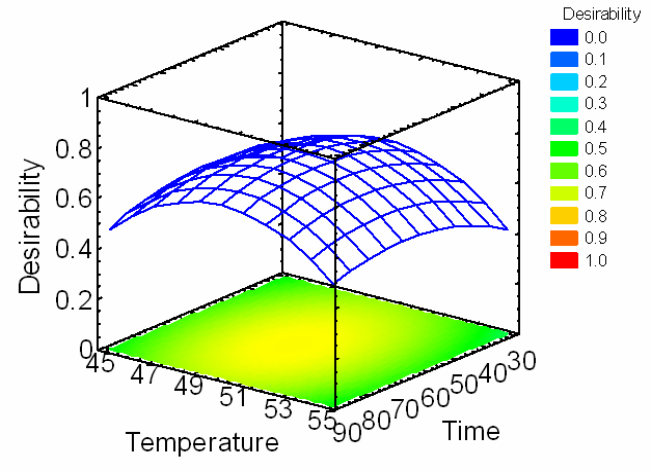

Figure 4.8 Response surface corresponding to the desirability function when the temperature (in°C), time (in min) and oligo quantity (in fmol) were optimised analysing two responses simultaneously.

Two- and three- dimensional contour plot showing interaction between temperature and time; The desirability function *d*(y) expressed the desirability of the response value equal to y on a scale of 0 to 1 indicated in the legend on the right side of the graph.

The models constructed with the new DOE-2 were adequate and a MRO was run. This model was found to be the most adequate for the optimisation objectives in terms of model fitting, and because it was the most efficient regarding incubation time and response variables in relation to the quantity of oligo used. The optimum conditions of incubation, *i.e.,* 58 min at 49ºC, were used to perform the titration of the fluorescent oligo as a validation study (Table 4-11). The comparison between experimental titration and the model prediction was then undertaken.

Table 4-11 Optimum conditions and responses

Factor	*Optimum*	Response	*Optimum*	*d*
Temperature (ºC)	57	**% Recovery**	77	
Time (min)	19	**Hybridisation Signal**	450	**0.90**
Concentration (fmol)	1341			

4.3.3. Hybridisation titration with optimum conditions

- **Hybridisation titration**

The hybridisation method was designed for future optimisation of the detection of multiplex DNA markers for genotyping application such as forensic genetics and molecular diagnostics. An important aspect of this assay was related to the sensitivity of the QDEM probes. To validate the optimised conditions defined by the design of experiment (Table 4-11) and investigate the sensitivity found in the assay, a hybridisation titration was undertaken. QDEM-probes were hybridised with increasing quantity of a complementary oligo labelled with Cy3 (Figure 4.9). The QDEM bioconjugates developed with a specific methodology in Chapter 3 were adapted to a hybridisation suspension assay using FC and therefore were compatible with conventional calibration bead kits. The number of fluorescent probes hybridising to the QDEM bioconjugates was evaluated with the QuantiBRITE PE Calibration kit (Section 4.2.7).

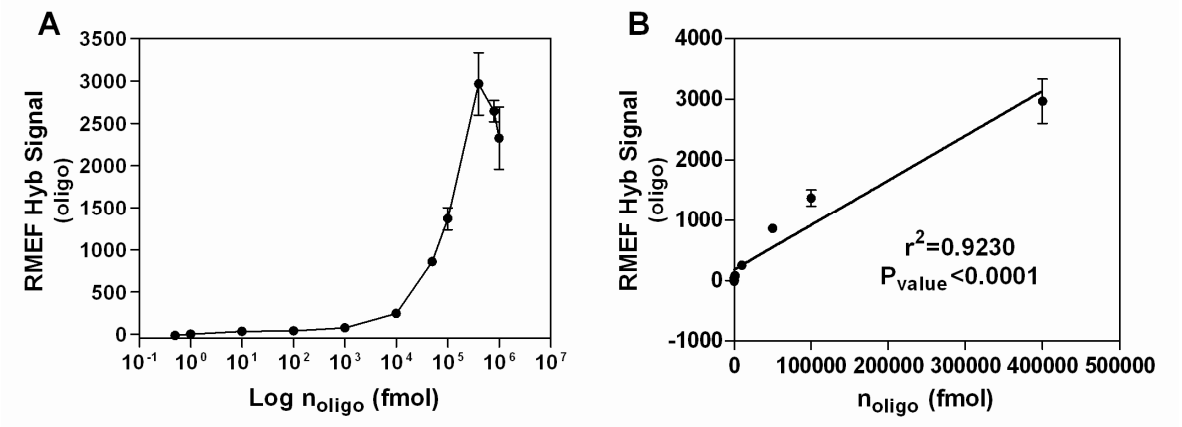

Figure 4.9 QDEM bioconjugate hybridisation titration curves.

A: RMEF (corrected molecule of fluorophore, in number of oligo) versus n_{oligo} (oligo quantity in fmol); the x-axis is in log scale. **B**: Linear regression plot of RMEF versus n_{oligo} before saturation (0 to 4 x 10^5 fmol).

QDEM bioconjugates (~8000) were hybridised in the optimum condition defined by the DOE-2, in 6X SSC, 0.5% SDS (pH 7.0) hybridisation buffer at 49ºC for 1 hour with increasing quantity of indirect fluorescent probe ranging from 0.5 fmol to 1000 pmol. A hybridisation titration curve was drawn with the mean average of three replicates (± SEM) of Cy3 RMEF (Figure 4.9A). A linear quantitative relationship ($r^2 = 0.92$) between targeted oligo and RMEF values was found over the dynamic range of DNA quantities where RMEF increased (0.5 fmol to 400 pmol). The limit of detection of 29 pM was obtained with the hybridisation of ~8000 QDEM bioconjugates (5 μm diameter) to 0.5 fmol of Cy3 oligo target. From 800 pmol to 1000 pmol of targeted probe the maximum hybridisation signal was lowered by ~11% to 22% (Figure 4.9A).

- **Comparison of predicted hybridisation optimum values with empirical data**

Hybridisation experiments were undertaken to test the optimum conditions defined by the DOE-2 in 6 X SSC hybridisation buffer. Approximately 8000 525QDEM were used for each of the three replicates incubated with 1.34 pmol of Cy3 oligo at 49ºC for 1 hour. The results obtained experimentally were presented as the median (± SEM) in Table 4-12 in comparison with the value predicted by the model.

Table 4-12 Comparison of experimental and DOE-2 model values

Parameters / values	Hybridisation signal	% Recovery
	Mean of RMFI (FL2)	Mean of Relative %Events
Experimental	190 (± 22.9)	55 (± 2.5)
Model	420	77

The hybridisation signal detected in the experiments was ~220-260 a.u. inferior to the predicted values. The experimental percentage of recovery value was on average 20-25% lower than the model prediction. These results indicated that the model over estimated the response values.

- **Impact of the ASO assay on the QDEM technology**

The stability of the microsphere structure and the code consistency of the QDEMs were analysed simultaneously to the hybridisation optimisation study. The average coefficient of variation (CV) for all replicates was 22.53 for FL1 and 7.11 for FL2. On average, the percentage of positive QDEM recovery after the conjugation and hybridisation procedure was 42%. Figure 4.10 shows the values obtained for the percentage of recovery and the code consistency of the hybridised QDEM populations for each quantity used in the titration experiment.

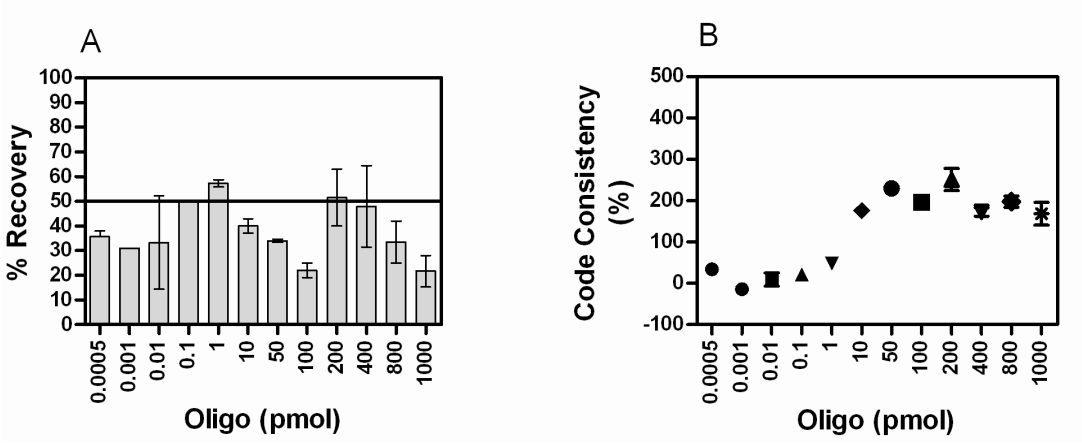

Figure 4.10 QDEM bioconjugates (A) structural stability and (B) fluorescent code consistency.

Data are presented as the mean of replicates ± SEM; the bar in graph (A) illustrates the 50% y-scale limit. Quantities of oligo are represented in pmol to ease the scale annotation on the graphical representation.

Figure 4.10A shows the decrease of the bead recovery in relation to the changes of QDEM working solution. During the titration three different working solutions were used. The first working solution was used for the DOE empirical work and the volume left was sufficient to perform the sample replicates from 0.5 fmol to 10 fmol. The working solutions were then

renewed at 0.1 pmol and at 200 pmol. The lowest recovery corresponded to ~22% of hybridised QDEMs, and the maximum recovery with a fresh working solution corresponded to 57%.

The code consistency was evaluated for each batch experiment by comparing the fluorescent code of hybridised 525QDEMs with the negative control population, which was, in this experiment, the 525QDEM population bioconjugated with NF direct probes (Table 4-2). The fluorescent code of 525QDEMs was detected in FL1 (Table 4-3). At low quantities of indirect Cy3 probe (0.5 fmol to 1 pmol), the code consistency of the 525QDEMs was close to zero. Figure 4.10B shows, on average, an increase of ~200% in the variation of QDEM fluorescent code from 10 pmol to 800 pmol of indirect probe. From 400 pmol to the end of the titration, the variation in code consistency decreases from > 200% to < 200% compared with its maximum.

4.4. Discussion

A 18-mer poly(T) sequence was chosen to evaluate the hybridisation efficiency as a way to mimic the potential hybridisation of a targeted sequence with low content of G/C nucleotide. The number, the composition, and the type of bases composing the sequence as well as the position of the SNP mismatch base influence the probe hybridisation temperature, or melting temperature. The hybridisation decreases when the G/C content is lower, presumably reflecting the lower affinity of the oligo for their PCR target. The A/T interactions being weaker than the G/C liaisons, the optimisation of hybridisation with short poly(T) oligo to a poly(A) probe sequence would therefore potentially assure the specificity of the experimental conditions adapted to high affinity DNA-DNA interactions (Wallace *et al.*, 1979). Further, previous studies reported that shorter probes had higher affinity and discrimination properties (Ikuta *et al.*, 1987). Typically, 17-mer probes are used to obtain unambiguous SNP genotypes. A short oligo sequence of 18 bp was chosen since short oligos were reported to display a higher hybridisation specificity (Armstrong *et al.*, 2000).

Previous studies used a fluorescent oligo with a sequence complementary to a specific probe sequence identifying a particular gene to optimise the hybridisation procedure on the microsphere surface (Fulton *et al.*, 1997; Son *et al.*, 2007). This approach was limited as it optimised hybridisation conditions for a specific type of oligo. The experimental approach of using Cy3-poly(A) aimed to optimise the hybridisation assay for more general applications. Fulton *et al.* (1997) initial work to develop the first commercialised multiplex bead-based assay (FlowMetrix™ system, Luminex Corp, Austin, TX, USA) used a single oligo sequence selected from the allelic sequence designed from the exon of an HLA gene to optimise the hybridisation conditions. This group tested the impact of oligo concentration, time and temperature of incubation with three separate experimentations to define optimum conditions for the multiplex bead-based assay. The limitations of using a specific allelic sequence to test the effect of target concentration on hybridisation properties has been reported (Armstrong *et al.*, 2000). A second limitation of the method was to use a sequential approach for the optimisation process (see 4.1 Introduction).

4.4.1. The design of experiments approach

DOE was first applied in two different types of experimentation using different stringency of SSC hybridisation buffer, oligo quantity and time range. This first set of experiments aimed to evaluate different variables to interpret their interaction and influence on the constructions of the model and on the multiple response optimisation responses. 3X SSC experimental design results presented, on average, a lower percentage of recovery compared with 6X SSC experiments. This difference could indicate a higher sensitivity of QDEMs to the hybridisation conditions in 3X SSC buffer (Figure 4.4, Figure 4.5). This result could therefore explain the lower signal of hybridisation observed in 3 X SSC: the more the structural integrity of the QDEM was disrupted by the incubation conditions, the more the QDEM structural property to bind DNA was reduced. As a conclusion, the 3X SSC stringent hybridisation buffer had a detrimental effect on QDEM stability, which induced a global low efficiency in the hybridisation process. This result could explain the global low level of desirability in the MRO with 3X SSC. The range used in 6 X SSC

experimental design was ten times wider (0 -1000 pmol) than with the 3X SSC experiment (0-100 pmol). The differences in the oligo target quantity range could therefore also explain the wider differences between minimum and maximum optimum of hybridisation signal and desirability values.

The RSM designed with 6X SSC for the hybridisation signal response presented a significant lack-of-fit. This result was related to the high range of oligo quantities used in this DOE that created high variability in the responses observed. The lack-of-fit, as stated earlier, was designed to determine if the selected model was adequate to describe the observed data or if a more complicated model should be used. At high oligo quantities (400 to 1000 pmol), a phenomenon of saturation could occur, which could induce a plateau followed by a decrease of the hybridisation signal. The diminution of the hybridisation signal could be related to a lower diffusion of ssDNA in the suspension and a saturation of the QDEM hybridisation sites (Livshits and Mirzabekov, 1996a; Armstrong *et al.*, 2000). Under this consideration and since 90% of the data were represented by the model, 6X SSC RSM model was used to build a MRO model.

The MRO showed that the optimum conditions defined with 6X SSC were more efficient than those predicted with 3X SSC. However, the optimum quantity of oligo target predicted by 6X SSC MRO and the low model fitting of the hybridisation data were less efficient than with 3X SSC buffer. To resolve these issues, a new DOE using the 6X SSC buffer was undertaken with lower fluorescent probe quantity to improve assay sensitivity and to improve the statistical model. The first DOE was necessary as a preliminary experiment to define the later precise the range of the factors with the more efficient hybridisation buffer (6X SSC). The second DOE was therefore adapted to ASO hybridisation assay in liquid format. It predicted optimum conditions for a maximum of hybridisation and bead recovery using minute quantities of DNA target with a model significantly fitting the data.

4.4.2. Validation of optimum conditions

The titration of QDEM bioconjugates was performed to evaluate the impact of the DNA target quantity on the hybridisation signal (Figure 4.9A). The number of fluorescent probes hybridising to the QDEM bioconjugates was evaluated with the QuantiBRITE PE kit (BD Biosciences). A linear quantitative relationship (r^2 = 0.92) between targeted oligo and RMEF values was found (Figure 4.9B). A detection limit of 29 pM was calculated for the fluorescent target which was lower than the 4 nM target DNA detection reported with QD-based solid microarrays (Gerion *et al.*, 2003) and than the 20 nM reported by Cao *et al.* (2006a) using QD-doped polystyrene microspheres. The factors influencing the hybridisation detection limit include: the detection method, the bead diameter, the carboxylation coverage, the coupling efficiency, the probe and target length, and the method to evaluate the sensitivity. The detection limit of hybridisation obtained with QDEM bioconjugates was satisfactory for bead-based assay requirements (Lowe *et al.*, 2004). The results obtained by Cao *et al.* (2006a) could be explained by a twenty times higher microsphere surface of detection (100 μm diameter). From 800 pmol to 1000 pmol of targeted probe the maximum hybridisation signal was lowered by ~11% to 22% (Figure 4.9A). Steric hindrance, competition effect, lower diffusion of ssDNA, and negative forces repulsion could explain the diminution of the signal. The quenching of Cy3 fluorophore and QDEM emission spectrum could also lead to a global decrease of the fluorescence emission at high concentrations of fluorescent probe (Section 3.3.1. and 3.3.3).

The experiments conducted here represent an initial demonstration of the sensitivity of the QDEM hybridisation assay. The optimum conditions defined with the DOE provided thus, a DNA limit of detection compatible with the quantity range expected for the analysis of biological samples limited in DNA material (Chung *et al.*, 2004). As a consequence, the method developed here has the potential to wider its genotyping application to the specific analysis of degraded DNA, soiled samples, complex biological mixtures, ancient DNA and so forth.

4.4.3. QDEM-probe stability in the hybridisation assay

The global impact of the bioconjugation associated to the hybridisation process on the 525QDEM stability was more specifically studied. The average coefficient of variation for all the replicates of the titration experiments was 22.53 MFI in FL1 and 7.11 MFI in FL2, with, on average, a recovery of ~42% of QDEMs at the end of the procedure.

The high CV detected for the 525QDEM fluorescent code and the low percentage of final bead recovery could be explained by the effect of the treatments on the 525QDEM. The percentage of bead recovery was shown to be dependent on the age and utilisation frequency of the 525QDEM working solution. Repeated treatments, *i.e.,* sonication frequency, vortexing intensity, centrifugation (time and speed), buffers, temperature, time exposure and buffers composition were shown to have an impact on QDEM percentage of recovery (Chapter 2 and 3). The study of the code consistency with increasing quantities of oligo presented a similar graph tendency as the hybridisation titration graph (Figure 4.9A and Figure 4.10B).

High quantities of fluorescent oligos induced a positive variation of the 525QDEM fluorescent code, increasing the fluorescence detected in FL1, the detector channel specific to the 525QDEM. This phenomenon was explained by an overspill of the fluorescence emitted by the molecules of fluorophore covering the surface of the microsphere and detected in FL2 (detector channel close to FL1). The observed overspill emission stabilised and started decreasing from 400 pmol, which could be explained as the reverse effect of a high quantity of fluorescent probe: high concentration of Cy3 probes induce a quenching of the QD fluorescent emission due to high density of Cy3 and close proximity of Cy3 and QD particles. As a consequence the global overspill emission was limited at 400 pmol of Cy3-oligo. The potential saturation effect linked to Cy3 fluorophore and oligo probe were detailed in previous chapter (Section 3.4).

To conclude, the main objective of this research project was to develop an optimised allele-specific oligonucleotide (ASO) detection method in a liquid format using QDEM-probe and FC detection. A crucial step in the identification of specific allele detection is the specific hybridisation of the probes to the DNA target. DNA hybridisation requires highly optimised conditions for the probes to anneal only to their corresponding allele, especially in complex mixtures. A novel approach, the design of experiments (DOE), was evaluated to develop highly optimised QDEM hybridisation suspension assay. Experimental design has shown to consume less time, effort and resources than one-factor-at-a-time procedures (Ryan *et al.*, 2009). DOE provides also a large amount of information, while minimising the amount of experimental work. DOE with RSM was applied to the QDEM suspension assay for the hybridisation optimisation step. Two hybridisation buffers were tested with 2^3 + star central composite design (CCD). RSM using central composite design (CCD) enabled the production of surface plot responses that help to understand the variation of the responses in relation with the variation of the conditions studied. The benefit gained from the DOE specifically applied to QDEM suspension assays could be undermined as the final multiple optimisation response model showed poor correlation with the validation study.
However, the difficulty of optimising the hybridisation process using sensitive material as QDEMs was nevertheless overcome and precise optimum experimental conditions were defined to apply the assay to SNP target detections. The DOE predicted optimum conditions adapted to the development of a QDEM assay with a competitive DNA target detection limit in the range of previous results obtained in QD-doped particle genotyping based assay (Xu *et al.*, 2003).

To conclude, an optimum hybridisation signal and bead recovery was obtained with the incubation of a volume of 8000 QDEM-probes in 6X SSC buffer, 1.3 pmol of target oligo, incubated at 49ºC for 58 min in the dark. The utilisation of the design of experiment showed the potential to facilitate and to improve experimental protocol in suspension array and more generally in bioassays.

Chapter 5

Investigation of the QDEM-probe Technology for the Genotyping of Single Nucleotide Polymorphisms

5. INVESTIGATION OF THE QDEM-PROBE TECHNOLOGY FOR THE GENOTYPING OF SINGLE NUCLEOTIDE POLYMORPHISMS

5.1. Introduction

SNPs screening is used in disease genetic studies to identify SNP markers that participate to the changes of biological cellular mechanism which participate to pathological events (Tost and Gut, 2005; Glinsky, 2008). The effect of a SNP is investigated to understand the response to a drug in patients since the development of adverse drug reactions has become a significant clinical issue. Hence, the growing interests of using SNPs as markers for pharmacogenomics studies and personalised medication (Zhang *et al.*, 2008). Reviews on SNP applications have also supported their valuable participation to specialised forensic applications. The reported growing interest in SNP forensics informed the selection of SNPs for this particular application (Budowle and Van Daal, 2008). Disease genetics, pharmacogenomics, population studies or human genotyping applications require the genotyping of a large number of SNPs in equally large sample collection (Gill *et al.*, 2004; Wetton *et al.*, 2005; Gunderson *et al.*, 2006). Hence, genotyping assay require a high level of throughput.

Current genotyping platforms adapted to SNP genotyping have been reviewed in the main introduction (Section 1.3.1). Briefly, robust genotyping methods have been developed and commercialised. The requirements of accuracy, efficiency, and throughput of SNP genotyping have been addressed with advanced assay design such as BeadARRAY™, Luminex®xMAP™, GeneChip®, or SNPlex™ platforms (Section 1.3.3). Multiplex capabilities (a maximum of 10^5 SNPs per assay can be achieved), cost –efficiency (cost reduced to 1-10 cents per genotype), and increased sample collection analysis have been the main advances provided by these methods (Kim and Misra, 2007). However, academic and industrial research continues to develop new genotyping technologies and data mining tools to extract more information from SNP DNA markers, with more efficient methods (May,

2008). Further improvements of current assays and new technologies are still needed to improve routine large-scale analysis of SNPs genotyping, in large samples collections, with cost and time efficiency. The use of SNPs in population studies, pharmacogenetics, and disease association studies is well-established, through there is still a need to pursue the development of new technology to improve the sensitivity and capacity of high throughput SNPs genotyping adapted to specific applications (Section 1.3.1).

SNPs have become the principal DNA markers used to investigate human genetic variation, for technological and genetic reasons. SNP genotyping technology, previously described, provides a level of throughput and cost-effectiveness largely superior to other genotyping methods based on alternatives markers such as microsatellites (Nelson, 2001). Furthermore the extensive development of SNP databases, SNP population studies, and SNP multiplex PCR (52-plex autosomal SNPs) is also showing the ability of SNPs to contribute the human identification applications (Nelson, 2001; Sanchez *et al.*, 2006; May, 2008). Hence, SNPs have found specialised applications in human evolution and forensic genetics that became essential in human genotyping.

The selection of SNP markers for a genotyping assay is based on multiple criteria (Henegariu *et al.*, 1997; Butler *et al.*, 2003; Sanchez and Endicott, 2006). First, the validation status of the marker is essential to ensure that the Y-SNP selected is real and not confused with a sequencing error, but also that the SNP under investigation is mapped only once, which testifies its unique appearance along the human genome (Petkovski *et al.*, 2003). Secondly, linkage disequilibrium between SNP markers should be avoided (Non-random associations between SNP at different loci in population genetics are measured by the degree of linkage disequilibrium). Some fragments of chromosome or blocks hold SNPs associated to genes with a higher frequency in a population than would be expected from a random formation of haplotypes from alleles based on their frequencies. It has been accepted that if a minimum distance of 100 kb is used between a SNP candidate and the neighbour gene, very few markers are likely to be in linkage disequilibrium beyond this distance (De la Vega *et al.*, 2005). The degree of polymorphism of the SNP, often

measured in reported allele heterozygosity of SNPs in the population, is another essential criterion of selection. A minimum of 0.3 heterozygosity at a locus is required to satisfy the general polymorphic guidelines described by Phillips *et al.* (2004). The reliability of the marker's flanking regions is an important criterion that will determine the robustness of the single- and multiplex PCR reactions. PCR success depends on the sequence surrounding the SNP. A sequence is considered reliable when free from mutation or polymorphism potentially interfering with primer binding sites. Finally, the A/T, C/G and C/T base modifications of bi-allelic polymorphism are preferentially selected, since G/T mismatches have shown to be more difficult to distinguish because of their thermodynamic stability (Werntges *et al.*, 1986). These criteria can be verified through the databank information provided by dbSNP with the SNP accession number under study (Sherry *et al.*, 2001). The selection and the amplification of genetic markers has been largely described in the literature and detailed protocols are available to guide researchers in the development of single- and multiplex SNP PCR (Henegariu *et al.*, 1997; Sanchez *et al.*, 2006).

One application of SNPs genotyping focuses on the Y chromosomal SNPs (Jobling and Tyler-Smith, 2003; Krausz *et al.*, 2004). The Y-chromosome sequence determines the male sex type and is approximately 57.7 megabases (Mb) long (Underhill *et al.*, 2000). The Human Genome Project has identified more than 200 Y-SNPs along the Y sequence. The Y-chromosome behaves like a male-haploid chromosome because the majority of the Y chromosome does not recombine with the X chromosome (recombination results in the formation of new allele combinations through meiotic crossing over during cell division). As a consequence, individuals are hemizygous or haploid for a SNP allele on the non recombining region of the Y chromosome (NRY).

SNP markers on the NRY are conservatively inherited from father to son. (Quintana-Murci *et al.*, 2001; Tilford *et al.*, 2001). Only mutation events will bring genetic diversity. Historical accumulations of mutations are then transmitted from generation to generation. The Y chromosome, therefore, can be a useful tool for the prediction of population-of-origin as human social behaviour suggests a pattern of male geographical distribution: woman tended

to follow their husbands (Jobling and Tyler-Smith, 2003). Publications that describe population data with Y SNP-chromosome markers are now widely available (Di Giacomo *et al.*, 2003; Vallone and Butler, 2004; Lee *et al.*, 2005). Recent studies focus on the identification of relevant SNPs among different sets of the worldwide population (Butler, 2004; Fechner *et al.*, 2008; Zalloua *et al.*, 2008). Brion *et al.* (2005a) have reported that NRY markers are appropriate to identify distinct geographical patterns across Europe as well as micro-geographical scale population structure. The main findings of this study have shown that although the genetic differences within the European male lineage are small, they are nevertheless well correlated with geographical distances. Y-SNPs have also shown the potential to infer the population-of-origin or the geographical origin of a DNA sample (Halder *et al.*, 2008). Wetton *et al.* (2005) suggested that Y-SNPs could predict likely-ethnic appearance since they are strongly correlated with the physical appearance of the corresponding ethnic group (Wetton *et al.*, 2005). Alternatively, the genotyping of Y-SNP markers may be applied to missing person's databases where paternal lineage is relevant. Y-SNP haplotypes can give an insight to associate the profile under investigation with potential paternal linage even if Y-SNP profiles are unsuitable for specific paternity tests. This first stage of profiling, early in the investigation, aims to implement DNA techniques for forensic human identification strategies (Budowle and Van Daal, 2008). To test QDEM-probes technology, the selection of SNP markers was focused on the male specific region of the Y chromosome (MSY) referred to as the NRY.

After the selection of the Y-SNP markers, the next steps in the development of an ASO assay involved the production of optimised QDEM-bioconjugates and the optimisation of the hybridisation conditions adapted to the QDEM technology (Figure 1.15). This work has been undertaken and reported in the previous chapter presented in this thesis (Chapter 3 and 4).

The last step in the assay was, then, the identification of the hybridised complex, *i.e.,* biotinylated-PCR product/QDEM-allelic probe, with a reporter dye. Streptavidin bioconjugated to organic fluorophores have been widely used as reporter dyes to identify

the biotinylated target hybridised with the probe (Xu *et al.*, 2003; Fitzgerald *et al.*, 2007; Tian *et al.*, 2008). Organic dyes are highly limited by their excitation lifetime, by their excitation and emission spectra, and are more likely to overlap with other fluorescent tags in a multiplex assay format (section 1.1.2). A quantum dot-streptavidin bioconjugate (QD-SA) was used as an inorganic reporter dye to reveal the genotype of the DNA template in order to develop an assay adaptable to future multiplex format and to maximise the hybridisation signal of detection. QD-SA was also chosen in order to demonstrate the potential of the QD technology in the development of a bioassay using only inorganic dyes. QD-SA bioconjugates have been commonly used in immunoassays, and commercialised products with standardised protocols are available (Section 1.1.3 and 1.2.3). QD-SA were chosen with a single emission signal emitting at 665 nm to avoid potential encroachment with multicolour beads. Eastman *et al.* (2006) reported the use of QD-SA665 for multiplex gene expression analysis using QD-doped particle. The specificity of the platform was described in section 1.2.3.

Previous work and commercialised particles facilitated the design of a specific protocol adapted for the detection of SNP allelic probes in suspension. The final objective of this research was to investigate the potential of QDEM-probes in a genotyping experiment. The genotyping of single nucleotide polymorphisms (SNP) with an allele-specific oligonucleotide (ASO) hybridisation assay and QDEM-probes involved: (**1)** the selection of SNP markers and the amplification of the DNA targets with biotinylated primers; (**2**) the design of the fluorescent probes, heat-denaturation of the PCR products and hybridisation of the probes to the denaturated biotinylated PCR products; (**3**) the addition of the fluorescent reporter dye linked to a streptavidin and interaction with the complex [biotinylated target fluorescent probe]; (**4**) the detection of the fluorescent signals in the suspension. Each probe should have a unique fluorescent tag. The detection of the reporter dye and the fluorescent probe simultaneously identified which allele has been hybridised (Figure 1.19).

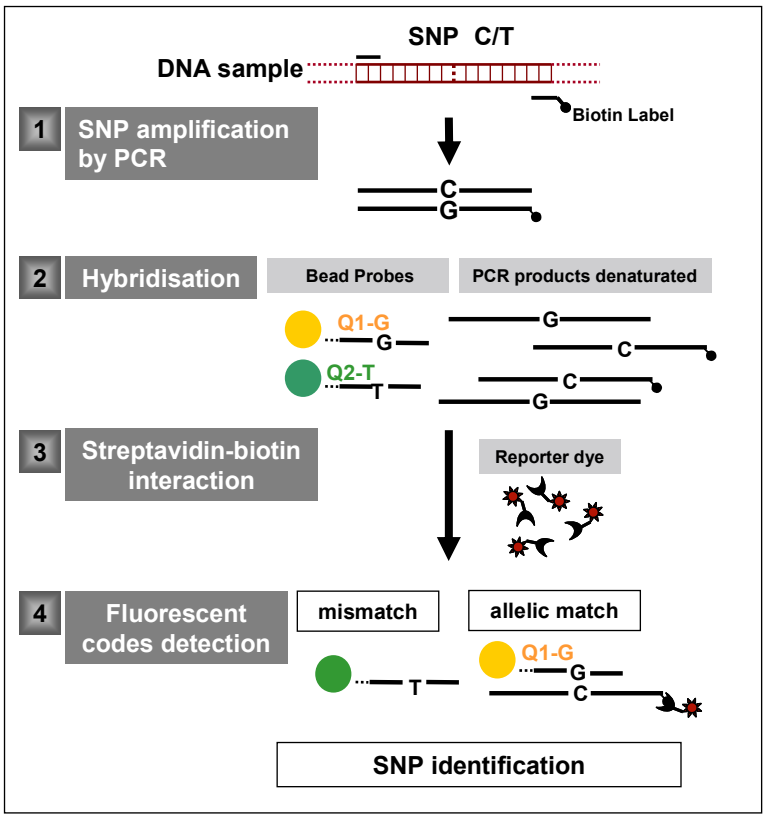

Figure 1.19 Schematic of the general ASO-SNP genotyping bead-based method (reprinted to facilitate reading).

Therefore, the main objectives of the work presented here was to select and amplify Y-SNPs in singleplex, and then to demonstrate the feasibility of an ASO genotyping assay using the optimum experimental conditions defined previously (Chapter 4) with exclusively inorganic fluorescent markers. The ASO QDEM suspension assay was tested with the genotyping of two different SNPs. The aim of this initial study was to provide a proof-of-principle of the potential of the QDEM-probe technology with the potential for future development in multiplex experiment format and male identification in forensic genetics.

5.2. Materials and methods

5.2.1. DNA templates

The male cell line ARPE19 (reference: CRT-2302) was supplied by the American Type Culture Collection (ATCC, Manassas, VA, USA), and was originated from human male retinal-pigmented epithelium. The female cell line RT112/84 (reference: 85061106) was supplied by the European Collection of Cell Culture (ECACC, Salisbury, UK) and belonged to human bladder slow growing tumour.

DNA from the male cell line (ARPE19, ATCC CRT-2302, VA, USA) was used as a positive control and DNA from the female cell line (RT112/84, ECACC 85061106, Wiltshire, UK) was used as a negative control for the amplification of the targeted DNA. Cell culture was carried out as described in Appendix L.

DNA was extracted using the QIamp DNA mini extraction kit (Qiagen, Crawley, West Sussex, UK) following supplier's instructions. QIamp DNA mini extraction kit uses Proteinase K procedure to lyse cells and a purification system on spin columns. Extracted and purified DNA was eluted in TE buffer (Tris-EDTA pH8.0, Sigma, Andover, UK). The DNA concentration and purity were evaluated after extraction by spectroscopy with a WPA light wave spectrophotometer (Biochrom, Cambridge, UK), and a 10 mm path length cell with an optical density (OD) of 1.0. The OD of the sample (typically diluted in 1/300) was read at absorbance 260 nm (A_{260}) and 280 nm. An OD of 1 at 260 nm corresponds to 50 µg/ml of double-stranded DNA. The DNA concentration was then calculated as followed:

$$C\ (\mu g/ml) = A_{260} \times 50 \times \text{dilution factor}$$

The purity was determined using the ratio of absorbance at 280 nm and 260 nm (A_{280}:A_{260}). Pure DNA preparations have expected ratios of ~1.8.

5.2.2. Design of a SNP polymerase chain reaction (PCR)

- **SNP selection**

The SNP selection involved the parameters detailed in the introduction of this chapter, namely: the validation status, the linkage between markers, the heterozygotie of the markers, the flanking regions reliability, and the mismatches composition.

Y-SNPs were selected from the SNP database (dbSNP) of the National Centre for Biotechnology Information (NCBI) that comprises 2,243,761 unique SNPs discovered from centres contributing to the public Human Genome Mapping Project (HGMP) (http://www.ncbi.nlm.nih.gov/entrez/SNP/), and from previous methodology developed for Y-SNPs genotyping assays (Sanchez *et al.*, 2003; Phillips, 2004; Carracedo and Sanchez-Diz, 2005; Sanchez *et al.*, 2006). The data collected on the SNP sequences were used to perform: (i) the compilation of the corresponding sequences of reference, (ii) the determination of the gene sizes and allele sizes, and (iii) the run of an initial alignment of sequences using the Basic Local Alignment Search Tool (BLAST, (Altschul *et al.*, 1990), www.ncbi.nlm.nih.gov/BLAST/), that helps to create a consensus sequence). A step-by-step protocol was then established to design Y- SNP primers and probes, for SNP amplification and genotyping (Henegariu *et al.*, 1997; Butler *et al.*, 2003; Sanchez and Endicott, 2006).

- **Primer and amplicon design strategy**

The Y-SNP sequence defined with previous multi criteria methodology was used for the design the Y-SNP primers with the software Primer3 (Rozen and Skaletsky, 2000) and according to published primers and probes design protocols (Henegariu *et al.*, 1997; Butler *et al.*, 2003; Sanchez *et al.*, 2003). The Y-SNP primers consisted of short nucleotide sequence (20 – 24 nt) labelled with a biotin at the 5'end (Figure 5.1).

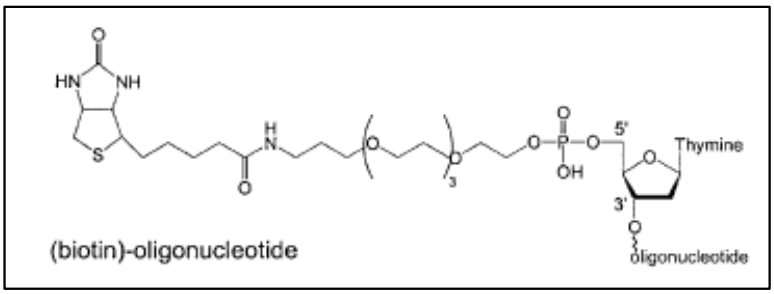

Figure 5.1 Oligonucleotide linked to a biotin molecule.

The primers were designed in order to obtain a PCR product that avoided duplex formation and non specific binding (with PCR products and probe sequences). Primer design aimed to amplify a small size range of amplicons between 90 to 200 bp. Small amplicon sizes are expected to facilitate and balance amplification efficiency, and therefore to optimise the PCR.

Control primers were used to amplify the beta-actin gene, a widely used housekeeping gene for internal positive control of PCR reactions (Dubreuil *et al.*, 1993). The beta-actin sequence and primer sequences can be found in Appendix O. The beta-actin primers amplify a 116 bp fragment, in the size range of the SNP amplicons.

The general parameters for the design of the primers selected on Primer3 software were:

- A percentage of DNA pyrimidine bases (G, C content) of 35% to 60% or a Pyrimidine:Purine ratio close to 1: 1
- Primer lengths ranging from 19 to 24 bp
- Primer annealing temperatures ranging between 55 and 65 °C
- Avoid unstable flanking regions, *i.e.,* palendromic sequences or long polynucleotide stretches

A series of primers were generated with the software. The pairs of primers that presented the best option matches were selected and tested for their suitability in PCR conditions with an *in silico* test simultaneously with the probes designed for the SNP identification.

- **Y-SNP probe design strategy**

Probe sequences were designed simultaneously with the primers using the same software (Primer3, (Rozen and Skaletsky, 2000)). The criteria for the design of the probes to be conjugated to a microsphere are listed (Fuchs *et al.*, 2005).

- Probes should be of 18 to 24 nucleotides in length; 21 nucleotides was chosen as an optimum length
- The point of mutation (or SNP) should ideally be positioned at the centre of the probe sequence
- Probes have to be synthesised for both SNP alleles
- Probes should be designed with a primary amino group at the 5' end, to provide bio-conjugation properties

Several authors suggested the synthesis of the oligo with a 5' amine-spacer to improve bioconjugation efficiency (Cao *et al.*, 2006a; Wittebolle *et al.*, 2006). A separate study was undertaken to determine the importance of the length of the carbon spacer in the coupling experiment (see Chapter 3). As a result, a 6 carbon spacer was found to be sufficient to provide efficient conjugation and hybridisation identification properties

Probes and primers were purchased from Thermo Electron (Thermo Fisher supplier, Hemel Hempstead, UK). Probe and primer stock solutions were prepared by the dissolution of the lyophilised primers in nuclease free water (nfH_2O, BRK200, Fisher Scientific Ltd, Leicestershire, UK) to a final concentration of 100 pmol/µL. Aliquots of 20 pmol/µL were used as working solution. Oligo solutions were stored at - 20 °C.

- **Test *in silico***

The suitable genomic region of the Y-SNP selected with phylogenetic criteria was screened using NCBI Map viewer with the alignments and the physical criteria guidelines described previously (Phillips, 2004). Table 5-1 summarises the main information which characterises the two SNPs selected to test the QDEM-probe technology. The two alleles reported for the SNP M9 loci are a guanine (G) / cytosine (C) transvertion. The two alleles reported for M60 are the absence of insert (NoIns) or the insertion of thymine (T) at the mutation point.

Table 5-1 Data on the SNPs selected *

SNP loci	dbSNP accession	Sequence of flanking regions (5' → 3')			Average estimated heterozygosity
		5' Near Seq (~ 30 bp)	Alleles	3' Near Seq (~ 30 bp)	
M9	rs3900	AAAGAAACGGCCTAAGATGGTTGAAT	**[C/G]**	CTCTTTATTTTTCTTTAATTTAGAC	0.499
M60	rs2032623	TACATTTCAAAATGCATGACTTAAAG	**[-/T]**	ATCAGGCACACAGTGGTTACTCAAT	0.137

* Source of data: SNP database (dbSNP); Seq: sequence; A,T,C,G: adenine, thymine, cytosine, guanine; the polymorphic site is indicated in brackets

A series of tests were undertaken to check the complementarities of the probes to their targeted SNP. Oligo sequences were tested *in silico* with the AutoDimer software (Vallone and Butler, 2004) to verify that no super secondary structure appeared with the probes, between primer and probe sequences, and between probes and PCR product sequence. First Primer-dimer formation was investigated.

The primer stability is usually measured in the length (bp) of DNA duplex, the GC/AT ratio, and in kcal/mol (duplex formation free energy, ΔG) at the melting point (Tm). The AutoDimer software (Vallone and Butler, 2004) was used to test primer dimer formation between the different sets of primers. Some of the most important parameters taken into account by the software are listed.

- The ΔG Temperature; the free energy (ΔG) evaluated the energy needed for the formation of stable oligo duplex; the lower the ΔG, the stronger the association. The ΔG Temperature was the T at which ΔG was calculated *i.e.,* T of annealing in the PCR process.
- The score; the score reflected the general stability or tendency of the potential interaction to exist in solution; a score threshold of 7 or 8 is considered as satisfactory
- The visualisation of oligo interactions; the alignment found with the program were listed and analysed one by one based on the 3'end binding, AT or CG content (%GC), and the context mismatches; strong association corresponded to a preferential 3' binding and higher GC content.

In parallel, the basic alignment search tool (BLAST) was used to test the specificity of the primers for the human Y-chromosome. A nucleotide-search for short nearly exact matches was used to look for non specific hybridisation on the human genome sequence (Altschul *et al.*, 1990). The E-value described as *"the probability due to chance that there is another alignment with a similarity greater than the given S score",* where the S score measures the similarity between the query and another oligo sequence, was used to analyse the results (Altschul *et al.*, 1990). An E-value < e^{-5} of the alignment of the primers with the corresponding SNP sequence, and no other genomic sequence was considered as a highly unique alignment, and not due to error.

5.2.3. PCR experiments

- **PCR product amplification**

All DNA amplifications were performed in a TC-512 thermal cycler (Techne, Barloworld Scientific Ltd, Stone, Staffordshire, UK). PCR products were stored at 4°C and kept at -20°C for daily experiment. The primer pairs (20 pmol/μL) were individually tested under identical amplification conditions with the same DNA template concentration. First, the optimal annealing temperature of the targeted SNPs in a singleplex format was determined

by T-gradient PCR procedure. Approximately one µg of male DNA (ARPE19 cell line) was amplified by PCR in a 25 µl reaction volume containing 1X Buffer, 2 mM $MgCl_2$, 200 µM of each dNTP, 0.4 µM of each primer, and 0.6 units of Taq DNA polymerase (Taq PCR core kit Qiagen, Crawley, West Sussex, UK) at 94°C for 5 min followed by 30 cycles of 30 s at 95°C, 30 s at 58°C-Δ20°C, 30 s at 72°C, ending by a final extension at 72°C for 5 min. The curve of the gradient calculator, Δ, of the annealing temperature ranges from 48.6°C to 68.3°C, with 12 temperature steps (Figure 5.2).

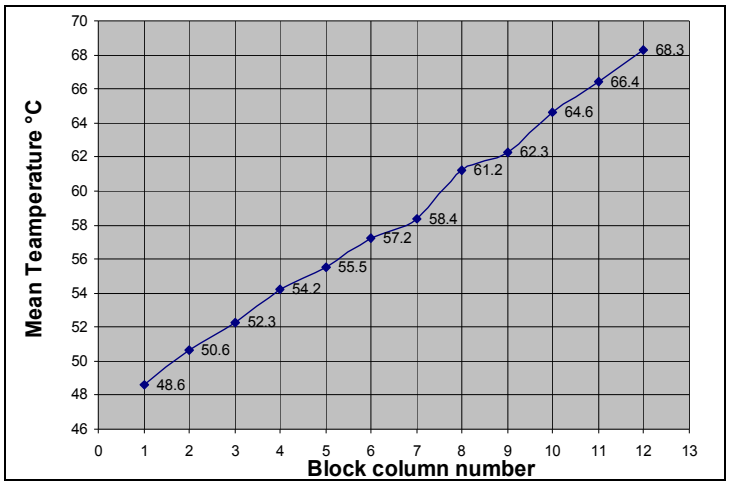

Figure 5.2 Curve representing the gradient for annealing temperature of 58°C, Δ20°C.
The curve was drawn with Excel (Windows, 2000, Microsoft Corp, USA), with the values given by the gradient calculator (Techne, Staffordshire, UK).

The final optimised PCR conditions were as follows: one µg of DNA template (female and male) was amplified by PCR in a 25 µl reaction volume containing 1X Buffer, 2 mM $MgCl_2$, 200 µM of each dNTP, 0.4 µM of each primer, and 0.6 units of Taq DNA polymerase (QiagenWest Sussex, UK) at 94°C for 5 min followed by 35 cycles of 30 s at 95°C, 30 s at 58°C, 30 s at 72°C, ending by a final extension at 72°C for 5 min. For each PCR experiment, the amplification was performed with nfH_2O (Fisher Scientific, UK) that replaced the DNA template as a negative control.

- **PCR product analysis**

Agarose gel electrophoresis

Singleplex PCR products were analysed by electrophoresis in a 3% agarose gel (Appendix M) (Sigma product purchase through Fisher Scientific, Leicestershire, UK). 1X TAE buffer (Tris-Acetate-EDTA, 40 mM Tris, 20 mM Acetic acid, 1 mM EDTA, Fisher Scientific, Leicestershire, UK) was used as electrophoresis running buffer.

The 100 bp DNA ladder (Promega, Southampton, Hampshire, UK) with size ladder ranging from 100 bp to 1500 bp and 6X bromophenol blue-orange G loading dye (Promega, UK) was used to identify the size of the bands on the gel. 2 µl of 100 bp ladder mixed with 3 µl of 6X loading dye (Promega, Hampshire, UK), and 5 µl of PCR product mixed with 3 µl of blue-orange dye were loaded on to the gel, and run at 25 V for 45 min with RunOne™ electrophoresis cell and power supply from EmbiTec (Web Scientific Ltd BTC, Crewe, Cheshire, UK).

Agarose gels were then stained in 400 mL of deionised water containing 0.5 µg/ml ethidium bromide solution for 45 min. Images were taken with the GenGenius Bio imaging system instrument from Syngene (Synoptics, Cambridgeshire, UK).

Sequencing

SNP PCR products were purified with the MiniElute PCR purification kit (Qiagen, West Sussex, UK), and quantified. Five µl at 1ng/µl per 100bp of purified PCR product and 5 µl of each primer at 3.2pmol/ µl per reaction, were sent to Geneservice Ltd (Cambridge, Cambridgeshire, UK) to be sequenced by capillary electrophoresis with an Applied Biosystems 3730 DNA analysers. The sequencing results were analysed using BLAST 2 sequences online tool (Tatusova and Madden, 1999).

- **PCR product quantification**

The concentration of PCR products was determined by two different methods. The first method was described in section 5.2.1. The second method used the GeneTools analysis software 3.02.00 (Syngene, division of Synoptics Ltd, Cambridge, Cambridgeshire, UK) to determine the relative concentration of the PCR products on agarose gel by comparison with a DNA ladder (Promega, Southampton, Hampshire, UK). Five microliters (650 ng) of DNA ladder contains approximately 150 ng of the 500 bp DNA fragment and 50 ng of each other ten DNA fragments. The concentration of DNA corresponding to the bands of the ladder was used to create a quantification scale depending on the fluorescence emitted by the band on the gel. The DNA quantity of the PCR fragments was then evaluated proportionally to this scale and as a function of their fluorescence. The concentrations obtained in g/L were then converted in molar concentration (C in mol/L) with the formula:

$$C = m / (MW \times V)$$

where m: quantity of PCR product in g; V: volume of PCR product loaded onto the gel in L; MW: molecular weight of the corresponding SNP PCR product analysed in g/mol.

5.2.4. Dot blot experiment

A dot blot protocol was employed to assess the specific hybridisation of the probes to the targeted SNP. The general procedure of dot blotting involves taking an aqueous solution of DNA target (the SNP PCR product), and to spotting it on a membrane. The denatured DNA sequences immobilised on the membrane are then exposed to a solution that contains single strand (ss) labelled probe sequences. After sufficient incubation time for the probe to hybridise to the target, the membrane is washed, dried and exposed to a film to reveal DNA-DNA hybridisation.

- **Membrane preparation**

A positively charged nylon membrane (Hybond N^+, GE Healthcare Life Sciences, Amersham place, Bucks, UK) was first washed in nfH_2O (Fisher Scientific, UK). PCR samples were mixed with a denaturation solution made of 0.4 M NaOH, 10 mM EDTA (pH 8.2), and then boiled for 10 min to separate the DNA strands and allow the single strand to immobilise on the membrane.

Approximately 100 ng of PCR products in solution were spotted on to the membrane, 2 µL at a time. The membrane was then placed under UV light for 30 s to cross-link the DNA to the membrane.

- **Probe labelling**

Probes were labelled with the enhanced chemiluminescent (ECL) direct labelling kit (GE Healthcare, UK) for chemiluminescent detection. Probes were first diluted to a final concentration of 10 ng/µL. 5 µL of each probe solution was denatured in boiling water for 10 min, and immediately placed on ice. After a brief centrifugation, 10 µL of acridan-based labelling reagent was added to the denaturated DNA and mixed. 10 µL of gluteraldehyde was then added to the mix and spun briefly. The mix was incubated at 37 °C for 10 min, and if not used immediately, was kept on ice for 10-15 min.

- **Probe-target hybridisation and signal detection**

Hybridisation was performed in the Gold Hybridisation Buffer (5 mM NaCl and 25 mM EDTA, GE Healthcare) with the 5% (w/v) non fat dried milk blocking agent provided by the supplier (ECL kit, GE Healthcare, UK). Before hybridisation, the membrane was washed briefly in 2X SSC, 0.1%SDS (Section 2.2.1). If more than one membrane was prepared at a time each membrane was then placed in a separate glass bottle and a pre-hybridisation step was undertaken at 42°C for 1 h in the pre-warmed hybridisation buffer

(42°C) under gentle agitation. Two labelled probes identifying both SNP alleles were added (ratio 1:1) to the hybridisation solution, avoiding direct contact with the membrane. The incubation continued over-night. The next morning the membrane was washed as described in Table 5-2 under medium speed agitation.

Table 5-2 Post-hybridisation washing steps *

Wash	Solution	Condition
2 time	0.5X SSC, 0.04% SDS	At 42°C for 20 min
2 times	0.5X SSC, 0.1% SDS	At RT for 5 min
Rinse in	2X SSC	At RT, 1 min

* RT: room temperature

The chemiluminescent detection of the DNA dot blot was carried out with the ECL detection reagents (GE Healthcare, UK). Reagent A was mixed with reagent B in a 40:1 ratio and applied to the membrane for 1 min at room temperature (RT). The excess of solution was then discarded, and the membrane was placed in a plastic bag, with all the air removed before being placed in a film cassette. An Amersham Hyperfilm ECL™ (GE Healthcare) was place in the cassette for two hours at RT, and then developed using Kodak developer and fixer (Eastman Kodak Sàrl, Geneva, Switzerland).

The film was placed in the developer for a few seconds until the spot of interest appeared, washed in water, immersed for 5 min in the fixer solution, placed in water for 5 min to rinse, and finally left to air-dry.

5.2.5. QDEM probes

Chemicals and instrumentation for the conjugation and the hybridisation experiment were as previously described (Section 3.2 and 4.2). The two SNPs M9 and M60 were used to test QDEM-probe technology in an ASO genotyping assay. SNP oligo probes for conjugation were designed as previously described (Section 3.2.2.) with an amino active group attached through a carbon spacer (6 carbon spacer, 6C) at the 5' extremity of the specific SNP allele probe sequence. Each probe was conjugated with a different QDEM fluorescent code.
The QDEM fluorescent codes used in the assay were: 525(1:0), 575(0:1), (525;575)(1:1), and (525;575)(1:2) (Appendix A). These QDEMs were chosen because their fluorescent codes were in the same range of colours and intensities which satisfied the criteria defined for multiplex analysis (Section 2.3.3). QDEMs and QDEM bioconjugates were enumerated as previously described (Appendix C), using a haemocytometer (Reichert, USA) (Appendix A). The name of each probe is presented in Table 5-4. As an example, the QDEM fluorescent code of the microsphere encoded with 525 nm QDs is symbolised by the code (1:0)Q and the name of the SNP allele it identified is placed after *e.g.,* M9-G or M9-C.

The initial QDEM solutions and QDEM bioconjugates were used as negative controls to evaluate the QDEM fluorescent code and the percentage of bead recovery at the end of the experiments. For each batch experiment, the bioconjugate populations were used to define a region on the flow cytometer. This region was then used to gate and to analyse the hybridised samples of the experiment batch. A population of 525QDEM bioconjugates were used in singleplex experiment to test the effect of the target concentration on the hybridisation efficiency of each allelic probe.

Quantum dots emitting at 665 nm (detection in FL4) bioconjugated to streptavidin molecules (665QD-SA) were used as reporter dyes to bind the biotinylated PCR products (Section 5.1). 665QD-SA was purchased from Crystalplex (PA, USA) at a concentration of $1.82 \text{ X } 10^{11}$ particle/mL.

5.2.6. Conjugation and hybridisation protocol

- **General procedure**

The conjugation procedure used in these experiments was obtained from the former part of the research where an optimised methodology adapted to carbodiimide attachment of short oligo to the QDEM materials was developed (Section3.2.2, and 4.2.7). For each conjugation experiment a volume of 10,000 QDEMs (quantification method in Appendix C) of each population were used to prepare a unique QDEM-probe, which aimed to bind specifically one of the alleles of the targeted SNP.

Approximately 8000 QDEM-probes were recovered at the end of the conjugation procedure in 10 µL of hybridisation buffer. For each batch experiment an extra QDEM bioconjugate sample was undertaken as a negative control. PCR samples obtained in a range of 400 to 800 ng with singleplex PCR experiments were diluted to the concentration needed for each specific hybridisation experiment (Section 5.2.3).The hybridisation procedure was then undertaken with 2 µL of the expected quantity of M9 and M60 PCR products. The hybridisation was undertaken in the optimised hybridisation conditions of ~1 hour incubation time at 49 ºC defined in the previous study (Chapter 4). An additional step in the hybridisation process consisted of the denaturation of the target or PCR products for 10 min at 100 ºC using the PCR machine (Techne, Staffordshire, UK) to obtain single strand DNA, before adding the target to the QDEM bioconjugates solution.

The initial QDEM solutions and QDEM bioconjugates were used as negative controls to determine the effect of the procedure on the background and hybridisation signals, and also on the internal QDEM fluorescent code.

- **665QD-SA labelling**

The last step in the QDEM ASO assay after the hybridisation of the QDEM-probes to the PCR products was the identification of the hybridised complex with 665QD-SA. First, a theoretical calculation of the number of 665QD-SA was undertaken (Agrawal *et al.*, 2008) (Wu *et al.*, 2007). As a result, 6.28 x 10^5 QD-SA were required for the hybridisation of 8,000 QDEM probes (Appendix N). The concentration of QD-SA being 1.82 x 10^{11} QD/mL, 3.5 µL of QD-SA solution was needed for each singleplex hybridisation experiment (Appendix N). 7 µL were used for duplex hybridisation assays. The incubation and washing steps of 665QD-SA labelling protocol were adapted from Eastman *et al.* (2006). The hybridisation mix was incubated at RT for 20 min, and mixed manually every 4 min. The samples were then washed four times in 300 µL of storage buffer 1 X TBS, 1% BSA, 0.01% azide (1 min, 400 rpm, RT). Centrifugations were performed at 1133 g for 3 min. Samples were resuspended in 400 µL of filtered TE buffer (FC running buffer) for analysis on the flow cytometer (Section 3.2.3).

- **Singleplex titration experiment**

The two allelic QDEM-probes corresponding to each SNP were first tested separately with increasing quantities of their corresponding SNP PCR product. An equal quantity of 8000 QDEM-probes for each allelic probe was used. The titration of the DNA target was undertaken using increasing quantity of PCR products ranging from 1.5 to 300 fmol. PCR products were diluted to obtain the expected quantity in 2 µL, in order to keep the final volume constant (10 µL of QDEM-probes, 2 µL target, 3.5 µL of 665QD-SA). The final concentration of each hybridisation solution was then approximately 520 QDEM / µL. Titration of PCR product was undertaken with molar quantities of products where an increasing fluorescent signal was obtained during the titration of the fluorescent probe testing the optimal conditions (Section 4.3.3). Target quantities in the fmol ranges (<1 pmol) were used to demonstrate the sensitivity and efficiency of the ASO QDEM genotyping system in singleplex.

QDEMs-probes incubated with the negative control of the PCR (PCR mix incubated with water instead of the DNA templates), was used as a negative control. Two replicates were performed for each PCR product quantity tested, and a negative control was performed for each batch experiment. A specific FC protocol was developed to maximise the detection signal of the QDEM codes of the probes in FL1 and FL2, simultaneously to the FL4 hybridisation signal. The protocol was adapted to detect the four probes with the same parameter settings in order to record comparable hybridisation signal.

- **Duplex genotyping assay testing 4 QDEM allelic probes**

For the genotyping of two SNPs, 2 allelic probes were required for each SNP. Each probe was conjugated to a single type of QDEMs. Four different QDEM codes were thus required to create the bioconjugated probes (Table 5-4). QDEM-probe samples were diluted separately in the hybridisation buffer to obtain 20 µL of bioconjugate solution. 10 µL of each QDEM-probe were pooled in a single experimental tube. The experiment that evaluated the effect of the target concentration on the hybridisation experiment revealed a good hybridisation signal simultaneously as a good discrimination signal for both SNPs in the range of PCR products quantities between 60 and 150 fmol.

These ranges of concentration were used for the duplex genotyping assay. M9 and M60 PCR product solutions were diluted to obtain the same concentration: ~100 fmol/µL. Approximately 100 fmol, corresponding to 1 µL of each PCR product was added to the hybridisation mix. 7 µL of 665QD-SA reporter dye was then adjoined to obtain a final hybridisation mix of 49 µL. The final concentration of the duplex hybridisation solution was then ~330 QDEM / µL. The multiplex assay was replicated with three experiments. The negative control of the PCR experiment was used to perform the negative hybridisation control reaction with the 4 QDEM-probes. Hybridisation conditions and washing steps were as previously described (Section 5.2.6).

5.2.7. Flow cytometry data analysis

Samples were analysed under FC and confocal microscopy as previously described (Section 2.2.5, and 2.2.6). The median fluorescence intensity (MFI) was recorded in FC detector channels and corrected with the MFI of the negative control to calculate the RMFI for each sample, as previously described (Section 3.2.3). The relative percentage of events was calculated at the end of the duplex hybridisation experiment. The relative percentage of events calculated in the duplex experiment for each QDEM population took into account that half of the bioconjugate probes were used for each QDEM population in this experiment:

$$R\%Events = \%Events\ (h) / (50\%\ of \%Events\ (c))$$

Where (h) represents the hybridised QDEM-probes, and (c) the QDEM bioconjugates before hybridisation.

The code consistency was estimated with the relative variation in the fluorescent code detected in the FL channel from the initial QDEM control population (in a.u.) The code consistency was evaluated in FL1 and FL2 since the QDEM probes had a fluorescent code encoded with QDs emitting at 525 nm and 575 nm wavelength detected in both of these detector channels (Appendix A). QDEM-probes after hybridisation were analysed with the logical gate defined with the QDEM bioconjugates control population. FC data were analysed with WinMDI2.8 software (the SRI, USA). A specific FC protocol was design for the analysis of single- and duplex ASO genotyping experiments (System II Data Acquisition and display software version 2.0 (Beckman-Coulter, FL, USA)).

Data were presented as the mean of replicates ± the standard error (SEM). Curves and statistics were designed with GraphPad Prism5.01 (GraphPad Software, CA, USA).

5.3. Results

5.3.1. Primer and probe sequences

Primer and probe sequences were designed with the Y-SNP genomic sequences available in the supplementary materials in Appendix O. Primers and probes satisfied the criteria defined previously (Section 5.2.2). Of all the possible oligo interactions between primers, probes, and amplicons, none of the alignment scores were greater than seven. Alignment scores greater than seven (the default value in Primer 3 and AutoDimer program for single primer comparison) lead to significant primer-dimer formation under typical PCR amplification conditions (Beasley *et al.*, 1999). The lack of significant primer-dimers along with the design of similar primer Tm values suggested that the primers were successfully optimised *in silico* for the PCR experiment. The standard nucleotide BLAST searches showed E value << e^{-5} for all the primers tested. These results indicated the specificity of the primers for their target. The data suggested very low probabilities of primers binding sites in the human genome other than the Y-SNPs marker of interest.

The beta-actin gene was used as a positive control in all PCR reactions. Specific primers provided an amplicon in the size range of the Y-SNPs PCR products to be able to use the same experimental PCR conditions and to analyse the PCR samples on the same gel electrophoresis analysis.

Amplicon size, primer length, Tm and GC contents were in the ranges expected and required: respectively between 90-200 bp, 19-24 bp, 55-65 °C, and 35-60% GC (Section 5.2.2). The primers were reverse-phase HPLC purified (Thermo Electron, Hemel Hempstead, UK). The sequences of the primers and probes are presented in Table 5-3.

The sequences of the probes were designed simultaneously with the primers to test their compatibility with primers and PCR products. The polymorphic sites are indicated in bold in Table 5-4.

Table 5-3 Primer sequences for Y-SNPs and beta-actin *

Y-SNP loci / dbSNP id	Primer	sequence 5' → 3'	Length (bp)	Tm (ºC)	GC%	Amplicon size (bp)
M9 / rs3900	forward (F)	AATACAGAACTGCAAAGAAAC	21	60.7	33.3	96
	reverse (R)	CTAAGTATGTAAGACATTGAACG	23	60.64	34.8	
M60 / rs2032623	F	CCCTGATGTGGACTCAACCTT	21	61.32	52	196
	R	GGTGGTCAAGAGCAGAGCTT	20	59.6	55	
Control						
Beta Actin	F	TCGTCATACTCCTGCTTGCTGATCCA	26	60	50	116
	R	TCCTCAGATCATTGCTCCTCCTGAGC	26	61	54	

Table 5-4 Probe sequences for the Y-SNP M9 and M60 *

Y-SNP loci / dbSNP id	Probe sequence 5' → 3'	Length (bp)	GC%	Tm (ºC)
M9 / rs3900	AATAAAGAG**c**ATTCAACC AT	20	30	44
	AATAAAGAG**g**ATTCAACCAT	20	30	45
M60 / rs2032623	AAAGATCAGGCACACAGTGGTT	22	45	54
	AAAG**t**ATCAGGCACACAGTGGTT	22	43	54

* dbSNP id: SNP database identification number; Tm: melting temperature; %GC: percentage of GC in the sequence; bp: base pair; the polymorphic site is indicated in bold in lower case in the probe sequence

The polymorphic site of the probes was located in a central position of the sequence, or a minimum of 5 nt separated the polymorphic site to one end (5' or 3') of the sequence. Since it is commonly accepted that the polymorphic site is required to be in the middle of the sequence or not less than 3 nt from the end to obtain efficient SNP probes, the designed *in silico* of the Y-SNP probes was validated as follows (Fuchs *et al.*, 2005).

All primers and probes presented a $\Delta G < 0$ for all the primer dimer tests performed between the oligo sequences of the primers, the probes, and the amplicons. Probes were typically giving a $\Delta G \geq +17$ Kj when tested for complementarities with the corresponding sequence of the SNP target. To conclude, the *in silico* optimisation of the design of allelic specific probes for most favourable SNP detection was successfully achieved for the SNP selected.

5.3.2. DNA extraction

The high concentration and high purity of the DNA recovered was expected from the extraction of cell lines using the QIamp DNA mini extraction kit (Qiagen, West Sussex, UK). The concentrations of the DNA samples extracted from the cell lines were in average of approximately 600 µg/ml. Extracted DNA had a purity factors in the range of 1.5 to 1.8. The DNA freshly extracted was systematically tested for the amplification of the housekeeping gene beta-actin.

5.3.3. Amplification of SNP target

- **PCR assays**

The gradient PCR experiment was undertaken for each SNP to identify the optimum annealing temperatures that amplified the expected fragments with the highest yield (Appendix P). Y-SNPs were amplified on a microplate in singleplex with a 20°C gradient of annealing temperature ranging from 56°C to 68.3°C, with ~2°C gradient step (Gel photos in Appendix P). The lowest and the highest Tm predicted from the primer design, respectively 59.6°C and 61.3°C, were therefore in the middle of the gradient range separated by one step (Figure 5.2). As a result, the two Y-SNPs were amplified in singleplex with a 58°C annealing temperature (Figure 5.3).

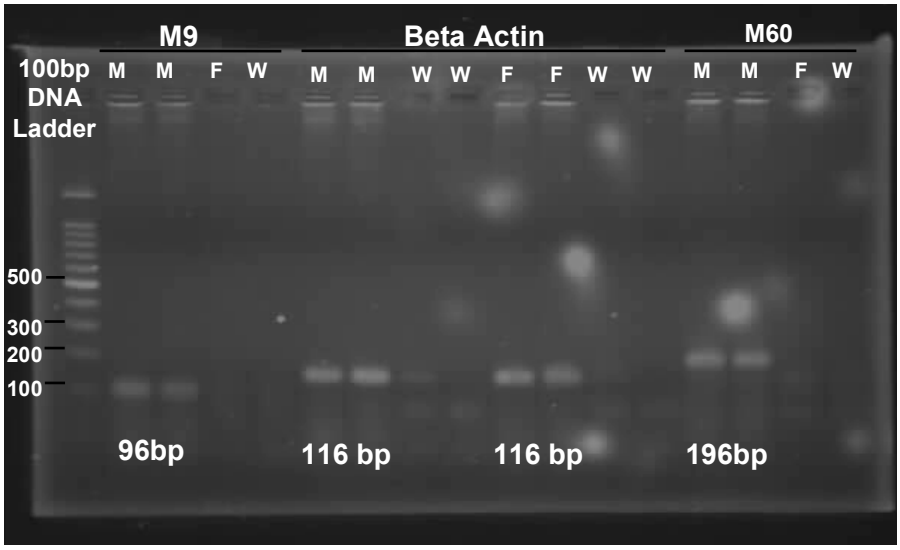

Figure 5.3 3% stained agarose gels showing singleplex PCR testing the Y-SNPs for their male specificity.

Each well is labelled: M for male template, F for female template, W for clean water. The sizes of the band of interest are indicated on the left side of the 100 bp step DNA ladder. The names of the PCR products and their expected sizes are indicated above the wells where they were run.

The male template ARPE19 was used as a positive control, whereas the female template and clean water were used as negative controls. Two PCR experiments were undertaken for each template. Similar yields of amplification of the expected bands were observed, which demonstrated the reproducibility of the amplification protocol. The analytical separation of the PCR fragments on a 3% agarose gel provided time efficient results to analyse the quality and the efficiency of the primer designed. The Y-SNPs primers showed no amplification with female DNA template and water. The Y-SNPs and the beta-actin fragments appeared at the expected size with the male template. Figure 5.3 shows a specific amplification of the expected size of beta-actin PCR product with the female DNA template. No amplification was observed with clean water. These results confirmed the specificity of the SNP primer design for the genotyping of the Y-chromosome.

The efficacy or the yields of amplification was quantitatively and qualitatively assessed by comparing the fluorescence of the product bands with the beta-actin as a positive control. M9 showed a lower amplification yield than M60 of ~ 35 %. Typical concentrations of the PCR products obtained ranged from ~500 to 800 ng of DNA per µL.

- **PCR product sequencing**

The sequencing of the PCR products was used as a comparative method to verify the sequence of the Y-SNP amplified. The sequences of the PCR products obtained with the male DNA template ARPE19 were compared with the genomic sequence used to design the primers and the probes (Appendix O).

The alignment of the sequences was performed with the Basic Local Alignment Search Tool (BLAST, www.ncbi.nlm.nih.gov/BLAST/, (Altschul *et al.*, 1990)). Each strand of the PCR products was sequenced to verify the reproducibility of the sequencing reaction. The genotype of ARPE19 for M9 and M60 are presented in Table 5-5. M9 and M60 are haploid in ARPE19 for respectively the allele G and the allele NoInsert (Appendix Q). The information on the allele frequencies provided by the dbSNP and summarised in Table 5-5 showed that the most frequent alleles were present in the selected male template.

Table 5-5 M9 and M60 genotyping results *

SNP loci	dbSNP accession	Alelles		Genotype for
		Alleles	Frequencies	
M9	rs3900	G/C	0.7 / 0.3	G/G
M60	rs2032623	-/T	0.926 / 0.074	-/-

* Frequencies obtained from the SNP database (http://www.ncbi.nlm.nih.gov/projects/SNP/)

5.3.4. Testing the probe specificity

The Y-SNP M9 and M60 were chosen for the preliminary experiments in the development of the ASO QDEM genotyping assay. These SNPs presented a robust and male specific amplification with the singleplex PCR experiment. The ASO probes corresponding to the SNP M9 and M60 were initially tested for their specificity to the PCR product amplified in the singleplex PCR with a dot blot experiment (Figure 5.4).

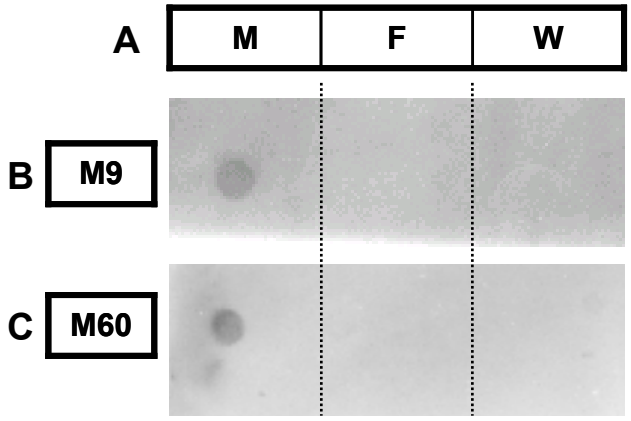

Figure 5.4 Dot blot analysis testing probes M9 and M60 specificity (scanned imagine).
A diagram indicates the positions of the spot deposit on the membranes (M: male, F: female, W: clean water). Pointed line were added to ease the interpretation of the pictures.

Approximately 35 ng of each PCR product was spotted on the membranes (Figure 5.4B and C). A positive hybridisation of the probes M9 and M60 was observed for their matching PCR products. No hybridisation was observed with the PCR samples obtianed with the female template and the water (see diagram Figure 5.4A). The probes designed for the identification of the Y-SNPs M60 and M9 were thus specific to the male DNA and their targeted amplicon.

5.3.5. The QDEM allele-specific probes

The four QDEMS were successfully conjugated to the four allelic probes. Approximately the same quantity of QDEM-probes were analysed under FC. Figure 5.5 shows the dot plot representation of the four QDEM-probes in FL1 and FL2 detector channel.

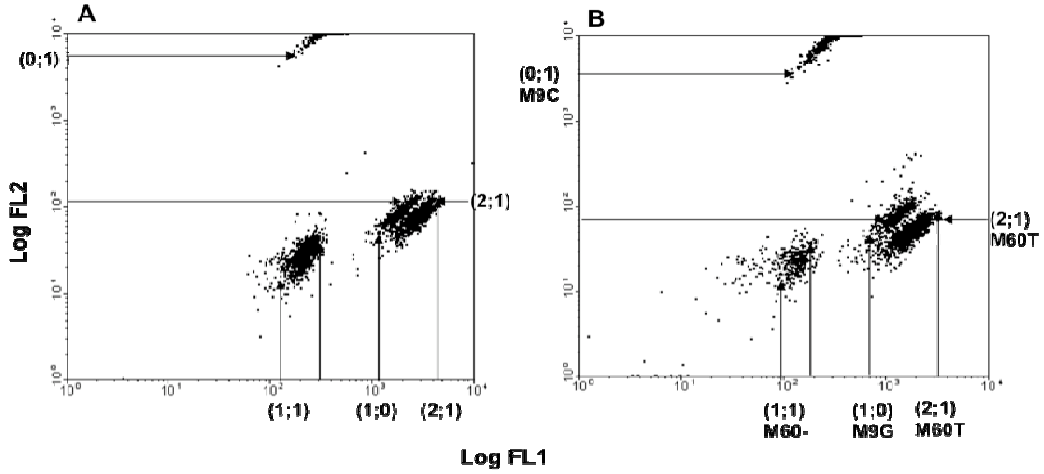

Figure 5.5 Dot plot analysis of (A) QDEMs and (B) QDEM-probes.

The initial four QDEMs (0:1)(1:0)(1:1)(2:1) and the four QDEM-probes (M9C, M9G, M60- or no insert, M60T) were analysed by flow cytometry; Dot plot representation in Log of FL1 (x-axis) versus Log of FL2 (y-axis); The population corresponding to each fluorescent code and probe are indicated by the black arrows on the graph.

The four control QDEM populations and QDEM-probes bioconjugates were visualised on the dot plot analysis. After conjugation the aspect of the population was modified. More debris was observed in the first Log of both detector channels, and populations encoded with 525 nm QDs *i.e.,* (1:0)(1:1)(2:1) presented a small decrease (< Log10) of FL1, similar to the decrease observed in FL2 for QDEMs encoded with 575 nm QDs *i.e.,* (1:1)(2:1)(0:1). The displacements of respective populations were symbolised by the displacement of the black arrows that delimitated the populations on the log scale of the x and y axis in Figure 5.5.

5.3.6. Effect of target concentrations on hybridisation in singleplex

The titration of each QDEM-probe was performed to evaluate the impact of the DNA target quantity on the hybridisation signal and probe affinity. This experiment also helped to determine which PCR concentrations would potentially be optimal for the identification of the SNP in a multiplex format (Figure 5.6).

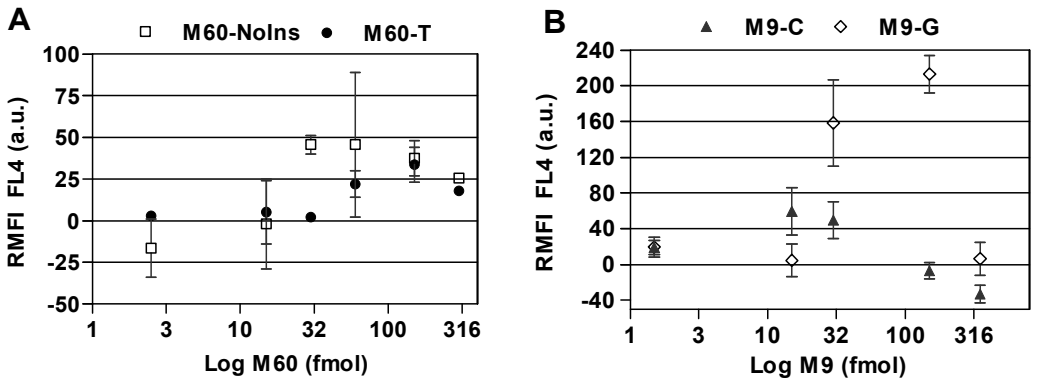

Figure 5.6 Hybridisation titration of PCR products (A) M60 and (B) M9.

A: Titration of M60 with increasing quantities of PCR products ranging from 1.5 to 300 fmol; **B**: Titration of M60 with increasing quantities of PCR products ranging from 1.5 to 300 fmol data were represented as the mean of replicates ± SEM.

M9 and M60 PCR products from the haploid male template (ARPE 19 cell line) were prepared in singleplex PCR experiments (Section 5.2.3) and quantified by gel electrophoresis fluorescence analysis (Section 5.2.1). The same quantity of each QDEM-probe was used in the experiment to hybridise the PCR products. The hybridisation signal detected in FL4 with the negative control was used to normalise the hybridisation signal detected with the positive samples (Figure 5.6).

The hybridisation signal detected with M60 amplicons was globally higher with the allele with no insert than with the insertion of the T base (Figure 5.6A). The titration curve of the 'M60-No insert' allele revealed no hybridisation signal from 0 to ~10 fmol and an increased of the hybridisation signal detected in FL4 from 0 to 50 a.u. from 10 to ~60 fmol. The signal decreased from 50 to 25 a.u. for PCR products quantities higher than 100 fmol. The M60-T allele was detected with amplicon quantities higher than 30 fmol and the maximum of hybridisation signal, at 25 a.u., was observed with 150 fmol of PCR products. Then the signal started to decrease in the same proportion as the signal of the other allele.

The results obtained with the titration of M60 showed a higher affinity (~50 a.u.) of the probes M60-No insert than the probe M60-T for the 150 fmol of amplicon. The large variation between replicates for M60-Noinsert, represented by the error bar on the graph at 150 fmol prevented the conclusion that the hybridisation signal for this target quantity was significantly different than the hybridisation signal with M60-T. Thus, an equivalent hybridisation signal was observed with both alleles for PCR quantities ranging from 150 to 300 fmol.

Figure 5.6B shows a significant higher hybridisation signal with the allele M9-G than with the allele M9-C. For PCR product quantities ranging from 30 to 150 fmol, a hybridisation signal of 150 to 200 a.u. was detected. For higher DNA concentration, the hybridisation signal decreased to ~0 a.u. A lower hybridisation signal, ranging from 0 to ~50 a.u. was recorded for the allele M9-C, with DNA quantities ranging from 1.5 to 30 fmol. With high PCR product quantities (> 150 fmol) both alleles had negative hybridisation signals.

5.3.7. A 4-plex QDEM ASO genotyping assay

An equivalent number of the four QDEM probes (4000 beads) were used in a duplex assay with approximately 100 fmol of each Y-SNP PCR product. The quantity of PCR products was chosen from the titration results and aimed to provide a significant hybridisation signal with a high discrimination level.

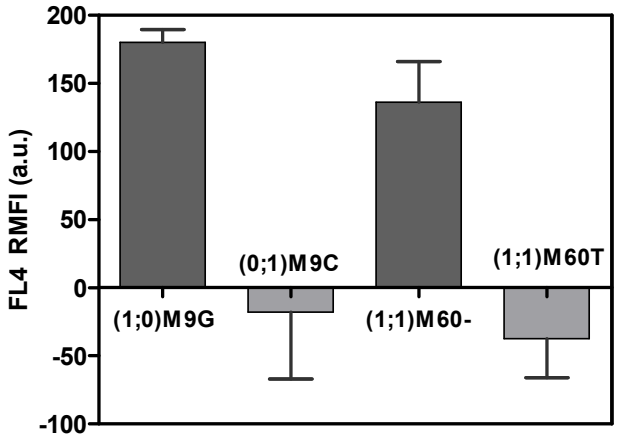

Figure 5.7 A duplex QDEM hybridisation genotyping assay.

(1:0)QM9-G identifies allele M9G; (0:1)M9-C identifies allele C; (1:1)M60- identifies M60 with no insert; (2:1)M60-T identifies allele M60T. Data presented as the RMFI ± SEM: the mean of fluorescence intensity (MFI) detected with the positive samples minus the MFI of negative control corresponding ± standard error (SEM).

The hybridisation signal represented by the fluorescent intensity of 665Q-SA attached to biotinylated PCR products was significantly higher for (1:1) and (1:0) QDEM-probe populations. Allele M60-No insert and allele M9G were detected respectively with ~140 and ~180 a.u. of FL4 RMFI. A FL4 RMFI background signal < 50 a.u. was recorded with the two other alleles.

The consistency of the QDEM fluorescent codes for each probe was evaluated by calculating the relative percentage of fluorescence in FL1 and FL2 for each hybridised population in comparison with its corresponding QDEM-probe bioconjugate population. No significant variation of the code consistency was identified: the relative fluorescence was between 90 and 100% for the four different hybridised QDEM populations. The percentage of events on the contrary significantly decreased; 18 to 45% of QDEM-probes were calculated at the end of the hybridisation procedure.

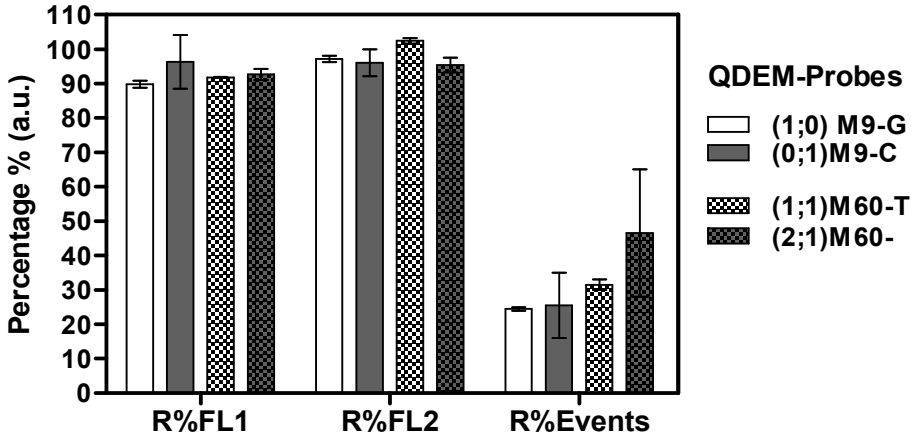

Figure 5.8 Stability of the QDEM-probe populations after hybridisation.

Legend is indicated on the left side of the graph; R%FL1, R%FL2 and R%Events were the Relative percentage of fluorescence and events detected at the end of the hybridisation procedure. Data were presented as the mean of R% ± SEM.

5.4. Discussion

A QDEM ASO genotyping assay was applied to the identification of Y-SNPs M9 and M60 in single and duplex format.

M9 and M60 amplicons were designed with sizes of respectively 96bp and 196 bp. The size of the PCR product influences the specificity of the probe attachment in the QDEM ASO methods, since the length of the DNA target determines the accessibility of the oligo attached on the surface of the 5 μm diameters QDEM. The length and the concentration of the amplicon potentially affect the renaturation of the PCR product in solution and the level of DNA saturation of the hybridisation mix (Armstrong *et al.*, 2000). M9 and M60 were also chosen regarding their content of base G/C (%GC) and the Tm of their respective allelic probes (Wetmur, 1991). Tm and %GC are the main parameters that influence the specificity and efficiency of hybridisation genotyping reactions. M60 presented a high Tm, associated with a high %GC, whereas M9 presented the inverse characteristics. The demonstration of a successful QDEM ASO genotyping assay with challenging allelic probes provided an initial proof of the performance of the method for future validation. The sequencing results were used to interpret the results observed with the genotyping assays.

The gradient PCR method is a technique that allows the empirical determination of an optimal annealing temperature using a minimum of experimental steps. This optimisation can often be achieved in one experiment (Preziozo and Jahns, 2000). The temperature-gradient (T-gradient) PCR method proved to be an efficient approach to optimise the specific amplification of loci M9 and M60. It accelerated the identification and selection of the PCR conditions that allowed the simultaneous amplification of both loci. M9, M60, and the beta-actin control gene were then amplified with the male and female DNA template, and with clean water. The absence of detection of PCR product formation with the female and water with the Y-SNPs illustrate the specificity of the primer design. The band at the expected size was observed with male template. The beta-actin products appeared on the gel at a position relatively higher compared with the size expected (116 bp). This

phenomenon was interpreted as a slower migration of the beta-actin products, compared with the other products analysed on the gel, due to the high yield of beta-actin PCR products that run through the gel. The housekeeping beta-actin gene showed a high efficiency of amplification, with a PCR product quantity higher than the SNP PCR product (on average, > 900 ng / μL). The high concentration of DNA from the beta-actin product could therefore restrain its migration through the matrix of the 3 % agarose gel, which could explain the electrophoretic results observed in Figure 5.3. The fluorescence detected in the initial wells, where the PCR products were loaded, illustrated the high quantity of DNA in the sample analysed. The fluorescence dots observed on the gel were due to these ethidium-bromide staining.

The sequence of the two SNPs M9 and M60 were verified by the sequencing of the PCR products obtained in singleplex with the male cell line ARPE19 (ATCC CRT-2302, VA, USA). By definition, the male template was haploid for the allele M9-G and M60-NoInsert. The sequencing was performed on the two DNA strands as a control experiment to confirm the sequencing results. With both M9 and M60 sequencing reactions, the genotype found with the first sequencing experiment was confirmed with the second one. These results also allowed the verification of the sequence of the amplicons in comparison with the theoretical sequence selected for the genotyping experiment (Appendix O and Q). The reproducibility of the amplification and sequencing reactions demonstrated the quality of the purified PCR products obtained with the PCR conditions adapted to the amplification of short amplicon (size range of 90-200bp).

The dot-blot hybridisation method is a rapid screening method which often employs allele-specific oligonucleotide probes to discriminate between alleles differing at a single nucleotide position. The specificity of the probes, designed for the identification of the Y-SNPs M9 and M60, were assessed with dot blot experiments. M9 and M60 positive dot blot showed a specific hybridisation of the allelic probes for their respective DNA target. These results were essential to demonstrate, in a second stage, the efficiency and specificity of the hybridisation of the QDEM ASO probes in a suspension assay.

Four QDEM-probes were produced with the optimised method of carbodiimide coupling of 10,000 QDEMs with amino active oligo developed in Chapter 3. The probes were first run through the flow cytometer to verify their specific fluorescent code by analysing the QDEM-probe recover at the end of the bioconjugation process. The regions defined with the initial control QDEM populations identified the stable QDEM-probe populations. A displacement (<< Log10) of the four QDEM bioconjugate populations was observed for the fluorescence detected in FL1 and FL2 (Figure 5.8). These modifications could be associated with the internal variation of the flow cytometer detectors, or with a low modification of the intensity emitted by the QDEMs due to the bioconjugation process.

An increase of the fluorescence intensity was detected in FL1 with 0QDEM bioconjugated to DNA probe in Chapter 3 (Figure 3.9). This modification of the fluorescence signal of the blank bead was related to the potential phenomenon of autofluorescence. Autofluorescence can be due to trace impurities of molecules that contain single or conjugated pi-bonding (such as aromatic molecules). These molecules can be produced by oxidation of impurities that were accumulated during manufacturing and storage of the bead materials. The adsorption of impurities, which can result in significant autofluorescence, could also be due to the storage and manipulation of the QDEMs in a buffer containing organic molecule such as BSA.

In this chapter, a decrease of the fluorescent signal was observed with the one and two colour encoded microsphere bioconjugates. This phenomenon was interpreted as a potential effect of the quenching of the bead fluorescence due to DNA and autofluorescence emission. Autofluorescence is a major contributor to the background signal in microarray experiments (Raghavachari *et al.*, 2003). This event has also been observed with bead-based assay, but has not been specifically investigated. The autofluorescence of polystyrene beads was reported to overlap with the dye detection of a ASO method for SNP detection (Russom *et al.*, 2004). Since the origin of autofluorescence has not been well studied and that there are various possible causes for this phenomenon, the conventional approach to reduce or eliminate it, is by chemical means (such as treatments with borohydride solutions

that reduce double bonds in conjugated systems) (Raghavachari *et al.*, 2003). The QDEMs being sensitive to chemicals treatments, this strategy could not be considered in this research. An effective analytical approach was therefore privileged to solve the issue of fluorescent code modification.

Initial regions were defined for each bioconjugate population separately, which allowed an efficient gating and a specific discrimination of the conjugated and hybridised populations in the genotyping assay. The gates identified the QDEM-probes that had conserved their initial fluorescent code. The modification of the fluorescent code of the QDEMs were therefore not significant (<< 10%) for all the 4 populations used in the experiment (Figure 5.8). The definition of a region for each QDEM-bioconjugate populations is an essential step for the later analysis of the hybridisation experiment, but also to be able to evaluate the impact of the hybridisation experiment on the code consistency and bead stability.

The gating process allowed the enumeration of the conserved QDEM populations at the end of the procedure. A low recovery of microspheres was calculated after the hybridisation in duplex experiment; between 30% and 50% of QDEMs exhibiting a fluorescent code similar to the initial population were detected simultaneously as the positive hybridisation signal. The QDEM material was found sensitive to bioconjugation and hybridisation procedure (Chapter 3, 4). The percentage of recovery after bioconjugation and hybridisation was lower than the average 75% bead recovery obtained after conjugation experiment only (Section 3.3.3). These results were expected since the instability of the QDEMs was shown to increase proportionally with the repeated number of treatments applied to the material (Chapter 2). The results obtained in this chapter were also in accordance with the 42% bead recovery observed during the hybridisation titration optimisation process in Chapter 4 (Section 4.4.3). The report of the bead loss during conjugation and hybridisation process has not been found in the literature. These results are essential to demonstrate the instability of the QDEM in aqueous solution, a major issue that need to be addressed and overcome if QDEMs have to become widely used for biomedical applications.

The QDEM-probes were then tested individually for their affinity with the DNA template. Hybridisation kinetics and thermodynamics affinities of the probes showed to be dependent on the SNP target concentration (Wetmur, 1991). To obtain a good signal of hybridisation with a good discrimination level it was important to determine the range of concentrations of the targeted DNA. The titration of M60 PCR product presumably presented a similar range of hybridisation signal for both M60 probes. M60-No insert demonstrated nevertheless a higher affinity for lower DNA quantity than M60-T probe. These results illustrated the different kinetics and thermodynamics of the probe hybridisation to the target. Since the genotype of the template was found haploid for the allele M60-NoInsert, the signal of hybridisation observed with M60-T revealed the levels of non specific bindings, ≤40 a.u., in singleplex hybridisation experiment for PCR product quantities superior to 60 fmol (Figure 5.6A).

Unlike M60 probes, the M9 probes presented a very different affinity for their targeted DNA. The probe M9G had a significantly higher hybridisation signal (three to four times higher) than the probe M9C. The optimum hybridisation signal was detected for PCR product quantities ranging from 60 to 150 fmol. M9 probes were designed with 13-15% lower %GC, 3 bp shorter oligo, 10-11°C Tm lower than the M60 probes (Table 5-4). A high content of G/C was shown to diminish the hybridisation signal, affecting the affinity of the oligo for their PCR targets (Armstrong *et al.*, 2000). Similarly, the effect of mismatch was greater on shorter oligo; unambiguous genotypes are typically obtained with 17 bp probes (Livshits and Mirzabekov, 1996b). The global lower affinity and specificity of the probe M60 in singleplex could therefore be explained by a less efficient *in silico* design of the probe sequences. The hybridisation signal intensities for haploid individual was similar with M60 (Figure 5.6) or different with M9 (Figure 5.6B), which illustrated similar binding affinities or high levels of non specific hybridisation.

The negative values calculated with the lowest and highest quantity of PCR products titrated with M60 and M9 probes corresponded to the fluorescent background and non specific hybridisation signal detected with the negative control (Figure 5.6). The hybridisation signal decreased with target quantities superior to the saturation point of the titration. The QDEM ASO assay involves the hybridisation of mobile DNA strands with mobile complementary DNA strands on a bead to form duplexes. The overall duplex formation rate is dependent on the rate of transport of the probe and the target in solution and on the kinetic of the hybridisation reaction (Gadgil *et al.*, 2004). Limited diffusion in solution has been reported to affect the DNA hybridisation (Armstrong *et al.*, 2000; Gadgil *et al.*, 2004). Chan *et al.* (1995) presented a model that correlates the DNA hybridisation rate with the diffusion constants, strand size, and the hybridisation probabilities per collision between the probes in a solution and a target attached to a solid surface. This model was developed for microarray hybridisation experiments. Considering that microspheres are a solid support, these considerations could also explain the inhibition of the hybridisation rate with the saturated mix solution. The probability of the QDEM-probe to encounter its target can be reduced due to the lower diffusion constant in the hybridisation solution, saturated with PCR products and QDEM-probes. High concentration of PCR products (> 100 fmol) can also increase the phenomenon of renaturation of the PCR products (previously heated to separate the DNA strands), which could limit the access of the QDEM-probes to their ssDNA. The potential hybridisation inhibition of DNA saturation and PCR product renaturation was avoided by using a quantity of targeted DNA inferior or equal to the saturation point of probe hybridisation in the duplex experiment.

A difference of hybridisation intensity was found between the singleplex and the duplex experiment. M60 and M9 probes reached a maximum of respectively ~50 and ~210 a.u. in singleplex compared with ~140 and ~180 a.u in duplex experiment. The variations of level of hybridisation intensities observed between single and duplex experiment for each probe can be due to variation in replicates and QDEM solution used for the conjugation. The modification of the final hybridisation volume in singleplex and duplex could also affect the DNA and QDEM-probes diffusion rate, facilitating or decreasing the formation of

duplexes. Singleplex titration experiment had a final concentration of 520 QDEM / µL compared with 320 for the duplex suspension array. The higher signal detected for M60-No insert in duplex appeared as a higher hybridisation efficiency of the probe for its target. It could be explained by more efficient duplex hybridisation mix than the singleplex, more advantageous to facilitate M60 probe efficiency of hybridisation (Armstrong *et al.*, 2000). The results of the probes titration illustrated some of the issues that can limit ASO SNP genotyping method, with different SNP loci having different hybridisation kinetics.

However, the allelic probe titration revealed a detection limit of ~32 fmol (Figure 4A,B). The method developed here showed a superior sensitivity in comparison with the average limit of detection of 37 fmol described by Horejsh *et al.* (2005) with a FC molecular beacon bead-based assay, and the 0.5 ng PCR products necessary to obtain the correct genotype of one SNP with a single base chain extension microsphere-based assay reported by Chen *et al.* (2000).

The determination of the DNA template genotypes for the Y-SNPs M60 and M9 was undertaken by signal-to-noise analyses. The higher relative hybridisation signals of the four signal-to-noise hybridisation (> 100 a.u.) only for the allele M9G and M60-. The average signal-to-noise for non specific hybridisation signal with the mismatch allelic-probes was ~6.5 (Figure 5.7) compared with a ratio ≥ 7 for Luminex bead-based assay applied to the detection of single-base changes in cystic fibrosis transmembrane conductance regulator gene (Dunbar and Jacobson, 2000). Non specific hybridisation signal contributing to the noise can vary upon probe sequence, mismatches (some less destabilising than other), and the flanking regions (Werntges *et al.*, 1986). The factors influencing the hybridisation detection limit include also: the detection method, the bead diameter, the carboxylation coverage, the coupling efficiency, the probe and target length, and the method to evaluate the sensitivity.

The assay developed here identified a male template as haploid for both alleles obtained with the sequencing experiments. The signal of non specific hybridisation, contributing to the noise, to other QDEM-probes was shown to vary upon probe sequence, mismatches, and flanking regions (Werntges *et al.*, 1986). The experiments conducted in this study represented an initial demonstration of the sensitivity and specificity of DNA detection using QDEM as fluorescent tag conjugated to short oligo probes. The development of a multiplex assay using multiple QDEM fluorescent codes, multiple SNP target, and computational data analysis is the next step in the development of the assay to demonstrate the potential of commercialised QDEMs in multiplex SNP genotyping experiments with potential application to forensic genotyping and/or molecular diagnostics.

Chapter 6

Final Discussion

6. FINAL DISCUSSION

The aim of this thesis was to develop a genotyping assay using quantum dot-encoded microsphere (QDEM) materials in order to demonstrate the potential of this technology for biological applications. The properties and reactivity of the technology for bead-based biological applications was first investigated (Chapter2). Then, the allele specific oligonucleotide (ASO) method was chosen to adapt QDEM technology to the genotyping of single nucleotide polymorphism in suspension format (Chapter 3,4,5).

Five main stages were identified in the development of the assay. The first stage involved the conception of optimised fluorescent probes specifically adapted to DNA marker detection. The second stage involved the development of molecular biological tools for an optimum application to SNPs genotyping. The targeted DNA markers, *i.e.,* single nucleotide polymorphisms (SNPs), were selected and oligos that amplified the targeted region, *i.e.,* the primers, were designed. Simultaneously, the oligonucleotides (oligos) identifying the targeted DNA markers, *i.e.,* the probes, were designed *in silico* to optimise the specificity of SNPs-DNA recognition. Thirdly, the optimisation of the fluorescent probe hybridisation to ssDNA in suspension was undertaken. In the last stage, QD-SA reporters were employed in the ASO assay for the specific identification of the selected SNPs hybridised to QDEM-probes. The targeted SNPs were amplified with biotinylated primers, hybridised with QDEMs-probe and QD-streptavidin bioconjugates were used to reveal the complex. Finally, the simultaneous detection of the QDEMs and the QDs signal indicated which allele had been hybridised. Hence, specific data analysis and flow cytometry (FC) protocols were developed for the simultaneous multiple fluorescent code detection. The work presented in this thesis can be illustrated by the schematic in Figure 6.1 representing the final QDEM ASO assay

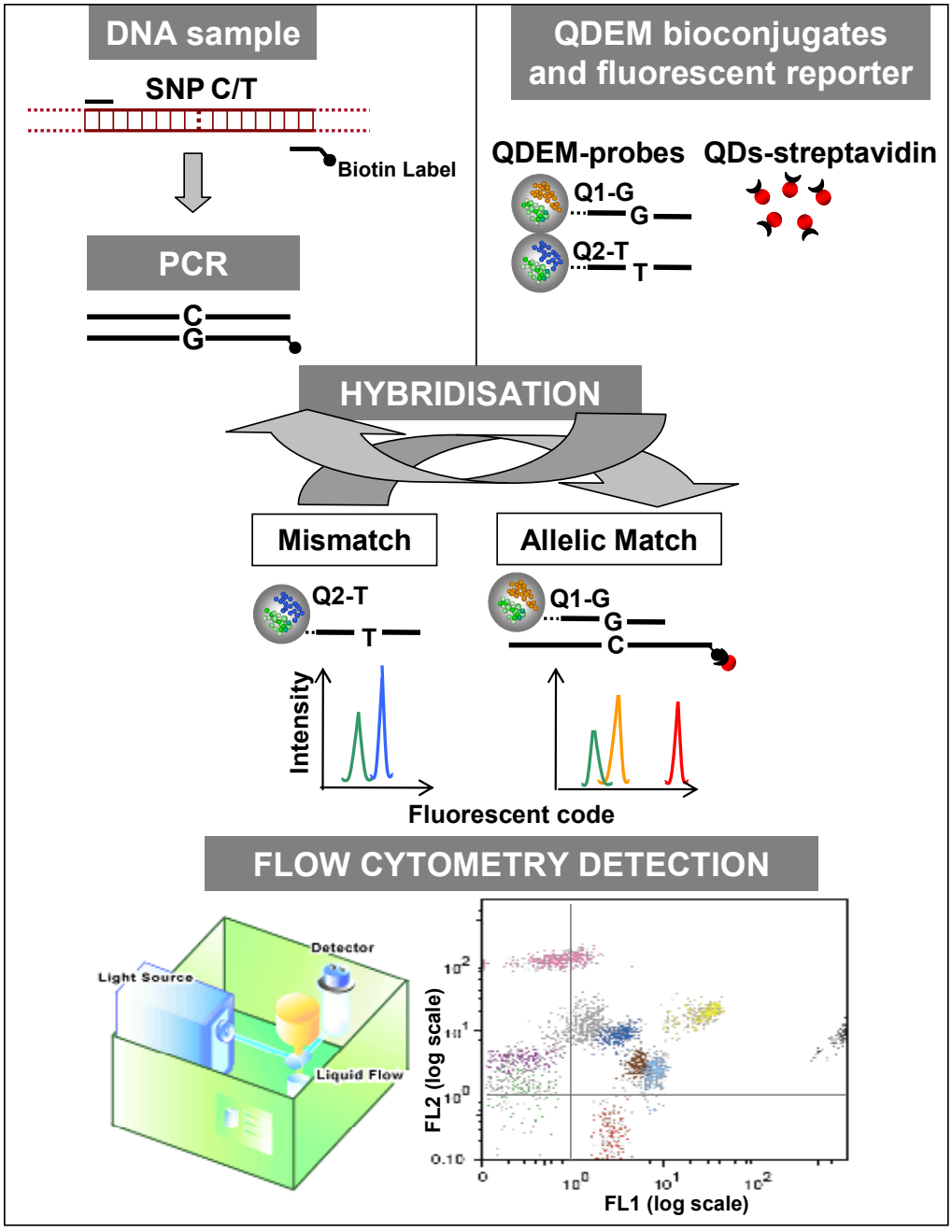

Figure 6.1 Schematic of the QDEM SNP ASO genotyping method.

SNP: single nucleotide polymorphism, G/C: guanine/cytosine nucleotide, PCR: polymerase chain reaction, QDEM: quantum dot encoded microsphere, QDs: quantum dots, FL1/FL2: the flow cytometer fluorescent detectors channel 1 and 2.

6.1. QDs and QD-doped particles technology for bioanalytical sciences

QDs offer unique advantages compared to conventional dyes because of their distinctive optical properties due to their composition and structural characteristics. QDs can be dispersed or dissolved in nearly any solvent and incorporated in a variety of inorganic and organic environment by bonding appropriate molecules to their surface (Sui *et al.*, 2003; Choi *et al.*, 2007). Their wide range of emission wavelengths (from 490 nm to 900 nm) allows multiplexed assays over a wide spectrum, with an improved signal-to-noise ratio. QD populations are excited using a single excitation source, simplifying the multiplex detection platform (Chan *et al.*, 2005). These properties have been used to embed microsphere structures (such as polystyrene or silica beads) with QDs to create QD-doped particles encoded in terms of intensity, corresponding to the quantity of each QD, and colours, defined by the wavelength emission of each QD population (Medintz *et al.*, 2005).

Because of QD properties, the QD-encoded microspheres present the following improvements over traditional fluorescent tag: (i) they are more photostable; (ii) they possess a greater extinction coefficient (probability of absorption or absorption efficiency) due to their ability to absorb more photons which implies a brighter signal for imaging; (iii) QD wide broad excitation source enables the emission of multiple colours in a same experiment with limited interferences between the excitation and emission source; (iv) the peak emission wavelength for a typical QD material is bell-shaped (Gaussian), very sharp, with narrow emission red tail, in contrast to organic dyes, which can facilitate the distinction of emission signals between different QD-encoded beads (Medintz *et al.*, 2005). Despite the advantageous properties demonstrated by the QDs and QD-encoded particles as molecular probes and the active research ongoing in this field, there is still a lack of extensive commercialised products and validated clinical applications of these materials for biological studies (Huo, 2007). Reports in the literature helped partially to identify the complex factors that potentially jeopardised the performance of the QD technology as a class of bioconjugates. The following paragraph discusses the relevance of some of theses factors in relation to the findings presented in this research project.

Nirmal *et al.* (1996) discovered that QDs suffer from an intermittent on-off emission under continuous excitation. Kuno *et al.* (2001) have investigated the kinetics of the "On"/"off" fluorescence intermittency or "blinking" of QD. Two modes of behaviour are distinguishable: (i) sustained "on" episodes of rapid laser absorption/fluorescence cycling, followed by (ii) sustained "off" episodes where essentially no light is emitted despite continuous laser excitation. The results of this study indicate the presence of distributed kinetics in the blinking phenomenon and the absence of unique rate for turning the QD on or off (Nirmal *et al.*, 1996; Kuno *et al.*, 2001). The exact origin of blinking is still not fully understood. This phenomenon is the first limitation of QD for some applications. Single QD signal might be missed by fluorescent detector if QD are "off" due to the blinking. However, the blinking of a certain portion of the QD population should not prevent the accurate detection of the global signal coming from thousand of identical replicated PCR products, each attached to the same unique fluorescent probe. In the case of the method developed here, the intensity of the signal for an experiment at a specific time could be modified, which would prevent quantitative interpretation of the results. These observations also applied to the fluorescent signature of QD-doped particles which is highly dependent on the QDs emission intensity (number of encoded QD in the bead). This phenomenon could therefore also modify the fluorescent signature of QDEMs during the bioassay.

The analysis of the fluorescent codes of the QDEM stock solutions, after limited resuspension treatments, is in accordance with the performance of the QDEM fluorescent properties stated earlier. QDEM fluorescent profiles of multicolour beads from control solutions (encoded with one, two, and four colours of QDs) showed highly specific emission profiles, which could be observed continuously in the flow stream of the flow cytometer without a decrease or modification of the emission intensities. The blinking effect described by Nirmal *et al.* (1996) was, thus, not observed when analysing different colour beads under flow cytometry (FC) and confocal microscopy (CM). The results obtained with the evaluation of the QDEM code consistency for the control population also confirmed these observations. Surfactants, capping groups or ligands (organic molecules, thiols being the most frequent ligands used) are usually chemically attached to the surface

of the nanocrystals to protect, to provide chemical functions, and to increase the stability of the material (Aldana *et al.*, 2001). The addition of the polystyrene matrix and the protective layer on the surface of the QDEMs could also contribute to the stability of the fluorescent emission of the QDs trapped inside the microspheres. Recent work demonstrates that bathing CdSe(ZnS) QDs in a solution of an antioxidant chemical used as a food additive apparently prevent the QD from blinking off (Fomento and Nesbitt, 2008). This discovery could further improve the fluorescent code stability of QDs and QDEMs.

Nevertheless, the instability of the fluorescent code of the QDEMs has been demonstrated due to environmental modifications. The specific evaluation of the materials in various conditions in the Chapter 2 of this thesis, along with the development of the ASO genotyping assay showed a decrease of the fluorescent code of the QDEMs under biological treatments. The observation of the instability of the QDEM materials in bioassay experimental conditions questioned the stability of the method used to dope the QDs in the polystyrene microspheres. Two distinguishable phenomena were observed when manipulating the Crystalplex QDEM encoded by the swelling procedure: (1) a significant decrease of fluorescence interpreted as a leach out of the QDs from the beads and (2) the disruption of the microsphere shell structure. Treatments (sonication frequency, vortex intensity, centrifugation time and speed), time exposure and the solvents used for microsphere suspension had a dramatic impact on QDEM stability in solution. QDEM stability was maximised during the conjugation reaction by the use of imidazole buffer, low-frequency of sonication, low speed vortexing, and medium-high speed centrifugation. The same drawback phenomenon described previously occurred when QDEM-probes were processed for the hybridisation experiments with oligos. A maximum of 50% of the initial QDEM bioconjugate population was detected by FC after one hour incubation at 49 °C in 6 X SSC hybridisation buffer (Figure 2.16). These results were confirmed by the observations of the physical disruption of QDEM shell structure under confocal microscopy (Figure 2.20, 2.21).

To date, the different synthesis methods presented in detail in the introduction (Section 1.2.2) have not proven to resolve the problems of instability encountered with the QD-doped particle technology. Six methods were reported: 1- swelling method (Gao and Nie, 2004); 2- layer-by-layer (LBL) strategy (Wang and Tan, 2006); 3- silica coating (Chan *et al.*, 2004); 4- modified suspension polymerisation method (Li *et al.*, 2005); 5- *in situ* encapsulation with chemical bound (Sheng *et al.*, 2006); 6- spray-dryness and thermal denaturation strategy (Chu *et al.*, 2006). Sheng *et al.* (2006) and Chan *et al.* (2004), initiators respectively of the fifth and third method reported without showing any data that their methods produced stable QD-doped particles under high-frequency sonication, solvent exchange and long term storage. The first and second methods, with QDs physically captured inside the polymer matrix but not chemically attached to it, were reported to produce instable materials under different chemical environment. QDs were described to leach out of the microsphere under certain conditions. These authors suggested that sonication and washes in polar or non-polar solvents could result in a loss of QDs form the microsphere due to the absence of chemically bound between the QDs and the polymer matrix of the bead (Chan *et al.*, 2004).

Shen's and Chan's groups were working with highly concentrated silica bead solutions which could indeed be more resistant to various external treatments, but which could also be increasingly challenging to work with in biomedical experiments (Chan *et al.*, 2004; Sheng *et al.*, 2006). Silica beads are more difficult to disperse in solution than polystyrene beads. Multiplexed bead-based bioassay requires a monodispersed concentrated bead solution, easy to quantify and to manipulate for effective and reproducible coupling procedure (Han *et al.*, 2001). Sathe *et al.* (2006) have produced silica microbeads embedded with QDs and iron oxide nanocrystals with magnetic separation properties. The capture of the microspheres facilitates bead washing steps, and general sample manipulation. It therefore reduces experimental time, and the expenses by avoiding other costly washing procedures (*i.e.,* filtration), and it also increases the encoded yield (Wilson *et al.*, 2007). QD-doped particle based on silica bead materials could therefore improve the stability of the materials in biological studies. The loss of half of the QDEM fluorescent

intensity and specific fluorescent signature during the suspension assay is a major limitation for the further development of the assay. For the ASO QDEM genotyping method to be cost-effective, quantitative and robust, the stability of the QDEM material requires to be improved. The specific and efficient analysis of multiple analyte in suspension relies on the recovery of a maximum of QDEM fluorescent probes at the end of the assay.

The properties of the QD technology (*i.e.,* QDs and QDEMs) are not only dependent on its stability but are also strongly dependent on the nanocrystals and microspheres sizes and compositions. The reproducibility of synthesis procedures remains a controversial topic in QD research. The variation in QDs technology size distribution from batch-to-batch under the same experimental conditions is often between 10 to 20% (Klostranec and Chan, 2006). The quality control of QD technology size distribution needs to improve to assure optical properties reproducibility and comparability for medical applications (Ozkan, 2004). As an example, QD size variation can generate false results with DNA sequencing using QD as fluorescent marker and capillary electrophoresis detection methods. The variation of QD size can mislead the migration of labelled analytes through the polymer network. QD-doped particles optical properties and size are also essential to assure the reproducibility of the bead fluorescent signature and the bioconjugation procedure. Since the bioconjugation is surface dependent, polydispersed solutions of QD-doped particles can alter the reproducibility of the conjugation efficiency, and therefore increase experimental variation. The reproducibility of QD and QD-doped particle synthesis procedures is a major concern that needs to be address before extensive research can be pursued for commercialised applications.

No significant variations were observed with the new Crystalplex (PA, USA) batches of QDEM solutions. On average, QDEM synthesis procedure appeared to be reproducible. However, the variable experimental error standards of the mean obtained during the bioassay treatments on a single batch could range from 2% to 30% (Chapter 2). These figures illustrated the sensitivity of the materials to treatments. The same range of

percentages was observed between replicates of the conjugation titration (Chapter 3). Working solutions started to show significantly higher variations between replicates when they had been used for multiple experiment. Repeated treatments on QDEM working solutions could alter their monodispersity and therefore impact on the experimental variation. The initial study on QDEM materials presented in this thesis showed how polydispersed bead solution due to experimental treatment could impact on bioconjugation reproducibility procedures (section 2.3 and section 3.3). To conclude, QDEM synthesis process showed a good batch-to-batch reproducibility, but with a poor robustness of the QDEM material.

The phenomenon of QDs leaching out of the microspheres described earlier is also a major concern in the development of QDEM bioassay, since the impact of QDs in solution on the experimentator manipulation and waste disposal has not yet been assessed. The potential risks on human health and the environment of the QD technology needs to be regarded as an important issue since this technology is becoming increasingly popular and generally widespread in other fields of research such as medicine, plastics, energy, and electronics. QDEM toxicity is directly dependent on the individual QD physiochemical characteristics encoded in the microspheres and from the environmental conditions applied to the bead. QD core composition, size, charge, concentration, outer coating (*i.e.,* capping material and functional groups), and oxidative, photolytic, and mechanical stability are factors participating to QD toxicity. The QDs chemical instability is mainly due to the photooxidation of the nanocrystal/ ligands complex. Studies reported that surface oxidation can occur under combined exposure to aqueous environments and UV-light excitation (Derfus *et al.*, 2004).

The release of QDs out of the polystyrene lattice implies the potential exposure of QD to photooxidation and therefore the release of cadmium ions in the case of CdSe-based QD, which is the main toxic threat. Cadmium and selenium have shown to cause severe and chronic toxicities in vertebrates. Hence, they present a high risks for human health and environment (Fan *et al.*, 2002; Henson and Chedrese, 2004; Satarug and Moore, 2004;

Satarug *et al.*, 2005). However, the inconsistency of the type of QDs used with variable QD dosage/exposure concentrations, participates to the divergence of reports on QD toxicity in the current literature. The injection of QDs in the bloodstream of living pigs and in mice up to four months did not show any toxic effect (Larson *et al.*, 2003; Ballou *et al.*, 2004; Hoshino *et al.*, 2004). Similarly, QD toxicity was not detected in cells loaded with QDs and grown for two weeks (Kim *et al.*, 2004). These studies were performed by nanotechnology researchers and not toxicologists or health scientist. A lack of specific QD toxicology-based studies, such as dose, duration, frequency of exposure, mechanism of action study, has been reported in the literature (Hardman, 2006). Research on QD synthesis tries to reduce its inherent toxicity by adding large band-gap-semiconductor, protein, or different type of cocapping agent (Derfus *et al.*, 2004; Hardman, 2006). Byrne *et al.* (2007) demonstrated that a gelatin polymer interacting with the cadmium precursors improves stability and reduces the toxic effects of QDs once incubated in the presence of human cells (Byrne *et al.*, 2007). The potential cytotoxicity of QD materials requires to be addressed before a potential use of QDEMs for routine and *in* vivo applications (drug carrier or imaging). The impact of QDs and QDEMs on human health, their long-term effect on the host organism's health, is a controversial issue. Risk assessments for laboratory practise and standardised guidelines for waste disposal are some of the topics that need to be rapidly addressed if QDEMs are to be used in routine laboratory work.

The other effect of the QD's photochemical instability due to ligands photocatalytic oxidation, is the modification of their optical properties and the their precipitation and aggregation in aqueous environment (Jaiswal *et al.*, 2004). The colloidal nature of QDs in aqueous environments makes them susceptible to irreversible aggregation depending on pH environment changes, heating, long term storage, or even freezing. Agglomeration in larger clusters illustrates one of the major difficulties when working with QDs for biological applications. Moreover, hydrophilic modifications on QD shell decrease both the stability and the quantum yield due to the sensitivity of QD structure and fluorescence to environmental factors such as pH, salts and oxidation (Jyoti and Sanford, 2005).

The clustering of QDs could have a negative impact on the uniform distribution of the QD-streptavidin reporter used in the ASO method. It could lead to use more reporter than needed to obtain a significant detection signal because of the lack of accessibility of the QD-SA streptavidin functionalities, due to the clustering of the QD reporters in solution. Furthermore, the genotyping of multiple SNPs in the QDEM ASO method should require higher concentration of QDs reporter, potentially increasing the clusterisation effect. The treatment applied to the QD bioconjugates during the assay could also impact on their long term stability. QD-SA were used at the end of the research project for the development of the last stage. Since QD-SA are widely used and commercialised, the material was not investigated for its stability. QD-SA have been used by Eastman *et al.* (2006) in a DNA biotinylated recognition assay; no data were reported on the effect of the specific DNA hybridisation condition on the material. To finalise the optimisation of the QDEM ASO method in single- and multi-plex, the evaluation of the efficiency of the QD-SA would need to be further investigated. The results in Chapter 2 showed that repeated sonication and vortexing treatment applied to QDEMs solution had a dramatic impact on their structural stability, fluorescent profile, but also on their long term use efficiency. The agglomeration of QDs and QDEMs implies the use of resuspension methods to obtain a homogeneous distribution of the materials in solution. The clustering of QDEM in solution and their instability in buffers and experimental conditions is a main drawback for the technology to be applied to suspension biological application.

It has been established that the spectroscopic properties of fluorophores are sensitive to their microenvironment (Resch-Genger *et al.*, 2008). Typically, since conjugated molecules are a relevant factor of the microenvironment, they affect the spectral position, the lifetime, the intensity of absorption and emission of organic dye, and mainly the fluorescent quantum yield and behaviour of QDEMs (Chapter 1). The bioconjugation usually leads to a decline of the fluorescence quantum yield for both types of dyes which is mainly dependent on the oligo length, the length of the spacer, the type of nucleotides in close proximity to the dye surface (Resch-Genger *et al.*, 2008). However, a limited number of systematic studies have examined the effect of the microenvironment on QD spectral properties, and

no study was found on the effect of bioconjugation on QD-doped particle spectroscopic properties. The observations made on the bioconjugate populations synthesised with the method developed in this thesis showed a modification of the fluorescent code of the QDEMs after attachment of oligos to their surface (Figure 3.9 and Figure 3.10). The fluorescent code variations due to bioconjugation need to be addressed in multiplexed bead-based flow cytometric assay. Fluorescent code modifications potentially decrease the fluorescent spacing between QDEM populations or misplace the fluorescent signature of a population. It therefore potentially increases fluorescent signature overlaps which lead to an increase likelihood of QDEM population misclassification and the contamination of an analyte signal with another QDEM population. This phenomenon could thereby be a source of error for QDEM population identification and quantification. The term "encroaching population" was defined by Yang *et al.* (2007) to designate bead population whose fluorescent signature overlap another population, and/or whose analyte they are attached to, will be associated to another bead population. The results of the four-plex QDEM genotyping assay showed that a reliable population gating method provided a highly specific signal-to-noise ratio of the analyte identification (section 5.4). These results could illustrate that bead encroachment did not affect significantly the analyte signal.

However, the modification of the optical characteristics and properties of the QDEMs introduced by the bioconjugation process is believed to have an impact on the multiplex application of the QDEM technology. The increasing number of fluorescent code and the increasing complexity of the encoding with different QDs at different intensities require a systematic study to determine the impact of bead encroachment on the sensitivity and specificity of the analyte identification in multiplex assays.

Eastman *et al.* (2006), demonstrated that a 100 complex mixed of QDEM could be analysed through a special scanner, designed specifically for the QDEM reading (the Mosaic Q1000 scanner, Quantum Dot corp., CA, USA). As previously described in Chapter 1, the Luminex platform reaches also a maximum of 100 detection codes adapted to a specific fluorescent device, the Luminex 100 (SP1 software, version 1.7.69; Luminex Corp.) or the

Bio-Rad Bio-Plex (Bio-Rad's version of the identical Luminex 100 flow cytometer) using the Bio-Plex Manager software 2.0. Each system integrates lasers, optics, fluidics, electronics, and signal processing to identify each set of fluorescent-coded microspheres and measure the total fluorescence at the surface of each microsphere to quantify the amount of reporter bound to it.

QDEMs have not yet been proved to be able to reach this level of high throughput using a common FC instrument. The approaches for the identification of individual QDEM from FC data are limited. Some studies have relied on traditional FC dot plot; others have modified FC instrumentation to include a spectrometer to be able to get distinctive fluorescent signals (Meissner *et al.*, 2003; Ma *et al.*, 2007). A maximum of 10 QDEM codes was successfully used for DNA genotyping in a single experiment to date (Xu *et al.*, 2003) with conventional dot plot FC analysis. Meissner *et al.* (2003) have reported the use of flow cytometers for high speed read-out of single-colour QD-tagged microsphere with DNA probes for DNA hybridisation. They also show the read-out of a two-colour bead and propose flow cytometer instrumentation as an optional efficient technique to perform the high speed readout of fluid-based microarrays.

The identification of QDEMs reported in this thesis was easily and rapidly achieved by histogram analysis using free conventional FC softwares available (*e.g.,* MdFI, FloJo) with 15 different QDEM fluorescent codes. These softwares are however not adapted for high throughput experiments. The results of the read-out investigation of 21 different QDEMs (of one-, two-, and four-colour beads) in a single experiment presented in Chapter 2, showed that manual analysis of multiplex fluorescent codes could be time consuming, required large quantity of QDEMs for analysis, and could limit the number of fluorescent codes to be analysed in a single tubes. The modification of the FC equipment describe previously, to facilitate QDEMs identification ends up devaluating the QDEM genotyping method by increasing the costs involved. Hence, a computational approach would be undoubtedly advantageous, and would allow the simultaneous analysis of a multiple number of unique QDEM codes using standard FC instrumentations available. A study has

been undertaken simultaneously to this project of research to evaluate statistical methods as a support for the detection of sixteen different QDEMs using the same standard FC instruments used in this report (Clarke *et al.*, 2005). This research project aimed to develop a software (The NanoSNP software) compatible with basic office computer, and which offer the automated identification of QDEMs fluorescent code from FC data. Further work is still needed to prove the validity of the model at a high throughput level.

Spectral broadening, leakage of QDs out of the microbeads, energy transfer between QDs or between QDs and fluorescent tag attached on the QD or on the QD-doped particle surface, aggregation, and structural sensitivity to reagents and mechanical forces are some of the pitfalls that limit the applications of QD technology to bioassays. The challenges of the QD technology presented here need to be addressed in order to expect a wide application of QDs and QD-doped particles in biological studies. The limited availability of commercialised QD material restrains their accessibility for research. The restricted chemical and structural information provided by the distributors also prevents from conducting reliable and comparable fluorescence measurements. These comparative studies are required to show the reproducibility of fluorescent label physicochemical properties and for the development of standard evaluation methods. The lack of structural information therefore holds back the non biased and scientific evaluation of the different strategies of synthesis, which are still controversial. Further, the absence of specific studies on the structural and optical stability of different types of QDEMs in biological experimental condition is a major issue for the development of QDEM bioassays.

The swelling method was the first historical method developed to produce QD-doped particles, and the first method to be used to proof the utility of the materials for the identification of multiplex analytes (Han *et al.*, 2001; Xu *et al.*, 2003; Eastman *et al.*, 2006). The study of QD-doped particles commercially available and synthesised with this method, which is presented in this thesis, is therefore a valuable contribution to the development of a standardised use of this material (Crystalplex, PA, USA). This report also described the first successful simultaneous specific identification of 21 different QDEM

populations, encoded with one to four different QDs at different intensities, using a conventional flow cytometer instruments and simple analytical tools. These results are a promising step in the demonstration of the high throughput potential of the QDEM technology.

However, the initial set-up cost for instrumentation could be a limitation of the QDEM method to be amenable to high throughput (Chapter 1). The QDEM SNP detection platform needs a flow cytometer, with at least four colour detections. A basic fluorescent detection machine is believed to able to reach great multiplex capabilities thanks to QD fluorescent specificity. The other fundamental instrumentation required in the platform is a PCR machine, which is also a common lab instrument, useful for other types of experimentation. Regarding reagents and molecular material, the type and number of oligos (oligo modified or not) also affect the cost per genotype. The method developed here requires four relatively simple oligo structures: two primers (one biotinylated) for SNP amplification of 18-20 bp and two probes for allele detection of 21-25bp with a 6 carbon spacer and an amine modification. Other popular genotyping technology can require a superior number of oligos (Figure 1.18 and Figure 1.20), or more complex and longer oligo structures which increase the methods' running costs such as bead-based SBE assay (Hsu *et al.*, 2001) and the SNPlex™ genotyping system workflow using OLA (Ballester *et al.*, 2007). Furthermore, the extra cost incurred by the reagents of the QDEM ASO method (*i.e.*, QD-streptavidin conjugate, QDEMs, modified probes) is expected to be competitive, in comparison with the other reagents such as dye terminators, molecular beacons or Taqman™ probes (£ 115- £ 230) required for commercialised genotyping methods. In addition, the QDEM assay does not require additional expensive step of purification or specific reagents to modify oligo backbone (in order to facilitate the purification, separation of PCR or extension products) (Chen and Sullivan, 2003). QDEM genotyping method is not yet the most cost-effective strategy for SNP genotyping, but it promises to offer considerable end-use benefits. The starting set-up and fixed costs per sample genotyped may initially appear to be higher than other technologies because QDEMs and QDs are new materials on the fluorescent label market and are still more expensive than classic dyes. However, to compensate this limitation, research

facilities have the possibility to acquire the knowledge of QD-doped particle synthesis. The development of their own QDEMs library would reduce asset-up costs over a long term of use. Furthermore, the high flexibility of the technology can reduce the cost per genotype since the same QDEM code can be re-used and combined to different SNP allelic probes. The methodology presents practical flexibility as it is *a priori* adaptable to other biological applications (such as autosomal or mtDNA SNP genotyping, immunodetection, *in vivo* imaging). QDEM technology possesses many advantages as potentially preferred fluorescent markers for screening genotyping assay.

6.2. Critical assessment of the methodological and analytical approaches

Flow cytometers are one of the less costly instruments of the genotyping platforms. They are commonly used in university laboratories, medical schools, industrial research facilities and hospitals as they are widely used for immunology, pathology, and clinical research (Simmer, 2008). The development of standardised and unbiased calibration and validation protocol for FC systems for the detection of QDEMs is needed to be able to compare the efficiency of different methodology and their reproducibility. This issue was addressed for confocal spectral imaging microscope systems (CSI), which is why CSI was chosen as an additional and comparative method in this report (Zucker *et al.*, 2007). FC and confocal microscopy were used to characterise QDEMs materials and to develop a suspension bead-based assay for DNA genotyping.

Fluorescent microscopy techniques identify the source location and topography of the fluorescent signature of the analyte under observation. Confocal microscopy proved to be useful to characterise the fluorescence and the structure of the materials and to evaluate QDEM-non specific fluorescent (section 2.3.2 and section 3.3.2). CSI provided the visualisation of the QD distribution within the sphere and the attachment of the fluorescent probes to its surface. It also showed the effect of the biological treatments on the QDEMs'

fluorescent and structural properties (section 2.3.4 and section 3.3.3). The results obtained with confocal microscopy in the different chapter of the thesis not only described the fluorescent profile of the QDEM materials but also successfully identified bioconjugate samples, fluorescent interference and/or inhibition as well as structural modifications. Finally, four different level of intensity 575QDEMs (emitting at 575 nm, Appendix A) were specifically identified with CSI, which illustrate the power and utility of this analytical tool for QDEM investigation.

FC identifies multiple fluorescence signatures, namely the multiple excitation and emission wavelengths of an analyte, with a fluorescence address location. FC detection method has the advantage to provide data that are convertible into numerical form by specific software publicly available for manipulation and storage. The FC standard file (or fcs file) provides a uniform file format that allows data analysis between different scientific platforms with the same different software (Seamer *et al.*, 1997). This flexibility and the free access of most FC software codes is a main advantage for the development of new standardised software for QDEM multiplex analysis.

The graphical interface of the representation of the data allows the physical observation of each event that flow through the detector channels of the instrument. Therefore, regions that determine an area of interest on a graph can be selected. Regions permit to isolate the cluster(s) of interest and gates, defined as one or more regions combined using Boolean (logic) operators (AND, NOT, OR), are used to compute statistics, to characterise the subsets of events selected, to get rid of the background noise, and to save space in the data storage. Clarke *et al.* (under revision) described the discrimination of multicolour QDEMs with the use of a supervised learning algorithm, support vector machines (SVMs), which accurately and automatically identify individual QDEM using a standard FC system. Multiparameter detection capabilities, speed, accuracy and sensitivity of flow cytometers have extended their area of applications while reducing the size and cost of the instruments thanks to improved lasers, optical devices and softwares (Bonetta, 2005). FC instrumentation and data analysis are a dynamic area of research. Current and future developments include: the improvement of

the sensitivity and the specificity of the detection parameters, the increased number of detectors (16-parameters, 13-colour for each particles, Partec, Münster, Germany), the higher flow speed with high throughput detections, and the miniaturisation of the instruments.

FC is thus an advantageous instrument for the development of QDEM suspension array technology (SAT). The main property of the QDEM suspension array is its flexibility and cost efficiency to create customised assays unlike solid microarray (Bonetta, 2005). Planar array, with fixed fluorescent address system for each individual analyte, allows the screening of large segments of the genome for single nucleotide polymorphism identification, but are not adapted for the screening of a large number of samples. Measurements on flat microarray present a low serial analysis rate. Each array represents a replicate for the different elements spotted on the array (100 to 1000 elements per square centimetre), and the scanning of a single array can take several minutes. Therefore, the analysis of series of microarrays is time consuming. In suspension array, each element in the array has a specific fluorescent signature and is represented by hundreds of microspheres of the same type. Each FC measurement of the same microsphere population is a replicate of an element of the array. FC platform can have a flow rate reaching 10,000 particles per second and automated sample handling. As a conclusion, flow cytometer equipped with automated sample delivery systems and adapted to multiwell plates present essential advantages over flat microarrays for high throughput analysis (Edwards *et al.*, 2004).

Another advantage of choosing FC instrumentation to demonstrate the potential of the QDEM technology in suspension is the quantitative analysis properties of FC technology. Quantitative FC offers the possibility to standardise protocols and practice between instruments but also between fluorescent bead technologies using the same type of equipment (Zenger *et al.*, 1998). Standard fluorescent calibration beads are used to calculate the quantity of fluorescent-tagged ligands (such as oligos, or proteins) on the particles (*e.g.,* cells, dye beads, QDEMs). Genotyping method efficiency can thus be evaluated and compared between laboratories and quality control can be performed for FC clinical applications. The recent development of QD calibration beads for quantitative assays with FC as a promising step in

the development of quantitative assay using QD as a fluorescent reporter (Wu *et al.*, 2007). QD-based beads have unique advantage over conventional calibration dyed-beads or molecule of soluble fluorophore beads (MEF). First, because MEF beads use organic fluorophore, the quantification of more than one fluorescent signal in a single experiment is highly limited by the spectral overlap of organic dyes, whereas QD-based calibration beads allow multiplex quantification detections because of their unique spectral properties described earlier (Chapter 1). Secondly, QD-based beads is a flexible technology since all QD can be streptavidin functionalised, synthesis procedures are identical and the procedure of synthesis and analysis demonstrated by Wu *et al.* (2007) can easily be applied to multiple calibration beads. The flexibility of the technology promises to facilitate the production of QD calibration beads adapted to specific experimental needs. Smith *et al.* (2008) developed a calibration method, based on QD fluorescent molecules, which extend the quantitative capabilities of FC for which no reliable calibration standards currently exists.

The choice of QD streptavidin bioconjugate as a reporter dye in this research project aimed to develop the QDEM genotyping method using only inorganic fluorophore to demonstrate the potential of this technology but also to implement knowledge on experimental assay using QD streptavidin bioconjugates as fluorescent tag in bead-based suspension array technology (SAT). The development of an allele-specific detection assay using QDEM as fluorescent bead and QD as reporter bioconjugate offers the promise for future development in high throughput format and multiple quantification experiments. The high specificity and efficiency of the QD reporter signals could guarantee the identification of the specific reporter signal when the number of fluorescent codes used in the assay increases in number and complexity, and could potentially provide allele quantification by using multiple specific reporter QD bioconjugates.

Suspension array using bead-based technology improves analytical performances and shows high flexibility for many assays with rapid analysis, high throughput, and robust quality control parameters. Several approaches have been developed to optimise the attachment of biomolecule on fluorescent beads in suspension format and FC detection (Nolan and Sklar,

2002). A limited number of studies though have quantitatively assessed the specific bioconjugation of oligos to QD-doped particles. The results in Chapter 3 present the quantitative evaluation of the bioconjugation efficiency with QDEM materials.

A similar experimental scheme was used for the conjugation and the hybridisation optimisation in the development of the QDEM ASO assay. Modified-oligos covalently linked to an organic fluorophore, the cyanine 3, were used to evaluate and quantify the conjugation efficiency and the hybridisation detection sensitivity (Figure 3.3 and Figure 4.3). Cyanine 3 fluorophore was chosen since it allowed the use of conventional calibration kit to quantify the fluorescence, its emission spectra did not overlap with the spectra of the beads selected to perform the optimisation, and for cost efficiency concern. Fluorescent energy transfer (FRET) had been described between 525 nm QDs and the Cy3 fluorophores covalently attached through a construct with distances separating both materials within a range of 5 to 10 nm. Clapp *et al.* (2004) showed that 525QDs and Cy3 probes excitation and emission spectra and the high level of functionalisation of Cy3 probes could potentially facilitate the FRET interactions. The changes observed in fluorescent detection with high functionalisation of Cy3-oligo on QDEM during conjugation and hybridisation experiments were mainly interpreted as fluorescent and physical saturation since the distance between QDs and Cy3 was theoretically calculated inadequate to allow FRET interactions. The results presented in chapter 3 and 4 highlighted that the distance between Cy3-oligo and QDs in the microsphere structure could vary depending on the QDs repartition inside the sphere and depending on the treatments applied to the QDEMs. These observations could thus put into question the role of FRET on the fluorescence quenching observed with high concentration of Cy3-oligo on the bead surface.

The quantification of the fluorescent labels changes in fluorescence intensity when they bind surfaces is difficult and other approaches are generally used to study the influence of binding events and of the solid surface on the label fluorescent emission (Tirri *et al.*, 2006). Changes in fluorescent lifetime reliably indicate the presence of dynamic quenching, energy transfer or other de-excitation processes. Tirri *et al.* (2006) studied the influence of

the binding of labelled protein conjugates, directly or few nanometre distant form the bead surface, to microsphere surface in a bead-based assay system under two-photon excitation. The changes in fluorescence lifetime of the labelled protein were recorded simultaneously as the polystyrene microsphere emission. The results detected fluorophore self-quenching of the label and label quenching by the polystyrene surface. These results could then explain the changes in fluorescence intensity observed in the conjugation and optimisation study with high QDEM Cy3 functionalisation. Typical immunoassay sandwich are already sufficient to overcome the surface-induced quenching in fluorescence detection. The effect of the surface can be avoided by increasing the distance between surface and label. This study answers one of the interrogations about the bio-affinity binding events and the bead surface quantitative impacts on the fluorescence of the label. On the solid support side, the study of the fluorescent life time of the QDEM emission would contribute to investigate the effect of the bio-affinity binding events on the QDEM fluorescence.

The saturation of the QDEM surface with oligos, illustrated by the decrease of the Cy3 fluorescence detected after bioconjugation with large oligo quantities, was also related to the instrumentation detection limit and the binding sites and steric saturation on the bead surface. These effects can be a limitation to the QDEM-probe efficiency. A highly functionalised QDEM bioconjugate does not assure of the efficiency of the hybridisation with its targeted single strand DNA. On the contrary, beads saturated with probes could prevent the successful recognition of the targeted DNA sequence (Section 3.4 and section 5.4). Therefore the quantification of the bioconjugation process was essential to assess the saturation point of the QDEM bioconjugates to select an optimum oligo quantity that would avoid this drawback. The bioconjugation methodology developed in this thesis was specifically adapted to the QDEM technology and provided the first optimisation of a QDEM-oligo probe. To further validate this approach, the methodology should be applied with QDEM of different sizes (20 µm, 12 µm diameter, and customised particle sizes are currently available). The application of the method to other types of QD-encoded particle would be a first step to compare and develop standardised method of bioconjugation adapted to QDs-doped microspheres.

Traditional approach to optimise hybridisation and buffer involved testing one-factor-at-a-time experiments. The quantity of the oligo or the value of a hybridisation conditions (time, temperature) are varied while the other components and conditions are held constant. The time, consumable and energy consumption of this methodology is extremely high. Running batch experiment for the optimisation of each condition implied months of experimental work and millions of QDEM and molar quantity of fluorescent oligos, both costly reagents. Even considering that all the one-factor-at-a-time experiments were completed, this approach would omit to test the combined effects of the different experimental conditions used and therefore it would miss the influences of their interactions in the optimisation process. A novel approach was investigated to identify optimum hybridisation conditions that applied to the particular QDEM material for hybridisation suspension assay (Chapter 4). The introductory part of this work presented in Chapter 4 identified four factors (*i.e.,* incubation time and temperature, oligo quantity, and hybridisation buffer) which played a major role in the optimisation of the QDEM hybridisation process. QDEM hybridisation was also highly dependent on the stability of the materials (Chapter 2).

The multivariate design of experiments (DOE) was a most valuable approach since it consumed less time, effort and resources than one-factor-at-a-time procedures. DOE provided also a large amount of information while minimising the number of experimental work (Noordam and Repping, 2006; Drago *et al.*, 2008; Ryan *et al.*, 2009). DOE method was applied to QDEM suspension array hybridisation optimisation procedure. RSM using central composite design (CCD) enabled to produce surface plot responses that helped to understand the variation of the responses in relation with the variation of the conditions studied (Didier *et al.*, 2007). As a drawback, RSM did not allow the use of non parametric variables, in our case the buffer solutions, for the design of experiments. Screening design could have been used to determine which of potentially many factors (time, temperature, concentration, buffers, vortex, sonication and so forth) had the greatest impact on the hybridisation responses. Screening elicits information from the experimentator about the goals of the experiment but provides a list of suitable designs (including necessary number of run and replicates). However, the RSM approach was used instead of the screening

experiments approach to test the efficiency of hybridisation buffers (Chapter 3). As the study undertaken in this thesis was time limited and aimed to evaluate the DOE for bioassay, it was decided to test one type of DOE under various conditions. The RSM with different buffers also helped to better understand the influence of the ranges of the other factors on the optimisation hybridisation process and on the RSM results. The results obtained in Chapter 4 and represented with the response plots validated the approach chosen. If the hybridisation signal continued to increase at one edges of the response surface design space, it would have indicated that the optimum probably lied outside the ranges of time and temperature tested in this experiment. The test of hybridisation buffer separately with RSM produced curves around the optima, which indicated the hybridisation signal or the percentage of events sensitivity to one or more experimental factors (time, temperature, oligo quantity). The application of the DOE to QDEM-probes hybridisation experiments was demonstrated, and showed its potential as a useful tool for the optimisation of complex biological protocol. The generalisation of the use of DOE should help to improve the optimisation of complex biological studies and to produce efficient protocols in short time.

The titration experiment with fluorescent hybridised probe was an important link between the QDEM-DNA coupling chemistry and the potential biological assay for which the platform was proposed. It was also a necessary step to evaluate the DOE approach. However, although the titration experiment showed the sensitivity and dynamic range of the hybridisation, biologically-relevant control probes to be titrated in the same way could have been included to provide more background noise information; in particular, the titration of a labelled probe with very little homology to the conjugated sequence, as well as the titration of a labelled probe with closer but inexact sequence homology (perhaps differing by a fixed set of base mismatches, mimicking SNP variations to the conjugated oligo). Such comparative titrations would extend the biological contribution of the work presented here and its potential application.

The principles of the genotyping approaches and commercialised platforms available were presented in detail in the introductory part of the thesis (Section 1.3). Some of the limitations and advantages of the SNP genotyping technologies were also presented (Section 1.3.3).

From these techniques, a majority of laboratories employ minisequencing, and especially the SNaPshot assay. An automated capillary electrophoresis sequencer analyses both SNP and STR assays, which optimises the instrumentation set-up costs. Minisequencing with Mass Spectrometry (MS) detection is also very popular for its high sensitivity, time efficiency, allele quantification, and mixture analysis application (Sobrino *et al.*, 2005). However, if the detection platform is not used for other throughput applications such as proteomics and metabolite identifications, the initial instrument and setup costs are then a major investment for laboratories. Moreover, the throughput of the method is highly dependent on the purity of multiplex PCR product which adds steps to the sample handling for PCR and minisequencing reaction. FRET methodologies (such as lightcycler, taqman, and molecular beacons) amplify and discriminate a limited number SNP alleles simultaneously. This technology is more adapted for validation of SNP candidates and for building DNA databases, than for SNP human identification casework analysis. Pyrosequencing™ also shows multiplex limitation whereas it has a high level of automation and presents the main advantage of quantifying the contribution of each SNP allele. The OLA methods exhibit high rates of efficiency, and necessitate genomic DNA template which is an important advantage when enough DNA template is provided. It saves time experiment and experimentator input. However, working with genomic DNA is a major issue when templates contain very low levels of DNA material (*e.g.,* forensics biological evidence, ancient DNA) (Chen and Sullivan, 2003). All the OLA reagents can be pooled together which minimises handwork and allow automation, but increases the difficulties of multiplex genotyping. A unique technology can hardly fit all the requirements involved in DNA markers genotyping. By definition genotyping experiments can have different particular technical aims, which involve specific criteria of analysis for different biological application objectives.

The protocol, the cost and the throughput of a SNP genotyping method depend on the mechanism for allele discrimination. However, the overall accuracy and specificity of a method also depend on its amplification strategy and detection format. The allele specific oligo hybridisation assay was chosen over other allele-specific genotyping method because it was identified as the most adapted technique for QDEM technology. The simplicity of the approach, its adaptability to high throughput and allele quantification, and the efficiency of time experiment were the main advantages of the method to demonstrate the adaptability of QDEMs to efficient DNA genotyping. Regarding the protocol, the QDEM ASO mechanism does not interfere with the target amplification step which implies that both steps can be combined and undertaken in parallel. This single-step procedure performed in a close tube simplifies the protocol and allows automation, which eventually enhances the speed of the assay. Figure 6.2 illustrates how QDEM ASO method fits both crucial challenges of high throughput genotyping assays. QDEM technology in association with ASO genotyping method displays *a priori* the criteria expected for the analysis of a large number of SNPs within a large number of samples: flexibility, high throughput, cost efficiency, automation.

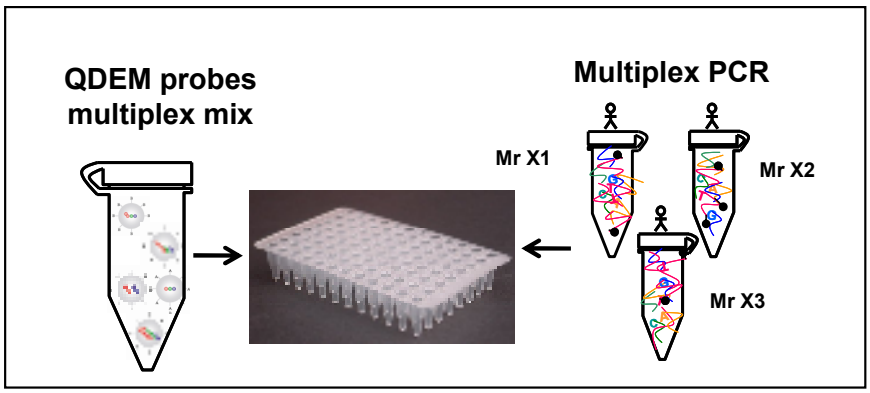

Figure 6.2 Multiplex bead detection of multiple DNA targets.

Multiple QDEM detection of multiple DNA target: A pool of analyte-specific oligo attached to QDEM are hybridised with SNP sequence amplified by polymerase chain reaction, in a single well, in a homogeneous format. Mr X: samples to be tested.

The limitations of the method are likely to come from the instrumentation detection capabilities, steric interference in a homogeneous format reaction, and multiplex fluorescent code identification.

The ASO strategy presented some limitations, mainly due to the hybridisation steps. The discrimination power of allele-specific hybridisation has been reported as relatively low compared to other methods like ligation (Chen and Sullivan, 2003). As described before, the optimisation of allele-specific hybridisation to a specific target in a complex mixture is a challenging process, which depends on the length and sequence of the probe, the location of the SNP in the probe, and the hybridisation conditions (Chapter 4) (Kim and Misra, 2007). Allele-specific hybridisation was not described as an optimal assay for bead-based genotyping. Authors agree to recommend the use of single base extension (SBE) or some form of oligo ligation assay (OLA). Nevertheless, ASO genotyping assay was chosen mainly because it involves a minimum of steps compared to other bead-based assays for the genotyping of ssDNA. QD-doped particles were shown to be unstable in aqueous environment according to a limited number of studies in the literature. Preliminary experiments performed on QDEMs (Crystalplex, USA) in the first stage of this research project had confirmed these observations. SBE or OLA assays require higher temperature and an increased number of washing and hybridisation steps than an ASO assay. As a consequence, SBE and OLA assays had the potential to significantly increase the instability of the QDEM material. We therefore considered that these assays were not adapted for the development of a genotyping method which employs QDEMs, the technology being insufficiently stable at the time of writing. QDEM stability was specifically tested for ASO experimental conditions and the assay developed aimed to limit the impact of the procedure on the QDEM material. This initial work with ASO method offers the possibility to later develop the QDEM technology for modified-ASO described in the literature, which have shown higher genotyping specificities (Howell *et al.*, 1999; Matsuzaki *et al.*, 2004). As an example, the use of multiple probes differing at a single position to analyse each SNP has shown to increase genotyping accuracy (Armstrong *et al.*, 2000; Cutler *et al.*, 2001).

SNP genotyping technologies have been rapidly developed in the last ten years. In practice, the choice or the development of a SNP genotyping method requires to consider technical and practical implications (Chen and Sullivan, 2003; Kim and Misra, 2007). As previously discussed, the cost per genotype is a major issue. Initial instrument and set-up costs, as well as fixed and running costs have to be considered. The advantages and disadvantages of current SNP genotyping methods were previously discussed, and illustrated the need to still further develop more efficient genotyping techniques (Section 1.3.3 and section 5.1). The ASO QDEM assay offers the potential to improve most of the technological requirements of high throughput SNP genotyping. First, as largely discussed earlier, QDEMs have the potential to supersede current fluorescent bead technology because of their multiplex capabilities due to the unique optical properties of the QD encoding material. The actual highest multiplex bead-based assay, the Luminex platform™ (TX, USA), is based on organic fluorophores, which therefore limits and increase the complexity of enlarging the number of fluorescent codes in a single tube experiment, because of fluorophore emission overlaps. Furthermore, the Luminex fluorescent beads require a specialised instrument which implies high set-up costs. The use of a conventional flow cytometer in the ASO QDEM assay with potentially higher multiplex fluorescent capacities is therefore an advantage over the Luminex technology. The specific allele detection and potential quantification of allele frequencies with the QD reporter dye also potentially offer better resolution than the use of the organic reporter dye in the Luminex assay. The development of QD-doped particle calibration kit promises to bring the QDEM ASO genotyping assay to quantitative FC applications. The flexibility of the QDEMs material is also an advantage over current fluorescent bead technology since the researcher could *a priori*, customised the fluorescent codes of the fluorescent microspheres depending on the assay requirements. Finally, the potential of the ASO QDEM method is a promising approach that could be applied to various genotyping experiments such as, human identification, analysis of environmental biological analyte, forensic genetics, association studies, and population genetics.

Chapter 7

Final Conclusion

7. FINAL CONCLUSION

Quantum dots (QDs) offer promise as novel labels for high throughput bioassays because of their unique electrical and optical properties due to their material compound, structure and size (Medintz *et al.*, 2008). Mixtures of QDs can be excited with a single source of light (488 nm), which provides a unique spectral code, dependent on the size and composition of the QDs. Encoded in spherical microspheres (QD-doped particles), this new type of fluorescent code can be applied to high throughput particle-based bioassay in liquid and solid format. Suspension array technology (SAT) applied to the quantification and identification of DNA sequence of environmental analyte, single nucleotide polymorphism (SNP) genotyping, and immunoassays has been reported in the literature. SAT has become a recognised and competitive method to planar microarray (Nolan and Mandy, 2001).

The research study reported in this thesis investigated the adaptability of the first commercialised quantum dot-encoded microspheres, QDEMs, to bioassay applications. The research focused on the evaluation of the technology for suspension array technology and more specifically on the application of QDEMs to the genotyping of SNP human markers with the allele-specific hybridisation (ASO) approach.

The first part of the research required the analysis of QDEMs in different suspension solutions and experimental conditions. This empirical evaluation of the materials helped to develop an optimised bioassay adapted to the QDEM structural characteristics. The fluorescent code consistency and complexity of the QDEMs are involved in the ability of the researcher to follow, along the development of the procedure, the signature of the probes to be developed. These new parameters needed to be considered during the QDEM bioassay experimental work. In the perspective of developing a multiplex suspension assay, the specificity and stability of the probe's fluorescent code signature require also a specific evaluation and optimisation. In the study presented here, these factors were intrinsically linked to the structural stability of the QDEMs, which is illustrated by the colour and

intensity of the encoded microspheres and the number of QDEMs recovered after the experimental treatments. The optimisation of the QDEM recovery would assure the method efficiency in terms of consumable and reproducibility.

Considering these new parameters the development of a QDEM genotyping platform adapted to flow cytometry instrumentation implied first a high optimisation of bioconjugate preparation, in terms of time, consumables, efficiency, stability, and reproducibility. The first experimental optimisation of commercialised QDEM bioconjugates was undertaken with a limited amount (10^4) of 5 µm QDEMs, *i.e.*, polystyrene microspheres encoded with TriLite™ nanocrystals, to be conjugated to specific DNA probes. The different coupling steps were evaluated by looking at different types of conjugation buffers; time conditions, probe structures, and oligo concentrations. Two methods were used to calibrate the fluorescent intensity. First, the median fluorescence intensity was selected for qualitative analysis as it provided a good indication of the central tendency of the population. Secondly, a fluorescent quantification kit was used for the estimation of the number of oligos attached to the surface of the QDEMs. The specific optimisation of QDEM-probes was achieved and experimental conditions were defined to obtain an optimum yield of coupling adapted to DNA-DNA hybridisation application, with good uniformity and relative stability of the QDEM populations. A fast and "economic" singleplex QDEM conjugation method, well adapted for future multiplex experiment, was thus developed. Bioconjugation experiments enlightened the drawback phenomenon on microsphere structure and fluorescent emission during the procedure. As a consequence, further investigation of the QDEM structural properties and responses to liquid environment were performed at each stage of the research.

QDEM optimised bioconjugates were then employed to develop an allele-specific hybridisation assay in suspension. A new approach was chosen for the hybridisation optimisation step. The design of experiments approach was evaluated for its beneficial contribution to the development of complex experimental bioassays. The multiple optimisations of the hybridisation responses under study, simultaneously to the

experimental parameters of the ASO was achieved. To finalise the development of the method the application of the optimum conditions were applied to single nucleotide polymorphism genotyping. The promising spectroscopic advantages of QDEM technology is believed to allow the genotyping of a great number of SNPs in a single tube experiment using a combinatorial library of QDEM bioconjugated to specific oligoss. A current application of SNP genotyping focuses on the identification of male genetic profile in forensic genetics. Because of its specific genetic properties, the Y-chromosome defines the male lineage and therefore provides a unique tool for the specific identification of masculine individuals. Y-chromosomal SNPs are transmitted from male generation to generation with approximately no modifications. An initial work was undertaken to develop a Y-SNP genotyping assay. QDEM specific ASO method successfully identified the genotype of a human male template for two different Y-SNPs.

A limited number of reports mentioned the instability of the QD-doped particles in aqueous environment. The research work presented in this thesis was a valuable contribution to a better understanding of the QD-doped particle materials behaviour in solution but also in bioassay experimental conditions. The method developed also importantly contributed to the global research aiming to adapted QD-doped particles for biomedical applications. QD-doped beads have been applied to biological systems, and mainly for DNA-DNA hybridisation experiment in liquid format. Most of these works were proof-of-principle that pointed out the potential of the technology for high through put biological assays. The limitation of commercial systems strongly prevent to study reproducibility and to compare the different methods developed. The development of bioconjugation and hybridisation protocols adapted to a specific type of commercialised QD-encoded microspheres in this research project is though to participate to standardisation and validation of protocols and to contribute to the evaluation of experimental procedures between laboratories. To conclude, the use of QD technology should be limited to case-by-case biological or technological issue and should continue to prove its potential and feasibility. Future developments in QD technology should be beneficial in specific fields of research where multi colour detection, high intensity and stability of fluorescent particles are essential.

Chapter 8

Suggestions for Future Work

SUGGESTIONS FOR FUTURE WORK

Further investigation of the QD-doped particle technology

The work reported in the chapter 2 and 3 presented a first attempt to characterise QD-doped particles in bioassay experimental conditions. To explain and specifically identify the physical and optical phenomena due to thermal, chemical and physical treatments applied to the QD-doped particle, the experimentations performed in the Chapter 2 and 3 should be reproduced on other type of QD-encoded microspheres, which differ by the method of encoding. An extensive search in the literature should help to select the different types of QD-doped particles susceptible to be used in suspension array. Comparing the stability between different types of QD-doped microspheres population could help to identify which encoding method provides robust beads for suspension array. It would also provide important chemical information to improve the stability of the QD-doped particles in aqueous environment. A challenging part of this work would be to obtain the materials from other researchers since no other types of beads were commercially accessible at the time of writing.

Further investigation of the QDEM-probe technology

The optimisation of allelic probe to QDEMs was described in Chapter 3, and the titration of the bioconjugate with its DNA complementary target was undertaken in Chapter 4. The titration of the hybridisation with different types of DNA probes (*i.e.,* poly-adenine fluorescent probe, single nucleotide polymorphism allelic probes) showed the sensitivity and dynamic range of the hybridisation in chapter 4 and 5. However, other types of DNA probes could be used for a quantitative hybridisation titration to further investigate the sensitivity and specificity of the assay. Hybridisation titration experiments could be undertaken with the Y-SNPs relevant biological probe attached to the beads and with its complementary sequence as a fluorescent labelled target, and with another labelled sequence with an inexact sequence homology, (as an example, sequence with a mismatch mimicking SNP variations). Such comparative titrations would enhance the optimisation of the hybridisation stage for its specific application to SNP genotyping.

Further development of the Y-SNP genotyping assay

The work reported in chapter 5 involved the development of a duplex genotyping assay for the identification of two Y-SNPs. The further development the ASO QDEM assay involves the development of the assay at the multiplex level. A multiplex genotyping assay for the identification of multiple Y-SNPs in the human genome requires:

- The selection of Y-SNP markers;
- The design of primers and probes compatible with multiplex PCR and genotyping experiments;
- The development of single and multiplex PCR amplifying the SNP markers;
- The verification of the SNP sequences amplified by sequencing;
- The validation of the specificity of the allelic probes designed for their DNA target using dot blot experiments and a human template
- The optimisation of hybridisation conditions for the specific hybridisation of the allelic probes for their target in a single tube experiment with a human template
- The optimisation of hybridisation conditions for the specific hybridisation of the allelic probes for their target in a complex mixture;
- The optimisation of the reporter fluorescent quantum dot (665QD-SA) quantity for the recognition of the multiple PCR products in a multiplex format

In the perspective of developing this method for high throughput hybridisation technology, further work may include to test the utility of the design of experiment to optimise the multiplex conditions of hybridisation, and the 665QD-SA reporter signal. The experimental factors to be optimised for the maximisation of the hybridisation signal for allele specific detection in the suspension assay include: 1) the QD665-SA reporter quantity; 2) The hybridisation complex quantity, 3) The time and speed shaking applied to reporter dye/complex incubation; and the responses: 1) the 665QD-SA fluorescent signal 2) the percentage of events; 3) QDEMs code consistency. Future work would include to compare DOE results and predictions with the theoretical (*i.e.,* chemistry prediction) and empirical conditions established in this report.

The validation of the genotyping assay involves the amplification of the Y-SNPs selected with different DNA templates in order to verify their polymorphism and to be able to evaluate the specificity of both allelic probes of each SNP with homozygote and heterozygote samples. This work implies the evaluation of the method through the genotyping of male DNA samples. The number of DNA templates should depend on the heterozygotie of the markers and would require ethic approvals for the collections of biological samples to obtain different type of DNA templates. Then, DNA extraction, Y-SNPs amplification, and the sequencing of the PCR products would have to be performed for each DNA templates.

This work would be useful to demonstrate the potential of Y-SNP markers for the identification of the population-of-origin of human sample in Forensic. Part of this future work was initiated during the last part of this research project.

Comparison with other SNP genotyping multiplex assays

The comparison of the method with other SNP genotyping multiplex assay, in terms of DNA detection sensitivity, SNP profiling accuracy, and cost and time efficiency, in order to further validate the efficiency of the method, and potentially commercialised it.

Future applications of QDEMs fluorescent technology in suspension array

The improvement of the stability of the QDEMs technology could lead to several promising applications in biomedical science. Realistically, QDEMs of µm size could be used for multiplex bead-based fluorescent immunoassays on microfluidic platforms (Riegger *et al.*, 2006). Further, the development of smaller and better portable flow cytometers would bring the QDEMs Y-SNP genotyping method to field analysis, enhancing the chance of finding a male genetic profile from very sensitive forensic sample (Bonetta, 2005). More interestingly, suspension bead array have been recently applied for rapid STR analysis (Villablanca *et al.*, 2008). STRs being the marker of choice for human identification, these new developments offer the promise of high through put individual genotyping using QDEMs technology in human identification applications.

References

REFERENCES

Agrawal, A., Deo, R., Wang, G., Wang, M., Nie, S., 2008. Nanometer-scale mapping and single-molecule detection with color-coded nanoparticle probes. *Proceedings of the National Academy of Sciences*, 105, 3298.

Akerman, M., Chan, W., Laakkonen, P., Bhatia, S., Ruoslahti, E., 2002. Nanocrystal targeting in vivo. *Proceedings of the National Academy of Sciences*, 99, 12617-12621.

Aldana, J., Wang, Y.A., Peng, X., 2001. Photochemical instability of CdSe nanocrystals coated by hydrophilic thiols. *Journal of the American Chemical Society*, 123, 8844-8850.

Alderborn, A., Kristofferson, A., Hammerling, U., 2000. Determination of Single-Nucleotide Polymorphisms by Real-time Pyrophosphate DNA Sequencing. Cold Spring Harbor Lab, pp. 1249-1258.

Alivisatos, A., Gu, W., Larabell, C., 2005. Quantum dots as cellular probes

Alivisatos, A.P., 1996. Semiconductor clusters, nanocrystals, and quantum dots. *Science*, 271, 933-937.

Alonso, A., Martin, P., Albarran, C., Garcia, P., Fernandez, d.S., Jesus, I.M., Fernandez-Rodriguez, A., Atienza, I., Capilla, J., Garcia-Hirschfeld, J., Martinez, P., Vallejo, G., Garcia, O., Garcia, E., Real, P., Alvarez, D., Leon, A., Sancho, M., 2005. Challenges of DNA profiling in mass disaster investigations. *Croat.Med.J*, 46, 540-548.

Altekar, M., Homon, C., Kashem, M., Mason, S., Nelson, R., Patnaude, L., Yingling, J., Taylor, P., 2007. Assay Optimization: A Statistical Design of Experiments Approach. *Clinics in Laboratory Medicine*, 27, 139-154.

Altschul, S., Gish, W., Miller, W., Myers, E., Lipman, D., 1990. Basic local alignment search tool. *J. Mol. Biol*, 215, 403-410.

Armstrong, B., Stewart, M., Mazumder, A., 2000. Suspension arrays for high throughput, multiplexed single nucleotide polymorphism genotyping. *Cytometry*, 40, 102-108.

Authier, L., Grossiord, C., Brossier, P., 2001. Gold nanoparticle-based quantitative electrochemical detection of amplified human cytomegalovirus DNA using disposable microband electrodes. *Anal.Chem.*, 73, 4450-4456.

Bailey, R., Smith, A., Nie, S., 2004. Quantum dots in biology and medicine. *Physica E: Low-dimensional Systems and Nanostructures*, 25, 1-12.

Bailey, R.E., Nie, S., 2003. Alloyed semiconductor quantum dots: Tuning the optical properties without changing the particle size. *Journal of the American Chemical Society*, 125, 7100-7106.

Baird, G.S., Zacharias, D.A., Tsien, R.Y., 2000. Biochemistry, mutagenesis, and oligomerization of DsRed, a red fluorescent protein from coral. *Proceedings of the National Academy of Sciences of the United States of America*, 97, 11984-11989.

Bakalova, R., Ohba, H., Zhelev, Z., Ishikawa, M., Baba, Y., 2004. Quantum dots as photosensitizers? *Nature Biotechnology*, 22, 1360-1361.

Ballester, M., Mercade, A., Van Haandel, B., Santamartina, J., Sanchez, A., 2007. Individual identification and genetic traceability in the pig using the SNPlex genotyping system. *Animal Genetics*, 38, 663-665.

Ballou, B., Lagerholm, B.C., Ernst, L.A., Bruchez, M.P., Waggoner, A.S., 2004. Noninvasive Imaging of Quantum Dots in Mice. *Bioconjugate Chemistry*, 15, 79-86.

Beasley, E.M., Myers, R.M., Cox, D.R., Lazzeroni, L.C., 1999. Statistical refinement of primer design parameters. *PCR Applications*, 55-71.

Berkhout, B., Back, N.K., De Ronde, A., Jurriaans, S., Bakker, M., Parkin, N.T., Van Der Hoek, L., 2006. Identification of alternative amino acid substitutions in drug-resistant variants of the HIV-1 reverse transcriptase. *AIDS*, 20, 1515-1520.

Boleda, M., Briones, P., Farres, J., Tyfield, L., Pi, R., 1996. Experimental design: a useful tool for PCR Optimization. *Biotechniques*, 21, 134-40.

Bonetta, L., 2005. Flow cytometry smaller and better. *Nature Methods*, 2, 785-795.

Botstein, D., White, R.L., Skolnick, M., Davis, R.W., 1980. Construction of a genetic linkage map in man using restriction fragment length polymorphisms. *Am.J Hum.Genet*, 32, 314-331.

Bradley, M., Bruno, N., Vincent, B., 2005. Distribution of CdSe quantum dots within swollen polystyrene microgel particles using confocal microscopy. *Langmuir*, 21, 2750-2753.

Brion, M., Sanchez, J.J., Balogh, K., Thacker, C., Blanco-Verea, A., Borsting, C., Stradmann-Bellinghausen, B., Bogus, M., Syndercombe, C., Schneider, P.M.,

Carracedo, A., Morling, N., 2005a. Introduction of an single nucleodite polymorphism-based "Major Y-chromosome haplogroup typing kit" suitable for predicting the geographical origin of male lineages. *Electrophoresis*, 26, 4411-4420.

Brion, M., Sobrino, B., Blanco-Verea, A., Lareu, M., Carracedo, A., 2005b. Hierarchical analysis of 30 Y-chromosome SNPs in European populations. *International Journal of Legal Medicine*, 119, 10-15.

Brookes, A.J., 1999. The essence of SNPs. *Gene*, 234, 177-186.

Bruchez Jr, M., Moronne, M., Gin, P., Weiss, S., Alivisatos, A.P., 1998. Semiconductor nanocrystals as fluorescent biological labels. *Science*, 281, 2013-2016.

Brus, L.E., 1984. Electron-electron and electron-hole interactions in small semiconductor crystallites: The size dependence of the lowest excited electronic state. *The Journal of Chemical Physics*, 80, 4403-4409.

Budowle, B., Van Daal, A., 2008. Forensically relevant SNP classes. *BioTechniques*, 44, 603-610.

Butler, J.M., Shen, Y., McCord, B.R., 2003. The development of reduced size STR amplicons as tools for analysis of degraded DNA. *Journal of Forensic Sciences*, 48, 1054-1064.

Butler, J.M., 2004. Short tandem repeat analysis for human identity testing. *Curr.Protoc.Hum.Genet*, Chapter 14, Unit.

Byrne, S.J., Williams, Y., Davies, A., Corr, S.A., Rakovich, A., Gun'ko, Y.K., Rakovich, Y.P., Donegan, J.F., Volkov, Y., 2007. "Jelly dots": Synthesis and cytotoxicity studies of CdTe quantum dot-gelatin nanocomposites. *Small*, 3, 1152-1156.

Cao, Y., Liu, T., Hua, X., Zhu, X., Wang, H., Huang, Z., Zhao, Y., Liu, M., Luo, Q., 2006a. Quantum dot optical encoded polystyrene beads for DNA detection. *Journal of Biomedical Optics*, 11, 054025.

Cao, Y.C., Huang, Z.L., Liu, T.C., Wang, H.Q., Zhu, X.X., Wang, Z., Zhao, Y.D., Liu, M.X., Luo, Q.M., 2006b. Preparation of silica encapsulated quantum dot encoded beads for multiplex assay and its properties. *Analytical Biochemistry*, 351, 193-200.

Carracedo, A., Sanchez-Diz, P., 2005. Forensic DNA-typing technologies: a review. *Methods Mol.Biol.*, 297, 1-12.

Chan, P., Yuen, T., Ruf, F., Gonzalez-Maeso, J., Sealfon, S., 2005. Method for multiplex cellular detection of mRNAs using quantum dot fluorescent in situ hybridization. *Nucleic Acids Research*, 33, e161.

Chan, V., Graves, D.J., McKenzie, S.E., 1995. The biophysics of DNA hybridization with immobilized oligonucleotide probes. *Biophysical Journal*, 69, 2243-2255.

Chan, W., Nie, S., 1998. Quantum Dot Bioconjugates for Ultrasensitive Nonisotopic Detection. *Science*, 281, 2016.

Chan, Y., Zimmer, J., Stroh, M., Steckel, J., Jain, R., Bawendi, M., 2004. Incorporation of Luminescent Nanocrystals into Monodisperse Core-Shell Silica Microspheres. *Advanced Materials*, 16, 2092-2097.

Chang, S., Zhou, M., Grover, C.P., 2004. Information coding and retrieving using fluorescent semiconductor nanocrystals for object identification. *Optics Express*, 12, 143-148.

Chen, J., Iannone, M.A., Li, M.S., Taylor, J.D., Rivers, P., Nelsen, A.J., Slentz-Kesler, K.A., Roses, A., Weiner, M.P., 2000. A microsphere-based assay for multiplexed single nucleotide polymorphism analysis using single base chain extension. *Genome Research*, 10, 549-557.

Chen, X., Sullivan, P.F., 2003. Single nucleotide polymorphism genotyping: biochemistry, protocol, cost and throughput. *Pharmacogenomics.J*, 3, 77-96.

Chestnoy, N., Harris, T.D., Hull, R., Brus, L.E., 1986. Luminescence and photophysics of CdS semiconductor clusters: The nature of the emitting electronic state. *Journal of Physical Chemistry*, 90, 3393-3399.

Choi, A., Cho, S., Desbarats, J., Lovric, J., Maysinger, D., 2007. Quantum dot-induced cell death involves Fas upregulation and lipid peroxidation in human neuroblastoma cells. *Journal of Nanobiotechnology*, 5, 1.

Chu, M., Zhou, L., Song, X., Pan, M., Zhang, L., Sun, Y., Zhu, J., Ding, Z., 2006. Incorporating quantum dots into polymer microspheres via a spray-drying and thermal-denaturizing approach. *Nanotechnology*, 17, 1791-1796.

Chung, D.T., Dra?bek, J., Opel, K.L., Butler, J.M., McCord, B.R., 2004. A study on the effects of degradation and template concentration on the amplification efficiency of the STR Miniplex primer sets. *Journal of Forensic Sciences*, 49, 733-740.

Clapp, A.R., Medintz, I.L., Mauro, J.M., Fisher, B.R., Bawendi, M.G., Mattoussi, H., 2004. Fluorescence Resonance Energy Transfer between Quantum Dot Donors and Dye-Labeled Protein Acceptors. *Journal of the American Chemical Society*, 126, 301-310.

Clarke, C., Malecha, M., Saini, S., 2005. BMC Bioinformatics. *BMC Bioinformatics*, 6, P5.

Clegg, R.M., 1992. Fluorescence resonance energy transfer and nucleic acids. *Methods Enzymol.*, 211, 353-388.

Cutler, D.J., Zwick, M.E., Carrasquillo, M.M., Yohn, C.T., Tobin, K.P., Kashuk, C., Mathews, D.J., Shah, N.A., Eichler, E.E., Warrington, J.A., Chakravarti, A., 2001. High-throughput variation detection and genotyping using microarrays. *Genome Research*, 11, 1913-1925.

Dabbousi, B., Bawendi, M., Onitsuka, O., Rubner, M., 1995. Electroluminescence from CdSe quantum-dot/polymer composites. *Applied Physics Letters*, 66, 1316.

Dabbousi, B., Rodriguez-Viejo, J., Mikulec, F., Heine, J., Mattoussi, H., Ober, R., Jensen, K., Bawendi, M., 1997. (CdSe) ZnS core-shell quantum dot: Synthesis and characterization of a size series of highly luminescent nanocrystallites *The Journal of physical chemistry. B, materials, surfaces, interfaces & biophysical*, 101, 9463-9475.

De la Vega, F.M., Isaac, H., Collins, A., Scafe, C.R., Halldorsson, B.V., Su, X.P., Lippert, R.A., Wang, Y., Laig-Webster, M., Koehler, R.T., Ziegle, J.S., Wogan, L.T., Stevens, J.F., Leinen, K.M., Olson, S.J., Guegler, K.J., You, X.Q., Xu, L.H., Hemken, H.G., Kalush, F*., et al.*, 2005. The linkage disequilibrium maps of three human chromosomes across four populations reflect their demographic history and a common underlying recombination pattern. *Genome Research*, 15, 454-462.

Derfus, A., Chen, A., Min, D., Ruoslahti, E., Bhatia, S., 2007. Targeted quantum dot conjugates for siRNA delivery. *Bioconjug. Chem*, 18, 1391-1396.

Derfus, A.M., Chan, W.C.W., Bhatia, S.N., 2004. Probing the Cytotoxicity of Semiconductor Quantum Dots. *Nano Letters*, 4, 11-18.

Di Giacomo, F., Luca, F., Anagnou, N., Ciavarella, G., Corbo, R.M., Cresta, M., Cucci, F., Di Stasi, L., Agostiano, V., Giparaki, M., Loutradis, A., Mammi, C., Michalodimitrakis, E.N., Papola, F., Pedicini, G., Plata, E., Terrenato, L., Tofanelli, S., Malaspina, P., Novelletto, A., 2003. Clinal patterns of human Y chromosomal diversity in continental Italy and Greece are dominated by drift and founder effects. *Molecular Phylogenetics and Evolution*, 28, 387-395.

Didier, C., Etcheverrigaray, M., Kratje, R., Goicoechea, H.C., 2007. Crossed mixture design and multiple response analysis for developing complex culture media used in recombinant protein production. *Chemometrics and Intelligent Laboratory Systems*, 86, 1-9.

Douglas, A.S., Monteith, C.A., 1994. Improvements to immunoassays by use of covalent binding assay plates. *Clinical Chemistry*, 40, 1833-1837.

Drago, S., González, R., Añón, M., 2008. Application of surface response methodology to optimize hydrolysis of wheat gluten and characterization of selected hydrolysate fractions. *Journal of the Science of Food and Agriculture*, 88, 1415-1422.

Dubertret, B., Skourides, P., Norris, D.J., Noireaux, V., Brivanlou, A.H., Libchaber, A., 2002. In vivo imaging of quantum dots encapsulated in phospholipid micelles. *Science*, 298, 1759-1762.

Dubreuil, R.M., Patel, J.M., Mendelow, B.V., 1993. Quantitation of Beta-Actin-Specific Messenger-Rna Transcripts Using Xeno-Competitive Pcr. *Pcr-Methods and Applications*, 3, 57-59.

Dugas, V., Depret, G., Chevalier, Y., Nesme, X., Souteyrand, É., 2004. Immobilization of single-stranded DNA fragments to solid surfaces and their repeatable specific hybridization: covalent binding or adsorption? *Sensors & Actuators: B. Chemical*, 101, 112-121.

Dunbar, S., Jacobson, J., 2000. Application of the Luminex LabMAP in rapid screening for mutations in the cystic fibrosis transmembrane conductance regulator gene: a pilot study. Am Assoc Clin Chem, pp. 1498-1500.

Dunbar, S., 2006. Applications of Luminex® xMAP™ technology for rapid, high-throughput multiplexed nucleic acid detection. *Clinica Chimica Acta*, 363, 71-82.

Eastman, P.S., Ruan, W., Doctolero, M., Nuttall, R., de Feo, G., Park, J.S., Chu, J.S., Cooke, P., Gray, J.W., Li, S., Chen, F.F., 2006. Qdot nanobarcodes for multiplexed gene expression analysis. *Nano.Lett.*, 6, 1059-1064.

Edwards, B.S., Oprea, T., Prossnitz, E.R., Sklar, L.A., 2004. Flow cytometry for high-throughput, high-content screening. *Current Opinion in Chemical Biology*, 8, 392-398.

Efros, A.L., Efros, A.L., 1982. Interband absorption of light in a semiconductor sphere *Soviet physics. Semiconductors*, 16, 772-775.

Enderlein, J., 2005. Dependence of the optical saturation of fluorescence on rotational diffusion. *Chemical Physics Letters*, 410, 452-456.

Ernst, L.A., Gupta, R.K., Mujumdar, R.B., Waggoner, A.S., 1989. Cyanine dye labeling reagents for sulfhydryl groups. *Cytometry*, 10, 3-10.

Fan, J.B., Hu, S.X., Craumer, W.C., Barker, D.L., 2005. BeadArray-based solutions for enabling the promise of pharmacogenomics. *BioTechniques.*, 39, 583-588.

Fan, T.W.M., Teh, S.J., Hinton, D.E., Higashi, R.M., 2002. Selenium toxicity: cause and effects in aquatic birds. *Aquatic Toxicology*, 57, 27-37.

Farahat, N., Lens, D., Zomas, A., Morilla, R., Matutes, E., Catovsky, D., 1995. Quantitative flow cytometry can distinguish between normal and leukaemic B-cell precursors. *British Journal of Haematology*, 91, 640-646.

Fechner, A., Quinque, D., Rychkov, S., Morozowa, I., Naumova, O., Schneider, Y., Willuweit, S., Zhukova, O., Roewer, L., Stoneking, M., 2008. Boundaries and clines in the West Eurasian Y-chromosome landscape: Insights from the European part of Russia. *American Journal of Physical Anthropology*, 137.

Fitzgerald, C., Collins, M., van Duyne, S., Mikoleit, M., Brown, T., Fields, P., 2007. Multiplex, Bead-Based Suspension Array for Molecular Determination of Common Salmonella Serogroups?†. *Journal of clinical microbiology*, 45, 3323-3334.

Fomento, V., Nesbitt, D.J., 2008. Solution control of radiative and nonradiative lifetimes: A novel contribution to quantum dot blinking suppression. *Nano Letters*, 8, 287-293.

Forsythe, G., Malcolm, M., Moler, C., 1977. Computer methods for mathematical computations. Prentice Hall Professional Technical Reference.

Fuchs, B.M., Woebken, D., Zubkov, M.V., Burkill, P., Amann, R., 2005. Molecular identification of picoplankton populations in contrasting waters of the Arabian Sea. *Aquatic Microbial Ecology*, 39, 145-157.

Fuja, T., Hou, S., Bryant, P., 2004. A multiplex microsphere bead assay for comparative RNA expression analysis using flow cytometry. *Journal of Biotechnology*, 108, 193-205.

Fulton, R.J., McDade, R.L., Smith, P.L., Kienker, L.J., Kettman, J.R., Jr., 1997. Advanced multiplexed analysis with the FlowMetrix system. *Clin.Chem.*, 43, 1749-1756.

Fundueanu, G., Constantin, M., Ascenzi, P., 2008. Preparation and characterization of pH- and temperature-sensitive pullulan microspheres for controlled release of drugs. *Biomaterials*, 29, 2767-2775.

Gadgil, C., Yeckel, A., Derby, J.J., Hu, W.S., 2004. A diffusion-reaction model for DNA microarray assays. *Journal of Biotechnology*, 114, 31-45.

Gao, X., Nie, S., 2003. Doping mesoporous materials with multicolor quantum dots. *Journal of Physical Chemistry B*, 107, 11575-11578.

Gao, X., Nie, S., 2004. Quantum dot-encoded mesoporous beads with high brightness and uniformity: rapid readout using flow cytometry. *Anal.Chem.*, 76, 2406-2410.

Gaponik, N., Talapin, D.V., Rogach, A.L., Hoppe, K., Shevchenko, E.V., Kornowski, A., Eychmu?ller, A., Weller, H., 2002. Thiol-capping of CDTe nanocrystals: An alternative to organometallic synthetic routes. *Journal of Physical Chemistry B*, 106, 7177-7185.

Gerion, D., Pinaud, F., Williams, S.C., Parak, W.J., Zanchet, D., Weiss, S., Alivisatos, A.P., 2001. Synthesis and properties of biocompatible water-soluble silica-coated CdSe/ZnS semiconductor quantum dots. *Journal of Physical Chemistry B*, 105, 8861-8871.

Gerion, D., Chen, F., Kannan, B., Fu, A., Parak, W., Chen, D., Majumdar, A., Alivisatos, A., 2003. Room-Temperature Single-Nucleotide Polymorphism and Multiallele DNA Detection Using Fluorescent Nanocrystals and Microarrays. *anal. Chem. Washington DC*, 75, 4766-4772.

Giepmans, B.N.G., Deerinck, T.J., Smarr, B.L., Jones, Y.Z., Ellisman, M.H., 2005. Correlated light and electron microscopic imaging of multiple endogenous proteins using Quantum dots. *Nature Methods*, 2, 743-749.

Gill, P., Werrett, D.J., Budowle, B., Guerrieri, R., 2004. An assessment of whether SNPs will replace STRs in national DNA databases--joint considerations of the DNA working group of the European Network of Forensic Science Institutes (ENFSI) and the Scientific Working Group on DNA Analysis Methods (SWGDAM). *Sci.Justice*, 44, 51-53.

Glinsky, G.V., 2008. SNP-guided microRNA maps (MirMaps) of 16 common human disorders identify a clinically accessible therapy reversing transcriptional aberrations of nuclear import and inflammasome pathways. *Cell Cycle*, 7, 3564-3576.

Goldman, E.R., Anderson, G.P., Tran, P.T., Mattoussi, H., Charles, P.T., Mauro, J.M., 2002. Conjugation of luminescent quantum dots with antibodies using an engineered adaptor protein to provide new reagents for fluoroimmunoassays. *Analytical Chemistry*, 74, 841-847.

Grecco, H.E., Lidke, K.A., Heintzmann, R., Lidke, D.S., Spagnuolo, C., Martinez, O.E., Jares-Erijman, E.A., Jovin, T.M., 2004. Ensemble and single particle photophysical properties (two-photon excitation, anisotropy, FRET, lifetime, spectral conversion) of commercial quantum dots in solution and in live cells. *Microsc.Res.Tech.*, 65, 169-179.

Grove, D., 1999. Quantitative real-time polymerase chain reaction for the core facility using TaqMan and the Perkin-Elmer/Applied Biosystems Division 7700 Sequence Detector. ABRF, pp. 11-16.

Gunderson, K.L., Kuhn, K.M., Steemers, F.J., Ng, P., Murray, S.S., Shen, R., 2006. Whole-genome genotyping of haplotype tag single nucleotide polymorphisms. *Pharmacogenomics*, 7, 641-648.

Guo, J., Yang, W., Wang, C., He, J., Chen, J., 2006. Poly(N-isopropylacrylamide)-coated luminescent/magnetic silica microspheres: Preparation, characterization, and biomedical applications. *Chemistry of Materials*, 18, 5554-5562.

Haaland, P., 1989. Experimental Design in Biotechnology. CRC Press.

Halder, I., Shriver, M., Thomas, M., Fernandez, J.R., Frudakis, T., 2008. A panel of ancestry informative markers for estimating individual biogeographical ancestry and admixture from four continents: Utility and applications. *Human Mutation*, 29, 648-658.

Han, M., Gao, X., Su, J., Nie, S., 2001. Quantum-dot-tagged microbeads for multiplexed optical coding of biomolecules. *Nature Biotechnology*, 19, 631-635.

Hand, L., 2002. SNP technology focuses on terror victims' IDs. *Scientist*, 16, 20.

Hanley, B.P., Xing, L., Cheng, R.H., 2007. Variance in multiplex suspension array assays: microsphere size variation impact. *Theor.Biol.Med.Model.*, 4, 31.

Hardman, R., 2006. A toxicologic review of quantum dots: toxicity depends on physicochemical and environmental factors. *Environmental health perspectives*, 114, 165.

Henegariu, O., Heerema, N.A., Dlouhy, S.R., Vance, G.H., Vogt, P.H., 1997. Multiplex PCR: critical parameters and step-by-step protocol. *Biotechniques*, 23, 504-511.

Henson, M.C., Chedrese, P.J., 2004. Endocrine Disruption by Cadmium, a Common Environmental Toxicant with Paradoxical Effects on Reproduction. *Experimental Biology and Medicine*, 229, 383-392.

Hermanson, G.T., Mallia, A.K., Smith, P.K., 1992. Immobilization of ligands. *Immobilized Affinity Ligand Techniques*.

Hermanson, G.T., 2008. Bioconjugation Techniques. *Academic Press*, 2nd ed., p. 582-627.

Hezinger, A.F.E., Temar, J., Gopferich, A., 2008. Polymer coating of quantum dots - A powerful tool toward diagnostics and sensorics. *European Journal of Pharmaceutics and Biopharmaceutics*, 68, 138-152.

Horan, P.K., Wheeless Jr, L.L., 1977. Quantitative single cell analysis and sorting. *Science*, 198, 149-157.

Horejsh, D., Martini, F., Poccia, F., Ippolito, G., Di Caro, A., Capobianchi, M., 2005. A molecular beacon, bead-based assay for the detection of nucleic acids by flow cytometry. *Nucleic Acids Research*, 33, e13.

Horton, R., Niblett, D., Milne, S., Palmer, S., Tubby, B., Trowsdale, J., Beck, S., 1998. Large-scale sequence comparisons reveal unusually high levels of variation in the HLA-DQB1 locus in the class II region of the human MHC. *J Mol.Biol.*, 282, 71-97.

Hoshino, A., Hanaki, K.I., Suzuki, K., Yamamoto, K., 2004. Applications of T-lymphoma labeled with fluorescent quantum dots to cell tracing markers in mouse body. *Biochemical and Biophysical Research Communications*, 314, 46-53.

Howell, W.M., Jobs, M., Gyllensten, U., Brookes, A.J., 1999. Dynamic allele-specific hybridization. *Nature Biotechnology*, 17, 87-88.

Hsu, T., Chen, X., Duan, S., Miller, R., Kwok, P., 2001. Universal SNP Genotyping Assay with Fluorescence Polarization Detection. *Biotechniques*, 31, 560-571.

Hughes, A.R., Spreen, W.R., Mosteller, M., Warren, L.L., Lai, E.H., Brothers, C.H., Cox, C., Nelsen, A.J., Hughes, S., Thorborn, D.E., Stancil, B., Hetherington, S.V., Burns, D.K., Roses, A.D., 2008. Pharmacogenetics of hypersensitivity to abacavir: From PGx hypothesis to confirmation to clinical utility. *Pharmacogenomics Journal*, 8, 365-374.

Huo, Q., 2007. A perspective on bioconjugated nanoparticles and quantum dots. *Colloids and Surfaces B: Biointerfaces*, 59, 1-10.

Hurley, J., Engle, L., Davis, J., Welsh, A., Landers, J., 2004. A simple, bead-based approach for multi-SNP molecular haplotyping. *Nucleic Acids Research*, 32, e186.

Iannone, M.A., Taylor, J.D., Chen, J., Li, M.S., Rivers, P., Slentz-Kesler, K.A., Weiner, M.P., 2000. Multiplexed single nucleotide polymorphism genotyping by oligonucleotide ligation and flow cytometry. *Cytometry*, 39, 131-140.

Ikuta, S., Takagi, K., Wallace, R.B., Itakura, K., 1987. Dissociation kinetics of 19 base paired oligonucleotide-DNA duplexes containing different single mismatched base pairs. *Nucleic Acids Research*, 15, 797-811.

InternationalHapMapConsortium, 2003. The International HapMap Project: The International HapMap Consortium. *Nature*, 426, 789-796.

InternationalHapMapConsortium, 2005. A haplotype map of the human genome. *Nature*, 437, 1299-1320.

Jaiswal, J.K., Goldman, E.R., Mattoussi, H., Simon, S.M., 2004. Use of quantum dots for live cell imaging. *Nat Methods*, 1, 73-78.

Jeffreys, A.J., Wilson, V., Thein, S.L., 1985. Individual-specific 'fingerprints' of human DNA. *Nature*, 316, 76-79.

Jiang, W., Kim, B.Y., Rutka, J.T., Chan, W.C., 2008. Nanoparticle-mediated cellular response is size-dependent. *Nat.Nanotechnol.*, 3, 145-150.

Jobling, M.A., Tyler-Smith, C., 1995. Fathers and sons: the Y chromosome and human evolution. *Trends Genet*, 11, 449-456.

Jobling, M.A., Tyler-Smith, C., 2003. The human Y chromosome: an evolutionary marker comes of age. *Nat.Rev.Genet*, 4, 598-612.

Jyoti, K., Sanford, M.S., 2005. Potentials and pitfalls of fluorescent quantum dots for biological imaging. *Trends in Cell Biology*, 14, 497-504.

Karas, M., Bahr, U., Ingendoh, A., Nordhoff, E., Stahl, B., Strupat, K., Hillenkamp, F., 1990. Principles and applications of matrix-assisted UV-laser desorption/ionization mass spectrometry. *Analytica Chimica Acta*, 241, 175-185.

Karger, A.E., 1996. Separation of DNA sequencing fragments using an automated capillary electrophoresis instrument. *Electrophoresis*, 17, 144-151.

Kellar, K., Iannone, M., 2002. Multiplexed microsphere-based flow cytometric assays. *Experimental Hematology*, 30, 1227-1237.

Kim, J.S., Kalb, J.W., 1996. Design of experiments: an overview and application example. *Medical Device and Diagnostic Industry*, 18.

Kim, S., Lim, Y.T., Soltesz, E.G., De Grand, A.M., Lee, J., Nakayama, A., Parker, J.A., Mihaljevic, T., Laurence, R.G., Dor, D.M., Cohn, L.H., Bawendi, M.G., Frangioni, J.V., 2004. Near-infrared fluorescent type II quantum dots for sentinel lymph node mapping. *Nature Biotechnology*, 22, 93-97.

Kim, S., Misra, A., 2007. SNP Genotyping: Technologies and Biomedical Applications.

Klostranec, J., Chan, W., 2006. Quantum dots in biological and biomedical research: recent progress and present challenges. *Adv. Mater*, 18, 1953–1964.

Krausz, C., Quintana-Murci, L., Forti, G., 2004. Y chromosome polymorphisms in medicine. *Ann.Med.*, 36, 573-583.

Kuhn, K., Baker, S.C., Chudin, E., Lieu, M.H., Oeser, S., Bennett, H., Rigault, P., Barker, D., McDaniel, T.K., Chee, M.S., 2004. A novel, high-performance random array platform for quantitative gene expression profiling. *Genome Research*, 14, 2347-2356.

Kulwinder, K., Edward, T., Sujata, B., 2001. Performance Evaluation of QuantiBRITE Phycoerythrin Beads. *Cytometry*, 45, 250-258.

Kuno, M., Fromm, D., Hamann, H., Gallagher, A., Nesbitt, D., 2001. "On"/"off" fluorescence intermittency of single semiconductor quantum dots. *The Journal of Chemical Physics*, 115, 1028.

Lagerholm, B.C., Wang, M., Ernst, L.A., Ly, D.H., Liu, H., Bruchez, M.P., Waggoner, A.S., 2004. Multicolor coding of cells with cationic peptide coated quantum dots. *Nano Letters*, 4, 2019-2022.

Lander, E.S., Linton, L.M., Birren, B., Nusbaum, C., Zody, M.C., Baldwin, J., Devon, K., Dewar, K., Doyle, M., Fitzhugh, W., Funke, R., Gage, D., Harris, K., Heaford, A., Howland, J., Kann, L., Lehoczky, J., Levine, R., McEwan, P., McKernan, K.*, et al.*, 2001. Initial sequencing and analysis of the human genome. *Nature*, 409, 860-921.

Larsen, L., Christiansen, M., Vuust, J., Andersen, P., 2000. High throughput mutation screening by automated capillary electrophoresis. *Combinatorial Chemistry & High Throughput Screening*, 3, 393-409.

Larson, D.R., Zipfel, W.R., Williams, R.M., Clark, S.W., Bruchez, M.P., Wise, F.W., Webb, W.W., 2003. Water-soluble quantum dots for multiphoton fluorescence imaging in vivo. *Science*, 300, 1434-1436.

Lee, H., Park, M., Yoo, J., Chung, U., Han, G., Shin, K., 2005. Selection of twenty-four highly informative SNP markers for human identification and paternity analysis in Koreans. *Forensic Science International*, 148, 107-112.

Li, Y., Liu, E., Pickett, N., Skabara, P., Cummins, S., Ryley, S., Sutherland, A., O'Brien, P., 2005. Synthesis and characterization of CdS quantum dots in polystyrene microbeads. *Journal of Materials Chemistry*, 15, 1238-1243.

Lidke, D., Nagy, P., Heintzmann, R., Arndt-Jovin, D., Post, J., Grecco, H., Jares-Erijman, E., Jovin, T., 2004. Quantum dot ligands provide new insights into erbB/HER receptor- mediated signal transduction. *Nature Biotechnology*, 22, 198-203.

Lidke, D.S., Lidke, K.A., Rieger, B., Jovin, T.M., Arndt-Jovin, D.J., 2005. Reaching out for signals: Filopodia sense EGF and respond by directed retrograde transport of activated receptors. *Journal of Cell Biology*, 170, 619-626.

Lim, T.C., Bailey, V.J., Ho, Y.P., Wang, T.H., 2008. Intercalating dye as an acceptor in quantum-dot-mediated FRET. *Nanotechnology*, 19.

Little, D.P., Chorush, R.A., Speir, J.P., Senko, M.W., Kelleher, N.L., McLafferty, F.W., 1994. Rapid sequencing of oligonucleotides by high-resolution mass spectrometry. *Journal of the American Chemical Society*, 116, 4893-4897.

Liu, F., Cheng, T., Shen, C., Tseng, W., Chiang, M., 2008. Synthesis of Cysteine-Capped Zn x Cd Se Alloyed Quantum Dots Emitting in the Blue-Green Spectral Range. *Langmuir*, 24, 2162-2167.

Livshits, M.A., Mirzabekov, A.D., 1996a. Theoretical analysis of the kinetics of DNA hybridization with gel- immobilized oligonucleotides. *Biophysical Journal*, 71, 2795-2801.

Livshits, M.A., Mirzabekov, A.D., 1996b. Kinetics of DNA hybridization with oligonucleotides immobilized in gel layer. *Molecular Biology*, 30, 694-698.

Longman-Jacobsen, N., Williamson, J.F., Dawkins, R.L., Gaudieri, S., 2003. In polymorphic genomic regions indels cluster with nucleotide polymorphism: Quantum genomics. *Gene*, 312, 257-261.

Lowe, M., Spiro, A., Summers, A.O., Wireman, J., 2001. Multiplexed identification and quantification of analyte DNAs in environmental samples using microspheres and flow cytometry. *Methods in Biotechnology: Environmental Biology: Methods and Protocols*, 51-74.

Lowe, M., Spiro, A., Summers, A., Wireman, J., 2004. Multiplexed Identification and Quantification of Analyte DNAs in Environmental Samples Using Microspheres and Flow Cytometry. *METHODS IN BIOTECHNOLOGY*, 16, 51-74.

Lutz, M., Menius, J., Choi, T., Gooding Laskody, R., Domanico, P., Goetz, A., Saussy, D., 1996. Experimental design for high-throughput screening. *Drug Discovery Today*, 1, 277-286.

Lyamichev, V., Mast, A.L., Hall, J.G., Prudent, J.R., Kaiser, M.W., Takova, T., Kwiatkowski, R.W., Sander, T.J., De Arruda, M., Arco, D.A., Neri, B.P., Brow, M.A.D., 1999. Polymorphism identification and quantitative detection of genomic DNA by invasive cleavage of oligonucleotide probes. *Nature Biotechnology*, 17, 292-296.

Ma, Q., Wang, X., Li, Y., Shi, Y., Su, X., 2007. Multicolor quantum dot-encoded microspheres for the detection of biomolecules. *Talanta*, 72, 1446-1452.

Maier, J., Panza, J., Bootman, M., 2007. Nanocrystal clusters in combination with spectral imaging to improve sensitivity in antibody labeling applications of fluorescent nanocrystals. SPIE, pp. 64480P.

Matsuzaki, H., Dong, S., Loi, H., Di, X., Liu, G., Hubbell, E., Law, J., Berntsen, T., Chadha, M., Hui, H., Yang, G., Kennedy, G.C., Webster, T.A., Cawley, S., Walsh, P.S., Jones, K.W., Fodor, S.P., Mei, R., 2004. Genotyping over 100,000 SNPs on a pair of oligonucleotide arrays. *Nat Methods*, 1, 109-111.

Mattoussi, H., Medintz, I.L., Clapp, A.R., Goldman, E.R., Jaiswal, J.K., Simon, S.M., Mauro, J.M., 2004. Luminescent quantum dot-bioconjugates in immunoassays, FRET, biosensing, and imaging applications. *JALA - Journal of the Association for Laboratory Automation*, 9, 28-32.

May, M., 2008. Business Office Feature:Life Science Technologies: Genotyping Technology--SNP-ing Out Information. *Science*, 320, 117.

Medintz, I., Uyeda, H., Goldman, E., Mattoussi, H., 2005. Quantum dot bioconjugates for imaging, labelling and sensing. *Nat. Mater*, 4, 435–446.

Medintz, I.L., Mattoussi, H., Clapp, A.R., 2008. Potential clinical applications of quantum dots. *Int J Nanomedicine*, 3, 151-67.

Meissner, K.E., Herz, E., Kruzelock, R.P., Spillman Jr, W.B., 2003. Quantum dot-tagged microspheres for fluid-based DNA microarrays. *Phys. Status Solidi C*, 4, 1355-1359.

Men'shikova, A.Y., Evseeva, T.G., Chekina, N.A., Ivanchev, S.S., 2001. Synthesis of polymethyl methacrylate microspheres in the presence of dextran and its derivatives. *Russian Journal of Applied Chemistry*, 74, 489-493.

MicroParticleGmBh, March 2008. *http://www.microparticles.de/*.

Montgomery, D., 1991. Design and analysis of experiments.

Montgomery, D.C., 1997. Response surface methods and other approaches to process optimization. *Design and Analysis of Experiments*, 427-510.

Morilla, R., Scolnik, M., 1998. Quantitative flow cytometry. *Proc. R. Microscop. Soc.*, 33, 267-270.

Mosteller, M., Hughes, A., Warren, L., 2006. Pharmacogenetic (PG) investigation of hypersensitivity to abacavir. *XVI International AIDS Conference*.

Mullis, K., Faloona, F., Scharf, S., Saiki, R., Horn, G., Erlich, H., 1986. Specific enzymatic amplification of DNA in vitro: the polymerase chain reaction. *Cold Spring Harb.Symp.Quant.Biol.*, 51 Pt 1, 263-273.

Murray, C.B., Norris, D.J., Bawendi, M.G., 1993. Synthesis and characterization of nearly monodisperse CdE (E = S, Se, Te) semiconductor nanocrystallites. *Journal of the American Chemical Society*, 115, 8706-8715.

Murray, C.B., Kagan, C.R., Bawendi, M.G., 1995. Self-organization of CdSe nanocrystallites into three-dimensional quantum dot superlattices. *Science*, 270, 1335-1338.

Myakishev, M.V., Khripin, Y., Hu, S., Hamer, D.H., 2001. High-throughput SNP genotyping by allele-specific PCR with universal energy-transfer-labeled primers. *Genome Research*, 11, 163-169.

Myers, R., Montgomery, D., 1995. Response surface methodology: process and product optimization using designed experiments, 1995. *John Wiley&Sons, New York*.

Myers, R., Montgomery, D., Response Surface Methodology. 2002. John Wiley & Sons. Inc.

Nakajima, N., Ikada, Y., 1995. Mechanism of amide formation by carbodiimide for bioconjugation in aqueous media. *Bioconjugate Chemistry*, 6, 123-130.

Nelson, D.L., 2001. SNPs, linkage disequilibrium, human genetic variation and Native American culture. *Trends in Genetics*, 17, 15-16.

Newton, C.R., Graham, A., Heptinstall, L.E., Powell, S.J., Summers, C., Kalsheker, N., Smith, J.C., Markham, A.F., 1989. Analysis of any point mutation in DNA. The aplivication refractory mutation system (ARMS). *Nucleic Acids Research*, 17, 2503-2516.

Nirmal, M., Dabbousi, B., Bawendi, M., Macklin, J., Trautman, J., Harris, T., Brus, L., 1996. Fluorescence intermittency in single cadmium selenide nanocrystals. *Nature*, 383, 802-804.

Nolan, J.P., Mandy, F.F., 2001. Suspension array technology: new tools for gene and protein analysis. *Cellular and Molecular Biology*, 47, 1241-1256.

Nolan, J., Sklar, L., 2002. Suspension array technology: evolution of the flat-array paradigm. *Trends in Biotechnology*, 20, 9-12.

Nolan, J.P., Mandy, F., 2006. Multiplexed and microparticle-based analyses? Quantitative tools for the large-scale analysis of biological systems. *Cytometry Part A*, 69, 318-325.

Noordam, M.J., Repping, S., 2006. The human Y chromosome: a masculine chromosome. *Curr.Opin.Genet Dev.*, 16, 225-232.

Norris, D., Efros, A., Rosen, M., Bawendi, M., 1996. Size dependence of exciton fine structure in CdSe quantum dots. *Physical Review B*, 53, 16347-16354.

Oliphant, A., Barker, D.L., Stuelpnagel, J.R., Chee, M.S., 2002. BeadArray technology: enabling an accurate, cost-effective approach to high-throughput genotyping. *Biotechniques*, Suppl, 56-1.

Ozkan, M., 2004. Quantum dots and other nanoparticles: What can they offer to drug discovery? *Drug Discovery Today*, 9, 1065-1071.

Pack, S.P., Kamisetty, N.K., Nonogawa, M., Devarayapalli, K.C., Ohtani, K., Yamada, K., Yoshida, Y., Kodaki, T., Makino, K., 2007. Direct immobilization of DNA oligomers onto the amine-functionalized glass surface for DNA microarray fabrication through the activation-free reaction of oxanine. *Nucleic Acids Research*, 35.

Pease, A.C., Solas, D., Sullivan, E.J., Cronin, M.T., Holmes, C.P., Fodor, S.P.A., 1994. Light-generated oligonucleotide arrays for rapid DNA sequence analysis. *Proceedings of the National Academy of Sciences of the United States of America*, 91, 5022-5026.

Pellegrino, T., Manna, L., Kudera, S., Liedl, T., Koktysh, D., Rogach, A.L., Keller, S., Ra?dler, J., Natile, G., Parak, W.J., 2004. Hydrophobic nanocrystals coated with an amphiphilic polymer shell: A general route to water soluble nanocrystals. *Nano Letters*, 4, 703-707.

Peng, X., 2003. Mechanisms for the shape-control and shape-evolution of colloidal semiconductor nanocrystals. *Advanced Materials*, 15, 459-463.

Peng, Z.A., Peng, X., 2001. Formation of high-quality CdTe, CdSe, and CdS nanocrystals using CdO as precursor [6]. *Journal of the American Chemical Society*, 123, 183-184.

Penn, S.G., He, L., Natan, M.J., 2003. Nanoparticles for bioanalysis. *Curr.Opin.Chem.Biol.*, 7, 609-615.

Peterson, A.W., Heaton, R.J., Georgiadis, R.M., 2001. The effect of surface probe density on DNA hybridization. *Nucleic Acids Research*, 29, 5163-5168.

Petkovski, E., Keyser, C., Ludes, B., Hienne, R., 2003. Validation of SNPs as markers for individual identification. *Int. Congress Series*, 1239, 33-36.

Phillips, C., 2004. Using online databases for developing SNP markers of forensic interest. *Methods in Molecular Biology*, 297, 83-106.

Pierce, K.E., Rice, J.E., Sanchez, J.A., Brenner, C., Wangh, L.J., 2000. Real-time PCR using molecular beacons for accurate detection of the Y chromosome in single human blastomeres. *Mol.Hum.Reprod.*, 6, 1155-1164.

Pillai, S.G., Chiano, M.N., White, N.J., Speer, M., Barnes, K.C., Carlsen, K., Gerritsen, J., Helms, P., Lenney, W., Silverman, M., Sly, P., Sundy, J., Tsanakas, J., von Berg, A., Whyte, M., Varsani, S., Skelding, P., Hauser, M., Vance, J., Pericak-Vance, M., *et al.*, 2006. A genome-wide search for linkage to asthma phenotypes in the genetics of asthma international network families: evidence for a major susceptibility locus on chromosome 2p. *Eur.J Hum.Genet*, 14, 307-316.

Preziozo, V., Jahns, A., 2000. Using Gradient PCR to Determine the Optimum Annealing Temperature. *Bioresearch Online, www.bioresearchonline.com, Last visited March 2009*.

Price, G., Smith, P., 1991. Ultrasonic Degradation of Polymer Solutions. I. Polystyrene Revisited. *Polymer International*, 24, 159-164.

Prozorov, T., Prozorov, R., Suslick, K.S., 2004. High velocity interparticle collisions driven by ultrasound. *Journal of the American Chemical Society*, 126, 13890-13891.

Qi, L., Gao, X., 2008. Emerging application of quantum dots for drug delivery and therapy. *Expert Opinion on Drug Delivery*, 5, 263-267.

Quintana-Murci, L., Krausz, C., McElreavey, K., 2001. The human Y chromosome: function, evolution and disease. *Forensic Sci.Int.*, 118, 169-181.

Raghavachari, N., Bao, Y.P., Li, G., Xie, X., Muller, U.R., 2003. Reduction of autofluorescence on DNA microarrays and slide surfaces by treatment with sodium borohydride. *Analytical Biochemistry*, 312, 101-105.

Resch-Genger, U., Grabolle, M., Cavaliere-Jaricot, S., Nitschke, R., Nann, T., 2008. Quantum dots versus organic dyes as fluorescent labels. *Nature Methods*, 5, 763-775.

Riegger, L., Grumann, M., Nann, T., Riegler, J., Ehlert, O., Bessler, W., Mittenbuehler, K., Urban, G., Pastewka, L., Brenner, T., Zengerle, R., Ducree, J., 2006. Read-out concepts for multiplexed bead-based fluorescence immunoassays on centrifugal microfluidic platforms. *Sensors and Actuators, A: Physical*, 126, 455-462.

Rieger, J., Ehlert, O., Nann, T., 2006. A facile method for coding and labeling assays on polystyrene beads with differently colored luminescent nanocrystals. *Analytical and Bioanalytical Chemistry*, 384, 645-650.

Rosenthal, S.J., Tomlinson, I., Adkins, E.M., Schroeter, S., Adams, S., Swafford, L., McBride, J., Wang, Y., DeFelice, L.J., Blakely, R.D., 2002. Targeting cell surface receptors with ligand-conjugated nanocrystals. *Journal of the American Chemical Society*, 124, 4586-4594.

Ross, P., Hall, L., Smirnov, I., Haff, L., 1998. High level multiplex genotyping by MALDI-TOF mass spectrometry. *Nature Biotechnology*, 16, 1347-1351.

Rozen, S., Skaletsky, H., 2000. Primer3 on the WWW for general users and for biologist programmers. *Methods Mol Biol*, 132, 365-86.

Ruan, W., Eastman, P.S., Cooke, P.A., Park, J.S., Chu, J.S.F., Gray, J.W., Li, S., Chen, F.F., 2007. Nanobarcode gene expression monitoring system for potential miniaturized space applications. *Advances in Space Research*, 40, 513-522.

Russom, A., Haasl, S., Ohlander, A., Mayr, T., Brookes, A.J., Andersson, H., Stemme, G., 2004. Genotyping by dynamic heating of monolayered beads on a microheated surface. *Electrophoresis*, 25, 3712-3719.

Ryan, J.E., Dhiman, N., Ovsyannikova, I.G., Vierkant, R.A., Pankratz, V.S., Poland, G.A., 2009. Response surface methodology to determine optimal cytokine responses in human peripheral blood mononuclear cells after smallpox vaccination. *Journal of Immunological Methods*, 341, 97-105.

Salas, V.M., Edwards, B.S., Sklar, L.A., 2008. Advances in Multiple Analyte Profiling Advances in Clinical Chemistry, pp. 47-74.

Sanchez, J.J., Borsting, C., Hallenberg, C., Buchard, A., Hernandez, A., Morling, N., 2003. Multiplex PCR and minisequencing of SNPs--a model with 35 Y chromosome SNPs. *Forensic Sci.Int.*, 137, 74-84.

Sanchez, J.J., Endicott, P., 2006. Developing multiplexed SNP assays with special reference to degraded DNA templates. *Nat.Protoc.*, 1, 1370-1378.

Sanchez, J.J., Phillips, C., Borsting, C., Balogh, K., Bogus, M., Fondevila, M., Harrison, C.D., Musgrave-Brown, E., Salas, A., Syndercombe, C., Schneider, P.M., Carracedo, A., Morling, N., 2006. A multiplex assay with 52 single nucleotide polymorphisms for human identification. *Electrophoresis*, 27, 1713-1724.

Sanger, F., Nicklen, S., Coulson, A.R., 1977. DNA sequencing with chain-terminating inhibitors. *Proceedings of the National Academy of Sciences of the United States of America*, 74, 5463-5467.

Satarug, S., Moore, M.R., 2004. Adverse health effects of chronic exposure to low-level cadmium in foodstuffs and cigarette smoke. *Environmental health perspectives*, 112, 1099-1103.

Satarug, S., Nishijo, M., Ujjin, P., Vanavanitkun, Y., Moore, M.R., 2005. Cadmium-induced nephropathy in the development of high blood pressure. *Toxicology Letters*, 157, 57-68.

Sathe, T.R., Agrawal, A., Nie, S., 2006. Mesoporous silica beads embedded with semiconductor quantum dots and iron oxide nanocrystals: Dual-function microcarriers for optical encoding and magnetic separation. *Analytical Chemistry*, 78, 5627-5632.

Schram, K.H., 1990. Mass spectrometry: Applications in the analysis of nucleosides, nucleotides and oligonucleotides. *Nucleosides and Nucleotides*, 9, 311-317.

Schröck, E., du, M.S., Veldman, T., Schoell, B., Wienberg, J., Ferguson-Smith, M.A., Ning, Y., Ledbetter, D.H., Bar-Am, I., Soenksen, D., Garini, Y., Ried, T., 1996. Multicolor spectral karyotyping of human chromosomes. *Science*, 273, 494-497.

Schwartz, A., Marti, G.E., Poon, R., Gratama, J.W., Ferna?ndez-Repollet, E., 1998. Standardizing flow cytometry: A classification system of fluorescence standards used for flow cytometry. *Cytometry*, 33, 106-114.

Scott Higgins, G., Little, D.P., Koster, H., 1997. Competitive oligonucleotide single-base extension combined with mass spectrometric detection for mutation screening. *BioTechniques*, 23, 710-714.

Seamer, L.C., Bagwell, C.B., Barden, L., Redelman, D., Salzman, G.C., Wood, J.C.S., Murphy, R.F., 1997. Proposed new data file standard for flow cytometry, version FCS 3.0. *Cytometry*, 28, 118-122.

Shen, R., Fan, J.B., Campbell, D., Chang, W., Chen, J., Doucet, D., Yeakley, J., Bibikova, M., Garcia, E.W., McBride, C., Steemers, F., Garcia, F., Kermani, B.G., Gunderson, K., Oliphant, A., 2005. High-throughput SNP genotyping on universal bead arrays. *Mutation Research - Fundamental and Molecular Mechanisms of Mutagenesis*, 573, 70-82.

Sheng, W., Kim, S., Lee, J., Kim, S., Jensen, K., Bawendi, M., 2006. In-situ encapsulation of quantum dots into polymer microspheres. *Langmuir*, 22, 3782-3790.

Sherry, S.T., Ward, M.H., Kholodov, M., Baker, J., Phan, L., Smigielski, E.M., Sirotkin, K., 2001. DbSNP: The NCBI database of genetic variation. *Nucleic Acids Research*, 29, 308-311.

Shim, S.E., Ghose, S., Isayev, A.I., 2002. Formation of bubbles during ultrasonic treatment of cured poly(dimethyl siloxane). *Polymer*, 43, 5535-5543.

Simmer, M., 2008. Flow cytometry: a technology to count and sort cells. *The Science Creative Quarterly*.

Singh, B., Kumar, R., Abuja, N., 2005. Optimizing drug delivery systems using systematic design of experiments. Part I: Fundamental aspects. *Critical reviews in therapeutic drug carrier systems*, 22, 27-105.

Sklar, L.A., Carter, M.B., Edwards, B.S., 2007. Flow cytometry for drug discovery, receptor pharmacology and high-throughput screening. *Current Opinion in Pharmacology*, 7, 527-534.

Smith, R.A., Giorgio, T.D., 2008. Quantitative measurement of multifunctional quantum dot binding to cellular targets using flow cytometry. *Cytometry Part A*, on line publication.

Sobrino, B., Brion, M., Carracedo, A., 2005. SNPs in forensic genetics: a review on SNP typing methodologies. *Forensic Sci.Int.*, 154, 181-194.

Sokolov, B.P., 1990. Primer extension technique for the detection of single nucleotide in genomic DNA. *Nucleic Acids Research*, 18, 3671.

Son, A., Dosev, D., Nichkova, M., Ma, Z., Kennedy, I.M., Scow, K.M., Hristova, K.R., 2007. Quantitative DNA hybridization in solution using magnetic/luminescent core-shell nanoparticles. *Analytical Biochemistry*, 370, 186-194.

Spiro, A., Lowe, M., Brown, D., 2000. A Bead-Based Method for Multiplexed Identification and Quantitation of DNA Sequences Using Flow Cytometry. *Applied and Environmental Microbiology*, 66, 4258-4265.

Spiro, A., Lowe, M., 2002. Quantitation of DNA sequences in environmental PCR products by a multiplexed, bead-based method. *Applied and Environmental Microbiology*, 68, 1010-1013.

Stsiapura, V., Sukhanova, A., Artemyev, M., Pluot, M., Cohen, J.H.M., Baranov, A.V., Oleinikov, V., Nabiev, I., 2004. Functionalized nanocrystal-tagged fluorescent polymer beads: Synthesis, physicochemical characterization, and immunolabeling application. *Analytical Biochemistry*, 334, 257-265.

Sui, G., Orbulescu, J., Ji, X., Gattás-Asfura, K., Leblanc, R., Micic, M., 2003. Surface Chemistry Studies of Quantum Dots (QDs) Modified with Surfactants. *Journal of Cluster Science*, 14, 123-133.

Sukhanova, A., Nabiev, I., 2008. Fluorescent nanocrystal-encoded microbeads for multiplexed cancer imaging and diagnosis. *Crit Rev Oncol Hematol*.

Suppl, C., Salas, V.M., Edwards, B.S., Sklar, L.A., 2008. Advances in Multiple Analyte Profiling Advances in Clinical Chemistry, pp. 47-74.

Suslick, K.S., Hammerton, D.A., Cline, R.E., 1986. The sonochemical hotspot. *J. Am. Chem. Soc.*, 106, 6856.

Suslick, K.S., 1995. Applications of ultrasound to materials chemistry. *MRS Bulletin*, 20, 29-34.

Swafford, L.A., Weigand, L.A., Bowers Ii, M.J., McBride, J.R., Rapaport, J.L., Watt, T.L., Dixit, S.K., Feldman, L.C., Rosenthal, S.J., 2006. Homogeneously alloyed CdSxSe1-x nanocrystals: Synthesis, characterization, and composition/size-dependent band gap. *Journal of the American Chemical Society*, 128, 12299-12306.

Tanaka, M., Sudo, A., Sanda, F., Endo, T., 2000. Samarium enolate on crosslinked polystyrene beads: Anionic initiator for well defined synthesis of polymethacrylate on a solid support. *Chemical Communications*, 2503-2504.

Tang, K., Fu, D.J., Julien, D., Braun, A., Cantor, C.R., Ko?stek, H., 1999. Chip-based genotyping by mass spectrometry. *Proceedings of the National Academy of Sciences of the United States of America*, 96, 10016-10020.

Tatusova, T.A., Madden, T.L., 1999. BLAST 2 SEQUENCES, a new tool for comparing protein and nucleotide sequences. *FEMS Microbiology Letters*, 174, 247-250.

Tian, F., Wu, Y., Zhou, Y., Liu, X., Visvikis-Siest, S., Xia, Y., 2008. A new single nucleotide polymorphism genotyping method based on gap ligase chain reaction and a microsphere detection assay. *Clinical chemistry and laboratory medicine: CCLM/FESCC*.

Tilford, C.A., Kuroda-Kawaguchi, T., Skaletsky, H., Rozen, S., Brown, L.G., Rosenberg, M., McPherson, J.D., Wylie, K., Sekhon, M., Kucaba, T.A., Waterston, R.H., Page, D.C., 2001. A physical map of the human Y chromosome. *Nature*, 409, 943-945.

Tirri, M.E., Wahlroos, R., Meltola, N.J., Toivonen, J., Hanninen, P.E., 2006. Effect of polystyrene microsphere surface to fluorescence lifetime under two-photon excitation. *Journal of Fluorescence*, 16, 809-816.

Tobler, A.R., Short, S., Anderson, M.R., Paner, T.M., Briggs, J.C., Lambert, S.M., Wu, P.P., Wang, Y., Spoonde, A.Y., Koehler, R.T., Peyret, N., Chen, C., Broomer, A.J., Ridzon, D.A., Zhou, H., Hoo, B.S., Hayashibara, K.C., Leong, L.N., Ma, C.N., Rosenblum, B.B.*, et al.*, 2005. *J. Biomol. Tech*, 16, 396.

Tost, J., Gut, I.G., 2005. Genotyping single nucleotide polymorphisms by MALDI mass spectrometry in clinical applications. *Clinical Biochemistry*, 38, 335-350.

Tsay, J., Trzoss, M., Shi, L., Kong, X., Selke, M., Jung, M., Weiss, S., 2007. Singlet Oxygen Production by Peptide-Coated Quantum Dot-Photosensitizer Conjugates. *Journal of the American Chemical Society*, 129, 6865-6871.

Tyagi, S., Bratu, D.P., Kramer, F.R., 1998. Multicolor molecular beacons for allele discrimination. *Nature Biotechnology*, 16, 49-53.

Tycko, D.H., Metz, M.H., Epstein, E.A., Grinbaum, A., 1985. Flow-cytometric light scattering measurement of red blood cell volume and hemoglobin concentration. *Appl. Opt.*, 24, 1355-1365.

Underhill, P., Shen, P., Lin, A., Jin, L., Passarino, G., Yang, W., Kauffman, E., Bonné-Tamir, B., Bertranpetit, J., Francalacci, P., 2000. Y chromosome sequence variation and the history of human populations. *Nature Genetics*, 26, 358-361.

Vallone, P.M., Butler, J.M., 2004. AutoDimer: a screening tool for primer-dimer and hairpin structures. *Biotechniques*, 37, 226-231.

Vijayalakshmi, S., Madras, G., 2004. Effect of temperature on the ultrasonic degradation of polyacrylamide and poly (ethylene oxide). *Polymer Degradation and Stability*, 84, 341-344.

Villablanca, A., Karhanek, M., Caramuta, S., Yu, H., Jejelowo, O., Webb, C.D., Pourmand, N., 2008. Suspension bead array branch migration displacement assay for rapid STR analysis. *Electrophoresis*, 29, 4109-4114.

Vu, T.Q., Maddipati, R., Blute, T.A., Nehilla, B.J., Nusblat, L., Desai, T.A., 2005. Ligand-conjugated quantum dots for targeted drug delivery to nerve cells 2005 3rd IEEE/EMBS Special Topic Conference on Microtechnology in Medicine and Biology, pp. 152-153.

Wallace, R.B., Shaffer, J., Murphy, R.F., Bonner, J., Hirose, T., Itakura, K., 1979. Hybridization of synthetic oligodeoxyribonucleotides to phi chi 174 DNA: the effect of single base pair mismatch. *Nucleic Acids Research*, 6, 3543-3557.

Wang, H., Liu, T., Cao, Y., Huang, Z., Wang, J., Li, X., Zhao, Y., 2006. A flow cytometric assay technology based on quantum dots-encoded beads. *Analytica Chimica Acta*, 580, 18-23.

Wang, H.Q., Wang, J.H., Li, Y.Q., Li, X.Q., Liu, T.C., Huang, Z.L., Zhao, Y.D., 2007. Multi-color encoding of polystyrene microbeads with CdSe/ZnS quantum dots and its application in immunoassay. *Journal of Colloid and Interface Science*, 316, 622-627.

Wang, J., Liu, G., Rivas, G., 2003. Encoded beads for electrochemical identification. *Analytical Chemistry*, 75, 4667-4671.

Wang, L., Tan, W., 2006. Multicolor FRET silica nanoparticles by single wavelength excitation. *Nano Letters*, 6, 84-88.

Watson, J.D., Crick, F.H., 1953. The structure of DNA. *Cold Spring Harb.Symp.Quant.Biol.*, 18, 123-131.

Werntges, H., Steger, G., Riesner, D., Fritz, H., 1986. Mismatches in DNA double strands: thermodynamic parameters and their correlation to repair efficiencies. *Nucleic Acids Res*, 14, 3773-3790.

Wetmur, J.G., 1991. DNA probes: Applications of the principles of nucleic acid hybridization. *Critical Reviews in Biochemistry and Molecular Biology*, 26, 227-259.

Wetton, J.H., Tsang, K.W., Khan, H., 2005. Inferring the population of origin of DNA evidence within the UK by allele-specific hybridization of Y-SNPs. *Forensic Sci.Int.*, 152, 45-53.

Wilson, R., Spiller, D., Prior, I., Bhatt, R., Hutchinson, A., 2007. Magnetic microspheres encoded with photoluminescent quantum dots for multiplexed detection. *Journal of Materials Chemistry*, 17, 4400-4406.

Wittebolle, L., Verstuyft, K., Verstraete, W., Boon, N., 2006. Technical Note Optimisation of the amino–carboxy coupling of oligonucleotides to beads used in liquid arrays. *Journal of Chemical Technology and Biotechnology*, 81.

Wong, S.S., 1991. Reactive groups of proteins and their modifying agents. *Chemistry of Protein Conjugation and Cross-Linking*, 13.

Wrobel, G., Schlingemann, J., Hummerich, L., Kramer, H., Lichter, P., Hahn, M., 2003. Optimization of high-density cDNA-microarray protocols by'design of experiments'. *Nucleic Acids Research*, 31, e67.

Wu, P., Xu, H., Sha, M., Wong, E., Treadway, J., Yong, H., Xu, Y., Wang, E., Chin, R., Jin, J., 2002. A multiplex assay platform using microparticles encoded with quantum dots, pp. 22–26.

Wu, X., Liu, H., Liu, J., Haley, K.N., Treadway, J.A., Larson, J.P., Ge, N., Peale, F., Bruchez, M.P., 2003. Immunofluorescent labeling of cancer marker Her2 and other cellular targets with semiconductor quantum dots. *Nature Biotechnology*, 21, 41-46.

Wu, Y., Campos, S., Lopez, G., Ozbun, M., Sklar, L., Buranda, T., 2007. The development of quantum dot calibration beads and quantitative multicolor bioassays in flow cytometry and microscopy. *Analytical Biochemistry*, 364, 180-192.

Xu, C., Bakker, E., 2007. Multicolor quantum dot encoding for polymeric particle-based optical ion sensors. *Analytical Chemistry*, 79, 3716-3723.

Xu, H., Sha, M., Wong, E., Uphoff, J., Xu, Y., Treadway, J., Truong, A., O'Brien, E., Asquith, S., Stubbins, M., 2003. Multiplexed SNP genotyping using the Qbead (TM) system: a quantum dot-encoded microsphere-based assay. *Nucleic Acids Research*, 31, e43.

Yang, P., Ando, M., Murase, N., 2007. Encapsulation of emitting CdTe QDs within silica beads to retain initial photoluminescence efficiency. *Journal of Colloid and Interface Science*, 316, 420-427.

Ye, F., Li, M., Taylor, J., Nguyen, Q., Colton, H., Casey, W., Wagner, M., Weiner, M., Chen, J., 2001. Fluorescent microsphere-based readout technology for multiplexed human single nucleotide polymorphism analysis and bacterial identification. *Human Mutation*, 17, 305-316.

Zalloua, P., Xue, Y., Khalife, J., Makhoul, N., Debiane, L., Platt, D., Royyuru, A., Herrera, R., Hernanz, D., Blue-Smith, J., 2008. Y-chromosomal diversity in Lebanon is structured by recent historical events. *The American Journal of Human Genetics*, 82, 873-882.

Zenger, V.E., Vogt, R., Mandy, F., Schwartz, A., Marti, G.E., 1998. Quantitative flow cytometry: Inter-laboratory variation. *Cytometry*, 33, 138-145.

Zhang, H., Cui, Z., Wang, Y., Zhang, K., Ji, X., Lu, C., Yang, B., Gao, M., 2003. From water-soluble CdTe nanocrystals to fluorescent nanocrystal-polymer transparent composites using polymerizable surfactants. *Advanced Materials*, 15, 777-780.

Zhang, W., Ratain, M., Dolan, M., 2008. The HapMap resource is providing new insights into ourselves and its application to pharmacogenomics. *Bioinformatics and biology insights*, 2, 15.

Zhong, X., Han, M., Dong, Z., White, T., Knoll, W., 2003. Compositiontunable ZnxCd1-xSe nanocrystals with high luminescence and stability (2003). *Journal of the American Chemical Society*, 125, 8589-8594.

Zhou, M., Chang, S., Grover, C.P., 2004. Cryptography based on the absorption/emission features of multicolor semiconductor nanocrystal quantum dots. *Optics Express*, 12, 2925-2931.

Zucker, R.M., Rigby, P., Clements, I., Salmon, W., Chua, M., 2007. Reliability of confocal microscopy spectral imaging systems: Use of multispectral beads. *Cytometry Part A*, 71, 174-189.

Appendices

APPENDIX A Quantum dot-encoded microsphere (QDEM) populations (Crystalplex, PA, USA)

Table 1 lists the QDEMs available, purchased during the research project. The optical specificities of the QDEMs are described as follow:

- Diameter (in µm);
- ***λe*** gave the emission wavelength (in nm) of the QDs trapped in the microsphere; when the bead are encoded with 2 or 3 different QDs, the emission wavelength of the QDs is indicated into brackets;
- ***I*** describe the relative intensity of each QD present in the bead compared to the others. The position of the intensity number into the brackets correspond to the emission wavelength at the same position in the brackets.

As an example, a two-colours QDEM (525;575) (2:1) was composed of two times more QDs emitting at 525 nm than QDs emitting at 575 nm. Single-colour beads could have also variable relative intensity. The precise amount of coloured QDs encoded in the microsphere defined the level of intensity. As an example, the 575QDEM of 20 µm diameters were encoded with 4 different levels of 575QDs intensity.

Table 1. Research project QDEM library *

QDEM	1 colour		2 colours		3 colours		4 colours		
Diameter (µm)	λe (nm)	Intensity (I) ratios	λe (nm)	I ratios	λe (nm)	I ratios	λe (nm)	I ratios	I ratios
5	0		(525:575)	(1:1)	(525:575:630)	(1:1:1)	(525:575:630:675)	(0:0:0:0)	(1:0:0:1)
	525	(1)		(2:1)	(575:615:675)	(1:1:1)		(1:0:0:0)	(1:1:0:1)
	575	(1)		(1:2)				(0:1:0:0)	(1:0:1:1)
	615	(1)		(3:1)				(0:0:1:0)	(1:0:1:0)
	630	(1)	(615:665)	(1:1)				(0:0:0:1)	(0:1:0:1)
	665	(1)	(575:675)	(1:1)				(1:1:0:0)	(0:1:1:0)
	675	(1)	(615:675)	(1:1)				(1:1:1:0)	(0:0:1:0)
								(0:1:1:1)	(1:1:1:1)
20	0								
	575	(1)							
		(2)							
		(3)							
		(4)							

* Numbers indicated for the intensity ratio are relative and not equal in terms of amount of QDs, all the codes of the QDEMs were obtained from Crystalplex (PA, USA).

APPENDIX B Quantum dot-encoded microspheres supplier's composition information sheet

Table 1. Composition, Information on Ingredients

(http://www.proteopure.com/proteocolor/proteocolor_plxbeads_msds.pdf)

Name	*CAS #*	*% by weight*
Water	7732-18-5	97.0-98.5
Polystyrene	9003-70-7	0.5-2.0
Sodium Chloride	7647-14-5	0.8
Tris (Hydroxymethyl) Aminomethane Free Base	77-86-1	0.11
Tris (Hydroxymethyl) Aminomethane Hydrochloride Salt	1185-53-1	0.02
Potassium chloride	7447-40-7	0.02
Divinyl benzene	1321-74-0	0.01
Sodium Azide	26628-22-8	0.01
BSA	9048-46-8	0-1
CdSe	1306-24-7	<0.001

APPENDIX C Quantum dot-encoded microspheres enumeration

QDEM stock solution were quantified using a Neubauer haemocytometer (Reichert, Bright-line®, NY, USA) was used for

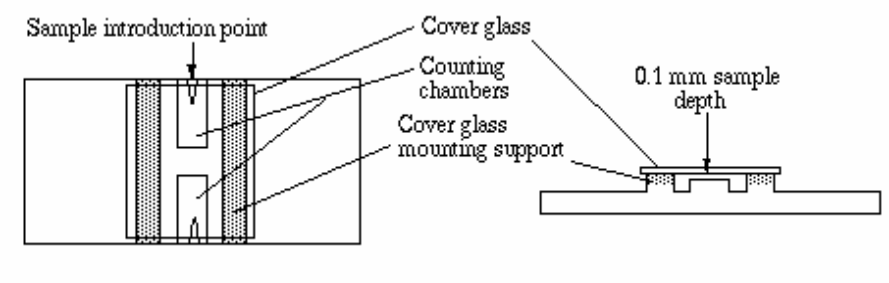

Figure 1. The haemocytometer (www.ruf.rice.edu, last visited sept 2008).

A cover slip is moistened and placed on the haemocytometer covering the 2 central channels. A drop of the bead dilution was placed underneath the cover slip at the sample introduction point and the whole counting chamber was then filled by capillary action. A cell count was then performed by following the methods described bellow.

The haemocytometer contains two identical grids one on the upper counting chamber and one on the lower counting chamber (Figure A.2). Each grid consists of four corner squares containing 16 smaller squares and one central square containing 25 little squares. When viewed under a microscope if the cellular number exceeded 200 when counting the central square alone, then only the two central squares on both grids were counted and an average was calculated. However if the bead number did not exceed 200, then all 4 corner squares were counted on each grid plus the central square.

- As an example: supposedly 187 particles were counted in the 25 little squares described. Each square has an area of 1/25 mm^2 (that is, 0.04 mm^2) and depth of 0.1 mm. The total volume in each square is (0.04) x (0.1) = 0.004 mm^3. You have 25 squares with combined volume of 25 x (0.004) = 0.1 mm^3. Thus you counted 187 particles in a volume of 0.1 mm^3, giving you 187 / 0.1 = 1870 particles per mm^3. There are 1000 cubic millimeters in one cubic centimeter (same as a milliliter), so the bead count is 1,870,000 per ml.

- Supposing a total number of beads in the four large corner squares plus the middle combined. was 125 beads; each square has surface area of 1 mm^2 and a depth of 0.1 mm, giving it a volume of 0.1 mm^2. You then have 125 cells per 0.5 mm^2, which is 250 cells / mm^2. Again, multiply by 1000 to determine cell count per ml (250,000).

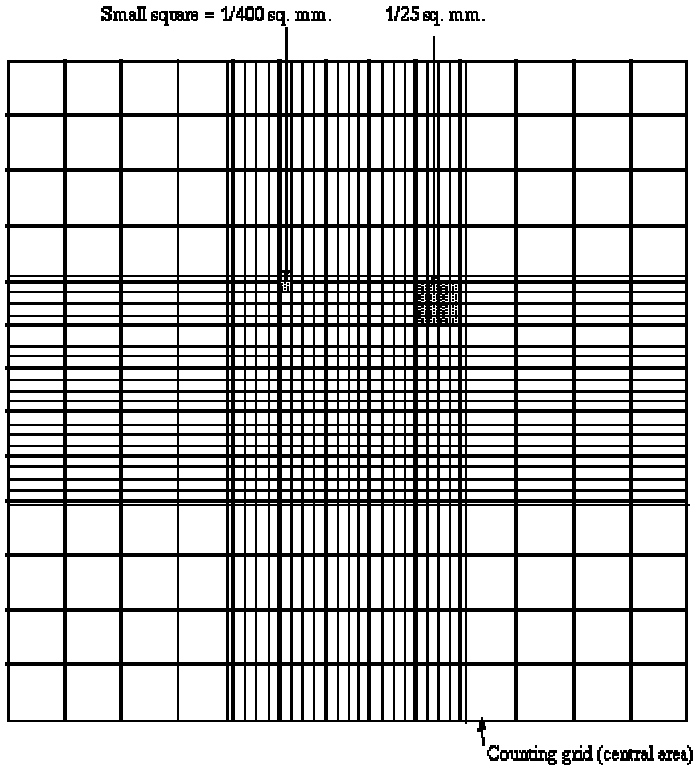

Figure 2. Diagram of the grid on the hemocytometer (www.ruf.rice.edu, last visited sept 2008).

Each of the 9 square is 1mm and the depth between the coverslip and grid is 0.1mm, (http://www.ruf.rice.edu/~bioslabs/methods/microscopy/cellcounting.html).

APPENDIX D Titration of the carboxylated groups on the polystyrene microspheres

The titration was undertaken with 6 µL of carboxyl functionalised 5 µm acrylic blank beads (*i.e.* not encoded with nanocrystals, taken from the initial solution in the glass vial), with a base solution of NaOH at 0.8 mM, and an acid solution of HCL at 1 mM.
The concentration (in $mol.L^{-1}$) of ($-CH_3COOH$) groups on the QDEM surface was calculated as followed using the titration curves (Figure C.1.).

The volume needed to reach the equivalence on the graph C.1.A was evaluated at 200 µL, therefore:

$$\mathbf{n_{OH}} = n_{HCL} = n_{COOH} = Veq \times C_{NaOH} = 200.10^{-6} \times 0.8.10^{-3} = 0.16\ \mu mol = \boldsymbol{0.16\ \mu eq}$$

The volume needed to reach the equivalence on the graph C.1.B was evaluated at 156 µL, which means a quantity of:

$$\mathbf{n_{HCL}} = n_{OH} = n_{COOH} = Veq \times C_{HCl} = 156.10^{-6} \times 1.10^{-3} = 0.156\ \mu mol = \boldsymbol{0.156\ \mu eq}$$

The concentration of the blank-QDEM solution (C_{QDEM}) is estimated by the supplier at $1.46.10^7$ $bead.mg^{-1}$ in 1 mL buffer solution, therefore:

- the number of beads titrated is:

$$6.10^{-3} \times 1.46.10^7 = 87{,}600 \text{ beads}$$

- the average of n_{COOH} per bead is (in mol or $eq.bead^{-1}$):

$$[(0.16 + 0.156)/2].10^{-6} / 87600 = 1.8 .10^{-12}\ mol.bead^{-1} = \boldsymbol{1.8 .10^{-12}\ eq.bead^{-1}}$$

- and the concentration **C** of (COOH) group per mL is (in mol or $eq.L^{-1}$):

$$C_{COOH} = n_{COOH} \times C_{QDEM} = \boldsymbol{26.3\ \mu mol.mL^{-1}\ or\ 26.3\ meq.g^{-1}}$$

Another way of presenting the data is to calculate the average density coverage of carboxylated group on the bead surface equivalent to 78.5 μm^2 (in mol or $eq.\mu m^2$):

$$d_{COOH} = (\text{average } n_{COOH} / S) = 1.8.10^{-12} / 78.5 = \boldsymbol{22.9\ mmol.m^2\ or\ 22.9\ meq.m^2}$$

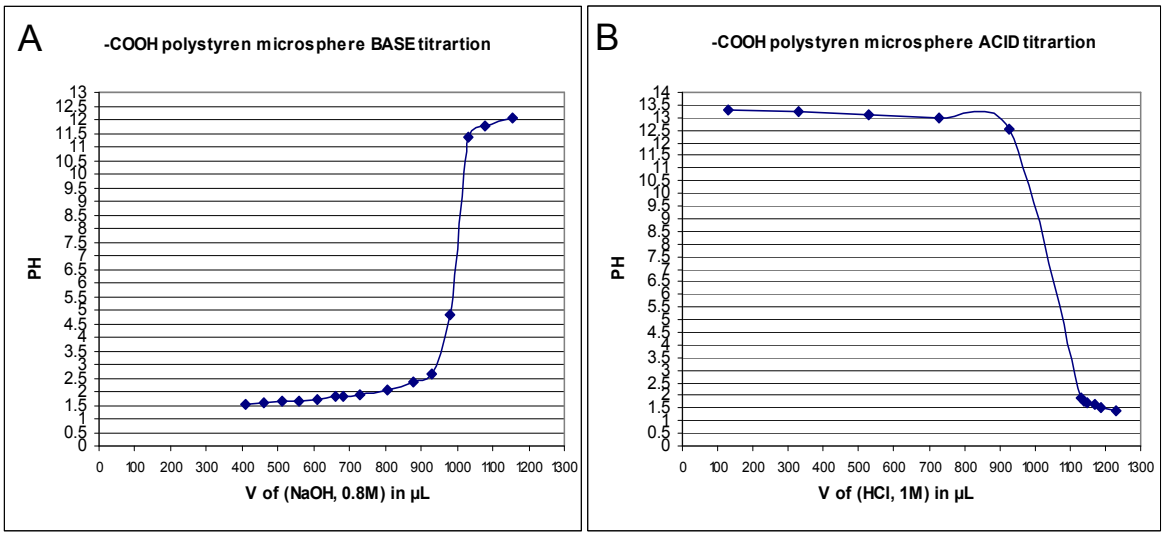

Figure 1. Acid/base titration curves

APPENDIX E The carbodiimide coupling reaction mechanism

Carbodiimides react with carboxyls to form an intermediate that can stabilize with reaction with amines, forming a peptidic bond, without spacer length. 1-Ethyl-3-(3-dimethylaminopropyl)-carbodiimide (EDC) is a water-soluble derivative of carbodiimide. Carbodiimide catalyzes the formation of amide bonds between carboxylic acids or phosphates and amines by activating carboxyl or phosphate to form an O-urea derivative. This derivative reacts readily with nucleophiles. The reagent can be used to make ether links from alcohol groups and ester links from acid and alcohols or phenols, and peptide bonds from acid and amines (Tedder *et al.* 1972). Carbodiimide is often used in the synthesis of peptides as the water-soluble derivative EDC or as the organic soluble derivative, *N,N′*-dicyclohexyl-carbodiimide (DCC).

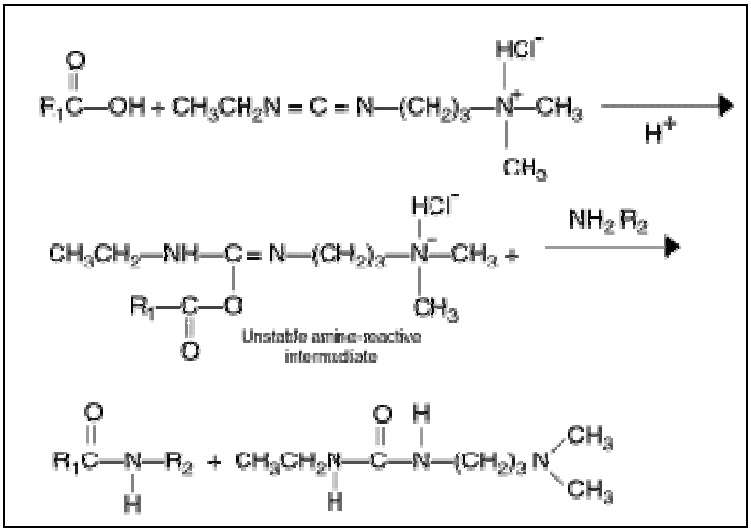

Figure 1 Mechanism of activation of carboxylic groups by EDC and further reaction with amines resulting in the amide bond formation

APPENDIX F Profile of 525-QDEM after homogenisation

(a)

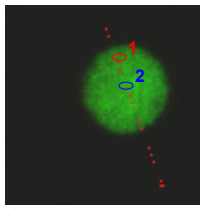

(b)

	Marker 1	marker 2	Difference
Disatnce (µm)	2.45	4.65	2.2
Intensity Ch1	126	149	23
Intensity Ch2	17	18	1

(c)

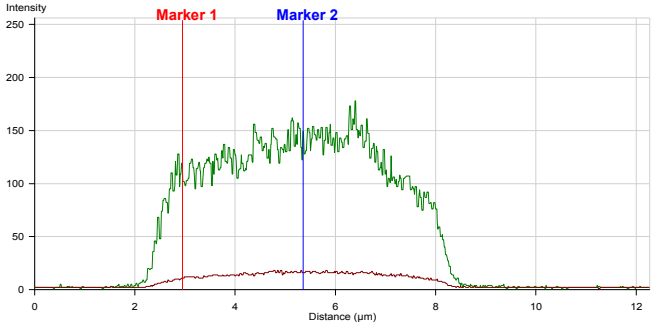

Figure 1. 525-QDEM confocal images

525-QDEM solution was vortexed (15 s) and sonicated (40 s) 3 times before microscopy analysis

APPENDIX G Long term storage in TE and in PBS

Long-term storage was also investigated. The fluorescent code and intensity as well as the microsphere concentration were stable in TBS storage buffer after months, whereas in TE buffer and PBS a significant decrease of the fluorescent code and of the number of QDEMs appeared after 24 h. High temperatures also increase these effects.

Fi

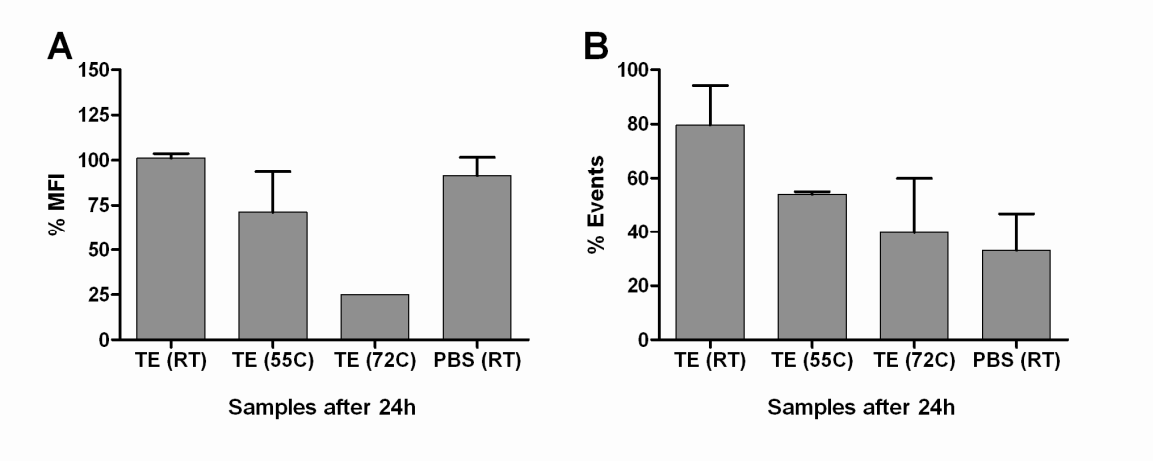

Figure 1 Effect of TE and PBS over time and temperature.

H: hour; RT: room temperature; temperature in °C.

APPENDIX H High resolution SEM images of 525QDEM stock solution

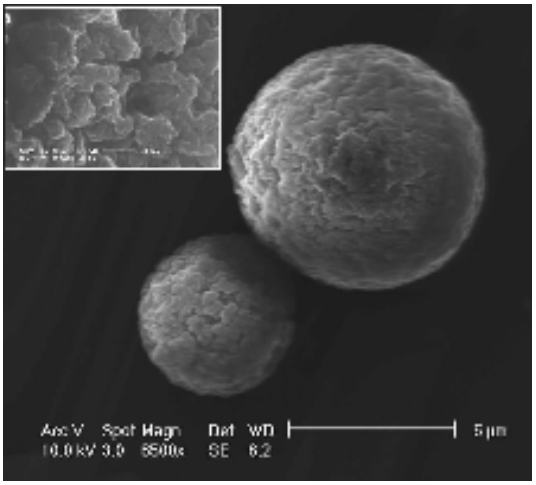

Figure 1. SEM images of 525-QDEM bio-conjugates

The inset is a 15.4-fold magnification of the QDEM surface, and imagined were taken in the same conditions.

APPENDIX I Supplementary materials for the statistical analysis of QDEM and QDEM bioconjugates population

Table 1.a MFI (in a.u.) and percentage of events for 0QDEM replicates*

0 QDEM										
Parameters / replicates	SSC 0 bioconj	FSC 0 bioconj	FL1 0 bioconj	FL2 0 bioconj	EVENTS % 0 bioconj	SSC 0	FSC 0	FL1 0	FL2 0	EVENTS % 0
1	181	227	197	78	49	152	197	88	271	95
2	183	252	230	95	50	184	255	29	284	82
3	201	252	292	113	66	230	272	128	319	83
4	176	271	272	115	60	206	277	95	327	88
5	178	233	242	116	68	184	249	45	339	87
6	204	248	253	79	61	240	406	83	270	93
7	185	253	189	94	40	240	406	83	243	93
8	191	246	267	114	84	237	386	0	352	95
9	199	256	256	113	62	240	406	60	286	86
10	188	239	305	117	62	132	451	196	350	80
11	195	264	147	100	58	177	219	264	210	96

* MFI calculated with WinMDI2.8 (CA, USA) on gated population

Table 1.b MFI (in a.u.) and percentage of events for 525QDEM replicates*

525 QDEM								
Parameters / replicates	SSC bioconj	FSC bioconj	FL1 bioconj	EVENTS % bioconj	SSC	FSC	FL1	Events %
1	244	372.5	502	56.1	236	421.5	801	89.43
2	236.5	405.5	583.5	67.39	224	380	766	89.43
3	240	403	582	65.98	212	380.5	786	85.23
4	225	382.5	574.5	29.7	227	391	793	84.81
5	234	375	543	81.42	224	380	766	87.52
6	239	379	514	67.33	212	380.5	786	85.23
7	234	383	561	79.55	233	411	807	89.49
8	237	361	430	54.69	241	431	793	89.03
9	233	399	569	72.24	241	431	793	89.03
10	235	386	529	74.11	233	411	807	89.49
11	234	386	539.6667	79.54333	212	380.5	786	85.23
12	219	348.6667	506	80.13	212	380.5	786	85.23

* MFI calculated with WinMDI2.8 (CA, USA) on gated population

Table 2.a Column statistics and normality tests of 0QDEM data

	0 QDEM									
Parameters / Statistics	**SSC bioconj**	**FSC bioconj**	**FL1 bioconj**	**FL2 bioconj**	**%Events bioconj**	**SSC**	**FSC**	**FL1**	**FL2**	**% Events**
Number of values	11	11	11	11	11	11	11	11	11	11
Minimum	176	227	147	78	40	132	197	0	210	80
25% Percentile	181	239	197	94	50	177	249	45	270	83
Median	188	252	253	113	61	206	277	83	286	88
75% Percentile	199	256	272	115	66	240	406	128	339	95
Maximum	204	271	305	117	84	240	451	264	352	96
Mean	189.2	249.2	240.9	103.1	60	202	320.4	97.36	295.5	88.91
Std. Deviation	9.569	12.81	47.22	14.78	11.45	38.77	90.8	75.65	45.98	5.77
Std. Error	2.885	3.863	14.24	4.457	3.451	11.69	27.38	22.81	13.86	1.74
Lower 95% CI of mean	182.8	240.6	209.2	93.16	52.31	176	259.4	46.54	264.7	85.03
Upper 95% CI of mean	195.6	257.8	272.6	113	67.69	228	381.4	148.2	326.4	92.79
D'Agostino & Pearson omnibus normality test										
K2	1.635	0.05685	1.243	1.95	1.646	1.377	4.525	4.459	0.605	2.729
P value	0.4415	0.972	0.5372	0.3771	0.4391	0.5023	0.1041	0.1076	0.739	0.2555
Passed normality test (alpha=0.05)?	Yes	Yes	Yes	Yes	Yes	Yes	Yes	Yes	Yes	Yes
P value summary	ns	ns	ns	ns	ns	ns	ns	ns	ns	ns
Coefficient of variation	5.06%	5.14%	19.60%	14.34%	19.08%	19.19%	28.34%	77.70%	15.56%	6.49%
Geometric mean	189	248.9	236.2	102.1	59	198.3	308.5		292.1	88.74
Lower 95% CI of geo. mean	182.7	240.4	204.3	92.12	51.78	172.7	253.6		261.8	84.92
Upper 95% CI of geo. mean	195.5	257.7	273	113.1	67.22	227.8	375.1		325.9	92.72
Sum	2081	2741	2650	1134	660	2222	3524	1071	3251	978

Table 2.b Column statistics and normality tests of 525QDEM data

	525 QDEM							
Parameters / Statistics	**SSC bioconj**	**FSC bioconj**	**FL bioconj**	**Events % bioconj**	**SSC**	**FSC**	**FL**	**Events %**
Number of values	12	12	12	12	12	12	12	12
Minimum	219	348.7	430	29.7	212	380	766	84.81
25% Percentile	233.3	373.1	508	58.57	212	380.5	786	85.23
Median	234.5	382.8	541.3	69.82	225.5	385.8	789.5	88.27
75% Percentile	238.5	395.8	573.1	79.55	235.3	418.9	799	89.43
Maximum	244	405.5	583.5	81.42	241	431	807	89.49
Mean	234.2	381.8	536.1	67.35	225.6	398.2	789.2	87.43
Std. Deviation	6.631	16.56	44.16	14.88	11.44	21.3	13.26	2.085
Std. Error	1.914	4.779	12.75	4.295	3.302	6.148	3.827	0.602
Lower 95% CI of mean	230	371.2	508.1	57.9	218.3	384.7	780.7	86.1
Upper 95% CI of mean	238.4	392.3	564.2	76.8	232.9	411.7	797.6	88.75
D'Agostino & Pearson omnibus normality test								
K2	5.123	0.6344	5.684	9.37	3.137	3.742	0.8714	10.4
P value	0.0772	0.7282	0.0583	0.0092	0.2084	0.154	0.6468	0.0055
Passed normality test (alpha=0.05)?	Yes	Yes	Yes	No	Yes	Yes	Yes	No
P value summary	ns	ns	ns	**	ns	ns	ns	**
Coefficient of variation	2.83%	4.34%	8.24%	22.09%	5.07%	5.35%	1.68%	2.39%
Geometric mean	234.1	381.4	534.4	65.32	225.3	397.7	789.1	87.41
Lower 95% CI of geo. mean	229.9	371	505.7	54.62	218.2	384.6	780.7	86.09
Upper 95% CI of geo. mean	238.4	392.2	564.6	78.11	232.7	411.3	797.6	88.74
Sum	2811	4581	6434	808.2	2707	4779	9470	1049

Table 3. ANOVA tables for 0 and 525QDEM analysis

Table Analyzed	0 QDEM			525 QDEM		
One-way analysis of variance						
P value	P<0.0001			P<0.0001		
P value summary	***			***		
Are means signif. different? (P < 0.05)	Yes			Yes		
Number of groups	8			6		
F	20.29			1063		
R squared	0.6284			0.9877		
ANOVA Table	***SS***	***df***	***MS***	***SS***	***df***	***MS***
Treatment (between columns)	512200	7	73170	2684000	5	536800
Residual (within columns)	202900	80	2536	33320	66	504.8
Total	715100	87		2718000	71	

* SS: sum-of-square; df: degree of freedom; MS: mean square

Table 4. D'Agostino & Pearson normality tests of paired data

	0 control - bioconjugate					525 control - bioconjugate			
Parameters / Statistics	**SSC**	**FSC**	**FL1**	**FL2**	**% Events**	**SSC**	**FSC**	**FL1**	**% Events**
Number of values	11	11	11	11	11	12	12	12	12
Minimum	-56	-45	-267	-238	11	-28	-25.5	182.5	5.1
25% Percentile	-18	3	-197	-223	18	-19.63	-3.75	219.6	7.06
Median	29	20	-170	-193	28	-7.5	16.75	246.2	17.35
75% Percentile	41	153	-109	-173	38	1.25	31.96	279.5	30.51
Maximum	55	212	117	-110	53	8	70	363	55.11
Mean	12.82	71.18	-143.5	-192.5	28.91	-8.625	16.44	253	20.08
Std. Deviation	35.2	91.27	99.03	37.81	12.96	11.92	28.27	48.92	14.7
Std. Error	10.61	27.52	29.86	11.4	3.907	3.441	8.16	14.12	4.244
Lower 95% CI of mean	-10.83	9.864	-210.1	-217.9	20.2	-16.2	-1.515	221.9	10.74
Upper 95% CI of mean	36.46	132.5	-77.02	-167.1	37.61	-1.052	34.4	284.1	29.42
D'Agostino & Pearson omnibus normality test									
K2	1.433	4.201	14.31	3.313	0.7928	1.057	0.1527	2.813	5.984
P value	0.4886	0.1224	0.0008	0.1908	0.6727	0.5895	0.9265	0.245	0.0502
Passed normality test (alpha=0.05)?	**Yes**	**Yes**	**No**	**Yes**	**Yes**	**Yes**	**Yes**	**Yes**	**Yes**
P value summary	ns	ns	***	ns	ns	ns	ns	ns	ns
Sum	141	783	-1579	-2117	318	-103.5	197.3	3036	241

* Std: standard; corrected paired data correspond to (control – bioconjugate) values

Table 5. Paired *t*-test results

Parameters/test	0 control vs bioconjugate				525 control vs bioconjugate			
Paired *t*-test	**SSC**	**FSC**	**FL2**	**%Events**	**SSC**	**FSC**	**FL2**	**%Events**
P value	0.2549	0.0271	P<0.0001	P<0.0001	0.0291	0.069	P<0.0001	P=0.0006
P value summary	**ns**	★	★★★	★★★	★	**ns**	★★★	★★★
Are means signif. different? (P < 0.05)	No	Yes	Yes	Yes	Yes	No	Yes	Yes
One- or two-tailed P value?	Two-tailed	Two-tailed	Two-tailed	Two-tailed	Two-tailed	Two-tailed	Two-tailed	Two-tailed
t, df	t=1.208 df=10	t=2.587 df=10	t=16.88 df=10	t=7.400 df=10	t=2.507 df=11	t=2.015 df=11	t=4.731 df=11	t=4.731 df=11
Number of pairs	11	11	11	11	12	12	12	12
How big is the difference?								
Mean of differences	12.82	71.18	-192.5	28.91	-8.625	16.44	20.08	20.08
95% confidence interval	-10.83 to 36.46	9.868 to 132.5	-217.9 to -167.1	20.20 to 37.61	-16.20 to -1.052	-1.515 to 34.40	10.74 to 29.42	10.74 to 29.42
R squared	0.1273	0.4008	0.9661	0.8456	0.3636	0.2697	0.6705	0.6705

* vs: versus; signif.: significantly; df: degree of freedom

Table 6. Wilcoxon matched pairs nonparametric test results

Parameter	**FL1**	
Table Analyzed	**0 QDEM**	**525 QDEM**
Wilcoxon signed rank test	control vs bioconj	control vs bioconj
P value	0.0112	0.0005
Exact or approximate P value?	Gaussian Approximation	Gaussian Approximation
P value summary	*	***
Are medians signif. different? (P < 0.05)	Yes	Yes
One- or two-tailed P value?	Two-tailed	Two-tailed
Sum of positive, negative ranks	4.00, -62.00	78, 0.00
Sum of signed ranks (W)	-58.0000	78.0000

Table 7. ANOVA tables of SSC, FSC analysis for 0 and 525QDEM corrected data (control (c)– bioconjugates (b))

Table Analyzed	**(SSC,FSC)**		
One-way analysis of variance			
P value	0.0039		
P value summary	**		
Are means signif. different? (P < 0.05)	Yes		
Number of groups	4		
F	5.17		
R squared	0.2697		
ANOVA Table	***SS***	***df***	***MS***
Treatment (between columns)	39160	3	13050
Residual (within columns)	106000	42	2525
Total	145200	45	

Table 8. Tukey-Kramer's multiple comparison test for SSC, FSC analysis of 0 and 525QDEM corrected data (control (c)– bioconjugates (b)).

Tukey's Multiple Comparison Test	Mean Diff.	q	Significant? P < 0.05?	Summary	95% CI of diff
0 SSC (c -b) vs 525 SSC (c -b)	21.44	1.446	No	ns	-34.70 to 77.59
0 FSC (c -b) vs 525 FSC (c -b)	54.74	3.691	No	ns	-1.409 to 110.9

* 0 : 0QDEM; 525: 0QDEM ; c for control samples and b for bioconjugates samples; Diff: difference; CI of diff: confidence interval of the difference

Table 9. Unpaired t test on the corrected percentage of events between 0 and 525QDEM population.

Parameters/test	**0 vs 525**
Unpaired *t*-test	**% Events**
P value	0.143
P value summary	**ns**
Are means signif. different? (P < 0.05)	No
One- or two-tailed P value?	Two-tailed
t, df	t=1.522 df=21
How big is the difference?	
Mean ± SEM of column C	28.91 ± 3.907 N=11
Mean ± SEM of column F	20.08 ± 4.244 N=12
Difference between means	8.829 ± 5.802
95% confidence interval	-3.239 to 20.90
R squared	0.09931
F test to compare variances	
F,DFn, Dfd	1.288, 11, 10
P value	0.6978
P value summary	ns
Are variances significantly different?	No

APPENDIX J Response surface experiment worksheet and results analysis obtained with the experimental data

Table 1 DOE-1 with 3X SSC hybridisation buffer

	Factors variables		
Number of Replicates	Temp (ºC)	Time (min)	Conc (pmol)
3	60	60	0.05
3	45	60	0.05
3	52.5	30	100
3	52.5	60	50.025
3	45	60	100
3	60	30	50.025
3	45	90	50.025
3	52.5	90	100
3	52.5	30	0.05
3	60	90	50.025
3	45	30	50.025
3	52.5	60	50.025
3	52.5	60	50.025
3	60	60	100
3	52.5	90	0.05

Table 2 DOE-1 with 6X SSC hybridisation buffer

	Factors variables		
Number of Replicates	Temp (ºC)	Time (min)	Conc (pmol)
3	55	90	1000.00
3	45	90	0.00
3	55	90	0.00
3	58.409	60	500.00
3	45	30	0.00
3	45	30	1000.00
3	55	30	1000.00
3	55	30	0.00
3	50	9.54622	500.00
3	50	60	500.00
3	50	60	500.00
3	41.591	60	500.00
3	50	60	0.00
3	45	90	1000.00
3	50	110.454	500.00
3	50	60	1340.90
3	50	60	500.00

Table 3 DOE-2 with 6X SSC hybridisation buffer

	Factors variables		
Number of Replicates	Temp (ºC)	Time (min)	Conc (pmol)
3	50	9.54622	500.25
3	50	60	500.25
3	55	90	1000.00
3	45	90	1000.00
3	55	30	0.50
3	50	110.454	500.25
3	50	60	500.25
3	41.591	60	500.25
3	50	60	1340.73
3	45	90	0.50
3	50	60	500.25
3	55	30	1000.00
3	50	60	0.00
3	58.409	60	500.25
3	55	90	0.50
3	45	30	1000.00
3	45	30	0.50

APPENDICES K and L ***Supplementary materials related to the statistical analysis of each response of the experimental design***

8. Design of Experiment (DOE) : General Remarks (Statgraphic Centurion XV, VA, USA)

The supplementary data for each DOE were composed of:

1. **The analysis of variance (ANOVA table)** of each response analysed (hybridisation signal and percentage of events) tested the statistical significance of the effects. The ANOVA table partitions the variability in Cy3 into separated pieces for each of the effects. It then tested the statistical significance of each effect by comparing the mean square against an estimate of the experimental error. The important results from the ANOVA table were:
    - The lack of fit test was designed to determine whether the selected model was adequate to describe the observed data, or whether a more complicated model should have been used. The test was performed by comparing the variability of the current model residuals to the variability between observations at replicate settings of the factors.
    - The R-Squared statistic indicated in percentage how the model, as fitted, explained the variability of the response studied.
2. **The equation that fitted the model.**
3. **The optimise response table** showed the combination of factor levels which maximised the hybridisation signal over the indicated region.
4. **The half-normal plot** represented the absolute value of the effect estimates against their cumulative normal probabilities.
5. **The plot of observed data versus predicted** helped to cross-check the validity of the model against the actual data set by plotting actual versus predicted data.

Only the tables and graphs mentioned in the general remarks were displayed in the supplementary materials for each analysis, in order to facilitate the understanding of the results.

8.1. Supplementary materials related to DOE-1 and 3 X SSC hybridisation buffer

8.1.1. Analyse Experiment – % Recovery

ANOVA table shows that for the analysis if the % of recovery, no effect had a P-value less than 0.05, meaning no effect appeared to affect the response studied. Since the P-value for lack-of-fit in the ANOVA table was greater or equal to 0.05, the model appeared to be adequate for the observed data at the 95.0% confidence level. The R-Squared statistic indicates that the model as fitted explains 58.7992% of the variability in % Recovery (Table 8-1).

Table 8-1 Analysis of Variance for the % Recovery

Source	*Sum of Squares*	*Df*	*Mean Square*	*F-Ratio*	*P-Value*
A:Temp C	11.1392	1	11.1392	0.11	0.7677
B:Time min	0.88445	1	0.88445	0.01	0.9328
C:Conc pmol	19.22	1	19.22	0.20	0.7006
AA	0.771416	1	0.771416	0.01	0.9373
AB	2.17563	1	2.17563	0.02	0.8950
AC	243.828	1	243.828	2.50	0.2548
BB	78.5402	1	78.5402	0.80	0.4644
BC	169.911	1	169.911	1.74	0.3179
CC	8.56348	1	8.56348	0.09	0.7950
Lack-of-fit	182.424	3	60.8079	0.62	0.6643
Pure error	195.257	2	97.6286		
Total (corr.)	916.684	14			

R-squared = 58.7992 percent

The equation of the fitted model was:

% Recovery = 100.404 - 0.149486*Temp C + 0.558477*Time min - 1.44645*Conc pmol - 0.00812593*Temp C^2 - 0.00327778*Temp C*Time min + 0.0208304*Temp C*Conc pmol - 0.00512454*Time min^2 + 0.00434717*Time min*Conc pmol + 0.000609776*Conc pmol^2

Where the values of the variables were specified in their original units.

Finally, Table 8-2 shows the combination of factor levels, which maximizes % Recovery over the indicated region.

Table 8-2 Optimise Response

Goal	*Optimum value*	*Factor*	*Low*	*High*	*Optimum*
maximise % Recovery	85.4453	**Temp C**	45.0	60.0	45.0
		Time min	30.0	90.0	40.1202
		Conc pmol	0.05	100.0	0.0500012

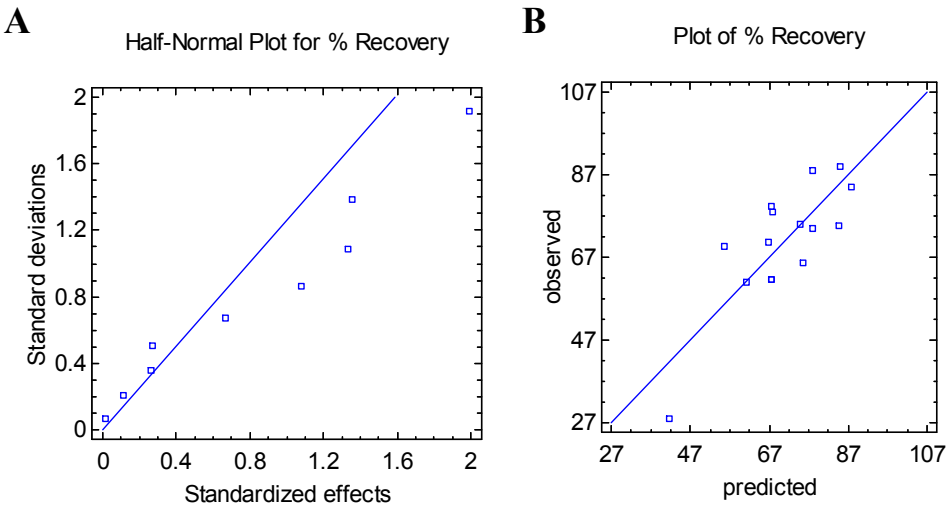

Figure 8-1 Half-Normal plot (A) and actual versus predicted plot (B)

(A) plot used for the identification of all significant effects; (B) plot used to inspect the correlation between the model predictions relative to the actual data.

8.1.2. Analyse Experiment – Cy3 (hybridisation signal)

ANOVA table shows that for the analysis of the hybridisation signal, oligo quantity had a P-value less than 0.05, meaning the quantity of oligo appeared to affect the response studied. Since the P-value for lack-of-fit in the ANOVA table was greater or equal to 0.05, the model appeared to be adequate for the observed data at the 95.0% confidence level. The R-Squared statistic indicates that the model as fitted explains 93.3883% of the variability in the hybridisation signal.

Table 8-3 Analysis of Variance for the hybridisation signal

Source	*Sum of Squares*	*Df*	*Mean Square*	*F-Ratio*	*P-Value*
A:Temp C	532.358	1	532.358	0.21	0.6638
B:Time min	591.336	1	591.336	0.24	0.6472
C:Conc pmol	134271.	1	134271.	53.74	0.0007
AA	2650.64	1	2650.64	1.06	0.3502
AB	0.0225	1	0.0225	0.00	0.9977
AC	4110.09	1	4110.09	1.65	0.2559
BB	916.311	1	916.311	0.37	0.5712
BC	1042.64	1	1042.64	0.42	0.5468
CC	34325.5	1	34325.5	13.74	0.0139
Lack-of-fit					0.4155
Total error	12492.1	5	2498.42		
Total (corr.)	188940.	14			

R-squared = 93.3883 percent

The equation of the fitted model was:

Hybridisation signal = 100.404 - 0.149486*Temp C + 0.558477*Time min - 1.44645*Conc pmol - 0.00812593*Temp C^2 - 0.00327778*Temp C*Time min + 0.0208304*Temp C*Conc pmol - 0.00512454*Time min^2 + 0.00434717*Time min*Conc pmol + 0.000609776*Conc pmol^2

Where the values of the variables were specified in their original units.

Table 8-4 shows the combination of factor levels, which maximises the hybridisation signal over the indicated region.

Table 8-4 Optimise Response

Goal	*Optimum value*	*Factor*	*Low*	*High*	*Optimum*
maximise Hybridisation signal	350.576	**Temp C**	45.0	60.0	54.6199
		Time min	30.0	90.0	62.9769
		Conc pmol	0.05	100.0	86.3611

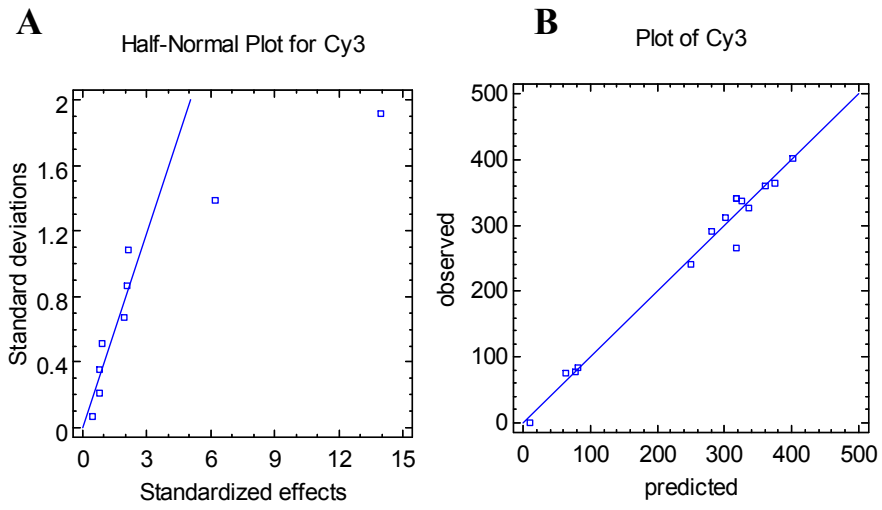

Figure 8-2 Half-Normal plot (A) and actual versus predicted plot (B)

(A) plot used for the identification of all significant effects; (B) plot used to inspect the correlation between the model predictions relative to the actual data.

8.2. Supplementary materials related to DOE-1 and 6 X SSC hybridisation buffer

8.2.1. Analyse Experiment – % Recovery

ANOVA table shows that for the analysis if the % of recovery, no effect a P-value less than 0.05, meaning the quantity of oligo appeared to affect the response studied.

Since the P-value for lack-of-fit in the ANOVA table was greater or equal to 0.05, the model appeared to be adequate for the observed data at the 95.0% confidence level. The R-Squared statistic indicates that the model as fitted explains 71.922% of the variability in % Recovery.

Table 8-5 Analysis of Variance for the % Recovery

Source	*Sum of Squares*	*Df*	*Mean Square*	*F-Ratio*	*P-Value*
A:Temp	3.8189	1	3.8189	0.35	0.6124
B:Time	0.391083	1	0.391083	0.04	0.8667
C:Conc pmol	0.637601	1	0.637601	0.06	0.8307
AA	184.461	1	184.461	17.08	0.0539
AB	1.39167	1	1.39167	0.13	0.7540
AC	106.799	1	106.799	9.89	0.0880
BB	45.5095	1	45.5095	4.21	0.1765
BC	0.160556	1	0.160556	0.01	0.9141
CC	1.54556	1	1.54556	0.14	0.7416
Lack-of-fit	107.419	5	21.4837	1.99	0.3676
Pure error	21.6048	2	10.8024		
Total (corr.)	459.522	16			

R-squared = 71.9222 percent

Table 8-6 Optimise Response

Goal	*Optimum value*	*Factor*	*Low*	*High*	*Optimum*
maximise % Recovery	78.1235	**Temp C**	41.59	58.4	45.7.082
		Time min	9.546	54.1	54.1222
		Conc pmol	0.0	1341	1340.9

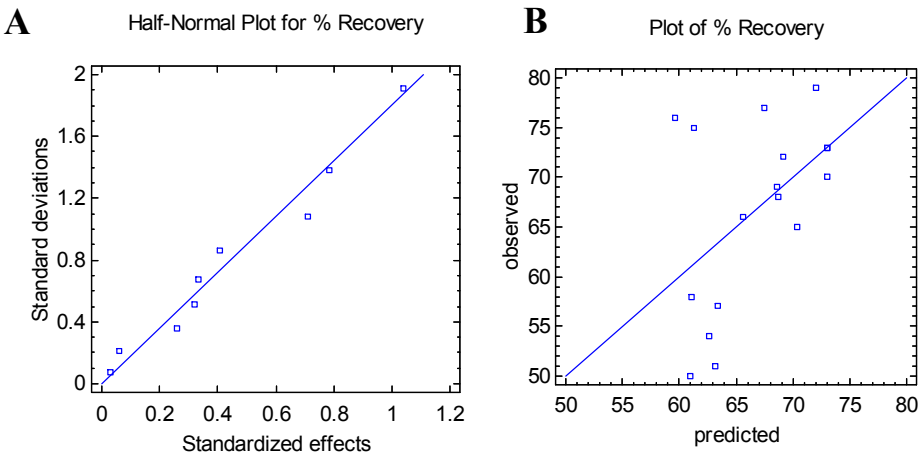

Figure 8-3 Actual versus predicted plot (A) and Half-Normal plot (B)

(A) plot used to inspect the correlation between the model predictions relative to the actual data; (B) plot used for the identification of all significant effects.

8.2.2. B.2.2. Analyse Experiment – Cy3 (hybridisation signal)

Table 8-7 shows that the 3 factor variables had a P-values ≤ 0.05, indicating that they were significantly different from zero at the 95.0% confidence level. Since the P-value for lack-of-fit in the ANOVA table was inferior to 0.05, the model appeared to be inadequate for the observed data at the 95.0% confidence level. The R-Squared statistic indicates that the model as fitted explains 89.47% of the variability in hybridisation signal.

Table 8-7 Analysis of Variance for the hybridisation signal

Source	*Sum of Squares*	*Df*	*Mean Square*	*F-Ratio*	*P-Value*
A:Temp	717.227	1	717.227	67.90	0.0144
B:Time	6443.39	1	6443.39	610.03	0.0016
C:Conc pmol	604172.	1	604172.	57199.70	0.0000
AA	3536.23	1	3536.23	334.79	0.0030
AB	4.01436	1	4.01436	0.38	0.6004
AC	316.676	1	316.676	29.98	0.0318
BB	13742.3	1	13742.3	1301.05	0.0008
BC	9022.74	1	9022.74	854.22	0.0012
CC	217677.	1	217677.	20608.45	0.0000
Lack-of-fit	80039.6	5	16007.9	1515.54	0.0007
Pure error	21.125	2	10.5625		
Total (corr.)	760815.	16			

R-squared = 89.477 percent

Table 8-8 Optimise Response

Goal	*Optimum value*	*Factor*	*Low*	*High*	*Optimum*
maximise Hybridisation signal	550	**Temp C**	41.59	58.4	50.4
		Time min	9.546	54.1	60.7991
		Conc pmol	0.0	1341	851.148

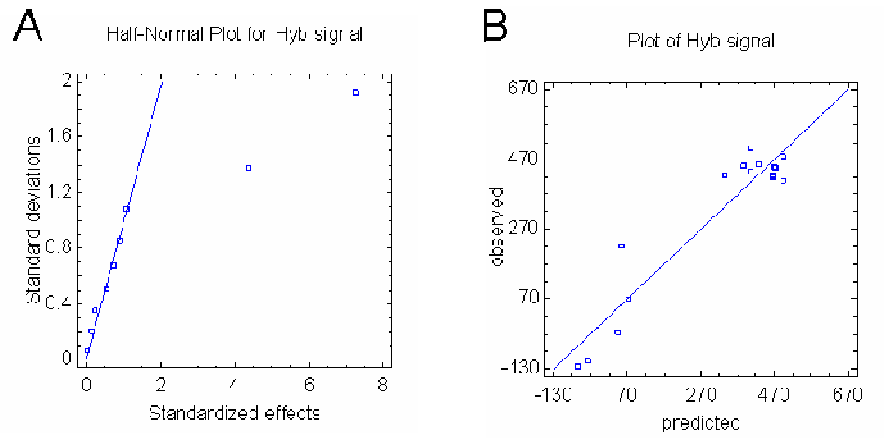

Figure 8-4 Half-Normal plot (A) and actual versus predicted plot (B)

(A) plot used for the identification of all significant effects; (B) plot used to inspect the correlation between the model predictions relative to the actual data.

8.3. Supplementary materials related to DOE-2 and 6 X SSC hybridisation buffer

8.3.1. Analyse Experiment – % Recovery

Table 8-9 shows that for the analysis if the % of recovery, no effect had a P-value ≤ than 0.05, meaning the no effect appeared to affect the response studied. Since the P-value for lack-of-fit in the ANOVA table was greater or equal to 0.05, the model appeared to be adequate for the observed data at the 95.0% confidence level. The R-Squared statistic indicates that the model as fitted explains 72.144% of the variability in % Recovery.

Table 8-9 Analysis of Variance for the % Recovery

Source	*Sum of Squares*	*Df*	*Mean Square*	*F-Ratio*	*P-Value*
A:Time	0.182479	1	0.182479	0.02	0.9085
B:Temperature	3.53021	1	3.53021	0.33	0.6252
C:Concentration oligoCy3	0.862384	1	0.862384	0.08	0.8041
AA	43.7402	1	43.7402	4.05	0.1818
AB	1.6456	1	1.6456	0.15	0.7340
AC	0.0885503	1	0.0885503	0.01	0.9361
BB	185.341	1	185.341	17.16	0.0536
BC	104.678	1	104.678	9.69	0.0896
CC	1.66448	1	1.66448	0.15	0.7325
Lack-of-fit	105.409	5	21.0817	1.95	0.3726
Pure error	21.6048	2	10.8024		
Total (corr.)	455.965	16			

R-squared = 72.144 percent

Table 8-10 Optimise Response

Goal	*Optimum value*	*Factor*	*Low*	*High*	*Optimum*
maximise % Recovery	78.1538	**41.59**	9.546	58.41	45.76
		Time min	9.546	110.4	54.7
		Conc pmol	0.05	1341	1340.9

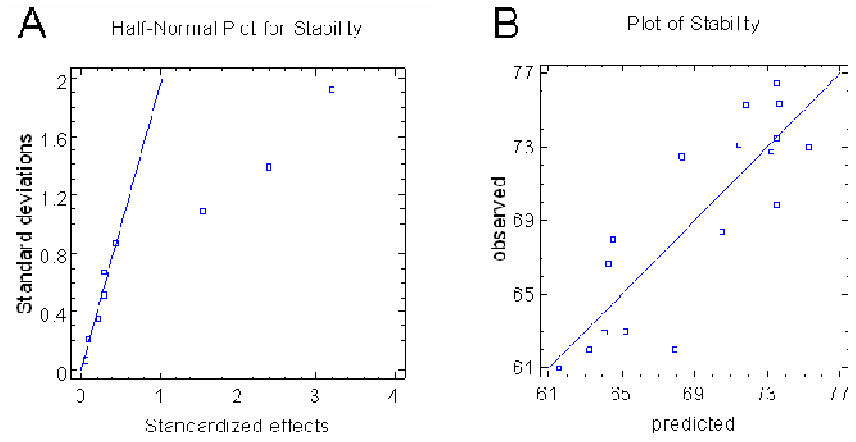

Figure 8-5 Half-Normal plot (A) and actual versus predicted plot (B)

(A) plot used for the identification of all significant effects; (B) plot used to inspect the correlation between the model predictions relative to the actual data.

8.3.2. Analyse Experiment – Cy3 (hybridisation signal)

Table 8-11a shows that for the analysis if the % of recovery, two effects (temperature and oligo quantity) had a P-value ≤ than 0.05, meaning the effect appeared to affect the response studied. Since the P-value for lack-of-fit in the ANOVA table was greater or equal to 0.05, the model appeared to be adequate for the observed data at the 95.0% confidence level. The R-Squared statistic indicates that the model as fitted explains 80.94% of the variability in % Recovery.

Table 8-11 Analysis of Variance for the hybridisation signal

Source	***Sum of Squares***	***Df***	***Mean Square***	***F-Ratio***	***P-Value***
A:Time	1908.62	1	1908.62	3.55	0.2000
B:Temperature	21.7309	1	21.7309	0.04	0.8592
C:Concentration oligoCy3	53624.3	1	53624.3	99.87	0.0099
AA	1973.28	1	1973.28	3.68	0.1953
AB	11.2813	1	11.2813	0.02	0.8980
AC	399.031	1	399.031	0.74	0.4795
BB	19907.6	1	19907.6	37.08	0.0259
BC	8944.53	1	8944.53	16.66	0.0551
CC	5571.73	1	5571.73	10.38	0.0844
Lack-of-fit	19041.4	5	3808.29	7.09	0.1282
Pure error	1073.85	2	536.926		
Total (corr.)	105539.	16			

R-squared = 80.9404 percent

Table 8-12 Optimise Response

Goal	***Optimum value***	***Factor***	***Low***	***High***	***Optimum***
maximise Hybridisation signal	482.632	**Temp C**	41.59	58.409	53.5248
		Time min	9.546	110.4	60.915
		Conc pmol	0.0	1341	1341

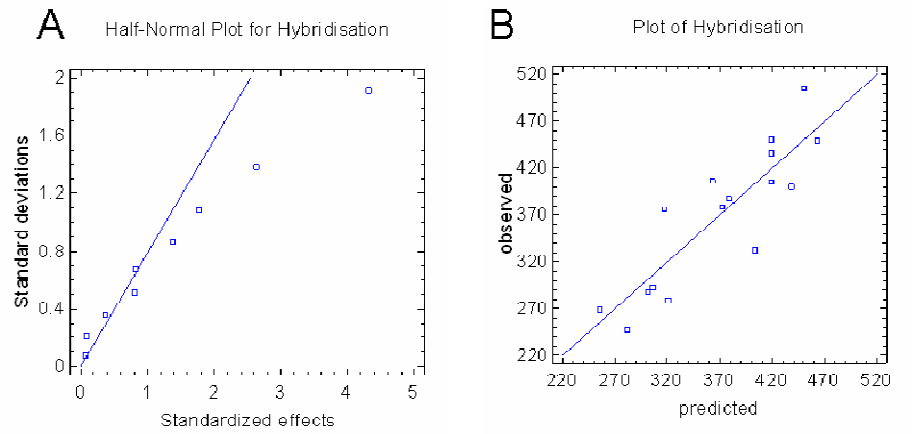

Figure 8-6 Half-Normal plot (A) and actual versus predicted plot (B)

(A) plot used for the identification of all significant effects; (B) plot used to inspect the correlation between the model predictions relative to the actual data.

9. Multiple Response Optimisation supplementary data (MRO)

9.1. DOE-1 Multiple response optimisation

9.1.1. 3X SSC

Table 9-1 The minimum and maximum values of the response variables over the experimental runs

	Observed	***Observed***
Response	***Minimum***	***Maximum***
% Recovery	27.84	88.88
Hybridisation signal	0.0	401.85

Table 9-2 The parameters of the desirability function

	Desirability	***Desirability***		***Weights***	***Weights***	
Response	***Low***	***High***	***Goal***	***First***	***Second***	***Impact***
% Recovery	27.84	88.88	Maximize	1.0		5.0
Hybridisation signal	0.0	401.85	Maximize	1.0		3.0

Table 9-3The observed values for each response and the predicted and observed values of desirability *

			Predicted	*Observed*
Row	***% Recovery***	***Hybridisation signal***	***Desirability***	***Desirability***
1	88.03	0.0	0.223663	0.0
2	84.1	74.6	0.498197	0.505381
3	74.05	401.85	0.884603	0.840332
4	61.55	341.84	0.697981	0.649381
5	65.62	311.11	0.769076	0.673129
6	75.08	290.44	0.742609	0.754322
7	61.07	240.21	0.57441	0.563826
8	78.08	360.22	0.738864	0.849837
9	74.62	78.3	0.518889	0.45858
10	27.84	336.4	0.366636	0.0
11	69.69	326.19	0.574153	0.730429
12	79.26	266.32	0.697981	0.769929
13	61.55	341.84	0.697981	0.649381
14	88.88	364.15	0.935162	0.963732
15	70.76	83.02	0.417428	0.444194

* % Recovery: relative percentage of events; Code consistency: corrected MFI in FL1; Cy3: hybridisation signal corresponding to corrected MFI in FL2

9.1.2. 6X SSC

Table 9-4 The minimum and maximum values of the response variables over the experimental runs

	Observed	*Observed*
Response	***Minimum***	***Maximum***
% Recovery	50.0	79.0
Hybridisation signal	-123.0	503.0

Table 9-5 The parameters of the desirability function

	Desirability	*Desirability*		*Weights*	*Weights*	
Response	***Low***	***High***	***Goal***	***First***	***Second***	***Impact***
% Recovery	50.0	79.0	Maximize	4.0		3.0
Hybridisation signal	-123.0	503.0	Maximize	3.0		5.0

Table 9-6 The observed values for each response and the predicted and observed values of desirability *

			Predicted	*Observed*
Row	***% Recovery***	***Hybridisation signal***	***Desirability***	***Desirability***
1	50.0	479.0	0.226942	0.0
2	66.0	-123.0	0.00490742	0.0
3	57.0	-105.667	0.00760025	0.000142351
4	75.0	457.0	0.19229	0.693687
5	68.0	-25.0	0.0449563	0.0151107
6	65.0	450.5	0.529976	0.315655
7	51.0	445.5	0.278468	0.00534498
8	58.0	71.0	0.027299	0.0161098
9	79.0	437.5	0.482742	0.812835
10	70.0	426.25	0.6315	0.448167
11	73.0	423.0	0.6315	0.54658
12	72.0	503.0	0.390675	0.66075
13	69.0	223.75	0.0495477	0.175181
14	54.0	411.0	0.280705	0.0380238
15	77.0	428.0	0.258725	0.707182
16	76.0	452.0	0.12887	0.723875
17	73.0	419.75	0.6315	0.540496

* % Recovery: relative percentage of events; Code consistency: corrected MFI in FL1; Cy3: hybridisation signal corresponding to corrected MFI in FL2

9.2. DOE-2 Multiple response optimisation

Table 9-7 The minimum and maximum values of the response variables over the experimental runs

Response	***Minimum***	***Maximum***
Stability	61.0	76.4567
Hybridisation	227.0	505.0

Table 9-8 The parameters of the desirability function

	Desirability	***Desirability***		***Weights***	***Weights***	
Response	***Low***	***High***	***Goal***	***First***	***Second***	***Impact***
Stability	61.0	76.4567	Maximize	1.0		3.0
Hybridisation	227.0	505.0	Maximize	1.0		3.0

Table 9-9 The observed values for each response and the predicted and observed values of desirability*

			Predicted	***Observed***
Row	***Stability***	***Hybridisation***	***Desirability***	***Desirability***
1	72.4533	405.667	0.48179	0.690092
2	76.4567	436.0	0.749445	0.867062
3	68.0	505.0	0.428996	0.672962
4	75.28	387.5	0.620158	0.730333
5	68.375	227.0	0.0	0.0
6	62.0	332.5	0.53271	0.156692
7	69.8933	450.333	0.749445	0.679874
8	62.0	288.0	0.197994	0.119147
9	73.0	448.667	0.886127	0.786792
10	66.6667	376.5	0.262998	0.444021
11	73.49	405.0	0.749445	0.719301
12	62.94	400.0	0.388986	0.279475
13	75.3033	279.0	0.527658	0.416044
14	61.0	292.0	0.0989917	0.0
15	73.13	269.0	0.262787	0.34433
16	72.76	378.5	0.641826	0.643916
17	63.0	248.0	0.232396	0.0988653

* % Recovery: relative percentage of events; Code consistency: corrected MFI in FL1; Cy3: hybridisation signal corresponding to corrected MFI in FL2

APPENDIX M Cell line Material and Methods

ALL CHEMICALS AND REAGENTS WERE SUPPLIED BY SIGMA-ALDRICH (POOLE, UK) UNLESS STATED OTHERWISE AND ALL EQUIPMENT USED IS LISTED IN *APPENDIX B*.

1 CELL CULTURE

1.1 MEDIA

TWO VARIETY OF CELL LINES WERE CULTURED: THEIR NAMES AND CELLULAR REQUIREMENTS ARE SHOWN IN TABLE C.1.

Table 1. The cell lines used and their media requirements.

Cell Line	Cell Type	Medium	Supplements
ARPE 19 (ATCC CRT-2302)	Human male retinal pigmented epithelium	Medium/Nutrient F-12 Ham (Eagle modified by Dulbecco)	1mM Glutamine, 10% (v/v) foetal calf bovine serum, 5 units/ml of Penicillin and 0.005mg/ml Streptomycin
RT112/84 (ECACC 85061106)	Human female Bladder slow growing tumor		

1.2 CELL CULTURE

CELL LINES WERE CULTURED IN AN INCUBATOR AT 37 °C WITH 5 % (V/V) CO_2, AND THE MEDIUM WAS CHANGED EVERY OTHER DAY. ONCE THE CELLS REACHED 70-80 % CONFLUENCES THEY WERE RINSED IN PHOSPHATE SALINE BUFFER (PBS) AND TREATED WITH A 1X TRYPSIN SOLUTION (APPROXIMATELY 5ML OF A 1X SOLUTION OF TRYPSIN WERE ADDED/ T75 FLASK). THE FLASKS WERE THEN INCUBATED AT 37°C FOR UP TO 5 MINUTES TO ALLOW THE TRYPSIN TO DISSOCIATE THE CELLS (CELLS WERE NEVER TRYPSINISED FOR LONGER THAN 5 MINUTES TO AVOID ANY CELLULAR DAMAGE). THE CELLULAR MIXTURE WAS THEN TRANSFERRED TO A 15ML CENTRIFUGE TUBE (FISHER SCIENTIFIC, LEICESTERSHIRE UK) AND AN EQUAL VOLUME OF MEDIUM CONTAINING SERUM WAS ADDED TO NEUTRALISE THE ACTION OF THE TRYPSIN. THE CELLS WERE THEN CENTRIFUGATED AT 105 G AT 4°C FOR 5 MIN AND THE SUPERNATANT REMOVED. THE PELLET WAS RE-SUSPENDED IN AN APPROPRIATE VOLUME OF MEDIUM.

APPENDIX N Recipe and procedure of lab routine experiment

Agarose gel 3 %

2.5 g of Agarose (powder, Fisher, UK)

80ml TAE 1X (Tris-Acetate-EDTA, 40 mM Tris, 20 mM Acetic acid, 1 mM EDTA, Sigma product purchase through Fisher Scientific, UK)

2min microwave

APPENDIX O Length separating microsphere to QD-SA bioconjugate

As described in Agrawal {, 2008}, the QDEM were hybridised to the PCR products which formed a rigid duplex DNA construct. The expected length could be extrapolated form the results obtained by this group on rigid structure. The approximate of the length of the QDEM construction was approximated using the hypothesis and calculations presented below.

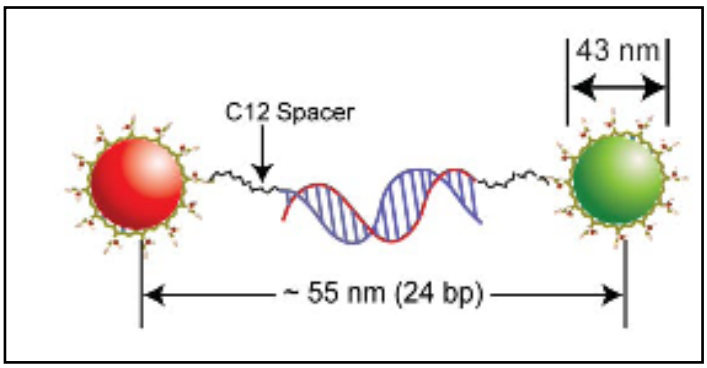

Figure 1. Schematic diagram of the structure of a rigid DNA/nanoparticle construct and its expected contour length (adapted from Agrawal {, 2008}).

The experimental distance result (54 nm) was matching the expected length (55 nm)

From Figure 1.:

- Distance between 2 nucleotides = 0.34 nm
- Radius of the nanoparticle: 43 / 2 = 21.5 nm
- Distance corresponding only to 24 bp DNA and 2 times 12C carbon spacer ~ 12 nm
- 24 bp correspond to ~ 0.34 X 24 = 8.16 nm in length

Therefore C 12 spacer length is approx (12 -8.16)/2 ~ 2 nm. From these data a 6C spacer should be ~ 1 nm, and a DNA sequence ranging from 18 to 25 bases should be between ~ 6 – 8.5 nm. As a conclusion the distance from the microsphere to the extremity of the oligonucleotide was estimated to range from 7-10 nm. QD-SA are typically coated with 8

to 10 SA molecules, which corresponds to a final size of bioconjugate of approx 8-10 nm {Wu, 2007}. The QD bioconjugate and the probe presented therefore approx the same size. The steric hindrance thus, limited the binding stoechiometry to a ratio of 1:1.

To work in excess of QD-SA, the hybridisation efficiency of the biotinylated PCR product to the probes on the bead surface was considered as maximal (all the site hybridised). These considerations allowed predicting the number of QD-SA needed to be certain to saturate all the binding sites of the microsphere. The number of QD-SA needed was then directly equivalent to the number of oligo probe attached on the surface of the QDEM.

The number of olio/ μm^2 calculated during coupling efficiency experiment provided the corresponding number of QD-SA that can potentially bind to the biotinylated PCR product. The number of oligo per microsphere was evaluated as followed, with the results obtained previously in chapter 4:

$$(MEF\ (s) - MEF\ (b)) / N = \text{number of oligo / bead}$$

Where MEF: molecule of equivalent of fluorophore; N: number of QDEM in samples; (s): sample; (b) background

With a probe quantity of ~ 100 pmol, ~78,500 MEF was obtained from the conjugation titration of 10,000 QDEMs (Chapter 3, figure 3.3). The hybridisation experiment were performed with 8000 QDEM, Therefore 6.28×10^5 QD-SA were required. The concentration of QD-SA being 1.82×10^{11} QD/mL, 3.5 µL of QD-SA solution was required for each hybridisation experiment.

APPENDIX P *Y-SNP and beta-actin sequences*

1. Y-SNPs sequences

All sequences are presented in fasta format; the bold letter positioned the allele;

M9 sequence

>gnl|dbSNP|rs3900|allelePos=201|totalLen=401|taxid=9606|snpclass=1|alleles='C/G'|mol=Genomic

ACATTTTCCT TACTTTACTC AACTCGTTCC TTTGAATACC GCAAAATTAA GACGGCGTTT AAAACAATCG AAATCCCTTT TCTTCTGGGG TTTGGTGCCT AAAGATTAGA AAAGTTTGCG CAAGGAATTC GCTGCAGCAT ATAAAACTTT CAGGACCCTG AAATACAGAA CTGCAAAGAA ACGGCCTAAG ATGGTTGAAT
S
CTCTTTATTT TTCTTTAATT TAGACATGTT CAAACGTTCA ATGTCTTACA TACTTAGTTA TGTAAGTAAG GTAGCGCTTA CTTCATTATG CATTTCAATA CTCAAAAAAA ATTCCTTTGT GAAATGTTGA AATATTTTTC TAATCTGTTT CACGAGCTTC AAAAATGAGG AAAAAAGATT CAGTTTACAT TTCAGCAAAA

M60 sequence

>gnl|dbSNP|rs2032623|allelePos=243|totalLen=389|taxid=9606|snpclass=2|alleles='-/T'|mol=Genomic|

GCACTGGCGT TCATCATCTG GGAGCAGCTC AAAAGCCTCT CGCTCAGCCT CCGTGACGCC CTGGGGGTGT TCAACCCACA TATACTGTAA AGACTAGGAG TAGGGTTGTG GACACCCCAC CTCAGCCAAC ACTGAGCCCT GATGTGGACT CAACCTTGTA AGGAAAGCTG TAGAGAAATT GGAAGAAAAA ATATAAACAC ATACAGACTC TGTCTTTACA TTTCAAAATG CATGACTTAA AG
N
ATCAGGCACA CAGTGGTTAC TCAATGTTGG TCTGTGTCTC TGTAACGTAA TATATGTGAC TAAATCCCTA AGCTCTGCTC TTGACCACCC ACCTTCTCCA AAAGGGCCTT TCGTAGACGT CGCTCCTCCT GAACCATAAT GAACAT

2. Beta-actin sequence

The following Beta-actin sequence and primer were supplied by Ryan Pink:

Beta actin Forward Primer 5' – TCGTCATACTCCTGCTTGCTGATCCA – 3'

Beta-actin Reverse Primer 5' – TCCTCAGATCATTGCTCCTCCTGAGC – 3'

GTCCGCCTAGAAGCATTTGCGGTGGACGATGGAGGGGCCGGAC*TCGTCATACTCCTGCTTGCTGATCCA*CA
TCTGCTGGAAGGTGGACAGCGAGGCCAGGATGGAGCCGCCGATCCACACGGAGTACTTGC*GCTCAGGAGGAGCAA*
*TGATCTGAGGA*GGGAAGGGGACAGGCAGTGAGGACCCTGGATGTGACAGCTCCCCACACACCACAGGACCCCACAG
CCGACCTGCCCAGGTCAGCTCAGGCAGGAAAGACACCCACCTTGATCTTCATTGTGCTGGGTGCCAGGGCAGTGATCTCC
TTCTGCATCCTGTCGGCAATGCCAGGGTACATGGTGGTGCCGCCAGACAGCACTGTGTTGGCGTACAGGTCTTTGCGGAT
GTCCACGTCACACTTCATGATGGAGTTGAAGGTAGTTTCGTGGATGCCACAGGACTCCATGCCTGAGAGGGAAATGAGGG
CAGGACTTAGCTTCCACAGCACAGCCCCGAGGGGTAACCCTCATGTCAGGCAGAGCCGGGAGACAGTCTCCACTCACCCA
GGAAGGAAGGCTGGAAGAGTGCCTCAGGGCAGCGGAACCGCTCATTGCCAATGGTGATGACCTGGCCGTCAGGCAGCTCG
TAGCTCTTCTCCAGGGAGGAGCTGGAAGCAGCCGTGGCCATCTCTTGCTCGAAGTCCAGGGCGACGTAGCACAGCTTCTC
CTTAATGTCACGCACGATTTCCCGCTCGGCCGTGGTGGTGAAGCTGTAGCCGCGCTCGGTGAGGATCTTCATGAGGTAGT
CAGTCAGGTCCCGGCCAGCCAGGTCCAGACGCAGGATGGCATGGGGGAGGGCATACCCCTCGTAGATGGGCACAGTGTGG
GTGACCCCGTCACCGG

The yellow highlights are the oligonucleotide target primer binding sites, amplifying a 116 bp fragment.

APPENDIX Q Temperature gradient PCR optimisation

3 % agarose electrophoresis gel analysis of PCR gradient experiment. For material and method, referred to Chapter 5

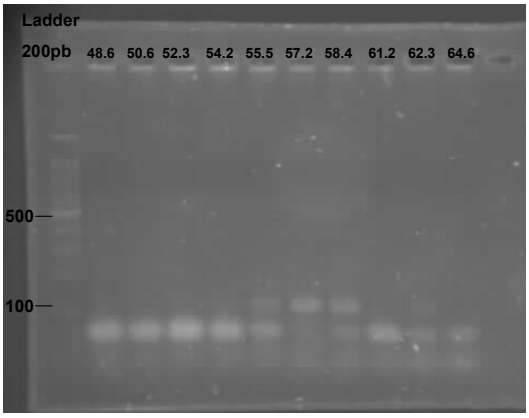

Figure 1. Photo of the T-gradient amplification agarose gel of Y-SNP M9 (96 bp)

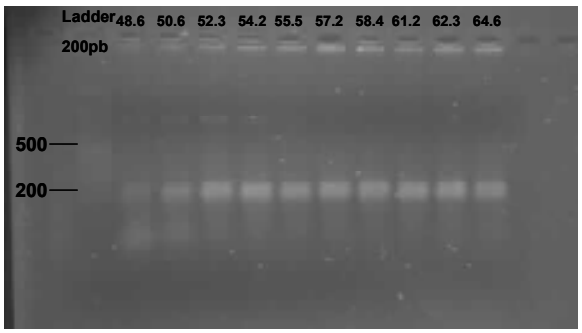

Figure 2. Photo of the T-gradient amplification agarose gel of Y-SNP M60 (196 bp)

APPENDIX R Sequence alignment output

The alignment of the sequences using the Basic Local Alignment Search Tool (BLAST, www.ncbi.nlm.nih.gov/BLAST/, Altschul *et al.* 1990) is presented below for Y-SNP M9 and M60. Each strand of the PCR products was sequenced and the SNP allele is indicated in bold.

1 M9 sequence

>M9 forward Similarity=94% for 49 bp

```
15      NTGA-ngntcttnatttttctttattt-agacatgttcaaacgttcaatgtcttaca    63
        |||||| ||||||||||||||||||||||||||||||||||||||||||||||||
43      ttgaatSctctttatttttctttaatttagacatgttcaaacgttcaatgtcttaca    91
```

>M9 reverse Similarity=98% for 48 bp

```
249         aatacagaactgcaaagaaacggcctaagatggttgaatgctctttat         296
            |||||||||||||||||||||||||||||||||||| ||||||||
2           aatacagaactgcaaagaaacggcctaagatggttgaatsctctttat         49
```

2 M60 sequence

>M60 Reverse: Similarity=99% for 130 bp

```
67 tgagtaaccactgtgtgcctgatactttaagtcatgcattttgaaatgtaaagacagagtctgt
   |||||||||||||||||||||| ||||||||||||||||||||||||||||||||||||||||
45 tgagtaaccactgtgtgcctgat-ctttaagtcatgcattttgaaatgtaaagacagagtctgt

atgtgtttatatttttttcttccaatttctctacagctttccttacaaggttgagtccacatcaggg 196
|||||||||||||||||||||||||||||||||||||||||||||||||||||||||||||||||||
atgtgtttatatttttttcttccaatttctctacagctttccttacaaggttgagtccacatcaggg  174
```

>M60 Forward Similarity=99% for 130 bp

```
67 tgagtaaccactgtgtgcctgatactttaagtcatgcattttgaaatgtaaagacagagtctgt
   |||||||||||||||||||||||||||||||||||||||||||||||||||||||||||||||||
45 tgagtaaccactgtgtgcctgat-ctttaagtcatgcattttgaaatgtaaagacagagtctgt

atgtgtttatatttttttcttccaatttctctacagctttccttacaaggttgagtccacatcaggg  196
|||||||||||||||||||||||||||||||||||||||||||||||||||||||||||||||||||
Atgtgtttatatttttttcttccaatttctctacagctttccttacaaggttgagtccacatcaggg  174
```